GLUTATHIONE S-TRANSFERASE PI-1 IN PANCREATIC CANCER PATHOGENESIS: MECHANISTIC INSIGHTS INTO ITS ROLE IN OXIDATIVE STRESS, CELL SIGNALING, AND METABOLIC PATHWAYS

A Dissertation
Submitted to the Graduate Faculty
of the
North Dakota State University
of Agriculture and Applied Science

By

Rahul Raj Singh

In Partial Fulfillment of the Requirements
for the Degree of
DOCTOR OF PHILOSOPHY

Major Program:
Cellular and Molecular Biology

October 2021

Fargo, North Dakota

North Dakota State University

Graduate School

Title

GLUTATHIONE S-TRANSFERASE PI-1 IN PANCREATIC CANCER PATHOGENESIS: MECHANISTIC INSIGHTS INTO ITS ROLE IN OXIDATIVE STRESS, CELL SIGNALING, AND METABOLIC PATHWAYS

By

Rahul Raj Singh

The Supervisory Committee certifies that this ***disquisition*** complies with North Dakota State University's regulations and meets the accepted standards for the degree of

DOCTOR OF PHILOSOPHY

SUPERVISORY COMMITTEE:

Katie M. Reindl, Ph.D.
Chair

John C. Wilkinson, Ph.D.

D.K. Srivastava, Ph.D.

Pawel Borowicz, Ph.D.

Approved:

11/5/2021
Date

Katie M. Reindl, Ph.D.
Department Chair

ABSTRACT

Pancreatic ductal adenocarcinoma (PDAC) is currently the third leading cause of cancer-related deaths in the US. Although surgery remains the most effective treatment option, only a few PDACs are resectable at diagnosis. Further, only a few PDAC patients respond to conventional chemotherapy making long-term survival notably challenging. Therefore, the identification of novel therapeutic targets is needed to improve PDAC treatment efficacy. Here, we investigated the role of glutathione S-transferase pi-1 (GSTP1) in PDAC pathogenicity. We postulated that a higher expression of GSTP1 provides selective advantages to PDAC cells by scavenging excessive reactive oxygen species (ROS) and promoting survival. Using shRNAs, we knocked down the expression of GSTP1 in metabolically diverse PDAC cells. We show loss of GSTP1 reduces PDAC cell growth and causes oxidative stress. Our results provide evidence that GSTP1 knockdown activates apoptotic signaling by phosphorylating c-Jun N-terminal kinase (JNK) and c-Jun. Further, supporting *in vitro* data, nude mice bearing orthotopically implanted GSTP1 knockdown PDAC cells showed a significant reduction in tumor size and volume and reduced Ki67 staining.

Further, using multi-omic techniques, we show that GSTP1 knockdown significantly changes the global transcriptomic and proteomic signatures of PDAC cells. Gene set enrichment analyses revealed that cellular metabolism and energy production pathways are most affected in GSTP1 knockdown PDAC cells. Specifically, we report a reduction in the mRNA and protein expression of aldehyde dehydrogenase 7A1 (ALDH7A1) and solute carrier 2A3 (SLC2A3) in GSTP1 knockdown cells compared to the control. We propose that the growth-inhibitory effects of GSTP1 knockdown are due to redox imbalance and impaired energy production pathways. Our data are the first steps of validating GSTP1 as a potential therapeutic target for PDAC.

Collectively, our results provide evidence that GSTP1 inhibitors combined with conventional chemotherapy can be an effective treatment for PDAC patients. However, understanding the function of GSTP1 in cancer cell metabolism requires further investigations. Because GSTP1 knockdown affects various metabolic genes, we will evaluate the bioenergetic changes in GSTP1 knockdown PDAC cells. Additionally, comparative evaluation of metabolites and lipids in control and GSTP1 knockdown cells will expand our knowledge of GSTP1 in cancer cell physiology and metabolism.

ACKNOWLEDGEMENTS

To Dr. Katie Reindl | I am greatly indebted to her for giving me the opportunity to work in her lab, for years of mentoring, and for providing constant motivation to complete my graduate studies. Her patience, guidance, and commitment to her students' success are remarkable. I have learned the importance of hard work, integrity, and a sound scientific mindset from her. Dr. Reindl makes sure that her students are held to the highest standards, and I hope that in future, I can emulate the degree of perfection and meticulousness that she expects of her students. Under her leadership, I have grown tremendously as a scientist, and her constant support has been instrumental in my success as a graduate student.

To my other mentors | I am incredibly thankful to the scientists I had the honor to work with. I thank my advisory committee- Dr. John Wilkinson, Dr. D.K. Srivastava, and Dr. Pawel Borowicz. It is because of their willingness to educate that I had a successful experience in graduate school. I highly appreciate Dr. Wilkinson for teaching me flow cytometry and giving me constructive feedback on numerous applications. Apart from my advisory committee, I was lucky to get guidance from some exceptional scientists. Dr. Jodie Haring has been a true inspiration throughout my graduate career, both as a scientist and as a human being. Dr. Jiha Kim, Dr. Kendra Greenlee, Dr. Megan Orr, and Dr. Jill Hamilton- thank you for offering advice and support. Most importantly, thank you all for taking the time to train me as a scientist. This is something that I value immensely.

To my colleagues | I was fortunate to work with amazing colleagues from across diverse disciplines. I am incredibly thankful for all the past and the present members of Reindl lab- Dr. Jiyan Mohammad, Dr. Shireen Chikara, Dr. Jagadish Loganathan, Gauthami Nair, Philip Salu, Jenna Duttenheffner, Jade Vipond, Nolan Schwarz, Pamoda Galhenage, Cody Riggle, Brandon

Haugrud, and Elena Linster- for all the support and great times spent in the lab. Jiyan- I am exceptionally thankful for your patience and guidance during the early stages at the lab. Your dedication and determination have since then motivated me to put in my best at everything. I appreciate your friendship and will never forget our fun-filled chats between experiments. My sincere appreciation goes to Jeffrey Kittilson for troubleshooting experiments and being available. Jeff- your company, support, and guidance mean a lot to me. In addition, I would like to thank Megan Ruch for her help with animal experiments and Jordan Flaten for assisting me with immunohistochemistry. Further, I would like to acknowledge members from Kim lab- Dr. Sangdeuk Ha, Alex Delgado, Reed Jacobson, Farid Solaymani, and Vikneshwari Natarajan- for sharing reagents and helping with fluorescence microscopy. Lastly, I would like to acknowledge all the faculty members from Biological Sciences, support staff (Wendy Leach and Chad Lachowitzer), and Danjel Nygard for their help, support, and patience.

To my family and friends | I owe an enormous debt to my family. Their generosity and guidance made me what I am today. Specifically, I would like to thank my parents for their untiring love and sacrifice, and my sisters for their constant encouragement. As an international student, graduate school would have been onerous and lonesome. I express my gratitude to my friends for making my stay in Fargo memorable. In particular, I thank Lydia, Megan, Mack, Courtney, Charlie, Deepak, Chris, Eric, Chad, Nick, and James for all the laughs, dinners, and camping trips. My life indeed would not be complete without you all.

DEDICATION

This thesis is dedicated to my parents, Geeta and Raj. Their untiring support, encouragement, and inspiration made this possible. Thank you for everything!

TABLE OF CONTENTS

LIST OF TABLES

LIST OF FIGURES

LIST OF ABBREVIATIONS

4-HNE	4-hydroxy nonenal
µM	Micromolar
ALDH7A1	Aldehyde dehydrogenase 7A1
AMPK	AMP-activated protein kinase
ASK1	Apoptosis signal-regulating kinase 1
ATP	Adenosine triphosphate
AVMA	American veterinary medical association
Bak	Bcl-2 homologous antagonist/killer
Bax	Bcl-2-like protein 4
Bcl-2	B cell lymphoma 2
CDK	Cyclin dependent kinase
cDNA	Complementary DNA
CM-H_2DCFDA	Chloromethyl-2',7'-dichlorodihydrofluorescein diacetate
CYP	Cytochrome P540
DAPI	4', 6-diamidino-2-phenylindole
DMEM	Dulbecco's modified Eagle medium
DMSO	Dimethyl sulfoxide
DNA	Deoxyribonucleic acid
Dox	Doxycycline
EGF	Epidermal growth factor
EGFR	Epidermal growth factor receptor
EMT	Epithelial-mesenchymal transition
ERK	Extracellular signal-regulated kinase

ETC .....Electron transport chain

FAO .....Fatty acid oxidation

FBS .....Fetal bovine serum

FOLFIRINOX .....Leucovorin, 5-fluorouracil, irinotecan, and oxaliplatin

GAPDH .....Glyceraldehyde 3-phosphate dehydrogenase

GFP .....Green fluorescent protein

GLUT3.....Glucose transporter 3

GPx .....Glutathione peroxidase

GSH .....Reduced Glutathione

GSSG .....Oxidized glutathione

GST.....Glutathione S-transferase

GSTA1.....Glutathione S-transferase alpha-1

GSTK1.....Glutathione S-transferase kappa-1

GSTM1 .....Glutathione S-transferase mu-1

GSTP1.....Glutathione S-transferase pi-1

GSTT1.....Glutathione S-transferase theta-1

GSTZ1 .....Glutathione S-transferase zeta-1

GTeX .....Genotype-tissue expression

HRP.....Horseradish peroxidase

IACUC.....Institutional animal care and use committee

i.p .....Intraperitoneal

JNK .....c-Jun N-terminal kinase

JNK1 .....c-Jun N-terminal kinase 1

JNK2 .....c-Jun N-terminal kinase 2

kDa/kD .....Kilodalton

Keap1	Kelch like ECH associated protein 1
KRAS	Kirsten rat sarcoma viral oncogene homolog
LC-MS/MS	Liquid Chromatography with tandem mass spectrometry
MAPK	Mitogen-activated protein kinase
mg	Milligram
mM	Millimolar
mRNA	Messenger RNA
MT-CYB	Mitochondrially encoded cytochrome b
MT-ND1	Mitochondrially encoded NADH:ubiquinone
MTT	3-(4, 5-dimethylthiazol-2-yl)-2, 5-dephenyltetrazolium bromide
NAB	Nanoparticle albumin-bound
NAC	N-acetylcysteine
NAD+/NADH	Nicotinamide adenine dinucleotide/Reduced NAD
NBDHEX	6-(7-nitro-2,1,3-benzoxadiazol-4-ylthio)hexanol
NDUFA9	NADH: ubiquinone oxidoreductase subunit A9
NDUFB8	NADH: ubiquinone oxidoreductase subunit B8
NF-κB	Nuclear factor κ-light-chain-enhancer of activated B cells
Nrf2	Nuclear factor erythroid 2-related factor 2
NS	Non-specific control
OXPHOS	Oxidative phosphorylation
PBS	Phosphate buffered saline
PCA	Principal component analysis
PCR	Polymerase chain reaction

PDAC.....Pancreatic ductal adenocarcinoma

PDIA6.....Protein disulfide isomerase A6

PI.....Propidium iodide

PI3K.....Phosphoinositide 3-kinase

PL.....Piperlongumine

PMSF.....Phenylmethylsulfonyl fluoride

PPP.....Pentose phosphate pathway

PRx.....Peroxiredoxin

PTEN.....Phosphatase and tensin homolog

PXR.....Pregnane X receptor

QC.....Quality control

qPCR.....Quantitative PCR

RNA.....Ribonucleic acid

RNAi.....RNA interference

RNA-Seq.....RNA sequencing

ROS.....Reactive oxygen species

RPMI 1640.....Roswell Park Memorial Institute 1640 medium

rRNA.....Ribosomal RNA

RT.....Reverse transcriptase

SDS.....Sodium dodecyl sulfate

SDS-PAGE.....Sodium dodecyl sulfate polyacrylamide gel electrophoresis

shRNA.....Short hairpin RNA

SLC.....Solute carrier proteins

Smad4.....Smad family member 4

SOD1.....Superoxide dismutase 1

TCA .....Tricarboxylic acid

TCGA .....The cancer genome atlas

TGF-β .....Transforming growth factor β1

TNF .....Tumor necrosis factor

TNFR .....TNF receptor

WB .....Western blot

I. INTRODUCTION: GLUTATHIONE S-TRANSFERASES IN CANCER[1]

Abstract

In humans, the glutathione S-transferase (GST) protein family is composed of seven members that present remarkable structural similarity and some degree of overlapping functionalities. GST proteins are crucial antioxidant enzymes that regulate stress-induced signaling pathways. Interestingly, overactive GST proteins are a frequent feature of many human cancers. Recent evidence has revealed that the biology of most GST proteins is complex and multifaceted and that these proteins actively participate in tumorigenic processes such as cell survival, cell proliferation, and drug resistance. Structural and pharmacological studies have identified various GST inhibitors, and these molecules have progressed to clinical trials for the treatment of cancer and other diseases. In this review, we discuss recent findings in GST protein biology and their roles in cancer development, their contribution in chemoresistance, and the development of GST inhibitors for cancer treatment.

Introduction

Glutathione S-transferases (GSTs) are a multigene family (EC 2.5.1.18) of eight dimeric enzymes that are classified based on their amino acid sequences and substrate specificity as alpha (A), kappa (K), mu (M), omega (O), pi (P), sigma (S), theta (T), and zeta (Z) [1]. Depending on their subcellular location, GSTs are grouped as cytoplasmic (A, P, M, S, T, Z), mitochondrial (K), or membrane-bound (Membrane Associated Proteins in Eicosanoid and Glutathione metabolism) [2].

[1] The content of this chapter is based in part on the following references:
Singh, R.R.; Reindl, K.M. Glutathione S-Transferases in Cancer. Antioxidants (**2021**), 10, 701.
R.R.S. and K.M.R. conceived the review. R.R.S. searched for previously published literature and selected studies for citations. R.R.S. wrote the manuscript with the supervision of K.M.R. All authors have read and agreed to the published version of the manuscript.

GSTs are phase-II detoxification enzymes found in most life forms and vital for maintaining cellular homeostasis [3]. GSTs play a cytoprotective role primarily by catalyzing the conjugation reaction of reduced glutathione (GSH) and reactive electrophiles generated by cytochrome P450 metabolism to form GSH conjugates [4]. The resulting GSH conjugates are either excreted via bile or transported to the kidney where: (1) the γ-glutamyl moiety is cleaved by γ-glutamyl transpeptidase; (2) the glycine is cleaved by dipeptidase; and (3) the cysteine is N-acetylated [5].

In addition to their detoxification roles, GSTs are known for their functions in cell signaling, post-translational modification, and resistance to chemotherapeutic agents [6]. For example, the pi and mu classes of GSTs regulate the mitogen-activated protein (MAP) kinase pathway that governs cell survival and cell death signals via direct interactions with c-Jun N-terminal kinase 1 (JNK1) and apoptosis signal-regulating kinase (ASK1) [7]. Additionally, GSTs form complexes with an array of intracellular proteins for their post-translational modification [8]. For instance, protein disulfide isomerase (PDI), peroxiredoxin-VI (Prdx VI), and p53 are common substrates of GST-mediated glutathionylation [9]. Similar to the detoxification process described above, antineoplastic drugs bound to GSH are expelled out of the cells by the membrane-bound GS-X pump, making cancer cells resistant to chemotherapy [10].

Since their discovery in 1961 in rat liver [11], GSTs have gained attention among cancer researchers. The expression of GSTs in all cell types and their abundance in aggressive cancer cells suggest that they play a key role in tumor progression and cancer pathogenicity [12]. Recent developments in the field of redox oncology have shed light on novel functions of GST proteins in cancer cells [13, 14]. This review summarizes newly identified functions of GST proteins and their roles in the cellular signaling, metabolism, and survival of cancer cells.

Structure of GSTs

Because GSTs are pivotal in drug metabolism, they were among the first cytosolic proteins to be structurally characterized. Porcine GST Pi-1 (GSTP1) was the first member of the family whose structure was determined [15]. Crystallographic studies have revealed that the catalytic GSTs display analogous tertiary structures and exist as homodimers in mammals (Figure 1.1A) [16]; however, heterodimers of a few cytosolic GSTs have been identified in plants [17]. Currently, no enzymatically active monomers of GST proteins are known [15]. Subsequent structural analyses revealed that all principal GST family members have a basic protein fold consisting of two domains: the N-terminal domain and the C-terminal domain. The GST N-terminal domain fold is similar to other cellular homeostasis and detoxification proteins such as glutathione peroxidases and glutaredoxins. The N-terminal domain constitutes approximately one-third of the protein structure and is made up of a β-α-β-α-β-β-α motif. The β-β-α motif in the N-terminal domain, also known as the G-site, is most conserved among the isoforms and provides the binding site for reduced glutathione (GSH) by recognizing the γ-glutamyl fragment of GSH (Figure 1.1B).

Interestingly, a proline residue, found at the N-terminal end of strand β3, is conserved among all cytosolic and mitochondrial GSTs. This proline forms hydrogen bond interactions with the backbone amine group of the GSH-cysteinyl moiety (Figure 1.1C) [16, 18, 19]. Global characterization of sequence and structure similarity of GST proteins show two major subgroups: (1) tyrosine-type GSTs (Y-GSTs), which use tyrosine to activate GSH; and (2) S/C-GSTs, which use serine (or cysteine in the case of GST Omega (GSTO)) to interact with GSH [20]. However, the C-terminal domain of GSTs constitutes the other two-thirds of the protein structure and is made up of a unique all-α-helical domain [19]. The hydrophobic substrates bind to a cleft between the N- and C-terminal domains known as the H-site. Unlike the G-site, the H-site is highly variable in

shape and chemical constitution between classes [21]. This variability in H-site structure determines the substrate selectivity of various GST isozymes [22].

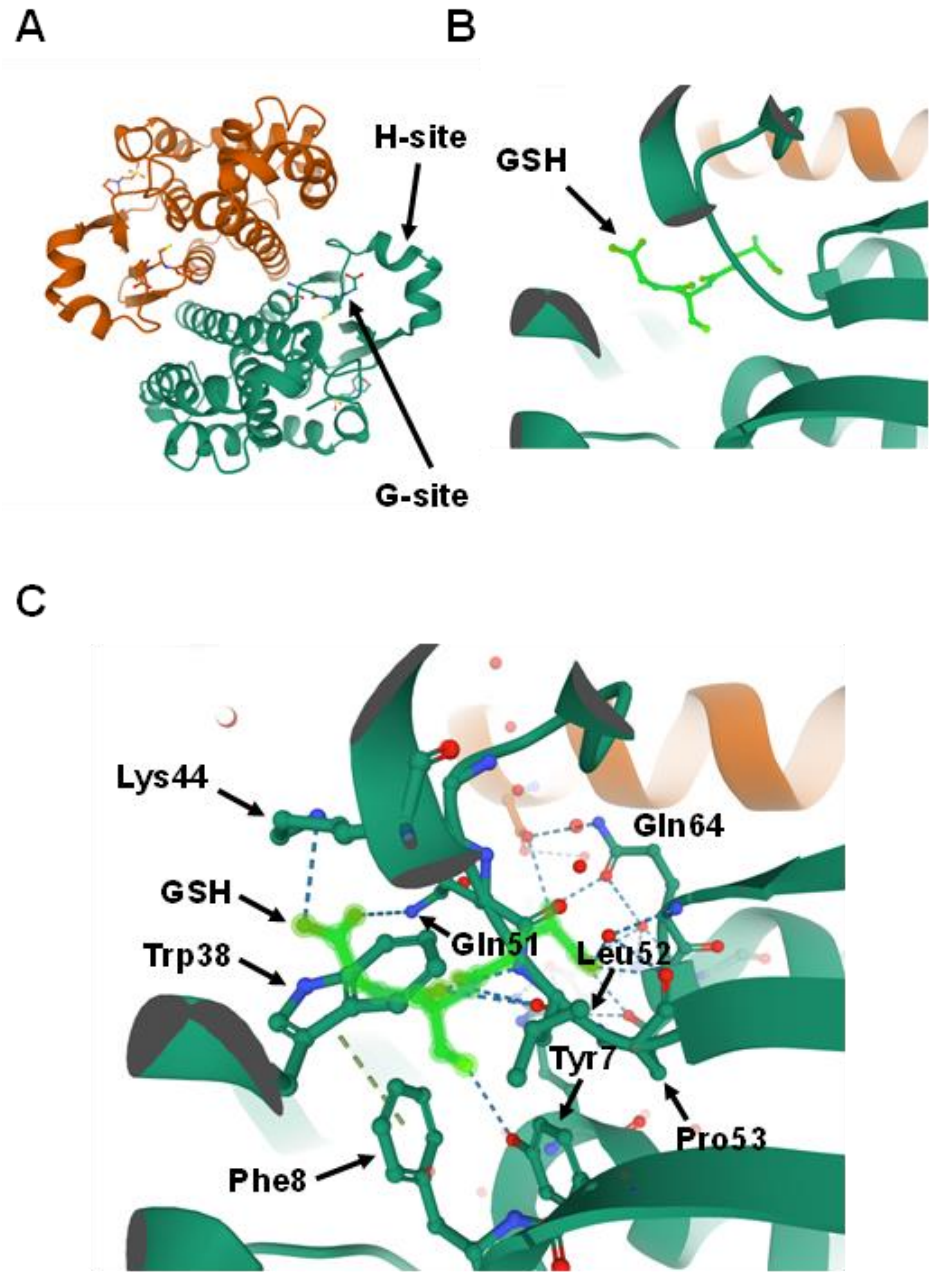

Figure 1.1. Structure of Glutathione S-transferase Pi-1 (GSTP1) (Protein Data Bank ID: 6GSS). (A) Homodimer assembly of GSTP1 showing G- and H-sites. (B) Magnified view of the G-site that is occupied by the ligand glutathione (GSH) (shown in light green). (C) Glutathione forms hydrogen-binding interactions with the surrounding amino acids found in the G-site pocket of GSTP1.

Metabolism of xenobiotic compounds

Exposure to several natural and manufactured substances in the environment accounts for more than two-thirds of all cancer cases in the United States [23]. These environmental factors range from lifestyle choices such as smoking, excessive alcohol consumption, and poor diet to exposure to certain medical drugs, radiation, and environmental chemicals present in the air, water, or food. Environmental carcinogens are known to generate reactive oxygen species (ROS) in the cells [24]. Strong evidence exists suggesting that oxidative stress promotes damage to the cellular components, including proteins, lipids, membranes, and DNA, that play a crucial role in cancer development [25].

Aerobic organisms have a cellular defense system composed of several enzymes that scavenge ROS and protect cells from macromolecular damage [26]. Phase-I detoxification enzymes process the primary steps of xenobiotic detoxification. For these reactions, an array of cytochrome P450 enzymes are utilized, and detoxification is achieved by a series of oxidation-reduction reactions. Due to their electrophilic nature, phase-I metabolites have a high affinity to form adducts with nucleic acids and proteins [27]. However, these cytotoxic intermediate metabolites are readily conjugated to hydrophilic moieties such as reduced glutathione (GSH), glucuronate, and sulfate by phase II enzymes, such as GSTs, uridine 5′-diphospho-glucuronosyltransferases (UGTs), sulfotransferases, and nicotinamide adenine dinucleotide phosphate-oxidase:quinone oxidoreductase (NQO) [28].

Carcinogens, industrial intermediates, pesticides, and environmental pollutants are the most common substrates for GSTs [29]. Environmental carcinogens such as polycyclic aromatic hydrocarbons (PAHs) that are converted to epoxides via P450 metabolism are pervasive in the modern industrial world and are a threat to general health [30]. PAHs, commonly found in engine

exhaust fumes and cigarette smoke, are conventional substrates of GSTs [31]. GSTs primarily carry out the catalytic detoxification of the above-mentioned exogenous compounds via synthesis of mercapturic acids [32]. The γ-glutamyl and the glycine fragment of the resulting glutathione conjugate are trimmed, followed by N-acetylation of the cysteine S-conjugates [33]. It is important to note that GSTs are a part of a unified cellular defense system. They rely on glutathione synthase activity to supply GSH [34] and transporter proteins to export the GSH conjugates [35, 36].

The tripeptide, γ-l-glutamyl-l-cysteinyl-glycine, known as glutathione (GSH), is an essential antioxidant in the cell [37]. The synthesis of GSH is a two-step enzymatic reaction mediated by: (1) γ-glutamylcysteine synthetase combining cysteine with glutamate; and (2) glutathione synthetase adding glycine to the dipeptide to produce GSH. The above reactions are coupled with adenosine triphosphate (ATP) hydrolysis [38]. GSH is primarily found in the cytosol with concentrations ranging from 1–3 mM [39]; however, it has also been reported in mitochondria [40] and the nucleus [41], where it functions in regulating apoptosis and cell division, respectively. Its primary role is to act as a free-radical scavenger and trap ROS that would otherwise cause irreparable damage to proteins, lipids, and nucleic acids [42]. The significance of the detoxification properties of GSH has been illustrated by depleting its intracellular levels and demonstrating the increased *in vitro* toxicities of compounds that depend on GSH metabolism, such as chromium [43], cadmium [44], arsenic [45], bleomycin [46], and mitomycin [47]. The detoxification reaction involving GSH is primarily catalyzed by glutathione peroxidases (GPx) through the following reaction:

$$2GSH + H_2O_2 \rightarrow GSSG + 2H_2O \quad (1)$$

where hydrogen peroxide (H_2O_2) is a low molecular weight, reactive oxygen species and GSSG is glutathione disulfide, the oxidized form of GSH. H_2O_2 is primarily produced by the superoxide anion via a dismutation reaction [48] and plays critical roles in hypoxia [49], inflammation [50],

apoptosis [51], and autophagy [52]. It is important to note that oxidized glutathione (GSSG) is reduced back to GSH by glutathione reductase and at the expense of NADPH through a GSH-restoring system [53] via following reaction:

$$GSSG + NADPH + H^+ \rightarrow 2GSH + NADP^+ \quad (2)$$

Cellular signaling

Besides their glutathione-conjugating activity, GSTs are known to bind structurally distinct non-substrate molecules. Several GST isozymes interact with the members of mitogen-activated protein kinase (MAPK) pathways involved in cell-survival and cell-death signaling mechanisms. This non-enzymatic function of GSTs is achieved by binding to the kinase protein in complex, thus preventing the activation of downstream targets. A specific subtype of the GST protein family, GSTP1, binds to the JNK complex [7, 54, 55]. Through fluorescence resonance energy-transfer measurements, it was revealed that the C- terminus of the JNK protein is essential for its interaction with GSTP1 [56]. Studies have revealed that dimerization of GSTP1 is critical for enzymatic activity and its interaction with JNK. It was shown that under non-stressed, normal conditions, monomeric GSTP1 binds to JNK and prevents its phosphorylation. However, under oxidative stress conditions, the GSTP1-JNK complex dissociates, allowing phosphorylation of JNK and dimerization of GSTP1 [7, 56]. In other words, GSTP1 acts as a sensor of oxidative stress and modulates the JNK signaling pathways for cell survival or apoptosis depending on the level of ROS encountered [56] (Figure 1.2A). The interaction between GSTP1 and JNK has also been demonstrated *in vivo* [7]. A higher and constitutive JNK activity was reported in the liver and lungs of transgenic mice in which GSTP1/2 were deleted (GSTP1/2(-/-)) compared to the wild-type control. In the same model system, increased DNA-binding activity of the transcription factor AP-1 was reported. In addition to establishing the role of GSTP1 as a JNK inhibitor, this study also

demonstrated the role of GSTP1 in regulating the expression of specific down-stream targets of the JNK signaling pathway [7].

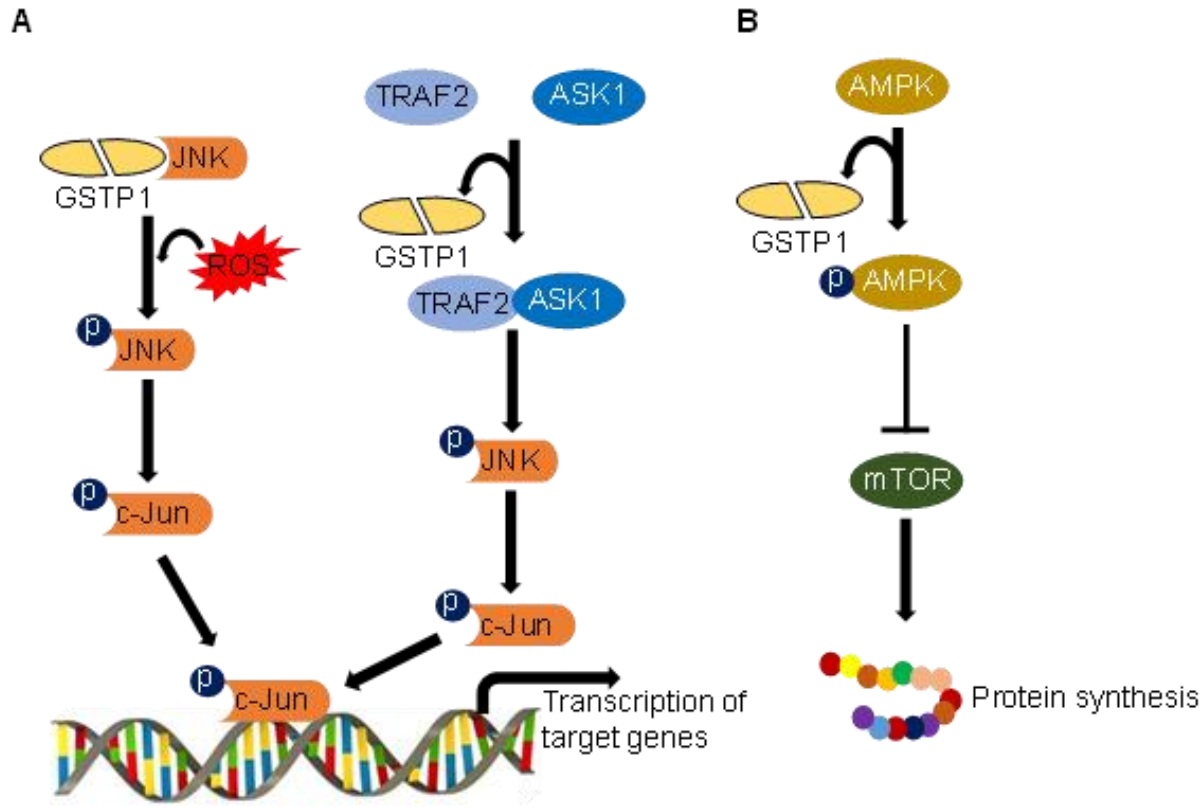

Figure 1.2. Multifarious roles of GSTP1 in cell signaling. (A) Under oxidative stress, the interaction between GSTP1 and c-Jun N-terminal kinase 1 (JNK1) is deterred and leads to phosphorylation of c-Jun and transcription of target genes. Similarly, in the absence of GSTP1, tumor necrosis factor (TNF)-receptor-associated factor 2 (TRAF2) and apoptosis signal-regulating kinase (ASK1) interact and cause phosphorylation of c-Jun. (B) Phosphorylation of 5' adenosine monophosphate-activated protein kinase (AMPK) in GSTP1 knockdown cells inhibits the mechanistic target of rapamycin (mTOR) pathway and impairs protein synthesis.

Additionally, GSTP1 interacts with and inhibits the activity of tumor necrosis factor (TNF)-receptor-associated factor 2 (TRAF2), a member of the TNF receptor-associated factor protein family [57]. Human cervical cancer HeLa cells overexpressing GSTP1 suppressed TRAF2-induced activation of both JNK and p38. Further, GSTP1 attenuated autophosphorylation of apoptosis signal-regulating kinase 1 (ASK1) and inhibited TRAF2-ASK1-induced apoptosis [58]. On the contrary, silencing of GSTP1 triggered TRAF2-ASK1 association and hyper-activation of

ASK1 and JNK [58]. Similar findings have been reported about the interaction of GSTM3 and TRAF6 in cervical cancer cells [13]. Further, GSTP1 knockdown in pancreatic [59] and GSTM knockdown in cervical cancer cells [13] showed reduced phosphorylation of extracellular signal-regulated kinase (ERK1/2), which plays a pivotal role in promoting cell growth and proliferation in many mammalian cell types. We have previously reported that GSTP1 knockdown pancreatic ductal adenocarcinoma (PDAC) cells have impaired growth compared to the control [59]. We hypothesize this phenotype is attributed to the reduced ERK activity upon GSTP1 knockdown. In addition, genetic and pharmacological inactivation of GSTP1 in triple-negative breast cancer showed increased phosphorylation of 5' adenosine monophosphate-activated protein kinase (AMPK) and acetyl-coenzyme-A carboxylase [12]. Phosphorylation and activation of AMPK have previously been demonstrated to reduce growth in breast cancer cells, primarily by inhibiting the mechanistic target of rapamycin (mTOR)-signaling pathway [60] (Figure 1.2B). Interestingly, GSTP1-knockdown mediated growth inhibition in these cells can be partly rescued by treatment with the AMP kinase inhibitor, dorsomorphin [12].

Other GST isozymes, such as GSTA1, are also known to negatively regulate the mTOR-signaling pathway. Liu *et al*. showed that overexpression of GSTA1 in hepatocellular carcinoma cells can increase AMPK activity and inhibit the mTOR pathway [61]. They found that hepatocellular carcinoma patients with higher GSTA1 had better prognoses, and GSTA1 overexpression can impair liver cancer cell proliferation and metastasis. Further, in human neuroblastoma cells, Saisawang *et al*. demonstrated that GSTO1 modulates protein kinase B and MAPK1/2 activation [62]. Using the GSTO1-specific inhibitor, ML175, they showed that GSTO1 enzyme activity inhibits the activation of these kinases and indirectly regulates the survival, growth, and metabolism of neuroblastoma cells.

Cellular metabolism

Cancer is often referred to as a metabolic disease, and aberrant metabolism is known to drive the pathogenicity of various neoplasms [63, 64]. Escalated aerobic glycolysis and lipid biosynthesis are key in generating cancer cell biomass and regulating signaling mechanisms [65]. Using a reactivity-based chemoproteomic platform, GSTP1 was identified as a chief player that controls cancer cell metabolism in triple-negative breast cancer cells [12]. Genetic or pharmacological inactivation of GSTP1 resulted in reduced lactic acid, ATP, nucleotides, and increased acylcarnitines and lysophospholipids. Upon mapping to metabolic pathways, it was found that inactivation of GSTP1 leads to impaired glycolytic metabolism resulting in reduced ATP as well as reductions in the levels of macromolecular building blocks. It was concluded that GSTP1 interacts with glyceraldehyde-3-phosphate dehydrogenase (GAPDH) and increases its enzymatic activity in breast cancer cells [12]. Recently, Hildebrandt *et al*. [66] and Moellering *et al*. [67] showed that GAPDH-mediated conversion of 3-phosphoglycerate to 1,3-bisphosphoglycerate is a rate-limiting glycolytic reaction in cancer cells that have heightened aerobic glycolysis. These studies validate that GSTP1-arbitrated GAPDH activation is a critical metabolic hub and, therefore, GSTP1 inhibitors are promising therapeutics for breast cancer patients.

Additionally, tetra-hydroxynonenal (4-HNE), a common byproduct of lipid peroxidation, was found to be reduced in GSTP1-positive prostate cancer patients compared to GSTP1-negative patients, indicating that GSTP1 protects lipids from oxidative damage [68]. The reactive 4-HNE adducts are mutagenic and are often accumulated in various pathological conditions [69, 70]. Further research is needed to identify and comprehensively characterize additional metabolic changes that are influenced by GST activity.

Chemoresistance

Ambiguous early symptoms and the lack of early diagnostic tools for many cancers results in a late diagnosis for many patients [71]. While surgery is the preferred line of treatment, only a small fraction of patients are eligible for resection surgery, especially for pancreatic cancer [72], non-small cell lung carcinoma [73], and glioblastoma [74]. Chemotherapy is used for patients with advanced and metastatic disease [75]. However, chemotherapy has largely been ineffective in many cancers, such as pancreatic ductal adeno-carcinoma [76, 77]. The primary reason for the dismal performance of various chemotherapies is the development of intrinsic or extrinsic resistance to antineoplastic reagents [78]. Several cellular signaling pathways are known to play critical roles in the development of chemoresistance. Pathways commonly associated with cell growth [79, 80], proliferation [81, 82], and detoxification [83] have a direct impact on drug efficacy in cancer cells.

Recent evidence supports that enzymes involved in maintaining cellular redox homeostasis, such as GSTs, can detoxify chemotherapeutic drugs [84]. For example, GSTP1′s role in chemoresistance is well established in human ovarian cancer. In Chinese ovarian cancer patients, positive correlations have been reported between the overexpression of GSTP1 and chemoresistance [85]. Interestingly, the response rate to chemotherapy for GSTP1-positive ovarian tumors was significantly lower than the GSTP1-negative tumors in a different cohort [86]. Similarly, an independent epidemiological study identified a drug-resistant phenotype in GSTP1-expressing ovarian tumors in Japanese women [87]. In this cohort, out of the eleven GSTP1-positive samples, ten were drug-resistant, and out of the seventeen GSTP1-negative samples, six showed the drug-resistant phenotype. Further, in the same group, the GSTP1-positive ovarian cancer patients showed shorter survival post-diagnosis than the GSTP1-negative cohort. They

concluded that GSTP1 expression in tumor cells is related to drug resistance of patients with epithelial ovarian cancer. Besides, GSTP1 knockdown ovarian cancer cells showed heightened sensitivity (IC50) to cisplatin and carboplatin by 2.3- and 4.8-fold, respectively. They reported that cell cycle progression was unaffected; however, cell invasion and migration were significantly reduced in GSTP1 knockdown cancer cells.

In addition to ovarian cancer, GSTP1 is involved in the chemoresistance of other cancer types. Proteomics analysis revealed that GSTP1 is overexpressed in cisplatin- and irinotecan-resistant glioma [88, 89], fluorouracil (5-FU)- and cisplatin-resistant gastric cancer cells [90], doxorubicin-resistant prostate cancer cells [91], and adriamycin-resistant breast cancer cells [92]. Further, Yang *et al*. demonstrated that small RNA-mediated knockdown of GSTP1 significantly increased the apoptosis and DNA damage in adriamycin-treated breast cancer cells [93]. Additionally, breast cancer cells were rescued from apoptosis by overexpressing GSTP1. GSTP1 was found to be upregulated in CLDN6-overexpressing and multidrug-resistant estrogen-receptor positive (ER+) breast cancer cells. Knockdown of CLDN6 reduced the expression and the enzyme activity of GSTP1 and increased the cytotoxicity of adriamycin, 5-FU, and cisplatin in ER+ breast cancer cells. Similar observations were made in triple-negative breast cancer cells [93]. Complementing the observations mentioned above, Ogino *et al*. found that the subcutaneous tumors generated from GSTP1 knockdown esophageal squamous cancer cells treated with cisplatin showed an impressive reduction in size compared to the GSTP1 knockdown and cisplatin treatment group alone [94]. Li *et al*. made similar observations where they showed GSTP1 inhibition sensitizes lung cancer stem cells to cisplatin treatment [95]. Small RNA-mediated knockdown of GSTP1 in lung cancer cells showed increased activation of JNK and increased camptothecin-induced apoptosis [96]. Camptothecin is a naturally occurring alkaloid that is known

for its antineoplastic activity because of its ability to target DNA topoisomerase I specifically. These emerging pieces of evidence suggest that the efficacy of chemotherapy and the overall outcome in cancer patients could be significantly improved if used in combination with GSTP1 inhibitors.

Tumor relapse has been linked to a small number of therapy-resistant cells known as cancer stem cells that survive treatment or develop during post-therapeutic remission [97]. Growing evidence suggests that cancer stem cells are responsible for tumor initiation [98], progression [99], metastasis [100], and drug resistance [101–103]. Higher protein levels of GST isoforms have been reported in cancer stem cells, which is a primary reason for their drug-resistant phenotype. Tanaka *et al*. observed that knockdown of GSTP1 in colorectal cancer stem cells significantly reduced tumor growth [104]. Further, increased chemo-resistance of stem-like non-small cell lung cancer cells is also linked to increased protein expression of GSTP1 [105]. Abundant levels of GST isozymes in cancer and cancer stem cells are correlated to the multidrug-resistant phenotype [106, 107]; however, most antineoplastic agents are poor substrates for GST isozymes [108]. Thus, the GST-mediated drug resistance could be explained by alternative roles of GSTs other than detoxification of chemotherapeutic drugs [6]. These studies have established the role of GSTP1 in the chemoresistance of anatomically diverse cancer cells. This has led to an increased focus on targeting the GST isozymes to increase the efficacy of chemotherapeutic drugs and improve patient survival [109–111]. The role of GSTP1 in resistance to chemotherapy and the respective cancer model is summarized in Table 1.1.

Table 1.1. The role of glutathione S-transferases (GST) proteins in the chemoresistance of different cancer model systems is summarized below.

Tumor model	Anti-neoplastic agent	Outcome	Reference
Ovarian cancer	Cisplatin, doxorubicin	Response rate lower in GSTP1-positive patients	[85–87]
Glioma	Cisplatin, irinotecan	GSTP1 is overexpressed in resistant tumors	[88, 89]
Gastric cancer	Fluorouracil (5-FU), cisplatin	GSTP1 is overexpressed in resistant tumors	[90]
Prostate cancer	Doxorubicin	GSTP1 is overexpressed in resistant tumors	[91]
Breast cancer	Adriamycin	GSTP1 is overexpressed in resistant tumors	[92]
Breast cancer	Adriamycin	Increased apoptosis and DNA damage upon GSTP1 knockdown	[93]
Esophageal squamous cancer cells	Cisplatin	Synergistic effect of GSTP1 knockdown and cisplatin treatment	[94]
Lung cancer stem cells	Cisplatin	Synergistic effect of GSTP1 inhibition and cisplatin treatment	[95]
Lung cancer	Camptothecin	Increased apoptosis upon GSTP1 knockdown and camptothecin treatment	[96]
Lung cancer stem cells	Cisplatin	miRNA-mediated inhibition of GSTP1 reverses cisplatin resistance	[105]

Antineoplastic agents such as cisplatin [112, 113], cytarabine [114], and gemcitabine [115, 116] induce cell death via JNK and p38 MAPK pathways. Given that GSTP1 is a direct inhibitor of JNK activity, it is speculated that GSTP1 overexpression is associated with many drug-resistant tumors [90–92]. Elevated levels of GSTP1 are shown in pancreatic [59] and triple-negative breast cancer cells [12], where it interferes with the cellular signaling processes that influence cell survival, proliferation, and apoptosis. These non-enzymatic functions of GSTP1 provide an explanation for drug-resistance in GSTP1-overexpressing tumors to chemotherapeutic agents that are poor substrates for this enzyme [108].

GSTs glutathionylate various proteins

S-glutathionylation occurs through the reversible addition of a glutathione donor to the thiolate moiety of cysteines in target proteins [117]. Like other post-translational modifications, glutathionylation can change the charge, mass, structure, and function of fully translated proteins [118]. Glutathionylation occurs primarily through a thiol-disulfide exchange reaction, as shown below, where ProSH represents the protein with a free cysteine residue [119].

$$ProSH + GSSG \rightarrow ProSSG + GSH \quad (3)$$

Glutathionylation is also known to occur via direct oxidation of a target protein as represented below:

$$GSH + ProSH \rightarrow ProSSG + 2e^- + 2H^+ \quad (4)$$

The GST-protein family members are known to post-translationally modify several target proteins by catalyzing the forward S-glutathionylation reaction [9]. The earliest evidence of their role in post-translational modification comes from GSTP1 knockout mice. Zhi-Wei *et al*. showed that GSTP1 knockout mice had reduced global protein glutathionylation levels compared to wild-type animals [120]. Additionally, they reported that cells expressing mutated GSTP1 polymorphic forms and lacking the catalytically active tyrosine residue had reduced glutathionylation activity.

Peroxiredoxins (Prxs), a family of thiol-specific peroxidase enzymes, are known targets for GSTP1-mediated reversible glutathionylation [121]. Ubiquitously expressed Prxs are found in all kingdoms and are located in all cellular components [122]. These enzymes perform their antioxidant function by reducing H_2O_2 and organic peroxides utilizing the intracellular thiols [123]. However, the catalytic cysteine in Prx enzymes is susceptible to oxidation and subsequent loss of peroxidase activity. GSTP1 facilitates the glutathionylation of the previously oxidized cysteine residue, thereby restoring the peroxidase activity [124]. The two major subclasses of Prxs, 1-cys Prx (also known as Prdx VI) and 2-cys Prx, are substrates for glutathionylation [121, 125].

Prdx VI, a multi-tasking antioxidant enzyme, is the only mammalian peroxiredoxin that can reduce phospholipid hydroperoxides through its glutathione peroxidase activity [126]. The catalytically active cys-47 residue is buried in the hydrophobic core of the Prdx VI protein. Following peroxide reduction, the oxidized cys-47 is accessed by GSH-loaded GSTP1 to reactivate Prdx VI [127]. Persuasive evidence suggests that different polymorphic forms of GSTP1 can differentially mediate Prdx VI activation and thereby affect the response to ROS/reactive nitrogen

species (RNS). For instance, GSTP1-1A, the most abundant polymorphic form of GSTP1, has a higher affinity for Prdx VI compared to GSTP1-1B or 1D [128]. Moreover, breast cancer cells transiently transfected with GSTP1-1A showed significantly higher peroxidase activity than those transfected with GSTP1-1B [128]. The differences in the activity can be attributed to the variation in the relative distance between oxidized cys-47 and the activated GSH bound to the GSTP1 molecule in the different polymorphic forms.

GST-mediated glutathionylation affects the function of additional proteins such as nitric oxide synthase (NOS). NOS contains highly conserved cys-689 and cys-908 residues that are susceptible to S-glutathionylation [129]. NOS activity is reduced upon glutathionylation, resulting in lower nitric oxide (NO) levels and impaired endothelium-dependent vasodilation [129]. Further, using *in vivo* hypertensive rat models, it was validated that endothelial-NOS glutathionylation increases with oxidative stress and has direct implications in vascular dysfunction [129].

Post-translational modification and folding of secretory and transmembrane proteins occur in the endoplasmic reticulum (ER). However, if the influx of nascent, unfolded polypeptides outpaces the folding capacity of ER and the homeostasis of ER is impaired resulting in unfolded protein response (UPR) [130]. Studies have shown that UPR is an underlying cellular mechanism of various human diseases such as ischemia, Friedreich's ataxia, Alzheimer's disease, type 2 diabetes, and cystic fibrosis [131–133]. Evidence increasingly shows interrelations between S-glutathionylation and UPR [134]. Protein disulfide isomerase (PDI) is a principal component of the cellular protein folding machinery [135]. Utilizing mass spectrometry and circular dichroism, Townsend *et al*. showed that S-glutathionylation decreases the isomerase activity of PDI and is potentially an upstream signaling event in UPR [134, 136].

Exposed thiol groups determine the supramolecular structure of cytoskeletal proteins [137]. It has been shown that glutathionylation of these sites can affect protein function by protecting them from irreversible oxidation [138] or inhibiting polymerization [139]. Actin has been identified as a common substrate for glutathionylation in endothelial [140] and gastric mucosal cells [138]. In response to oxidative stress, Dalle-Donne *et al*. reported that S-glutathionylation of cys-374 impairs the rate of actin polymerization [139]. The authors added that a reduced rate of actin polymerization was partially due to the slow addition of actin monomers to the growing actin filament chain. S-glutathionylation of actin deregulates the soluble:filamentous protein ratios and affects various cytoskeletal functions. In the ischemia-reperfusion injury rat model, Chen *et al*. described that glutathionylated ac-tin affects cell adhesion and has a weaker affinity for tropomyosin [141].

Additional cytoskeletal proteins are targets of glutathionylation. Rapid and reversible glutathionylation of beta-tubulin was observed in oxidation-stressed human endothelial cells [140]. In addition, using two-dimensional electrophoresis and mass spectrometry fingerprinting, Fratelli *et al*. reported that cytoskeletal proteins such as vimentin, cofilin, myosin, and profilin are glutathionylated in human T-cell blasts exposed to oxidative stress [8]. Further, using atomic force microscopy, electron microscopy, and hydrogen-deuterium exchange mass spectrometry, Kaus-Drobek *et al*. demonstrated that glutathionylation of cys-328 of human vimentin inhibits filament elongation [142]. In brief, S-glutathionylation of cytoskeletal proteins disrupts their polymerization and contributes to anti-metastatic activity in cancer cells.

p53, a principal transcription factor, plays a pivotal role in DNA repair, cell cycle control, differentiation, and tumor suppression through transcriptional activation of an array of target genes in response to a variety of endogenous and exogenous stimuli [143]. Functional inactivation of

p53 gives rise to various unstable genomes that cause more than 60% of all human cancers [144]. Human p53 is constituted of ten cysteine residues that reside in its DNA binding domain [145]. Velu *et al*. reported that p53 is a substrate for glutathionylation, and this post-translational modification reorganized p53′s structure and reduced its affinity for DNA binding [146]. Interestingly, Yusuf *et al*. observed that oxidative stress and DNA damage treatments increased the levels of glutathionylated p53 [147]. Moreover, using immunohistochemistry, they reported abundant levels of glutathionylated p53 in human prostate adenocarcinoma and melanoma tissues. Overall, glutathionylation of p53 might be a physiologically relevant phenomenon that occurs as a cellular defense mechanism in response to stress stimuli. This modification is known to re-vamp gene expression for cancer cell survival [148]. Further, increased GST activity in tumor cells could promote oncogenesis through glutathionylation and inhibition of key proteins such as p53.

Protein kinase C (PKC) isozymes are major cellular signaling molecules that play important roles in proliferation, invasion, tumorigenesis, and metastasis [149]. The earliest evidence suggesting the role of PKC in tumor progression was its identification as a cellular receptor for phorbol esters [150]. Since then, studies have shown that the overexpression of PKC drives tumor development via synergistic activation of several cell-survival and mitotic pathways, including nuclear factor-κB (NF-κB), signal transducer and activator of transcription 3 (Stat3), phosphatidylinositol 3-kinase/protein kinase B (PI3K/Akt), and extracellular signal-regulated kinase (ERK) [151, 152]. Ward *et al*. showed that PKC isolated from the rat brain is inactivated by glutathionylation in the presence of diamide and glutathione [153]. Importantly, they concluded that the antagonistic role of GSH in tumor progression is mediated via oxidative inactivation of PKC isozymes.

Glutathionylation is additionally known to inhibit the activity of various enzymes involved in energy metabolism. Complex I [154], cytochrome oxidase [8], ATPase [14], carbonic anhydrase [155], and pyruvate dehydrogenase [156] are known targets of glutathionylation. Glutathionylation inhibits the activity of these metabolic enzymes. These, and additional proteins that are post-translationally modified by glutathionylation, are summarized in Table 1.2.

Table 1.2. Proteins that are susceptible to glutathionylation and the resulting effects on their activity are summarized below. Prx, peroxiredoxins; NOS, nitric oxide synthase; PDI, protein disulfide isomerase; PKC, protein kinase C; ERK, extracellular signal-regulated kinase; GAPDH, glyceraldehyde-3-phosphate dehydrogenase.

Protein	Impact of Glutathionylation	Reference
1-cys Prx (Prdx VI)	restores peroxidase activity	[121, 157]
2-cys Prx	restores peroxidase activity	[121, 127, 128]
NOS	inhibits activity	[129]
PDI	inhibits isomerase activity	[134, 136]
Actin	inhibits polymerization	[138–140]
Vimentin	inhibits elongation	[8]
Cofilin	reduces depolymerization activity	[8, 158]
Myosin	increases Ca^{2+} sensitivity	[8, 159]
β-tubulin	inhibits polymerization	[140, 160]
p53	reduces DNA binding	[146, 147]
PKC	inhibits activity	[153]
Complex-I	inhibits activity	[154]
Cytochrome oxidase	inhibits activity	[8]
adenosine triphosphate (ATP)-ase	inhibits activity	[14]
Carbonic anhydrase	inhibits activity	[155]
Pyruvate dehydrogenase	inhibits activity	[156]
ERK	inhibits activity	[153]
protein-tyrosine phosphatase (PTP1B)	inhibits activity	[14]
Phosphatase and tensin homolog (PTEN)	inhibits activity	[161]
Aldolase	inhibits activity	[140]
Adenylate kinase 2	inhibits activity	[8]
Vimentin	inhibits activity	[8]
c-Jun	inhibits activity	[155]
NF-κB subunits 65 and 50	inhibits activity	[162]
HSP60	inhibits activity	[8]
HSP70	inhibits activity	[8]
S100 A1, S100 A4, S100 B	increases activity	[163]
Nicotinamide adenine dinucleotide hydrogen (NADH) ubiquinone reductase	inhibits activity	[164]
Inhibitor of nuclear factor kappa B kinase (IKK) β-subunit	inhibits activity	[165]
GAPDH	inhibits activity	[166]
Caspase 3	inhibits activity	[155, 167]
SerpinA1 and A3	inhibits activity	[168]
TRAF2	inhibits activity	[134]

Table 1.2. Proteins that are susceptible to glutathionylation and the resulting effects on their activity are summarized below (continued). Prx, peroxiredoxins; NOS, nitric oxide synthase; PDI, protein disulfide isomerase; PKC, protein kinase C; ERK, extracellular signal-regulated kinase; GAPDH, glyceraldehyde-3-phosphate dehydrogenase.

Protein	Impact of Glutathionylation	Reference
STAT3	inhibits activity	[169]
Src homology region 2 domain-containing phosphatase 1 and 2 (SHP-1, SHP-2)	inhibits activity	[170]
Thioredoxin (Trx)	inhibits activity	[171]
p12	inhibits activity	[167]
p17	inhibits activity	[167]
Sarco/endoplasmic reticulum Ca2+-ATPase (SERCA)	increases activity	[172]
CCAAT/enhancer-binding homologous protein (CHOP)	inhibits activity	[134]
Protein kinase B (Akt)	increases activity	[62]
Calreticulin	inhibits activity	[166]
Enolase 1 (Eno1)	inhibits activity	[166]
High mobility group box 1 (HMGB1)	inhibits activity	[173]
Ras	increases activity	[174]

GST inhibitors and their therapeutic implications

Considering the roles of GST proteins in promoting tumor pathogenicity and chemo-resistance, attempts have been made to develop specific GST inhibitors to reduce tumor growth and enhance the cytotoxic properties of chemotherapeutic drugs [109, 110, 175]. GST inhibitors are classified based on their binding activity and structure. Molecules that can bind to the G- or H-site of GST proteins, glutathione peptidomimetics, and several natural compounds have been identified as GST inhibitors. Some of the commonly studied GST inhibitors are discussed below.

Inhibitors that bind to the G-site

Crystallographical studies have found that different GST isoforms have unique G-site structures [176]. This information was instrumental in developing inhibitors for specific GST subtypes. Interestingly, the G-site accepts only glutathione as a substrate, and as a result, glutathione is used as a prototype to develop G-site inhibitors. However, the high intracellular concentration of glutathione presents the biggest challenge for the development of competitive G-

site inhibitors for GST proteins. Because the Tyr7 in the active site of GSTP1 extracts the thiol proton of glutathione, Shishido *et al*. designed GSTP1 inhibitors by placing the electrophilic reactive group around the thiol group of GSH [177]. CD spectral analysis revealed no structural modifications in the presence of the inhibitor, validating no evidence of protein denaturation. Liquid chromatography with tandem mass spectrometry (LC-MS/MS) confirmed the covalent binding of the inhibitor to GSTP1. To circumvent using high concentrations of the inhibitors, cell membrane permeable benzene sulfonyl fluoride (BSF)-type covalent inhibitors (Figure 1.3A) were developed by the same research group [178]. BSF-type covalent GST inhibitors used 1-chloro-2,4-dinitrobenzene (CDNB), a major substrate of GST proteins, as a structural backbone (Figure 1.3B).

The irreversible binding of the BSF-type inhibitors was analyzed by washout assays, and inhibition of GST enzymatic activity upon treatment by these compounds was analyzed in human non-small cell lung adenocarcinoma cells. Interestingly, covalent inhibitors showed prolonged inactivation of GST enzymes and hold promise for use as antineoplastic agents against GSTP1-overexpressing tumors. Additionally, amitriptyline, a commonly prescribed drug for clinical depression, significantly inhibits the activity of GSTP1 and GSTA1 by binding to their G-sites; however, the binding of amitriptyline to the GST proteins is reversible [179].

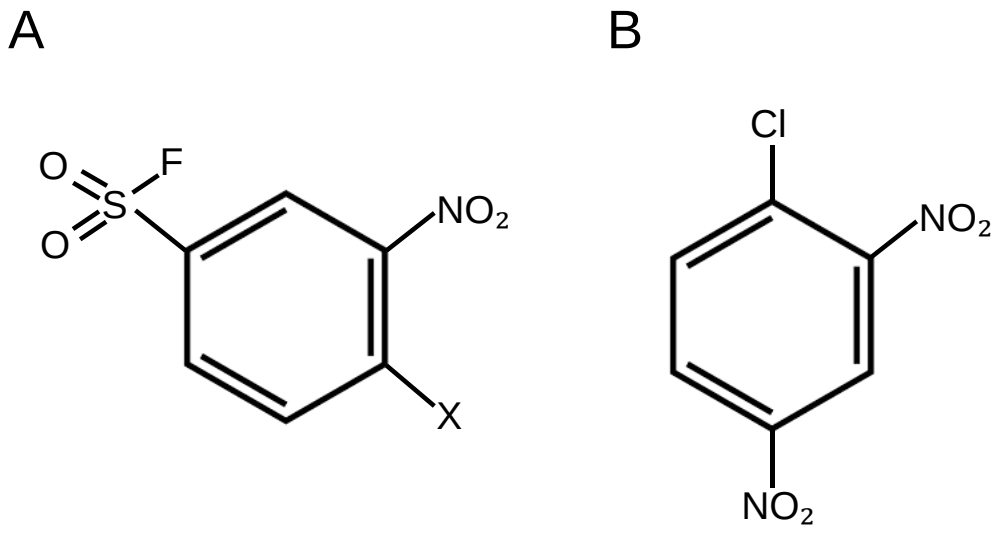

Figure 1.3. Structure of inhibitors that bind to the G-site of GST proteins. (A) Covalent inhibitor benzene sulfonyl fluoride (BSF)-type ligand (X=Cl, F) and (B) 1-chloro-2,4-dinitrobenzene (CDNB).

Using fluorescent-activity-based probes, Bachovchin *et al*. reported the identification of α-chloroacetamide compounds as specific GSTO1 inhibitors [180]. These compounds, specifically ML175 (Figure 1.4A) and KT53 (Figure 1.4B), react irreversibly with the cysteine in the active site of GSTO1. Interestingly, Tsuboi *et al*. demonstrated that the co-treatment of KT53 and cisplatin significantly decreased cell survival compared to KT53 and cisplatin alone [181]. Similar findings have been reported in cisplatin-resistant ovarian cancer cell lines [182, 183].

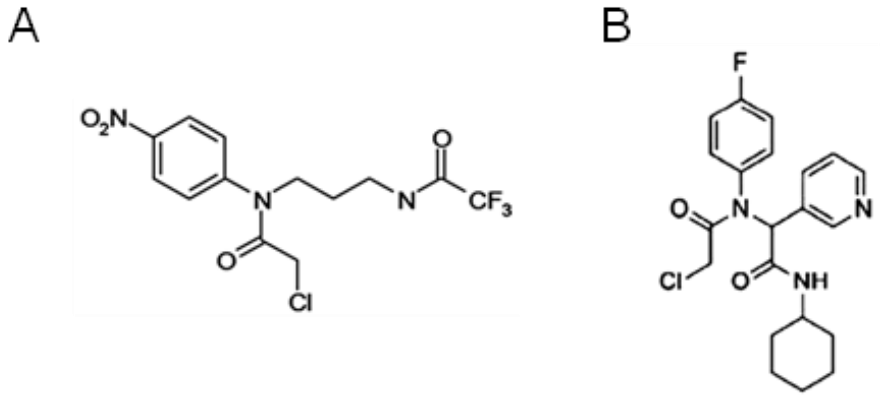

Figure 1.4. Structure of covalent inhibitors that specifically bind to the active site of Glutathione S-transferase Omega-1 (GSTO1) protein. (A) ML175 and (B) KT53.

Inhibitors that bind to the H-site

Several compounds can bind to the H-site of GST proteins and inhibit the enzymatic activity of the same. Since the H-site can be occupied by a variety of substrates, it is particularly difficult to develop specific inhibitors for GST subtypes targeting the H-site. Recently, a potent inhibitor of GSTs, 6-(7-nitro-2,1,3-benzoxadiazol-4-ylthio)hexanol (NBDHEX) (Figure 1.5A), was identified that showed anti-proliferative properties in various cancer cells [184,185]. Structural analysis of GSTP1 and GSTM1 bound to NBDHEX showed that it binds to these subtypes in a similar manner by interacting with aromatic side chains (Tyr108 of GSTP1 and Tyr115 of GSTM2) [186]. The inhibition of GST activity by NBDHEX was demonstrated by the release of GSTP1 from the GSTP1-JNK and GSTP1-TRAF2 complexes upon NBDHEX treatment [57, 187]. Further, increased caspase-dependent apoptosis was reported in NBDHEX treated cancer cells [3], including MDR1-expressing leukemia cells [185]. It was concluded that doxorubicin-resistant cancer cells are susceptible to drug treatment if treated with GSTP1 inhibitors such as NBDHEX. An additional H-site binder, ethacrynic acid (Figure 1.5B), has also been investigated for its GSTP1-inhibitory properties [188]. Li *et al*. reported significant cytotoxic effects of ethacrynic acid derivatives in human leukemia cells [189].

Furthermore, Crawford *et al*. synthesized a library of twenty dichlorotriazine probes via tosylating 4-pent-yn-1-ol [190]. Of the twenty compounds investigated, LAS17 (Figure 1.5C) was reported to specifically inhibit GSTP1 activity by covalent modifications. Moreover, Louie *et al*. showed that LAS17 treatment of triple-negative breast cancer cells impaired GSTP1 activity and reduced cell growth and proliferation [12]. Further, LAS17 treatment of the immunodeficient mice bearing xenograft breast tumors showed an impressive reduction in tumor weight and volume compared to the untreated controls.

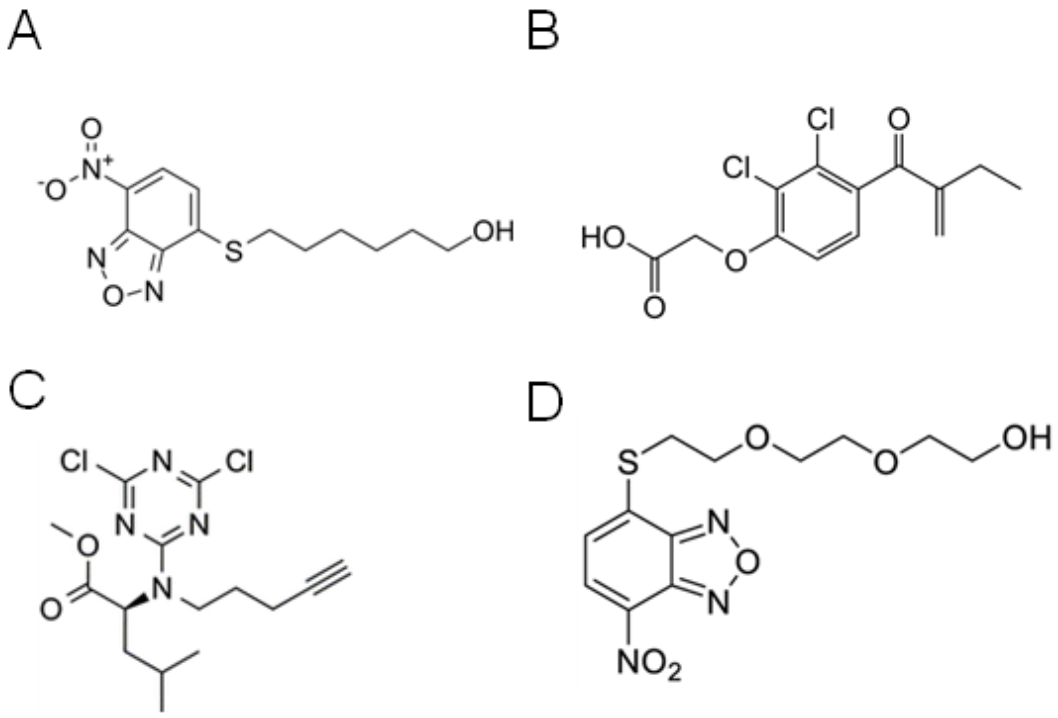

Figure 1.5. Structure of inhibitors that bind to the H-site of GST proteins. (A) 6-(7-nitro-2,1,3-benzoxadiazol-4-ylthio)hexanol (NBDHEX), (B) ethacrynic acid, (C) LAS17, and (D) MC3181 (2-(2-(2-((7-nitrobenzo[c][1,2,5]oxadiazol-4-yl)thio)ethoxy)ethoxy)ethanol), an NBDHEX analogue.

Glutathione peptidomimetics

γ-glutamyl-S-(benzyl)cysteinyl-R-(−)-phenyl glycine diethyl ester, commonly known as TER199, is the well-studied peptidomimetic analog of glutathione. O'Brien *et al*. demonstrated that TER199-treated mouse fibroblast cells showed increased expression of the multidrug resistance-associated protein, MRP1, and γ-glutamyl cysteine synthetase. They concluded that GSTP1 inhibition could increase the efficacy of chemotherapeutic drugs and glutathione biosynthesis [191]. Another glutathione peptidomimetic, TLK117 (Figure 1.6A), has been studied intensively in the context of lung fibrosis. McMillan *et al*. demonstrated that TLK117-mediated inhibition of GSTP1 blocked lung fibrogenesis through JNK signaling [192]. Ezatiostat, or TLK199 (Figure 1.6B), is a glutathione analog and a commonly used GSTP1 inhibitor. TLK199 treatment of mouse fibroblast cells showed disrupted GSTP1 binding to JNK and ERK2 [193].

Currently, TLK199 is commercially sold as Telintra® to treat myelodysplastic syndrome patients [193, 194].

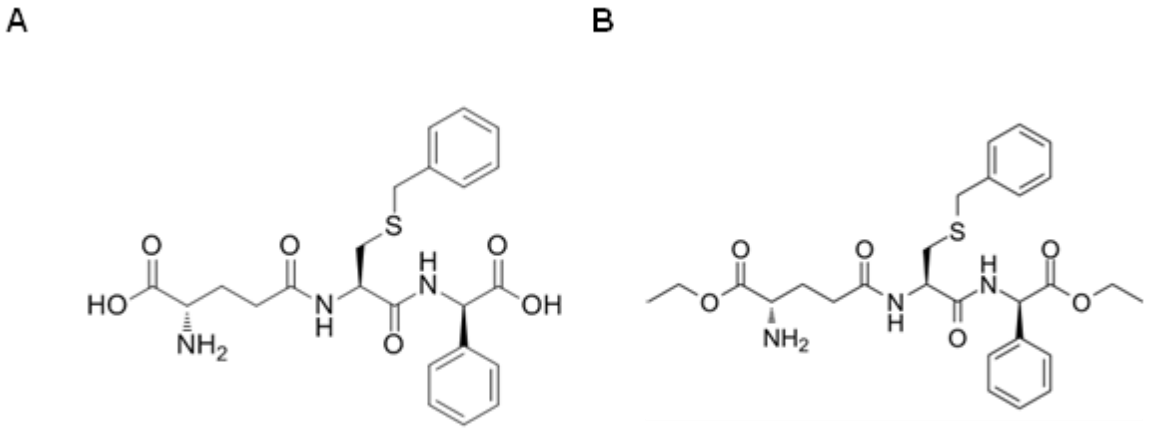

Figure 1.6. Structure of GSH peptidomimetics. (A) TLK117 and (B) Ezatiostat (TLK199).

Natural compounds

Chemotherapy is the primary treatment for patients with early and advanced stages of cancer. However, it is common for patients to respond poorly to conventional antineoplastic drugs. Lately, several independent studies have shown that various dietary agents, commonly used in Asian cuisine, show protective effects against multiple diseases, including cancer [195–197]. Interestingly, many of these compounds investigated target the cellular antioxidant system. For instance, a bioactive alkaloid compound obtained from *Piper longum*, piperlongumine (Figure 1.7A), is selectively toxic to cancer cells [198]. Structural and biochemical analyses using x-ray crystallography revealed that piperlongumine, upon entering a cell, hydrolyzes to hydroxypiperlongumine and binds to GSTP1 as a glutathione conjugate [199]. Hydroxypiperlongumine sits deeper into the H-site of GSTP1 that allows four hydrogen-bonding interactions overall. This unique positioning additionally mediates the formation of van der Waals interactions between the side chain of Ile104 and the aliphatic backbone of

hydroxypiperlongumine. Piperlongumine treatment causes oxidative stress by inhibiting the activity of GSTP1 and elevating the ROS levels [200]. Hang *et al*. showed piperlongumine treatment in head and neck cancer-xenograft mouse model reduced tumor growth and increased oxidative stress [201]. Similar results were found in a pancreatic orthotopic tumor mouse model [200].

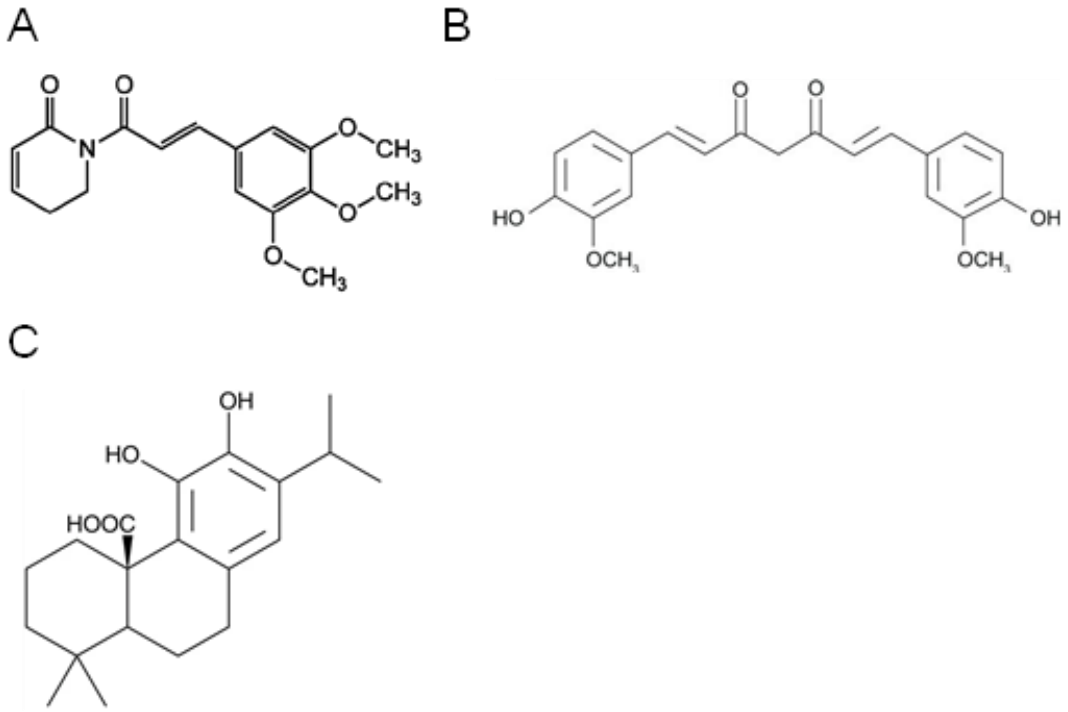

Figure 1.7. Structure of natural compounds that bind to the GST proteins and inhibit their activity. (A) Piperlongumine is a bioactive alkaloid obtained from *Piper longum*, (B) Curcumin is an anti-oxidant obtained from *Curcuma longa*, and (C) Carnosic acid is an antioxidant and an anti-inflammatory agent obtained from *Rosmarinus officinalis*.

Additionally, curcumin (Figure 1.7B), a natural compound extracted from *Curcuma longa*, has antioxidant and chemopreventive properties [202, 203]. Duvoix *et al*. demonstrated that the previously observed activation of NF-κB and anticancer properties in curcumin-treated cells is because of the inactivation of GSTP1 [204]. Carnosic acid (Figure 1.7C), a phenolic diterpene is extracted from *Rosmarinus officinalis* and is known for its antioxidant and anti-inflammatory

properties [202]. Ceylan *et al*. demonstrated that carnosic acid acts as a competitive inhibitor of GSTO1 [203].

Drug discovery and development have identified GST inhibitors as promising therapeutic agents to counter drug resistance in cancer patients. Convincing data suggest inhibiting GSTP1 protein levels and activity can increase oxidative stress, impair cancer-cell survival, reduce chemoresistance, and improve overall survival in patients [12, 13, 59]. However, one of the significant roadblocks that GST inhibitors encounter in clinical trials is their insufficient specificity. For example, it was reported that NBDHEX could impair enzyme activity of all GST enzymes, and exhibits a higher affinity to GSTM2 than any other GST isoform [186]. Therefore, to specifically inhibit GSTP1 and treat drug resistance, novel NDBHEX analogues have been developed and tested in human melanoma [205, 206]. Among them, 2-(2-(2-((7-nitrobenzo[c][1,2,5]oxadiazol-4-yl)thio)ethoxy)ethoxy)ethanol, also known as MC3181, (Figure 1.5D) significantly reduced cancer growth and metastasis in vemurafenib-resistant melanoma [207]. However, little is known about the efficacy of these analogues as stand-alone or combination therapeutics. Additionally, the toxicity of GST inhibitors in normal cells is not thoroughly investigated. Therefore, efforts are needed to identify and evaluate novel GST inhibitors that are isoform-specific, overcome drug resistance, and improve overall patient survival.

Conclusions and future directions

GST proteins have complex biology and play multifaceted roles in cancer cells. These enzymes are a crucial component of the cellular antioxidant system and play critical roles in maintaining cellular homeostasis. Under normal physiological conditions, GSTP1 can glutathionylate multiple proteins, including various transcription factors and oncogenes.

Conversely, under oxidative stress, GSTP1 can trigger MAPK- and caspase-mediated apoptotic signaling pathways. Interestingly, recent findings suggest that GST enzymes play important roles in cancer development and chemoresistance. However, kinetic and functional studies have revealed that most antineoplastic agents are poor substrates of GSTs with a weaker catalytic constant for the conjugation reaction. Therefore, researchers have shifted their focus to investigating the role of GSTs in various cellular functions, such as regulating kinases and the post-translational processes of diverse proteins.

Multiple studies have demonstrated that GST proteins are overexpressed in many human cancers. Their overexpression contributes to poor outcomes and is negatively correlated with patient survival. However, GSTP1 is not considered a diagnostic marker in clinical practices. We suggest that GSTP1, along with a combination of other biomarkers, may identify a high-risk population that is susceptible to developing cancer. In conclusion, recent studies have established the role of GSTP1 and other GST isozymes in cancer development, progression, metastasis, and resistance to antineoplastic drugs. Active research in the field of antioxidants and redox biology has narrowed to GSTP1 as a promising therapeutic target for cancer treatment. GSTP1 inhibitors can potentially be used in the future to enhance the efficacy of chemotherapy and overcoming drug resistance. However, to use these inhibitors safely for cancer treatment, research is needed to characterize their impact on normal cells and the long-term effects.

Author contributions

R.R.S. and K.M.R. conceived the review. R.R.S. searched for previously published literature and selected studies for citations. R.R.S. wrote the manuscript with the supervision of K.M.R.. All authors have read and agreed to the published version of the manuscript.

Funding

R.R.S. is supported by NIH COBRE Grant 1P20GM109024-04 and K.M.R. is supported by NIH Research Enhancement Award 1R15CA249714-01.

Acknowledgments

We thank Stephen Disrud for editorial feedback and comments.

Conflict of interest

The authors declare no conflict of interest.

References

1. Hayes, J.D., J.U. Flanagan, and I.R. Jowsey, *Glutathione transferases.* Annu Rev Pharmacol Toxicol, 2005. **45**: p. 51-88.

2. Chatterjee, A. and S. Gupta, *The multifaceted role of glutathione S-transferases in cancer.* Cancer Lett, 2018. **433**: p. 33-42.

3. Zhang, J., et al., *Pleiotropic functions of glutathione S-transferase P.* Adv Cancer Res, 2014. **122**: p. 143-75.

4. Kural, C., et al., *Glutathione S-Transferases and Cytochrome P450 Enzyme Expression in Patients with Intracranial Tumors: Preliminary Report of 55 Patients.* Med Princ Pract, 2019. **28**(1): p. 56-62.

5. Soleo, L. and R. Strzelczyk, *[Xenobiotics and glutathione].* G Ital Med Lav Ergon, 1999. **21**(4): p. 302-8.

6. Tew, K.D. and D.M. Townsend, *Regulatory functions of glutathione S-transferase P1-1 unrelated to detoxification.* Drug Metab Rev, 2011. **43**(2): p. 179-93.

7. Adler, V., et al., *Regulation of JNK signaling by GSTp.* EMBO J, 1999. **18**(5): p. 1321-34.

8. Fratelli, M., et al., *Identification by redox proteomics of glutathionylated proteins in oxidatively stressed human T lymphocytes.* Proc Natl Acad Sci U S A, 2002. **99**(6): p. 3505-10.

9. Townsend, D.M., et al., *Novel role for glutathione S-transferase pi. Regulator of protein S-Glutathionylation following oxidative and nitrosative stress.* J Biol Chem, 2009. **284**(1): p. 436-45.

10. de Bittencourt Junior, P.I., et al., *Glutathione metabolism and glutathione S-conjugate export ATPase (MRP1/GS-X pump) activity in cancer. II. Cell-to-cell variability, relation*

with cellular activation state and functional absence of GS-X pump in lymphocytes. Biochem Mol Biol Int, 1998. **45**(6): p. 1243-54.

11. Booth, J., E. Boyland, and P. Sims, *An enzyme from rat liver catalysing conjugations with glutathione.* Biochem J, 1961. **79**(3): p. 516-24.

12. Louie, S.M., et al., *GSTP1 Is a Driver of Triple-Negative Breast Cancer Cell Metabolism and Pathogenicity.* Cell Chem Biol, 2016. **23**(5): p. 567-578.

13. Checa-Rojas, A., et al., *GSTM3 and GSTP1: novel players driving tumor progression in cervical cancer.* Oncotarget, 2018. **9**(31): p. 21696-21714.

14. Townsend, D.M., et al., *A glutathione S-transferase pi-activated prodrug causes kinase activation concurrent with S-glutathionylation of proteins.* Mol Pharmacol, 2006. **69**(2): p. 501-8.

15. Reinemer, P., et al., *The three-dimensional structure of class pi glutathione S-transferase in complex with glutathione sulfonate at 2.3 A resolution.* EMBO J, 1991. **10**(8): p. 1997-2005.

16. Oakley, A., *Glutathione transferases: a structural perspective.* Drug Metab Rev, 2011. **43**(2): p. 138-51.

17. Kilili, K.G., et al., *Differential roles of tau class glutathione S-transferases in oxidative stress.* J Biol Chem, 2004. **279**(23): p. 24540-51.

18. Ladner, J.E., et al., *Parallel evolutionary pathways for glutathione transferases: structure and mechanism of the mitochondrial class kappa enzyme rGSTK1-1.* Biochemistry, 2004. **43**(2): p. 352-61.

19. Li, J., Z. Xia, and J. Ding, *Thioredoxin-like domain of human kappa class glutathione transferase reveals sequence homology and structure similarity to the theta class enzyme.* Protein Sci, 2005. **14**(9): p. 2361-9.

20. Atkinson, H.J. and P.C. Babbitt, *Glutathione transferases are structural and functional outliers in the thioredoxin fold.* Biochemistry, 2009. **48**(46): p. 11108-16.

21. Board, P.G., et al., *Identification, characterization, and crystal structure of the Omega class glutathione transferases.* J Biol Chem, 2000. **275**(32): p. 24798-806.

22. Wilce, M.C. and M.W. Parker, *Structure and function of glutathione S-transferases.* Biochim Biophys Acta, 1994. **1205**(1): p. 1-18.

23. Cohen, L. and A. Jefferies, *Environmental exposures and cancer: using the precautionary principle.* Ecancermedicalscience, 2019. **13**: p. ed91.

24. Valko, M., et al., *Free radicals, metals and antioxidants in oxidative stress-induced cancer.* Chem Biol Interact, 2006. **160**(1): p. 1-40.

25. Sosa, V., et al., *Oxidative stress and cancer: an overview.* Ageing Res Rev, 2013. **12**(1): p. 376-90.

26. He, L., et al., *Antioxidants Maintain Cellular Redox Homeostasis by Elimination of Reactive Oxygen Species.* Cell Physiol Biochem, 2017. **44**(2): p. 532-553.

27. Hakkola, J., et al., *Inhibition and induction of CYP enzymes in humans: an update.* Arch Toxicol, 2020. **94**(11): p. 3671-3722.

28. Jancova, P., P. Anzenbacher, and E. Anzenbacherova, *Phase II drug metabolizing enzymes.* Biomed Pap Med Fac Univ Palacky Olomouc Czech Repub, 2010. **154**(2): p. 103-16.

29. Bocedi, A., et al., *Glutathione Transferase P1-1 an Enzyme Useful in Biomedicine and as Biomarker in Clinical Practice and in Environmental Pollution.* Nutrients, 2019. **11**(8).

30. Kim, K.H., et al., *A review of airborne polycyclic aromatic hydrocarbons (PAHs) and their human health effects.* Environ Int, 2013. **60**: p. 71-80.

31. Kaisarevic, S., et al., *Differential expression of CYP1A1 and CYP1A2 genes in H4IIE rat hepatoma cells exposed to TCDD and PAHs.* Environ Toxicol Pharmacol, 2015. **39**(1): p. 358-68.

32. Bakhiya, N., et al., *Directing role of organic anion transporters in the excretion of mercapturic acids of alkylated polycyclic aromatic hydrocarbons.* Drug Metab Dispos, 2007. **35**(10): p. 1824-31.

33. Hanna, P.E. and M.W. Anders, *The mercapturic acid pathway.* Crit Rev Toxicol, 2019. **49**(10): p. 819-929.

34. Lu, S.C., *Glutathione synthesis.* Biochim Biophys Acta, 2013. **1830**(5): p. 3143-53.

35. Cole, S.P. and R.G. Deeley, *Transport of glutathione and glutathione conjugates by MRP1.* Trends Pharmacol Sci, 2006. **27**(8): p. 438-46.

36. Ballatori, N. and J.F. Rebbeor, *Roles of MRP2 and oatp1 in hepatocellular export of reduced glutathione.* Semin Liver Dis, 1998. **18**(4): p. 377-87.

37. Biswas, S.K. and I. Rahman, *Environmental toxicity, redox signaling and lung inflammation: the role of glutathione.* Mol Aspects Med, 2009. **30**(1-2): p. 60-76.

38. Meister, A., *Biosynthesis and functions of glutathione, an essential biofactor.* J Nutr Sci Vitaminol (Tokyo), 1992. **Spec No**: p. 1-6.

39. Meister, A., *Glutathione metabolism and its selective modification.* J Biol Chem, 1988. **263**(33): p. 17205-8.

40. Yuan, L. and N. Kaplowitz, *Glutathione in liver diseases and hepatotoxicity.* Mol Aspects Med, 2009. **30**(1-2): p. 29-41.

41. Pallardo, F.V., et al., *Role of nuclear glutathione as a key regulator of cell proliferation.* Mol Aspects Med, 2009. **30**(1-2): p. 77-85.

42. Storr, S.J., et al., *Redox environment, free radical, and oxidative DNA damage.* Antioxid Redox Signal, 2013. **18**(18): p. 2399-408.

43. Ning, J. and M.H. Grant, *The role of reduced glutathione and glutathione reductase in the cytotoxicity of chromium (VI) in osteoblasts.* Toxicol In Vitro, 2000. **14**(4): p. 329-35.

44. Kang, Y.J. and M.D. Enger, *Effect of cellular glutathione depletion on cadmium-induced cytotoxicity in human lung carcinoma cells.* Cell Biol Toxicol, 1987. **3**(4): p. 347-60.

45. Shimizu, M., et al., *Effect of glutathione depletion and metallothionein gene expression on arsenic-induced cytotoxicity and c-myc expression in vitro.* Toxicol Sci, 1998. **45**(2): p. 204-11.

46. Russo, A., et al., *Alteration of bleomycin cytotoxicity by glutathione depletion or elevation.* Int J Radiat Oncol Biol Phys, 1984. **10**(9): p. 1675-8.

47. Perry, R.R., et al., *Effect of treatment duration and glutathione depletion on mitomycin C cytotoxicity in vitro.* Cancer Res, 1992. **52**(17): p. 4608-12.

48. Loschen, G., et al., *Superoxide radicals as precursors of mitochondrial hydrogen peroxide.* FEBS Lett, 1974. **42**(1): p. 68-72.

49. Smith, K.A., G.B. Waypa, and P.T. Schumacker, *Redox signaling during hypoxia in mammalian cells.* Redox Biol, 2017. **13**: p. 228-234.

50. Li, L.C., et al., *MDG1 inhibits H_2O_2-induced apoptosis and inflammation in human umbilical vein endothelial cells.* Mol Med Rep, 2017. **16**(3): p. 3673-3679.

51. Riou, C., et al., *H_2O_2 induces apoptosis of pig thyrocytes in culture.* J Endocrinol, 1998. **156**(2): p. 315-22.

52. Finkel, T., *Signal transduction by mitochondrial oxidants.* J Biol Chem, 2012. **287**(7): p. 4434-40.

53. Dekant, W. and S. Vamvakas, *Glutathione-dependent bioactivation of xenobiotics.* Xenobiotica, 1993. **23**(8): p. 873-87.

54. Adler, V., et al., *Role of redox potential and reactive oxygen species in stress signaling.* Oncogene, 1999. **18**(45): p. 6104-11.

55. Gate, L., et al., *Increased myeloproliferation in glutathione S-transferase pi-deficient mice is associated with a deregulation of JNK and Janus kinase/STAT pathways.* J Biol Chem, 2004. **279**(10): p. 8608-16.

56. Wang, T., et al., *Glutathione S-transferase P1-1 (GSTP1-1) inhibits c-Jun N-terminal kinase (JNK1) signaling through interaction with the C terminus.* J Biol Chem, 2001. **276**(24): p. 20999-1003.

57. De Luca, A., et al., *The fine-tuning of TRAF2-GSTP1-1 interaction: effect of ligand binding and in situ detection of the complex.* Cell Death Dis, 2014. **5**: p. e1015.

58. Wu, Y., et al., *Human glutathione S-transferase P1-1 interacts with TRAF2 and regulates TRAF2-ASK1 signals.* Oncogene, 2006. **25**(42): p. 5787-800.

59. Singh, R.R., et al., *Glutathione S-Transferase pi-1 Knockdown Reduces Pancreatic Ductal Adenocarcinoma Growth by Activating Oxidative Stress Response Pathways.* Cancers (Basel), 2020. **12**(6).

60. Dowling, R.J., et al., *Metformin inhibits mammalian target of rapamycin-dependent translation initiation in breast cancer cells.* Cancer Res, 2007. **67**(22): p. 10804-12.

61. Liu, X., et al., *Glutathione S-transferase A1 suppresses tumor progression and indicates better prognosis of human primary hepatocellular carcinoma.* J Cancer, 2020. **11**(1): p. 83-91.

62. Saisawang, C., et al., *Glutathione transferase Omega 1-1 (GSTO1-1) modulates Akt and MEK1/2 signaling in human neuroblastoma cell SH-SY5Y.* Proteins, 2019. **87**(7): p. 588-595.

63. Halbrook, C.J. and C.A. Lyssiotis, *Employing Metabolism to Improve the Diagnosis and Treatment of Pancreatic Cancer.* Cancer Cell, 2017. **31**(1): p. 5-19.

64. Vazquez, A., et al., *Cancer metabolism at a glance.* J Cell Sci, 2016. **129**(18): p. 3367-73.

65. Li, Z. and H. Zhang, *Reprogramming of glucose, fatty acid and amino acid metabolism for cancer progression.* Cell Mol Life Sci, 2016. **73**(2): p. 377-92.

66. Hildebrandt, T., et al., *Cytosolic thiol switches regulating basic cellular functions: GAPDH as an information hub?* Biol Chem, 2015. **396**(5): p. 523-37.

67. Moellering, R.E. and B.F. Cravatt, *Functional lysine modification by an intrinsically reactive primary glycolytic metabolite.* Science, 2013. **341**(6145): p. 549-53.

68. Song, X., et al., *[Expressions of glutathione S-transferase P1 and 4- hydroxynonenal and the progression of prostate cancer].* Zhonghua Nan Ke Xue, 2017. **23**(5): p. 412-416.

69. Barbati, S., et al., *Secondary oxidation of cyclic 1,N2-propano and 1,N2-etheno-2'-deoxyguanosine DNA adducts. Consequences in oxidative stress biomarker development.* Chemosphere, 2010. **80**(9): p. 1081-7.

70. Bartsch, H., K. Arab, and J. Nair, *Biomarkers for hazard identification in humans.* Environ Health, 2011. **10 Suppl 1**: p. S11.

71. Koo, M.M., et al., *Presenting symptoms of cancer and stage at diagnosis: evidence from a cross-sectional, population-based study.* Lancet Oncol, 2020. **21**(1): p. 73-79.

72. Sabater, L., et al., *Borderline resectable pancreatic cancer. Challenges and controversies.* Cancer Treat Rev, 2018. **68**: p. 124-135.

73. Vijayvergia, N., P.C. Shah, and C.S. Denlinger, *Survivorship in Non-Small Cell Lung Cancer: Challenges Faced and Steps Forward.* J Natl Compr Canc Netw, 2015. **13**(9): p. 1151-61.

74. Tan, A.C., et al., *Management of glioblastoma: State of the art and future directions.* CA Cancer J Clin, 2020. **70**(4): p. 299-312.

75. Mehrling, T., *Chemotherapy is getting 'smarter'.* Future Oncol, 2015. **11**(4): p. 549-52.

76. Gupta, R., I. Amanam, and V. Chung, *Current and future therapies for advanced pancreatic cancer.* J Surg Oncol, 2017. **116**(1): p. 25-34.

77. Li, D., et al., *Pancreatic cancer.* Lancet, 2004. **363**(9414): p. 1049-57.

78. Zheng, H.C., *The molecular mechanisms of chemoresistance in cancers.* Oncotarget, 2017. **8**(35): p. 59950-59964.

79. Lakshmanan, I., et al., *MUC16 Regulates TSPYL5 for Lung Cancer Cell Growth and Chemoresistance by Suppressing p53.* Clin Cancer Res, 2017. **23**(14): p. 3906-3917.

80. Tang, J., et al., *Continuous exposure of non-small cell lung cancer cells with wild-type EGFR to an inhibitor of EGFR tyrosine kinase induces chemoresistance by activating STAT3.* Int J Oncol, 2015. **46**(5): p. 2083-95.

81. Kuroda, H., et al., *Inhibition of heme oxygenase-1 with an epidermal growth factor receptor inhibitor and cisplatin decreases proliferation of lung cancer A549 cells.* Lung Cancer, 2010. **67**(1): p. 31-6.

82. Miao, Y., et al., *MicroRNA-130b targets PTEN to mediate drug resistance and proliferation of breast cancer cells via the PI3K/Akt signaling pathway.* Sci Rep, 2017. **7**: p. 41942.

83. Deeley, R.G. and S.P. Cole, *Substrate recognition and transport by multidrug resistance protein 1 (ABCC1).* FEBS Lett, 2006. **580**(4): p. 1103-11.

84. Shen, H., L. Kauvar, and K.D. Tew, *Importance of glutathione and associated enzymes in drug response.* Oncol Res, 1997. **9**(6-7): p. 295-302.

85. Huang, J., M. Gu, and C. Chen, *[Expression of glutathione S-transferase-pi in operative specimens as marker of chemoresistance in patients with ovarian cancer].* Zhonghua Fu Chan Ke Za Zhi, 1997. **32**(8): p. 458-61.

86. Zhang, F., L. Qi, and H. Chen, *[Value of P-glycoprotein and glutathione S-transferase-pi as chemo-resistant indicators in ovarian cancers].* Zhonghua Zhong Liu Za Zhi, 2001. **23**(4): p. 313-6.

87. Satoh, T., et al., *[An immunohistological study on expression of glutathione S-transferase pi (form) in human ovarian carcinoma].* Nihon Sanka Fujinka Gakkai Zasshi, 1995. **47**(9): p. 931-8.

88. Mousseau, M., et al., *A study of the expression of four chemoresistance-related genes in human primary and metastatic brain tumours.* Eur J Cancer, 1993. **29A**(5): p. 753-9.

89. Fruehauf, J.P., et al., *In vitro drug response and molecular markers associated with drug resistance in malignant gliomas.* Clin Cancer Res, 2006. **12**(15): p. 4523-32.

90. Geng, M., et al., *The association between chemosensitivity and Pgp, GST-pi and Topo II expression in gastric cancer.* Diagn Pathol, 2013. **8**: p. 198.

91. Yu, D.S., D.S. Hsieh, and S.Y. Chang, *Increasing expression of GST-pi MIF, and ID1 genes in chemoresistant prostate cancer cells.* Arch Androl, 2006. **52**(4): p. 275-81.

92. Wang, Z., et al., *Identification of proteins responsible for adriamycin resistance in breast cancer cells using proteomics analysis.* Sci Rep, 2015. **5**: p. 9301.

93. Yang, M., et al., *CLDN6 promotes chemoresistance through GSTP1 in human breast cancer.* J Exp Clin Cancer Res, 2017. **36**(1): p. 157.

94. Ogino, S., et al., *Glutathione S-transferase Pi 1 is a valuable predictor for cancer drug resistance in esophageal squamous cell carcinoma.* Cancer Sci, 2019. **110**(2): p. 795-804.

95. Li, J., et al., *Transcriptional Activation of Gstp1 by MEK/ERK Signaling Confers Chemo-Resistance to Cisplatin in Lung Cancer Stem Cells.* Front Oncol, 2019. **9**: p. 476.

96. Ishii, T., S. Teramoto, and T. Matsuse, *GSTP1 affects chemoresistance against camptothecin in human lung adenocarcinoma cells.* Cancer Lett, 2004. **216**(1): p. 89-102.

97. Zhao, J., *Cancer stem cells and chemoresistance: The smartest survives the raid.* Pharmacol Ther, 2016. **160**: p. 145-58.

98. Batlle, E. and H. Clevers, *Cancer stem cells revisited.* Nat Med, 2017. **23**(10): p. 1124-1134.

99. Ayob, A.Z. and T.S. Ramasamy, *Cancer stem cells as key drivers of tumour progression.* J Biomed Sci, 2018. **25**(1): p. 20.

100. Nandy, S.B. and R. Lakshmanaswamy, *Cancer Stem Cells and Metastasis.* Prog Mol Biol Transl Sci, 2017. **151**: p. 137-176.

101. Liu, T., et al., *Establishment and characterization of multi-drug resistant, prostate carcinoma-initiating stem-like cells from human prostate cancer cell lines 22RV1.* Mol Cell Biochem, 2010. **340**(1-2): p. 265-73.

102. Shafee, N., et al., *Cancer stem cells contribute to cisplatin resistance in Brca1/p53-mediated mouse mammary tumors.* Cancer Res, 2008. **68**(9): p. 3243-50.

103. Broxterman, H.J., K.J. Gotink, and H.M. Verheul, *Understanding the causes of multidrug resistance in cancer: a comparison of doxorubicin and sunitinib.* Drug Resist Updat, 2009. **12**(4-5): p. 114-26.

104. Tanaka, G., et al., *Dual pharmacological inhibition of glutathione and thioredoxin systems synergizes to kill colorectal carcinoma stem cells.* Cancer Med, 2016. **5**(9): p. 2544-57.

105. Lin, C., et al., *miR-133b reverses cisplatin resistance by targeting GSTP1 in cisplatin-resistant lung cancer cells.* Int J Mol Med, 2018. **41**(4): p. 2050-2058.

106. Chen, J., C. Solomides, and H. Simpkins, *Sensitization of mesothelioma cells to platinum-based chemotherapy by GSTpi knockdown.* Biochem Biophys Res Commun, 2014. **447**(1): p. 77-82.

107. Hour, T.C., et al., *Characterization of chemoresistance mechanisms in a series of cisplatin-resistant transitional carcinoma cell lines.* Anticancer Res, 2000. **20**(5A): p. 3221-5.

108. Tew, K.D., et al., *The role of glutathione S-transferase P in signaling pathways and S-glutathionylation in cancer.* Free Radic Biol Med, 2011. **51**(2): p. 299-313.

109. Robin, S.K.D., M. Ansari, and C.R.S. Uppugunduri, *Spectrophotometric Screening for Potential Inhibitors of Cytosolic Glutathione S-Transferases.* J Vis Exp, 2020(164).

110. Lee, K.G.Z., et al., *Development of an Efficient Dual-Action GST-Inhibiting Anticancer Platinum(IV) Prodrug.* ChemMedChem, 2018. **13**(12): p. 1210-1217.

111. Abd El-Karim, S.S., et al., *Synthesis and molecular modeling of new benzimidazoles as glutathione S-transferase inhibitors and anticancer agents.* Future Med Chem, 2018. **10**(2): p. 157-181.

112. Brozovic, A., et al., *Long-term activation of SAPK/JNK, p38 kinase and fas-L expression by cisplatin is attenuated in human carcinoma cells that acquired drug resistance.* Int J Cancer, 2004. **112**(6): p. 974-85.

113. Mansouri, A., et al., *Sustained activation of JNK/p38 MAPK pathways in response to cisplatin leads to Fas ligand induction and cell death in ovarian carcinoma cells.* J Biol Chem, 2003. **278**(21): p. 19245-56.

114. Besirli, C.G. and E.M. Johnson, Jr., *JNK-independent activation of c-Jun during neuronal apoptosis induced by multiple DNA-damaging agents.* J Biol Chem, 2003. **278**(25): p. 22357-66.

115. Huang, X.L., et al., *Activation of a c-Jun N-terminal kinase-mediated autophagy pathway attenuates the anticancer activity of gemcitabine in human bladder cancer cells.* Anticancer Drugs, 2017. **28**(6): p. 596-602.

116. Li, J., X. Liang, and X. Yang, *Ursolic acid inhibits growth and induces apoptosis in gemcitabine-resistant human pancreatic cancer via the JNK and PI3K/Akt/NF-kappaB pathways.* Oncol Rep, 2012. **28**(2): p. 501-10.

117. Dominko, K. and D. Dikic, *Glutathionylation: a regulatory role of glutathione in physiological processes.* Arh Hig Rada Toksikol, 2018. **69**(1): p. 1-24.

118. Grek, C.L., et al., *Causes and consequences of cysteine S-glutathionylation.* J Biol Chem, 2013. **288**(37): p. 26497-504.

119. Gilbert, H.F., *Redox control of enzyme activities by thiol/disulfide exchange.* Methods Enzymol, 1984. **107**: p. 330-51.

120. Ye, Z.W., et al., *Glutathione S-Transferase P-Mediated Protein S-Glutathionylation of Resident Endoplasmic Reticulum Proteins Influences Sensitivity to Drug-Induced Unfolded Protein Response.* Antioxid Redox Signal, 2017. **26**(6): p. 247-261.

121. Chae, H.Z., et al., *Protein glutathionylation in the regulation of peroxiredoxins: a family of thiol-specific peroxidases that function as antioxidants, molecular chaperones, and signal modulators.* Antioxid Redox Signal, 2012. **16**(6): p. 506-23.

122. Rhee, S.G., H.Z. Chae, and K. Kim, *Peroxiredoxins: a historical overview and speculative preview of novel mechanisms and emerging concepts in cell signaling.* Free Radic Biol Med, 2005. **38**(12): p. 1543-52.

123. Hofmann, B., H.J. Hecht, and L. Flohe, *Peroxiredoxins.* Biol Chem, 2002. **383**(3-4): p. 347-64.

124. Noguera-Mazon, V., et al., *Glutathionylation induces the dissociation of 1-Cys D-peroxiredoxin non-covalent homodimer.* J Biol Chem, 2006. **281**(42): p. 31736-42.

125. Manevich, Y., S.I. Feinstein, and A.B. Fisher, *Activation of the antioxidant enzyme 1-CYS peroxiredoxin requires glutathionylation mediated by heterodimerization with pi GST.* Proc Natl Acad Sci U S A, 2004. **101**(11): p. 3780-5.

126. Arriga, R., et al., *Peroxiredoxin 6 Is a Key Antioxidant Enzyme in Modulating the Link between Glycemic and Lipogenic Metabolism.* Oxid Med Cell Longev, 2019. **2019**: p. 9685607.

127. Manevich, Y. and A.B. Fisher, *Peroxiredoxin 6, a 1-Cys peroxiredoxin, functions in antioxidant defense and lung phospholipid metabolism.* Free Radic Biol Med, 2005. **38**(11): p. 1422-32.

128. Manevich, Y., et al., *Allelic variants of glutathione S-transferase P1-1 differentially mediate the peroxidase function of peroxiredoxin VI and alter membrane lipid peroxidation.* Free Radic Biol Med, 2013. **54**: p. 62-70.

129. Chen, C.A., et al., *S-glutathionylation uncouples eNOS and regulates its cellular and vascular function.* Nature, 2010. **468**(7327): p. 1115-8.

130. Grootjans, J., et al., *The unfolded protein response in immunity and inflammation.* Nat Rev Immunol, 2016. **16**(8): p. 469-84.

131. Hetz, C. and S. Saxena, *ER stress and the unfolded protein response in neurodegeneration.* Nat Rev Neurol, 2017. **13**(8): p. 477-491.

132. Gerakis, Y. and C. Hetz, *Emerging roles of ER stress in the etiology and pathogenesis of Alzheimer's disease.* FEBS J, 2018. **285**(6): p. 995-1011.

133. Tripathy, D., et al., *Mutations in TGM6 induce the unfolded protein response in SCA35.* Hum Mol Genet, 2017. **26**(19): p. 3749-3762.

134. Townsend, D.M., *S-glutathionylation: indicator of cell stress and regulator of the unfolded protein response.* Mol Interv, 2007. **7**(6): p. 313-24.

135. Wilkinson, B. and H.F. Gilbert, *Protein disulfide isomerase.* Biochim Biophys Acta, 2004. **1699**(1-2): p. 35-44.

136. Townsend, D.M., et al., *Nitrosative stress-induced s-glutathionylation of protein disulfide isomerase leads to activation of the unfolded protein response.* Cancer Res, 2009. **69**(19): p. 7626-34.

137. Stournaras, C., et al., *Glutathionyl(cysteine-374) actin forms filaments of low mechanical stability.* Biochim Biophys Acta, 1990. **1037**(1): p. 86-91.

138. Rokutan, K., R.B. Johnston, Jr., and K. Kawai, *Oxidative stress induces S-thiolation of specific proteins in cultured gastric mucosal cells.* Am J Physiol, 1994. **266**(2 Pt 1): p. G247-54.

139. Dalle-Donne, I., et al., *Reversible S-glutathionylation of Cys 374 regulates actin filament formation by inducing structural changes in the actin molecule.* Free Radic Biol Med, 2003. **34**(1): p. 23-32.

140. Lind, C., et al., *Identification of S-glutathionylated cellular proteins during oxidative stress and constitutive metabolism by affinity purification and proteomic analysis.* Arch Biochem Biophys, 2002. **406**(2): p. 229-40.

141. Chen, W., et al., *Differential interaction of cardiac, skeletal muscle, and yeast tropomyosins with fluorescent (pyrene235) yeast actin.* Biophys J, 2006. **90**(4): p. 1308-18.

142. Kaus-Drobek, M., et al., *Vimentin S-glutathionylation at Cys328 inhibits filament elongation and induces severing of mature filaments in vitro.* FEBS J, 2020. **287**(24): p. 5304-5322.

143. Levine, A.J., *p53, the cellular gatekeeper for growth and division.* Cell, 1997. **88**(3): p. 323-31.

144. Bykov, V.J.N., et al., *Targeting mutant p53 for efficient cancer therapy.* Nat Rev Cancer, 2018. **18**(2): p. 89-102.

145. Rainwater, R., et al., *Role of cysteine residues in regulation of p53 function.* Mol Cell Biol, 1995. **15**(7): p. 3892-903.

146. Velu, C.S., et al., *Human p53 is inhibited by glutathionylation of cysteines present in the proximal DNA-binding domain during oxidative stress.* Biochemistry, 2007. **46**(26): p. 7765-80.

147. Yusuf, M.A., et al., *Cys-141 glutathionylation of human p53: Studies using specific polyclonal antibodies in cancer samples and cell lines.* Free Radic Biol Med, 2010. **49**(5): p. 908-17.

148. Moldogazieva, N.T., S.V. Lutsenko, and A.A. Terentiev, *Reactive Oxygen and Nitrogen Species-Induced Protein Modifications: Implication in Carcinogenesis and Anticancer Therapy.* Cancer Res, 2018. **78**(21): p. 6040-6047.

149. Wu-Zhang, A.X. and A.C. Newton, *Protein kinase C pharmacology: refining the toolbox.* Biochem J, 2013. **452**(2): p. 195-209.

150. Castagna, M., et al., *Direct activation of calcium-activated, phospholipid-dependent protein kinase by tumor-promoting phorbol esters.* J Biol Chem, 1982. **257**(13): p. 7847-51.

151. Benavides, F., et al., *Transgenic overexpression of PKCepsilon in the mouse prostate induces preneoplastic lesions.* Cell Cycle, 2011. **10**(2): p. 268-77.

152. Wang, H., et al., *Transcriptional regulation of oncogenic protein kinase C (PKC) by STAT1 and Sp1 proteins.* J Biol Chem, 2014. **289**(28): p. 19823-38.

153. Ward, N.E., et al., *Oxidant-induced S-glutathiolation inactivates protein kinase C-alpha (PKC-alpha): a potential mechanism of PKC isozyme regulation.* Biochemistry, 2000. **39**(33): p. 10319-29.

154. Taylor, E.R., et al., *Reversible glutathionylation of complex I increases mitochondrial superoxide formation.* J Biol Chem, 2003. **278**(22): p. 19603-10.

155. Klatt, P., et al., *Novel application of S-nitrosoglutathione-Sepharose to identify proteins that are potential targets for S-nitrosoglutathione-induced mixed-disulphide formation.* Biochem J, 2000. **349**(Pt 2): p. 567-78.

156. Odin, J.A., et al., *Bcl-2-dependent oxidation of pyruvate dehydrogenase-E2, a primary biliary cirrhosis autoantigen, during apoptosis.* J Clin Invest, 2001. **108**(2): p. 223-32.

157. Ralat, L.A., et al., *Direct evidence for the formation of a complex between 1-cysteine peroxiredoxin and glutathione S-transferase pi with activity changes in both enzymes.* Biochemistry, 2006. **45**(2): p. 360-72.

158. Kruyer, A., et al., *Post-translational S-glutathionylation of cofilin increases actin cycling during cocaine seeking.* PLoS One, 2019. **14**(9): p. e0223037.

159. Patel, B.G., T. Wilder, and R.J. Solaro, *Novel control of cardiac myofilament response to calcium by S-glutathionylation at specific sites of myosin binding protein C.* Front Physiol, 2013. **4**: p. 336.

160. Carletti, B., et al., *Effect of protein glutathionylation on neuronal cytoskeleton: a potential link to neurodegeneration.* Neuroscience, 2011. **192**: p. 285-94.

161. Yu, C.X., S. Li, and A.R. Whorton, *Redox regulation of PTEN by S-nitrosothiols.* Mol Pharmacol, 2005. **68**(3): p. 847-54.

162. Qanungo, S., et al., *Glutathione supplementation potentiates hypoxic apoptosis by S-glutathionylation of p65-NFkappaB.* J Biol Chem, 2007. **282**(25): p. 18427-36.

163. Goch, G., et al., *Affinity of S100A1 protein for calcium increases dramatically upon glutathionylation.* FEBS J, 2005. **272**(10): p. 2557-65.

164. Chen, C.L., et al., *Site-specific S-glutathiolation of mitochondrial NADH ubiquinone reductase.* Biochemistry, 2007. **46**(19): p. 5754-65.

165. Reynaert, N.L., et al., *Dynamic redox control of NF-kappaB through glutaredoxin-regulated S-glutathionylation of inhibitory kappaB kinase beta.* Proc Natl Acad Sci U S A, 2006. **103**(35): p. 13086-91.

166. Cianfruglia, L., et al., *KRIT1 Loss-Of-Function Associated with Cerebral Cavernous Malformation Disease Leads to Enhanced S-Glutathionylation of Distinct Structural and Regulatory Proteins.* Antioxidants (Basel), 2019. **8**(1).

167. Huang, Z., et al., *Inhibition of caspase-3 activity and activation by protein glutathionylation.* Biochem Pharmacol, 2008. **75**(11): p. 2234-44.

168. Grek, C.L., et al., *S-glutathionylated serine proteinase inhibitors as plasma biomarkers in assessing response to redox-modulating drugs.* Cancer Res, 2012. **72**(9): p. 2383-93.

169. Xie, Y., et al., *S-glutathionylation impairs signal transducer and activator of transcription 3 activation and signaling.* Endocrinology, 2009. **150**(3): p. 1122-31.

170. Rinna, A., M. Torres, and H.J. Forman, *Stimulation of the alveolar macrophage respiratory burst by ADP causes selective glutathionylation of protein tyrosine phosphatase 1B.* Free Radic Biol Med, 2006. **41**(1): p. 86-91.

171. Haendeler, J., *Thioredoxin-1 and posttranslational modifications.* Antioxid Redox Signal, 2006. **8**(9-10): p. 1723-8.

172. Adachi, T., et al., *S-Glutathiolation by peroxynitrite activates SERCA during arterial relaxation by nitric oxide.* Nat Med, 2004. **10**(11): p. 1200-7.

173. Hoppe, G., et al., *Molecular basis for the redox control of nuclear transport of the structural chromatin protein Hmgb1.* Exp Cell Res, 2006. **312**(18): p. 3526-38.

174. O'Brian, C.A. and F. Chu, *Post-translational disulfide modifications in cell signaling--role of inter-protein, intra-protein, S-glutathionyl, and S-cysteaminyl disulfide modifications in signal transmission.* Free Radic Res, 2005. **39**(5): p. 471-80.

175. Musdal, Y., et al., *FDA-approved drugs and other compounds tested as inhibitors of human glutathione transferase P1-1.* Chem Biol Interact, 2013. **205**(1): p. 53-62.

176. Wu, B. and D. Dong, *Human cytosolic glutathione transferases: structure, function, and drug discovery.* Trends Pharmacol Sci, 2012. **33**(12): p. 656-68.

177. Shishido, Y., et al., *A covalent G-site inhibitor for glutathione S-transferase Pi (GSTP1-1).* Chem Commun (Camb), 2017. **53**(81): p. 11138-11141.

178. Shishido, Y., et al., *A Covalent Inhibitor for Glutathione S-Transferase Pi (GSTP1-1) in Human Cells.* Chembiochem, 2019. **20**(7): p. 900-905.

179. Kulaksiz-Erkmen, G., et al., *Amitriptyline may have a supportive role in cancer treatment by inhibiting glutathione S-transferase pi (GST-pi) and alpha (GST-alpha).* J Enzyme Inhib Med Chem, 2013. **28**(1): p. 131-6.

180. Bachovchin, D.A., et al., *Identification of selective inhibitors of uncharacterized enzymes by high-throughput screening with fluorescent activity-based probes.* Nat Biotechnol, 2009. **27**(4): p. 387-94.

181. Tsuboi, K., et al., *Potent and selective inhibitors of glutathione S-transferase omega 1 that impair cancer drug resistance.* J Am Chem Soc, 2011. **133**(41): p. 16605-16.

182. Urzua, U., et al., *Transcriptomic analysis of an in vitro murine model of ovarian carcinoma: functional similarity to the human disease and identification of prospective tumoral markers and targets.* J Cell Physiol, 2006. **206**(3): p. 594-602.

183. Yan, X.D., et al., *Identification of platinum-resistance associated proteins through proteomic analysis of human ovarian cancer cells and their platinum-resistant sublines.* J Proteome Res, 2007. **6**(2): p. 772-80.

184. Turella, P., et al., *Proapoptotic activity of new glutathione S-transferase inhibitors.* Cancer Res, 2005. **65**(9): p. 3751-61.

185. Turella, P., et al., *A strong glutathione S-transferase inhibitor overcomes the P-glycoprotein-mediated resistance in tumor cells. 6-(7-Nitro-2,1,3-benzoxadiazol-4-ylthio)hexanol (NBDHEX) triggers a caspase-dependent apoptosis in MDR1-expressing leukemia cells.* J Biol Chem, 2006. **281**(33): p. 23725-32.

186. Federici, L., et al., *Structural basis for the binding of the anticancer compound 6-(7-nitro-2,1,3-benzoxadiazol-4-ylthio)hexanol to human glutathione s-transferases.* Cancer Res, 2009. **69**(20): p. 8025-34.

187. Tentori, L., et al., *The glutathione transferase inhibitor 6-(7-nitro-2,1,3-benzoxadiazol-4-ylthio)hexanol (NBDHEX) increases temozolomide efficacy against malignant melanoma.* Eur J Cancer, 2011. **47**(8): p. 1219-30.

188. Awasthi, S., et al., *Interactions of glutathione S-transferase-pi with ethacrynic acid and its glutathione conjugate.* Biochim Biophys Acta, 1993. **1164**(2): p. 173-8.

189. Li, T., et al., *The synthesis of ethacrynic acid thiazole derivatives as glutathione S-transferase pi inhibitors.* Bioorg Med Chem, 2012. **20**(7): p. 2316-22.

190. Crawford, L.A. and E. Weerapana, *A tyrosine-reactive irreversible inhibitor for glutathione S-transferase Pi (GSTP1).* Mol Biosyst, 2016. **12**(6): p. 1768-71.

191. O'Brien, M.L., et al., *Glutathione peptidomimetic drug modulator of multidrug resistance-associated protein.* J Pharmacol Exp Ther, 1999. **291**(3): p. 1348-55.

192. McMillan, D.H., et al., *Attenuation of lung fibrosis in mice with a clinically relevant inhibitor of glutathione-S-transferase pi.* JCI Insight, 2016. **1**(8).

193. Raza, A., et al., *Phase 1-2a multicenter dose-escalation study of ezatiostat hydrochloride liposomes for injection (Telintra, TLK199), a novel glutathione analog prodrug in patients with myelodysplastic syndrome.* J Hematol Oncol, 2009. **2**: p. 20.

194. Tew, J.Z.-W.Y.J.-H.M.T.D., *Development of Telintra as an Inhibitor of Glutathione S-Transferase P.* Reactive Oxygen Species, 2020. **264**.

195. Miyanaga, N., et al., *Prostate cancer chemoprevention study: an investigative randomized control study using purified isoflavones in men with rising prostate-specific antigen.* Cancer Sci, 2012. **103**(1): p. 125-30.

196. Nagata, C., et al., *Soy intake and breast cancer risk: an evaluation based on a systematic review of epidemiologic evidence among the Japanese population.* Jpn J Clin Oncol, 2014. **44**(3): p. 282-95.

197. Jian, L., et al., *Protective effect of green tea against prostate cancer: a case-control study in southeast China.* Int J Cancer, 2004. **108**(1): p. 130-5.

198. Roh, J.L., et al., *Piperlongumine selectively kills cancer cells and increases cisplatin antitumor activity in head and neck cancer.* Oncotarget, 2014. **5**(19): p. 9227-38.

199. Harshbarger, W., et al., *Structural and Biochemical Analyses Reveal the Mechanism of Glutathione S-Transferase Pi 1 Inhibition by the Anti-cancer Compound Piperlongumine.* J Biol Chem, 2017. **292**(1): p. 112-120.

200. Mohammad, J., et al., *Piperlongumine potentiates the effects of gemcitabine in in vitro and in vivo human pancreatic cancer models.* Oncotarget, 2018. **9**(12): p. 10457-10469.

201. Hang, W., et al., *Piperlongumine and p53-reactivator APR-246 selectively induce cell death in HNSCC by targeting GSTP1.* Oncogene, 2018. **37**(25): p. 3384-3398.

202. Tanaka, T., et al., *Chemoprevention of 4-nitroquinoline 1-oxide-induced oral carcinogenesis by dietary curcumin and hesperidin: comparison with the protective effect of beta-carotene.* Cancer Res, 1994. **54**(17): p. 4653-9.

203. Huang, M.T., et al., *Inhibitory effects of dietary curcumin on forestomach, duodenal, and colon carcinogenesis in mice.* Cancer Res, 1994. **54**(22): p. 5841-7.

204. Duvoix, A., et al., *Induction of apoptosis by curcumin: mediation by glutathione S-transferase P1-1 inhibition.* Biochem Pharmacol, 2003. **66**(8): p. 1475-83.

205. De Luca, A., et al., *A novel orally active water-soluble inhibitor of human glutathione transferase exerts a potent and selective antitumor activity against human melanoma xenografts.* Oncotarget, 2015. **6**(6): p. 4126-43.

206. Luisi, G., et al., *Nitrobenzoxadiazole-based GSTP1-1 inhibitors containing the full peptidyl moiety of (pseudo)glutathione.* J Enzyme Inhib Med Chem, 2016. **31**(6): p. 924-30.

207. De Luca, A., et al., *The nitrobenzoxadiazole derivative MC3181 blocks melanoma invasion and metastasis.* Oncotarget, 2017. **8**(9): p. 15520-15538.

II. A META-ANALYSIS OF GST PROTEIN EXPRESSION IN MAMMALIAN ORGANS AND THEIR PROGNOSTIC IMPACTS ON THE SURVIVAL OF CANCER PATIENTS[2]

Abstract

Glutathione S-transferase (GST) enzymes are key components of the antioxidant system. Recent evidence shows that these proteins play essential roles in carcinogenesis by contributing to cancer cell survival, proliferation, and cell signaling. Although GST proteins are ubiquitously expressed, mammalian organs have unique expression patterns. Moreover, it has been reported that neoplastic tissues show higher expression of some GST isoforms. In the present study, using publicly available datasets, we investigated the mRNA expression of GST isozymes in different mammalian organs and compared their relative abundance in normal and neoplastic tissues. We report that GST isoforms are differentially expressed in human organs. Further, some GST isoforms are overexpressed in human cancer tissues. We additionally found that overexpression of some GST isoforms is negatively correlated with survival post-diagnosis for cancer patients.

Introduction

Glutathione S-transferases (GSTs) are found in most life forms and are ubiquitously expressed by most mammalian cells [1]. However, different cell types and mammalian tissues express varying levels of GST proteins [2, 3]. Therefore, in mammals, every organ presents a unique protein expression profile for GSTs. The complicated themes of organ-specific GST isozyme expression teamed up with the isozyme specificity for the substrate determine the detoxification potential of various organs for xenobiotic detoxification and their susceptibility to chemical carcinogenesis [4, 5]. These expression profiles were characteristic of particular tissue

[2] The content of this chapter is based in part on the following references:
Singh, R.R.; Reindl, K.M. Glutathione S-Transferases in Cancer. Antioxidants (2021), 10, 701.
R.R.S. and K.M.R. conceived the review. R.R.S. searched for previously published literature and selected studies for citations. R.R.S. wrote the manuscript with the supervision of K.M.R. All authors have read and agreed to the published version of the manuscript.

types, and the tissue specificity of GST expression was found to be consistent in organs from different individuals [6].

GST proteins are of particular interest among cancer biologists because many isozymes are expressed at higher levels in various neoplastic tissues than the surrounding healthy tissues [7-10]. Further, some GST isozymes, such as GST Pi-1 (GSTP1), are overexpressed in drug-resistant cell lines and tumors [11-13]. However, the immediate involvement of GST isozymes with chemotherapy resistance is not well explained. With the established roles of GST proteins in cell survival [14], proliferation [7], and apoptosis [15], it is speculated that these proteins indirectly contribute to drug resistance.

We postulate that GST isozymes show varying mRNA expression in different mammalian tissues and have higher mRNA expression in neoplastic tissues compared to the healthy tissues. Moreover, we speculate that overexpression of GST isozymes is correlated with poor patient survival post-diagnosis and dismal overall outcomes for cancer patients.

Methods

To compare the GST isoform expression in different human organs and normal versus the cancer tissue, we retrieved the publicly available Gene Expression Omnibus (GEO) datasets submitted in the National Institutes of Health-National Center for Biotechnology Information (NIH-NCBI). The fragments per kilobase of transcript per million mapped reads (FPKM) values of GST isoforms for different groups were plotted as jitter plot (for different human organs) and dotplot (for normal and cancer tissues) using the ggplot function in RStudio. To investigate the survival outcome of GST overexpression in cancer patients, we retrieved the publicly available FPKM values for GST genes and the respective patient survival probability from The Human

Protein Atlas. We examined the correlation between expression level and patient survival by plotting the Kaplan-Meier survival plots.

Results

GSTs vary in expression in different organs

The expression of GST proteins in different organs was analyzed using publically available Gene Expression Omnibus (GEO) datasets. These datasets compare the mRNA expression of GST proteins in various adult human organs. Analysis of the publicly available GEO dataset, GDS1096, revealed that *GSTA1* (Figure 2.1A) is highly expressed in brain tissues and kidneys in normal individuals. In the same dataset, we also noted that *GSTK1* (Figure 2.1B) and *GSTM1* (Figure 2.1C) are abundantly expressed in hepatic tissues. However, the highest levels of *GSTP1* mRNA are found in extra-hepatic tissues (Figure 2.1D).

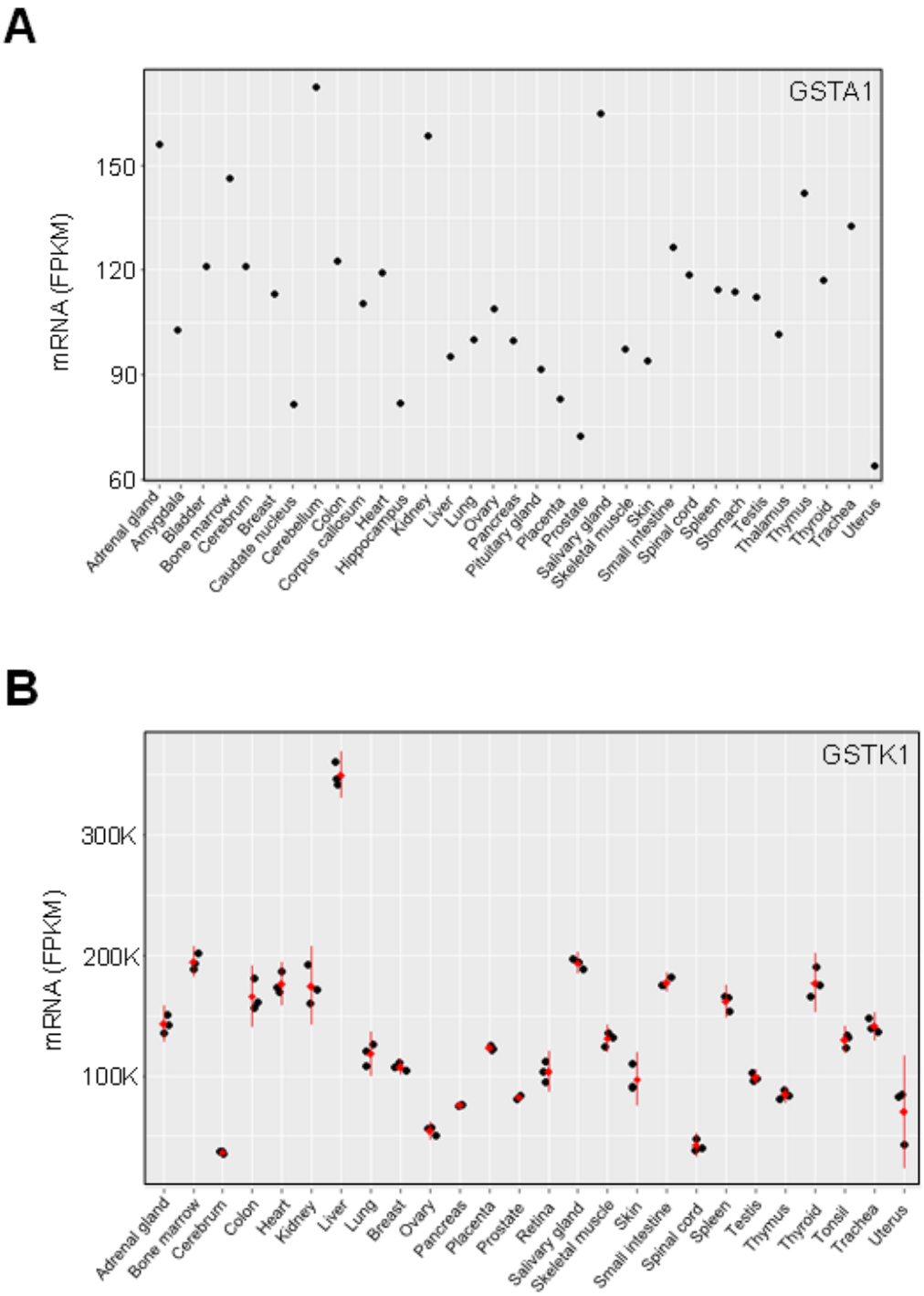

Figure 2.1. Glutathione S-transferases (GSTs) vary in expression in different human organs. Jitter plot showing the distribution of A) GSTA1, B) GSTK1, C) GSTM1, and D) GSTP1 in different human organs. The average of three technical replicates for GSTK1 and GSTP1 are shown in red.

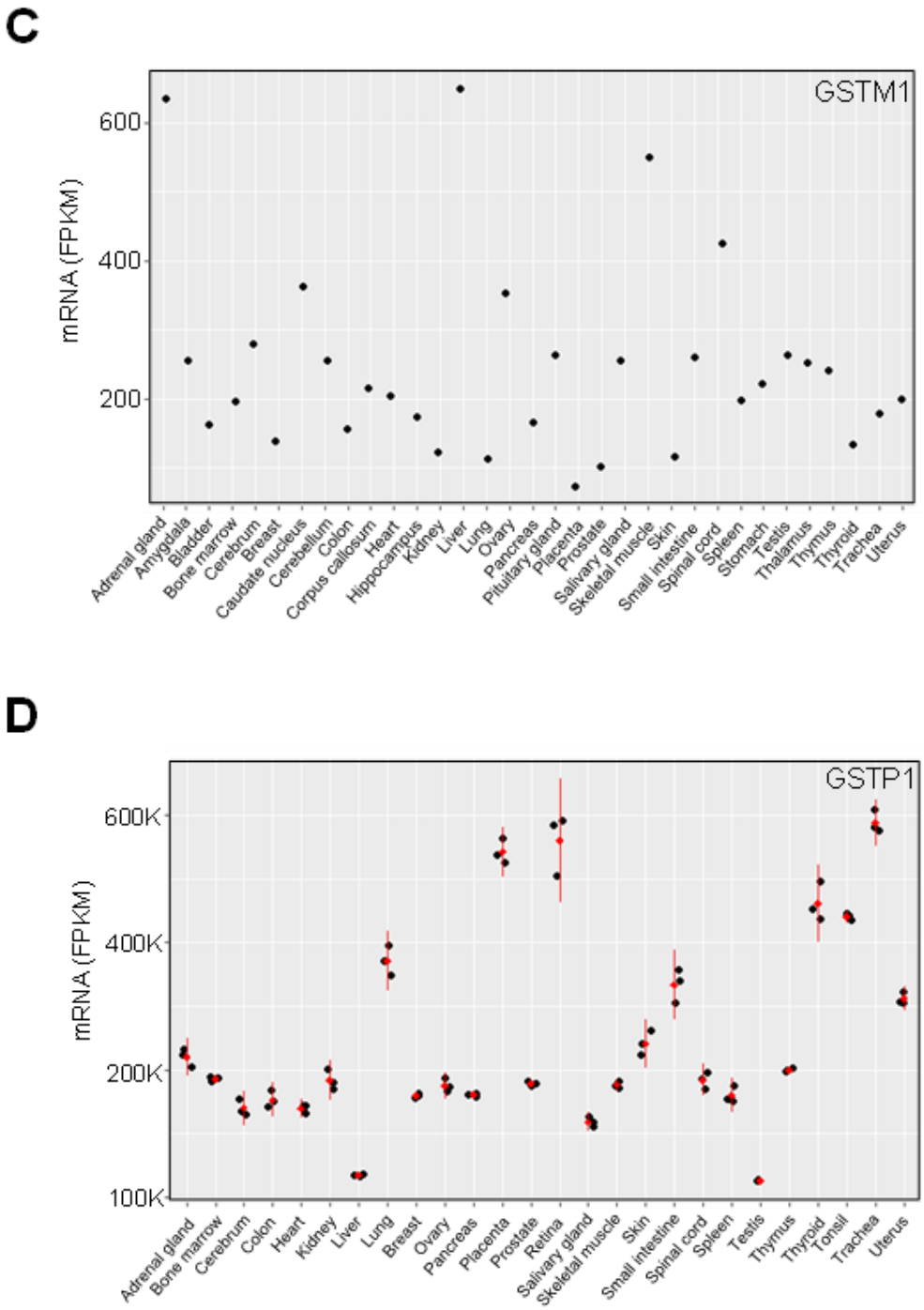

Figure 2.1. Glutathione S-transferases (GSTs) vary in expression in different human organs (continued). Jitter plot showing the distribution of A) GSTA1, B) GSTK1, C) GSTM1, and D) GSTP1 in different human organs. The average of three technical replicates for GSTK1 and GSTP1 are shown in red.

Some GST isoforms are overexpressed in human cancer

We compared the mRNA levels of different *GST* isoforms in human cancer and healthy tissues in the publicly available Gene Expression Omnibus (GEO) datasets. We found that *GSTP1* is significantly overexpressed in gastric (Figure 2.2A) and colorectal cancers (Figure 2.2B) compared to the respective healthy tissues (GDS1210 and GDS4382, respectively). Similarly, we report that *GSTK1* is overexpressed in prostate (Figure 2.2C) and pancreatic ductal adenocarcinoma (PDAC) (Figure 2.2D) tissues (GDS4824 and GDS4102, respectively). However, we did not find significant overexpression of *GSTP1* in head and neck (Figure 2.3A), and nasopharyngeal cancers (Figure 2.3B) (GDS2520 and GDS3341, respectively), *GSTM1* in head and neck cancers (Figure 2.3C) (GDS2520), and *GSTA1* in colorectal cancer tissues (Figure 2.3D) (GDS4382) compared to the respective healthy tissues.

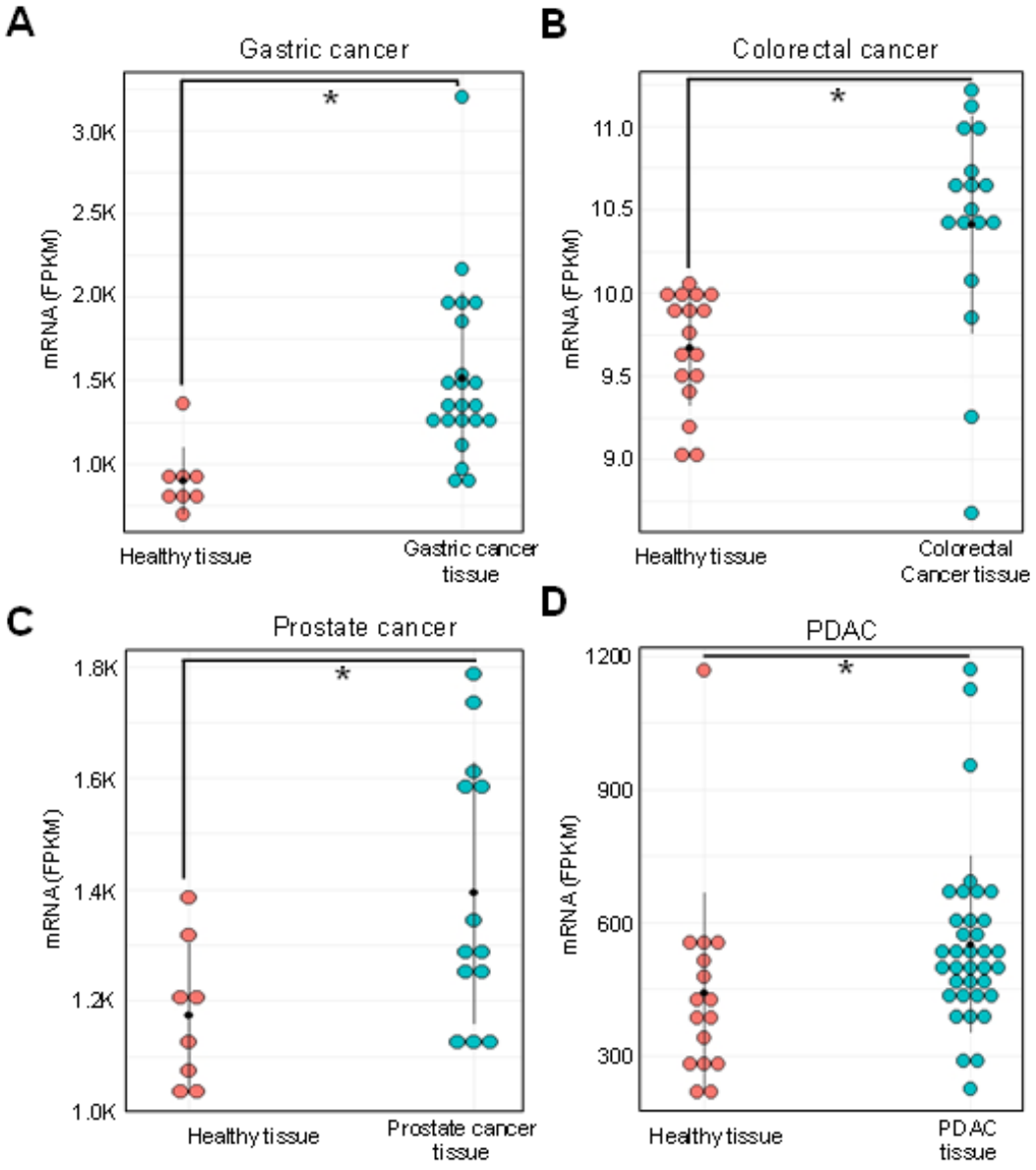

Figure 2.2. Some GSTs are overexpressed in neoplastic tissues. mRNA expression of different GST isoforms was compared in healthy tissue and the neoplastic tissues in the publicly available Gene Expression Omnibus (GEO) datasets. Student's t-test was used to analyze potential differences in GST mRNA expression in cancer tissue compared to the normal tissue. Significant changes in GST mRNA expression levels are denoted with * ($p < 0.05$). The data are shown for A) GSTP1 in gastric cancer, B) GSTP1 in colorectal cancer, C) GSTK1 in prostate cancer, and D) GSTK1 in pancreatic ductal adenocarcinoma (PDAC).

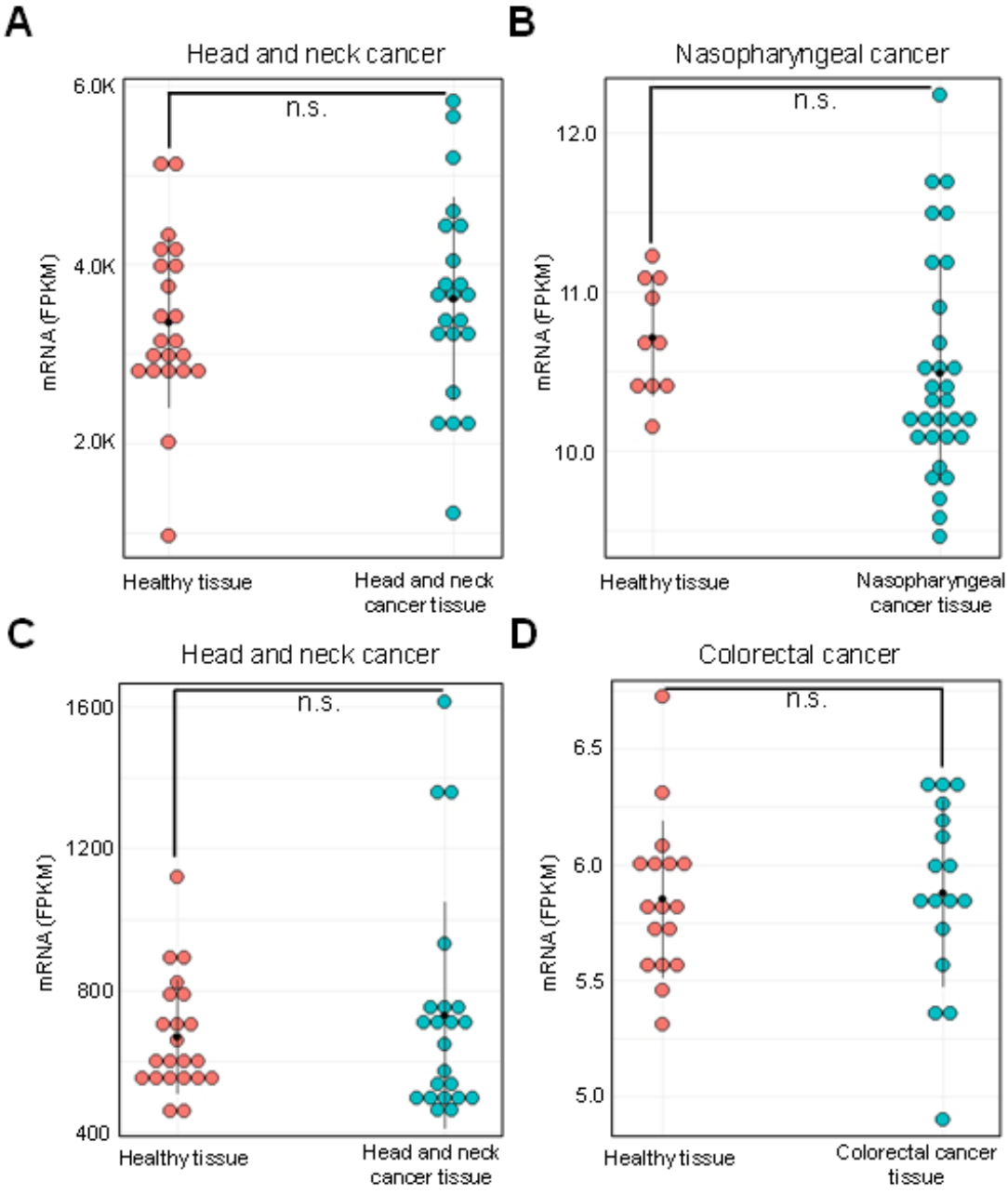

Figure 2.3. Some GST isoforms are not significantly overexpressed in neoplastic tissues. mRNA expression of different GST isoforms was compared in healthy tissue and the neoplastic tissues in the publicly available Gene Expression Omnibus (GEO) datasets. Student's t-test was used to analyze potential differences in GST mRNA expression in cancer tissue compared to the normal tissue. The data are shown for A) GSTP1 in head and neck cancer, B) GSTP1 in nasopharyngeal cancer, C) GSTM1 in head and neck cancer, and D) GSTA1 in colorectal cancer. n.s.: not significant.

Prognostic impact of GST protein expression

We determined that the overexpression of *GSTA1* is negatively correlated with patient survival post-diagnosis for renal (n = 877) (Figure 2.4A), stomach (n = 354) (Figure 2.4B), and endometrial (n = 541) (Figure 2.4C) cancer. Similarly, a negative correlation was identified between overexpression of *GSTK1* and patient survival for pancreatic cancer (n = 176) (Figure 2.4D), melanoma (n = 102) (Figure 2.4E), and glioma (n = 153) (Figure 2.4F) patients.

Further, identical correlations were found for *GSTM1* and *GSTP1* for glioma (n = 153) (Figure 2.4G), urothelial cancer (n = 406) (Figure 2.4H), ovarian cancer (n = 373) (Figure 2.4I), breast cancer (n = 1075) (Figure 2.4J), lung cancer (n = 994) (Figure 2.4K), and pancreatic cancer (n = 176) (Figure 2.4L) patients. However, poor patient survival with the overexpression of GST proteins is not uniformly corroborated. For example, high GSTP1 expression improved overall survival in epithelial ovarian cancer [16] and maxillary sinus squamous cell carcinoma patients from China [17]. Similarly, we found *GSTK1* overexpression is positively correlated with patient survival post-diagnosis for breast (n = 1075) (Figure 2.5A) and renal (n = 877) (Figure 2.5B) cancer.

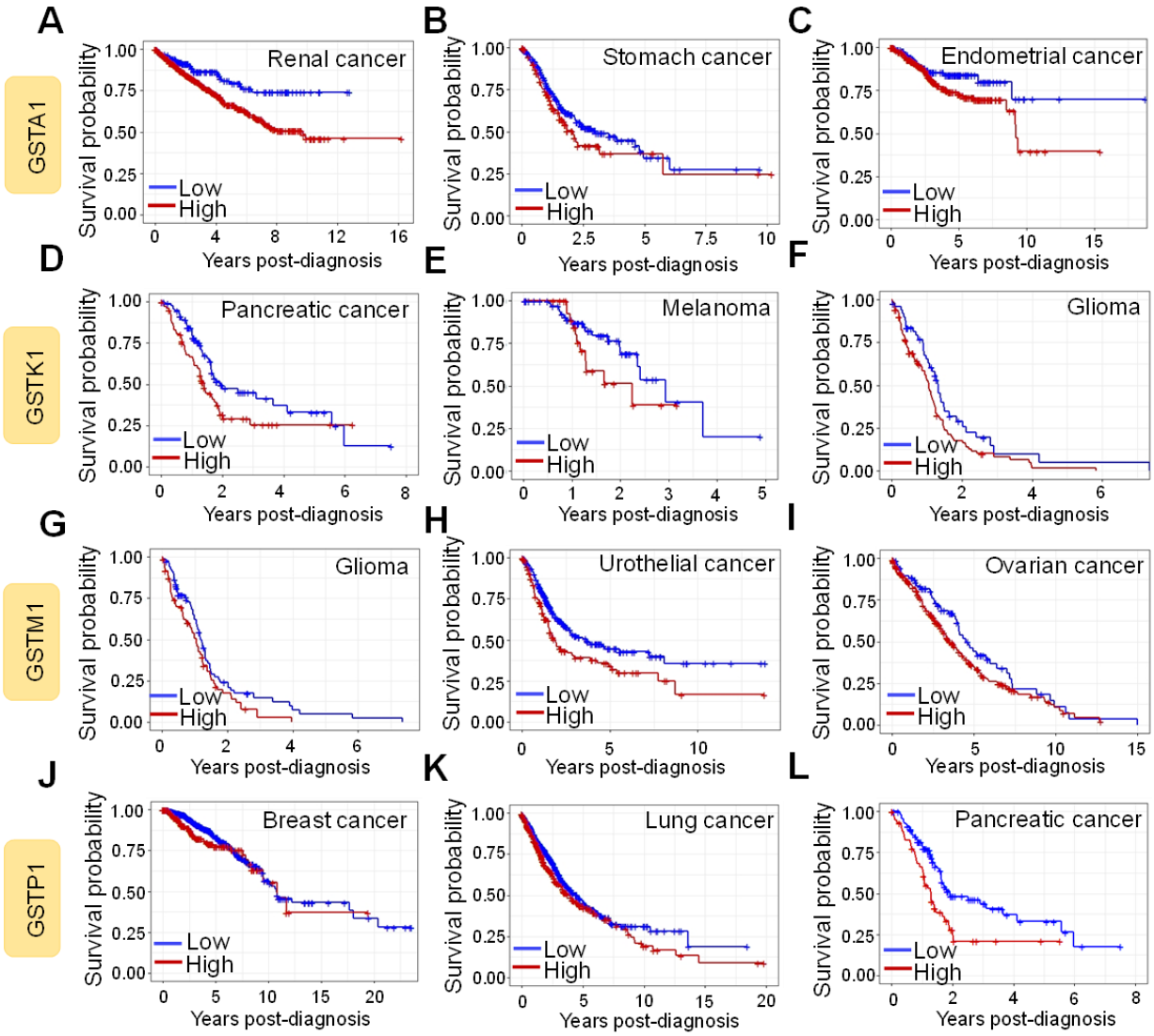

Figure 2.4. Expression of GST proteins is negatively correlated with patient survival for some human cancers. The Human Protein Atlas was mined for Glutathione S-transferase Alpha 1 (GSTA1) (A–C), Glutathione S-transferase Kappa 1 (GSTK1) (D–F), Glutathione S-transferase Mu 1 (GSTM1) (G–I), and Glutathione S-transferase Pi-1 (GSTP1) (J–L) mRNA expression in cancer patients relative to their corresponding years of survival post-diagnosis. The patients were divided in high- (red) and low- (blue) GST expressing groups. The Kaplan–Meier survival plots were constructed using survminer package in RStudio.

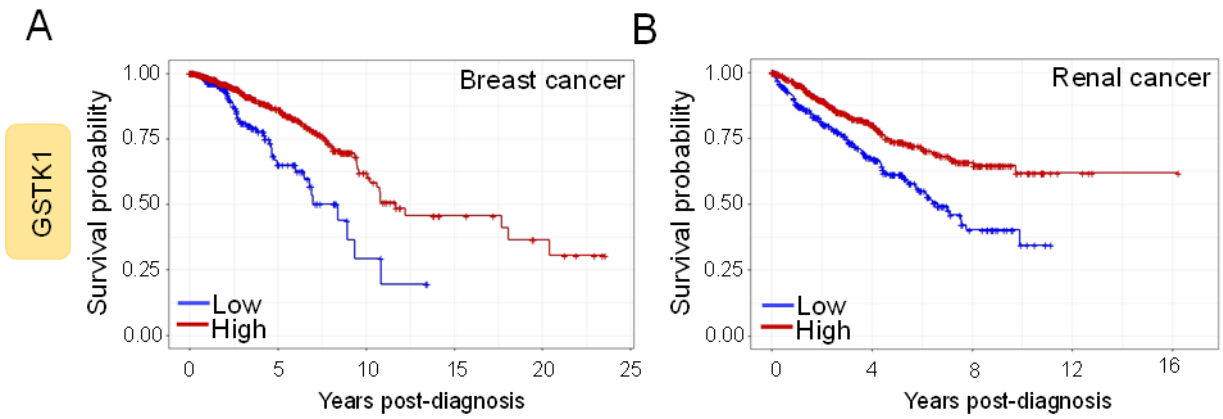

Figure 2.5. Expression of GST proteins is positively correlated with patient survival for some human cancers. The Human Protein Atlas was mined for Glutathione S-transferase Kappa 1 (GSTK1) expression in (A) breast and (B) renal cancer patients relative to their corresponding years of survival post-diagnosis. The patients were divided in high- (red) and low- (blue) GST expressing groups. The Kaplan–Meier survival plots were constructed using survminer package in RStudio.

Discussion

GSTs are a multigene family of eight isozymes [18]. GSTs are cytoprotective enzymes and are the primary components of the cellular antioxidant system [19]. In this study, we found that the mRNA of GST isoforms are expressed at varying levels in different human organs. Considering that GST proteins detoxify chemical carcinogens and are vital in maintaining cellular homeostasis, it is appealing to investigate how organ-specific dissimilarity in GST mRNA expression influences susceptibility to cancers. We found isoforms such as *GSTK1* and *GSTM1* were abundantly expressed in hepatic tissues. Given that liver is the epicenter for diverse physiological processes, including the catabolism of various xenobiotic compounds [20], it is not surprising to find some GST isozymes are overexpressed in hepatic tissues. However, other isozymes, such as *GSTP1*, were primarily found in extra-hepatic tissues. We found organs such as the cerebrum, breast, colon, ovaries, and testis show low expression of *GSTM1* and *GSTP1* proteins. We believe that the organs with lower GST activity are more susceptible to tumor development. Complementing our inference, Peters *et al*. demonstrated an inverse relationship between GST activity and cancer

incidence in the esophagus, stomach, and colon [21]. However, the interplay between the susceptibility of other human organs for tumor development and their unique GST isoform expression pattern is not clearly understood. We believe further epidemiological research is needed to comprehensively evaluate correlations between organ-specific GST expression, DNA damage, and carcinogenesis among populations.

The process of tumor development is coupled with hyperactive metabolism [22]. Consequently, byproducts of oxidative phosphorylation, such as reactive oxygen species (ROS), accumulate and cause DNA damage and senescence [23]. To counteract the oxidative stress, the cellular antioxidant system is often upregulated in cancer cells to scavenge the high ROS levels [24]. We found that GST isoforms such as *GSTK1* and *GSTP1* are overexpressed in neoplastic tissue compared to the surrounding healthy tissue. These observations are per the previous studies in ovarian cancer [25] and PDAC patients [7]. Others [14, 15, 26] and we [7] have previously shown that overexpression of GST proteins contributes to cell survival, proliferation, and prevents apoptosis. Additionally, significant evidence exists suggests that overexpression of GST isoforms, especially GSTP1, is associated with resistance to chemotherapy [27, 28]. Thus, we propose that GST proteins provide selective advantages to the cancer cells by maintaining cellular homeostasis and providing drug resistance.

Gene polymorphisms within the GST family of proteins are commonly reported in the human population [29]. Evidence suggests that the polymeric forms of GST proteins, most often arising from single-nucleotide polymorphisms (SNPs), have altered enzyme activity. This influences the detoxification of carcinogenic compounds, leads to the accumulation of DNA damage, and by implication, and increases the risk of cancer development [30, 31]. Although GST proteins are overexpressed in many tumor tissues, the analysis of the impact of their

overexpression on survival has generated differing results. We found that overexpression of some GST isoforms was negatively correlated with poor patient survival post-diagnosis. However, this observation was not uniform with all GST isoforms and all cancer types. The contrasting reports can be attributed to the patient population, polymeric forms of GST proteins [32], and treatment regime variations among the studies. Despite the lack of clarity on the impact of overactive GST proteins on the overall survival of cancer patients, there is a widespread consensus that higher expression of GST proteins drives tumor pathogenicity and results in poor outcomes [7, 14, 26, 33]. The conflicting data currently makes GST proteins an unreliable prognostic marker for cancer-patient survival.

References

1. Zhang, J., et al., *Pleiotropic functions of glutathione S-transferase P.* Adv Cancer Res, 2014. **122**: p. 143-75.

2. Chatterjee, A. and S. Gupta, *The multifaceted role of glutathione S-transferases in cancer.* Cancer Lett, 2018. **433**: p. 33-42.

3. Singh, S., *Cytoprotective and regulatory functions of glutathione S-transferases in cancer cell proliferation and cell death.* Cancer Chemother Pharmacol, 2015. **75**(1): p. 1-15.

4. Hayes, J.D. and D.J. Pulford, *The glutathione S-transferase supergene family: regulation of GST and the contribution of the isoenzymes to cancer chemoprotection and drug resistance.* Crit Rev Biochem Mol Biol, 1995. **30**(6): p. 445-600.

5. Dirven, H.A., B. van Ommen, and P.J. van Bladeren, *Glutathione conjugation of alkylating cytostatic drugs with a nitrogen mustard group and the role of glutathione S-transferases.* Chem Res Toxicol, 1996. **9**(2): p. 351-60.

6. Terrier, P., et al., *An immunohistochemical study of pi class glutathione S-transferase expression in normal human tissue.* Am J Pathol, 1990. **137**(4): p. 845-53.

7. Singh, R.R., et al., *Glutathione S-Transferase pi-1 Knockdown Reduces Pancreatic Ductal Adenocarcinoma Growth by Activating Oxidative Stress Response Pathways.* Cancers (Basel), 2020. **12**(6).

8. Kolwijck, E., et al., *GSTP1-1 in ovarian cyst fluid and disease outcome of patients with ovarian cancer.* Cancer Epidemiol Biomarkers Prev, 2009. **18**(8): p. 2176-81.

9. Simic, T., et al., *Glutathione S-transferases in kidney and urinary bladder tumors.* Nat Rev Urol, 2009. **6**(5): p. 281-9.

10. Sreenath, A.S., et al., *Evidence for the association of synaptotagmin with glutathione S-transferases: implications for a novel function in human breast cancer.* Clin Biochem, 2005. **38**(5): p. 436-43.

11. Mousseau, M., et al., *A study of the expression of four chemoresistance-related genes in human primary and metastatic brain tumours.* Eur J Cancer, 1993. **29A**(5): p. 753-9.

12. Geng, M., et al., *The association between chemosensitivity and Pgp, GST-pi and Topo II expression in gastric cancer.* Diagn Pathol, 2013. **8**: p. 198.

13. Wang, Z., et al., *Identification of proteins responsible for adriamycin resistance in breast cancer cells using proteomics analysis.* Sci Rep, 2015. **5**: p. 9301.

14. Louie, S.M., et al., *GSTP1 Is a Driver of Triple-Negative Breast Cancer Cell Metabolism and Pathogenicity.* Cell Chem Biol, 2016. **23**(5): p. 567-578.

15. Niitsu, Y., et al., *A CRAF/glutathione-S-transferase P1 complex sustains autocrine growth of cancers with KRAS and BRAF mutations.* Proc Natl Acad Sci U S A, 2020. **117**(32): p. 19435-19445.

16. Xu, L., et al., *Prognostic significance of several biomarkers in epithelial ovarian cancer: a meta-analysis of published studies.* J Cancer Res Clin Oncol, 2013. **139**(8): p. 1257-77.

17. Guo, G.F., et al., *[Correlation of GST-pi and PCNA expression to prognosis of advanced maxillary sinus squamous cell carcinoma].* Ai Zheng, 2005. **24**(10): p. 1267-71.

18. Hayes, J.D., J.U. Flanagan, and I.R. Jowsey, *Glutathione transferases.* Annu Rev Pharmacol Toxicol, 2005. **45**: p. 51-88.

19. Bocedi, A., et al., *Glutathione Transferase P1-1 an Enzyme Useful in Biomedicine and as Biomarker in Clinical Practice and in Environmental Pollution.* Nutrients, 2019. **11**(8).

20. Osterreicher, C.H. and M. Trauner, *Xenobiotic-induced liver injury and fibrosis.* Expert Opin Drug Metab Toxicol, 2012. **8**(5): p. 571-80.

21. Peters, W.H., et al., *Glutathione and glutathione S-transferases in Barrett's epithelium.* Br J Cancer, 1993. **67**(6): p. 1413-7.

22. Deberardinis, R.J., et al., *Brick by brick: metabolism and tumor cell growth.* Curr Opin Genet Dev, 2008. **18**(1): p. 54-61.

23. Takahashi, A., et al., *Mitogenic signalling and the p16INK4a-Rb pathway cooperate to enforce irreversible cellular senescence.* Nat Cell Biol, 2006. **8**(11): p. 1291-7.

24. Williamson, J.M., B. Boettcher, and A. Meister, *Intracellular cysteine delivery system that protects against toxicity by promoting glutathione synthesis.* Proc Natl Acad Sci U S A, 1982. **79**(20): p. 6246-9.

25. Ghalia, A.A., et al., *Estimation of glutathione S-transferase and its Pi isoenzyme in tumor tissues and sera of patients with ovarian cancer.* Anticancer Res, 2000. **20**(2B): p. 1229-35.

26. Checa-Rojas, A., et al., *GSTM3 and GSTP1: novel players driving tumor progression in cervical cancer.* Oncotarget, 2018. **9**(31): p. 21696-21714.

27. Ogino, S., et al., *Glutathione S-transferase Pi 1 is a valuable predictor for cancer drug resistance in esophageal squamous cell carcinoma.* Cancer Sci, 2019. **110**(2): p. 795-804.

28. Yang, M., et al., *CLDN6 promotes chemoresistance through GSTP1 in human breast cancer.* J Exp Clin Cancer Res, 2017. **36**(1): p. 157.

29. Economopoulos, K.P. and T.N. Sergentanis, *GSTM1, GSTT1, GSTP1, GSTA1 and colorectal cancer risk: a comprehensive meta-analysis.* Eur J Cancer, 2010. **46**(9): p. 1617-31.

30. McCarty, K.M., et al., *PAH-DNA adducts, cigarette smoking, GST polymorphisms, and breast cancer risk.* Environ Health Perspect, 2009. **117**(4): p. 552-8.

31. Was, J., et al., *The diagnostic potential of glutathione S-transferase (GST) polymorphisms in patients with colorectal cancer.* Adv Clin Exp Med, 2018. **27**(11): p. 1561-1566.

32. Gong, M., et al., *Genetic polymorphisms of GSTM1, GSTT1, and GSTP1 with prostate cancer risk: a meta-analysis of 57 studies.* PLoS One, 2012. **7**(11): p. e50587.

33. Harpole, D.H., Jr., et al., *The prognostic value of molecular marker analysis in patients treated with trimodality therapy for esophageal cancer.* Clin Cancer Res, 2001. **7**(3): p. 562-9.

III. GLUTATHIONE S-TRANSFERASE PI-1 KNOCKDOWN REDUCES PANCREATIC DUCTAL ADENOCARCINOMA GROWTH BY ACTIVATING OXIDATIVE STRESS RESPONSE PATHWAYS[3]

Abstract

Glutathione S-transferase pi-1 (GSTP1) plays an important role in regulating oxidative stress by conjugating glutathione to electrophiles. GSTP1 is overexpressed in breast, colon, lung, and prostate tumors, where it contributes to tumor progression and drug resistance; however, the role of GSTP1 in pancreatic ductal adenocarcinoma (PDAC) is not well understood. Using shRNA, we knocked down GSTP1 expression in three different PDAC cell lines and determined the effect on cell proliferation, cell cycle progression, and reactive oxygen species (ROS) levels. Our results show GSTP1 knockdown reduces PDAC cell growth, prolongs the G_0/G_1 phase, and elevates ROS in PDAC cells. Furthermore, GSTP1 knockdown results in the increased phosphorylation of c-Jun N-terminal kinase (JNK) and c-Jun and the decreased phosphorylation of extracellular signal-regulated kinase (ERK), p65, the reduced expression of specificity protein 1 (Sp1), and the increased expression of apoptosis-promoting genes. The addition of the antioxidant glutathione restored cell viability and returned protein expression levels to those found in control cells. Collectively, these data support the working hypothesis that the loss of GSTP1 elevates oxidative stress, which alters mitogen-activated protein (MAP) kinases and NF-κB signaling, and induces apoptosis.

[3] The content of this chapter is based in part on the following references:
Singh RR, Mohammad J, Orr M, Reindl KM. Glutathione S-Transferase pi-1 Knockdown Reduces Pancreatic Ductal Adenocarcinoma Growth by Activating Oxidative Stress Response Pathways. Cancers (Basel). 2020 Jun 9;12(6):1501.
R.R.S. and K.M.R. conceived and designed the study. All *in vitro* experiments were performed by R.R.S. *In vivo* experiments were performed by R.R.S. and J.M. M.O. performed the statistical analysis of the data. K.M.R. was responsible for the supervision and coordination of the project. All authors read and approve the final manuscript before submission.

In support of these *in vitro* data, nude mice bearing orthotopically implanted GSTP1-knockdown PDAC cells showed an impressive reduction in the size and weight of tumors compared to the controls. Additionally, we observed reduced levels of Ki-67 and increased expression of cleaved caspase-3 in GSTP1-knockdown tumors, suggesting GSTP1 knockdown impedes proliferation and upregulates apoptosis in PDAC cells. Together, these results indicate that GSTP1 plays a significant role in PDAC cell growth and provides support for the pursuit of GSTP1 inhibitors as therapeutic agents for PDAC.

Introduction

Pancreatic ductal adenocarcinoma (PDAC) is the third leading cause of cancer-related mortalities in the Western world and is responsible for more than 45,000 deaths per year in the US alone [1]. Less than 9% of PDAC patients survive for five years or more after diagnosis [2]. The conventional treatment approaches, such as chemotherapy, radiation therapy, surgery, and any combination of these, have had little impact on the course of this aggressive malignancy [3–6]. Therefore, new therapeutic strategies based on the unique molecular biology and physiology of pancreatic cancer are needed [7–9].

The constant need for cellular building blocks drives the overzealous metabolism in cancer cells [10]. As a result, abundant byproducts such as reactive oxygen species (ROS) and reactive nitrogen species persistently accumulate and dysregulate cellular homeostasis, causing DNA damage and inducing senescence [11, 12]. To maintain optimal redox balance in the cells, efficient and counteractive antioxidant machinery is required. Glutathione (GSH), nicotinamide adenine dinucleotide phosphate (NADPH), and redox regulatory proteins such as thioredoxin reductase and thioredoxin constitute the antioxidant enzyme system and scavenge the high levels of ROS [13].

Glutathione S-transferase pi-1 (GSTP1) is a principal component of the antioxidant system [14]. It plays a cytoprotective role by catalyzing the conjugation reaction of reduced glutathione (GSH) to reactive electrophiles generated by cytochrome P450 metabolism [15]. GSTP1 is ubiquitously expressed in mammalian tissues and is overexpressed in human tumors of diverse anatomic origin [16, 17], as well as in a wide variety of drug-resistant cell lines [18]. In addition to its role in cellular detoxification and glutathionylation, GSTP1 regulates stress-induced signaling by binding to and inhibiting the phosphorylation of c-Jun N-terminal kinase (JNK) [19]. Additionally, GSTP1 was recently shown to modulate glycolytic metabolism in breast cancer cells by enhancing Glyceraldehyde-3-phosphate dehydrogenase (GAPDH) activity [20]. These, and additional literature [15, 21–23], suggest that GSTP1 plays versatile roles in cancer cell survival, signaling mechanisms, and metabolism. With its established roles in breast [20] and cervical cancer [24], we postulate that overexpression of GSTP1 provides selective advantages to PDAC cells by scavenging elevated ROS and maintaining cellular homeostasis. In this present study, we provide evidence suggesting that GSTP1 contributes to pancreatic cancer cell growth and holds promise as a therapeutic target for PDAC.

Materials and methods

Chemicals

Puromycin was purchased from Sigma-Aldrich, St. Louis, MO, USA. A CellTiter-Glo® luminescent cell viability assay kit was purchased from Promega, Madison, WI, USA. Ki67 antibody was purchased from Vector Labs, Burlingame, CA, USA. GSTP1 antibody was obtained from Santa Cruz Biotechnology, Dallas, TX, USA. Antibodies to GAPDH, β-actin, phospho-JNK (Thr 183/Tyr 185), total JNK, p65, pERK, total ERK, cleaved caspase-3, total caspase-3, phospho-c-Jun (Ser 73), total c-Jun, and Sp1 were obtained from Cell Signaling Technology, Danvers, MA,

USA. Horseradish peroxidase (HRP)-linked anti-mouse and anti-rabbit IgG secondary antibodies were obtained from Cell Signaling Technology. CF633-conjugated goat anti-mouse IgG secondary antibody was obtained from Biotium, Fremont, CA, USA. CM-H_2DCFDA was purchased from Life Technologies, Carlsbad, CA, USA. Glutathione was purchased from Calbiochem, Burlington, MA, USA.

Cell culture

Human PDAC cell lines (MIA PaCa-2, PANC-1, HPAF-II, AsPC-1, and BxPC-3) were obtained from American Type Culture Collection, Manassas, VA, USA. hTERT-HPNE cells were obtained from Dr. Channing Der's laboratory at UNC, Chapel Hill, NC. MIA PaCa-2 cells were cultured in DMEM (Dulbecco's Modified Eagle Medium) high-glucose media (GE Healthcare Life Sciences, Chicago, IL, USA) containing 10% (v/v) fetal bovine serum (Atlanta Biologicals, Flowery Branch, GA, USA) and 2.5% (v/v) horse serum (Corning, Corning, NY, USA). PANC-1 cells were cultured in DMEM high-glucose media containing 10% (v/v) FBS. HPAF-II cells were cultured in Eagle's Minimum Essential Medium (EMEM) (Corning, Corning, NY, USA) containing 10% v/v Fetal Bovine Serum (FBS). AsPC-1 were cultured in RPMI-1640 (GE Healthcare Life Sciences) containing 10% FBS (v/v). Cells were maintained at 37°C with 5% CO2. The cell lines were subcultured by enzymatic digestion with 0.25% trypsin/1 mM EDTA solution (GE Healthcare Life Sciences, Chicago, IL, USA) when they were 80% confluent. All cell lines tested negative for Mycoplasma contamination.

Constructing knockdown cell lines

We used two independent short-hairpin oligonucleotides to knock down the expression of GSTP1. Lentiviral particles containing the shRNA (Sigma, St. Louis, MO, USA, catalogue# SHCLNV-NM_000852) were used to infect the target PDAC cell lines with polybrene (Sigma-

Aldrich, St. Louis, MO, USA). Transfected cells were selected over five days with 5 µg/ml puromycin. The short-hairpin sequences used to achieve the knockdown of GSTP1 expression were: shGSTP1-1, CCGGCCTCACCCTGTACCAGTCCAACTCGAGTTGGACTGGTACA GGGTGAGGTTTTG; shGSTP1-2, CCGGCGCTGACTACAACCTGCTGGACTCGAGT CCAGCAGGTTGTAGTCAGCGTTTTTG. Scrambled GSTP1 shRNA, empty vector (pLKO.1), and shRNA targeting GFP were used as controls. Knockdown was confirmed by qRT-PCR and western blotting techniques.

Western blotting

Cells and tissues were lysed in lysis buffer (Promega, Madison, WI, USA) containing both protease and phosphatase inhibitors. Denatured proteins were resolved on 11% SDS-polyacrylamide gel and transferred to nitrocellulose membrane (AmershamTM ProtranTM 0.2µM, GE Healthcare Life Sciences, Chicago, IL, USA) using the wet electroblotting system (BioRad, Hercules, CA, USA). Blots were blocked using 5% BSA in Tris-buffered saline containing Tween 20 (TBS-T) solution for 1 h at room temperature, washed in TBS-T, and probed with primary antibody overnight at 4 °C. Following washes with TBS-T, the blots were incubated with HRP-linked secondary antibody at room temperature for 1 h. Blots were treated with SuperSignal West Femto Maximum Sensitivity Substrate (Thermo Scientific, Waltham, MA, USA) and visualized using FluorChem FC2 imaging system. The expression levels were quantified using ImageJ software. The data represent average ± standard deviation for three independent experiments.

RNA extraction and gene expression by qRT-PCR

Total RNA was extracted using SurePrep TrueTotal RNA purification kit (Carlsbad, CA, USA) following the manufacturer's instructions. cDNA was synthesized using 500 ng of total RNA and the qScript cDNA synthesis kit (Quanta Biosciences, Beverly, MA, USA). Steady-state

RNA levels were determined as described elsewhere [60]. The relative change in gene expression was calculated using the 2−ΔΔCt method [61]. HPRT, β-actin, and β-tubulin were used as internal controls. The data represent the average ± standard deviation for three independent experiments with two technical replicates each. The primer sequences of the genes analyzed are listed in Table 3.1.

Table 3.1. Primer sequences used for measuring mRNA expression via quantitative polymerase chain reaction.

Gene	Forward Sequence	Reverse Sequence
HPRT	5'-GAA CGT CTT GCT CGA GAT GTG-3′	5'TCC AGC AGG TCA GCA AAG AAT-3'
β-Actin	5'-TTG CCG ACA GGA TGC AGA-3′	5'-GCC GAT CCA CAC GGA GTA CTT-3'
β-Tubulin	5'-GTT CGC TCA GGT CCT TTT GG-3′	5'-CCC TCT GTG TAG TGG CCT TTG-3'
GSTP1	5'-CAG GAG GGC TCA CTC AAA GC-3′	5'-AGG TGA CGC AGG ATG GTA TTG-3'
CDKN1A	5'-GGA CAG CAG AGG AAG ACC ATG T-3′	5'-GCC GTT TTC GAC CCT GAG A-3'
HMOX-1	5'-AAT TCT CTT GGC TGG CTT CCT-3′	5'-CAT AGG CTC CTT CCT CCT TTC C-3'
Bax	5′-TTG CTT CAG GGT TTC ATC CA-3′	5′-ACA CTC GCT CAG CTT CTT G-3′
Bak	5′-ACA TCA ACC GAC GCT ATG AC-3′	5′-TGG TGG CAA TCT TGG TGA A-3′
Bcl2	5′-CGC CCT GTG GAT GAC TGA GTA-3′	5′-CCT CAG CCC AGA CTC ATC A-3′

Cell viability assay

MIA PaCa-2, PANC-1, and HPAF-II cells (3000/well) were seeded in 96-well plates. The viability of control and GSTP1 knockdown cells after 24, 48, 72, and 96 h was evaluated by adding 100 µl of CellTiter-Glo® substrate to each well containing 100 µL of media. The plates were incubated for ten min at room temperature. The endpoint luminescence was measured using Synergy H1 Hybrid multi-mode plate reader (Winooski, VT, USA) located in the Core Biology Facility, Chemistry and Molecular Biology, North Dakota State University. The gain was maintained at 135 and the integration time of 1 second using the Gen5 v2.07 software. The data represent the average ± standard deviation of three independent experiments with eight technical replicates for each treatment.

Cell cycle arrest assay

Control and GSTP1 knockdown PDAC cell lines (MIA PaCa-2, PANC-1, and HPAF-II) were seeded in 6-well plates and incubated for 24 h. Cells were synchronized overnight using serum-free medium and harvested by trypsinization, washed, and re-suspended in 70% ethanol overnight at 4°C. Finally, 70% ethanol was removed, and cells were re-suspended in PBS containing 50 µg/mL propidium iodide (VWR Life Technologies) and 1 µg/mL RNase A (Biotium, Fremont, CA, USA). Flow cytometry was performed using BD Accuri C6 equipment to determine the cell population in each phase of the cell cycle. The data represent the average ± standard deviation of three independent experiments with three technical replicates for each treatment.

Detection of ROS levels by the 2,7-dichlorodihydrofluorescein diacetate (CM-H_2DCFDA) assay

Control and GSTP1 knockdown MIA PaCa-2 and HPAF-II cells were resuspended in 20 µM CM-H_2DCFDA (Life Technologies) in PBS and incubated at 37 ℃ for 30 min before flow cytometric analysis using a BD Accuri C6. Three technical replicates were included for each experiment, and the experiments were performed in biological triplicates for each cell line. FLOWJO software was used to create histograms. The data represent the average ± standard deviation of three independent experiments with three technical replicates for each treatment.

Orthotopic tumor studies

All animal experimental procedures were performed abiding by the protocol approved by North Dakota State University's Institutional Animal Care and Use Committee (IACUC). Six- to eight-week-old female athymic nude mice (nu/nu) were purchased from The Jackson Laboratory (Bar Harbor, ME, USA). The mice were maintained in sterile conditions using individually

ventilated cage (IVC) racks (Allentown and Innovive). The mice were acclimated for 1 week before tumor implantation. PDAC cells were washed twice with PBS, trypsinized, and harvested in serum-containing medium. Harvested cells were washed with serum-free medium and resuspended in PBS. Mice were anesthetized using 3% isoflurane. A small incision was made in the left abdominal flank and control or GSTP1 knockdown cells (7.5 × 105 in 25 µL) were injected into the pancreas using a 27-gauge needle. The abdomen was closed using chromic catgut and ethilon sutures by a 2-layer suture technique. Animals were monitored every day for their food and water intake and for the signs of distress and pain. The tumor volumes were estimated every ten days by abdominal ultrasounds. The mice in the HPAF-II experimental group were euthanized earlier than the previously planned endpoint, as the tumor volumes in the control group were approaching the highest acceptable values as defined in the IACUC protocol. Humane endpoints defined for removing animals from the project were: (1) if/when the tumor burden was estimated to be more than 10–15% of their body weight, if mice demonstrated significant signs of distress or pain, (2) if the tumor interfered with ambulation, if mice exhibited decreased eating or drinking, or (3) if they showed signs of infection [62]. After 4 weeks (HPAF-II group) or 6 weeks (MIA PaCa-2 and PANC-1), animals were euthanized using a CO_2 chamber (Quietek Model 1, Next Advantage, Troy, NY) that regulates the flow of CO_2 in the chamber at a rate of 10–30% of the chamber volume per minute. The equipment will not exceed 30% of the chamber volume per minute. These flow rates are compliant with the AVMA regulations for euthanasia of laboratory mice. Animal death was subsequently verified by cervical dislocation. The primary tumor in the pancreata was excised and measured for weight. Each tumor was paraformaldehyde fixed and paraffin embedded for immunohistochemistry. The data represent the average ± standard deviation for the biological replicates.

Ethics approval and consent to participate: All the animal experimental procedures were approved by North Dakota State University's Institutional Animal Care and Use Committee (protocol number: A17062). The permitted study period on the protocol was from May-2017 to April-2020. North Dakota State University maintains a Registration with the United Stated Department of Agriculture (45-R-002) and an Animal Welfare Assurance with the National Institute of Health-Office of Laboratory Animal Welfare (D16-00156).

Murine abdominal ultrasound imaging

The growth of pancreatic tumors was monitored via abdominal ultrasound imaging every ten days for all animals in the treatment groups (for the HPAF-II group, last ultrasound was performed on D27). A FUJIFILM Vevo3100 ultrasound imaging system (Toronto, ON, Canada) was used to image the pancreata. The animals were anesthetized using 3% isoflurane and were maintained at 2% isoflurane for the course of ultrasound. To support the optimal physiological conditions, mice were kept on the platform maintained at 37 °C. Intraperitoneal administration of 2 mL saline was performed to achieve a higher resolution of abdominal organs. Mice were retained in the supine position and the tumor volumes were calculated using an Mx250 transducer and Vevo Lab Software. The data represent the average ± standard deviation for the biological replicates.

Immunohistochemistry

Tumor tissues were collected and fixed for 24 h in formaldehyde. Paraffin-embedded 5-μm-thick sections of tumor tissues were prepared. Sections were deparaffinized with Histo-Clear and ethanol, followed by antigen retrieval in 10 mM sodium citrate buffer (0.05% Tween 20, pH 6.0) using an autoclave method. The sections were blocked for 20 min in blocking buffer (10% normal goat serum in TBS-T) and incubated with Ki67 (1:100) or cleaved caspase-3 (1:100) overnight at 4 °C. The following day, sections were incubated with CF633-conjugated goat anti-

mouse secondary antibody (1:250) for 1 h at room temperature. After mounting a coverslip using Hardset Mounting Medium with 4′,6-diamidino-2-phenylindole (DAPI) (Vector Labs, Burlingame, CA, USA), slides were visualized using a Zeiss inverted Axio Observer Z1 microscope. The percentage of Ki67- or cleaved caspase-3-positive cells was measured based on the number of pink-stained cells relative to the number of blue DAPI-stained nuclei. Immunohistochemistry was performed for all the tumor samples from different treatment groups. The data represent the average ± standard deviation for the biological replicates.

Statistical analyses

All outcome variables were analyzed using fixed-effects linear models with analysis of variance. For relative GSTP1 expression in different human PDAC cell lines, different cell lines and experimental replicate were the factors. Cell viability was analyzed separately for each PDAC cell line with knockdown line, time, and experimental replicate as the factors. The live and the dead cell population in the scrambled controls of three different cell lines were compared to the same populations in the GSTP1 knockdown cells. The G_0/G_1 and G_2/M populations of scrambled controls were compared to the same populations in GSTP1 knockdown cells. Relative protein expressions of p-JNK, p-ERK, and p-p65 in GSTP1 knockdown cells were analyzed with protein, knockdown line, and experimental replicate as the factors. The relative expression of phosphorylated proteins was compared to total proteins. Relative cleaved caspase-3 expressions were analyzed separately for PDAC cell lines with knockdown lines and experimental replicates as the factors. Pancreas volume was analyzed separately for each PDAC cell line, with knockdown line and day as the factors. Only the results for last ultrasound are presented. The relative tumor weight was analyzed separately for each PDAC cell line using fixed-effects models with knockdown lines as the factor. Welch's one-way analysis of variance was performed due to the

observed heterogeneity of variances. Relative tumor weight, Ki-67-positive cell population, and *in vivo* cleaved caspase-3 cell population were analyzed separately for each PDAC cell lines using fixed-effects models with knockdown lines as the factor. The Pearson correlation test was done to analyze the association between GSTP1 expression and the survival of patients, post-diagnosis of PDAC.

For any analysis in which an interaction effect was not significant, the interaction effect was dropped from the model for the final analysis. Post-hoc pairwise comparisons using Tukey were performed following significant findings in the overall analysis of variance. All analyses were performed using the MIXED procedure in SAS software version 9.4 (SAS Institute; Cary, NC, USA).

Results

GSTP1 is overexpressed in human PDAC cells

GSTP1 is expressed at high levels in many human cancers, including colon, lung, breast, and ovarian cancers [25]. A higher expression of GSTP1 is correlated with disease progression and resistance to chemotherapeutic drugs [18]. However, the expression of GSTP1 is not well documented in human PDAC cells and tissues. We investigated the expression of GSTP1 in various PDAC cell lines. Intriguingly, we show that GSTP1 is present at higher levels in pancreatic carcinoma cell lines (MIA PaCa-2, PANC-1, HPAF-II, AsPC-1, and BxPC-3) compared to normal Human Pancreatic Nestin-Expressing ductal cells (hTERT-HPNE) (Figures 3.1A and B). Additionally, we compared the GSTP1 mRNA levels in human PDAC and healthy pancreas tissues in the publicly available Gene Expression Omnibus (GEO) dataset (GDS4102/200824_at). We found that GSTP1 is significantly overexpressed in PDAC tissue compared to the healthy pancreas (Figure 3.1C). Furthermore, using gene expression and survival data from The Human Protein

Atlas [26], we determined that the overexpression of GSTP1 is negatively correlated with PDAC patient survival post-diagnosis (Figure 3.1D).

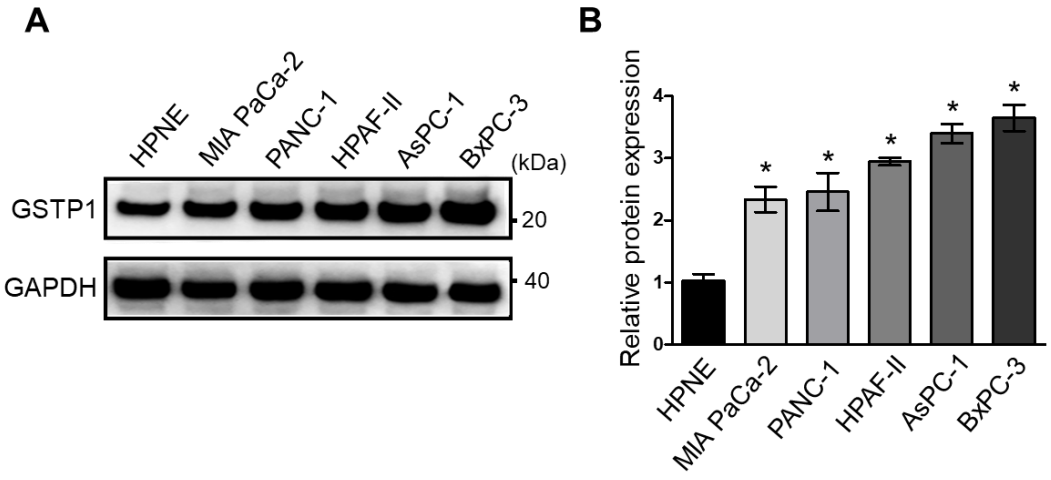

Figure 3.1. Glutathione S-transferase pi-1 (GSTP1) is overexpressed in human pancreatic ductal adenocarcinoma (PDAC) cells and tissues, and its expression is negatively correlated with patient survival. (A) GSTP1 expression in a normal pancreatic cell line (Human Pancreatic Nestin-Expressing ductal cells (hTERT-HPNE)) and a panel of human PDAC cell lines (MIA PaCa-2, PANC-1, HPAF-II, AsPC-1, and BxPC-3) was determined by western blotting. Glyceraldehyde-3-phosphate dehydrogenase (GAPDH) protein levels were used as loading control. The images are representative of three independent experiments. (B) GSTP1 expression in MIA PaCa-2, PANC-1, HPAF-II, AsPC-1, and BxPC-3 cells were compared to GSTP1 expression in hTERT-HPNE cells. Densitometry values were determined using ImageJ software and normalized to GAPDH values. Student's t-test was used to identify potential significant differences in expression in the tumor cell lines compared to hTERT-HPNE cells. Significant changes in GSTP1 protein expression are denoted with * ($p < 0.05$). (C) *GSTP1* mRNA expression was compared in normal pancreas and PDAC tissue in the Gene Expression Omnibus (GEO) dataset submitted by Liewei Wang *et al*. (2009). Student's t-test was used to analyze potential differences in *GSTP1* mRNA expression for PDAC tissue compared to normal pancreas tissue. Significant changes in *GSTP1* mRNA expression levels are denoted with * ($p < 0.05$). (D) The Human Protein Atlas was mined for *GSTP1* mRNA expression in PDAC patients ($n = 176$) relative to their corresponding years of survival post-diagnosis. The cut-off value of 327 FPKM was used to divide patients in high- (red) and low- (blue) *GSTP1*-expressing groups. The Kaplan–Meier survival plot was constructed in RStudio. FPKM: fragments per kilobase of transcript per million mapped reads. Unprocessed images for the western blotting results are shown in Figure S1.

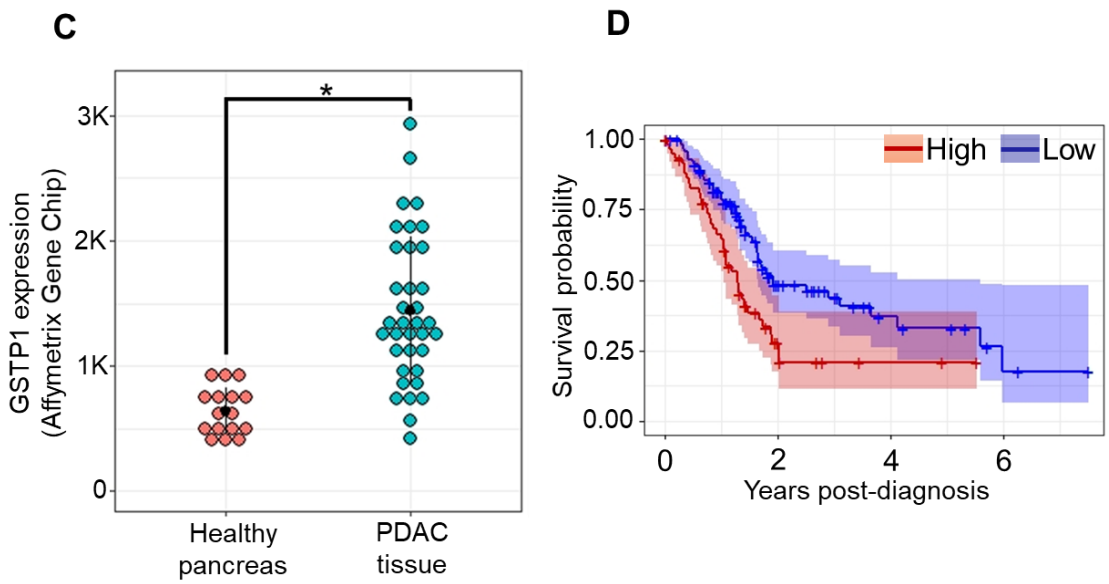

Figure 3.1. Glutathione S-transferase pi-1 (GSTP1) is overexpressed in human pancreatic ductal adenocarcinoma (PDAC) cells and tissues, and its expression is negatively correlated with patient survival (continued). (A) GSTP1 expression in a normal pancreatic cell line (Human Pancreatic Nestin-Expressing ductal cells (hTERT-HPNE)) and a panel of human PDAC cell lines (MIA PaCa-2, PANC-1, HPAF-II, AsPC-1, and BxPC-3) was determined by western blotting. Glyceraldehyde-3-phosphate dehydrogenase (GAPDH) protein levels were used as loading control. The images are representative of three independent experiments. (B) GSTP1 expression in MIA PaCa-2, PANC-1, HPAF-II, AsPC-1, and BxPC-3 cells were compared to GSTP1 expression in hTERT-HPNE cells. Densitometry values were determined using ImageJ software and normalized to GAPDH values. Student's t-test was used to identify potential significant differences in expression in the tumor cell lines compared to hTERT-HPNE cells. Significant changes in GSTP1 protein expression are denoted with * ($p < 0.05$). (C) *GSTP1* mRNA expression was compared in normal pancreas and PDAC tissue in the Gene Expression Omnibus (GEO) dataset submitted by Liewei Wang *et al*. (2009). Student's t-test was used to analyze potential differences in *GSTP1* mRNA expression for PDAC tissue compared to normal pancreas tissue. Significant changes in *GSTP1* mRNA expression levels are denoted with * ($p < 0.05$). (D) The Human Protein Atlas was mined for *GSTP1* mRNA expression in PDAC patients ($n = 176$) relative to their corresponding years of survival post-diagnosis. The cut-off value of 327 FPKM was used to divide patients in high- (red) and low- (blue) *GSTP1*-expressing groups. The Kaplan–Meier survival plot was constructed in RStudio. FPKM: fragments per kilobase of transcript per million mapped reads. Unprocessed images for the western blotting results are shown in Figure S1.

GSTP1 knockdown impairs PDAC cell growth

To elucidate the role of GSTP1 in PDAC cell survival, we developed two knockdown lines of GSTP1 (shGSTP1-1 and shGSTP1-2) in metabolically diverse human PDAC cells. MIA PaCa-2, PANC-1, and HPAF-II cells were transfected with GSTP1-specific shRNA and scrambled

shRNA control plasmid (scr-shRNA) as described in the Materials and methods section. MIA PaCa-2 and PANC-1 are mesenchymal in origin and lie towards the glycolytic end of the metabolic spectrum, while HPAF-II cells are epithelial and rely on lipolytic pathways for energy [27]. All these PDAC cells carry TP53 and KRAS mutations [28]. Following puromycin selection, the antibiotic-resistant cells were screened for GSTP1 knockdown by western blot and quantitative real-time (qRT)-PCR analysis. Both shGSTP1-1 and GSTP1-2 resulted in more than a 95% reduction in GSTP1 protein expression (Figures 3.2A and B) and mRNA expression (Figure 3.2C) in all the three cell lines. To determine if GSTP1 knockdown can impair the viability of PDAC cells, we conducted CellTiter-Glo® assays. We show that GSTP1 knockdown impairs cell viability for MIA PaCa-2, PANC-1 cells, and HPAF-II cells, by more than 50% for 72 and 96 hours (Figure 3.2D). Similarly, trypan blue exclusion assays showed that GSTP1 knockdown increased the percentage of dead cells for all three PDAC cell lines by 25–30% compared to the control (Figure 3.2E). Supporting these results, we also show that GSTP1 knockdown reduces the clonogenic survival of PDAC cells (Figure S2).

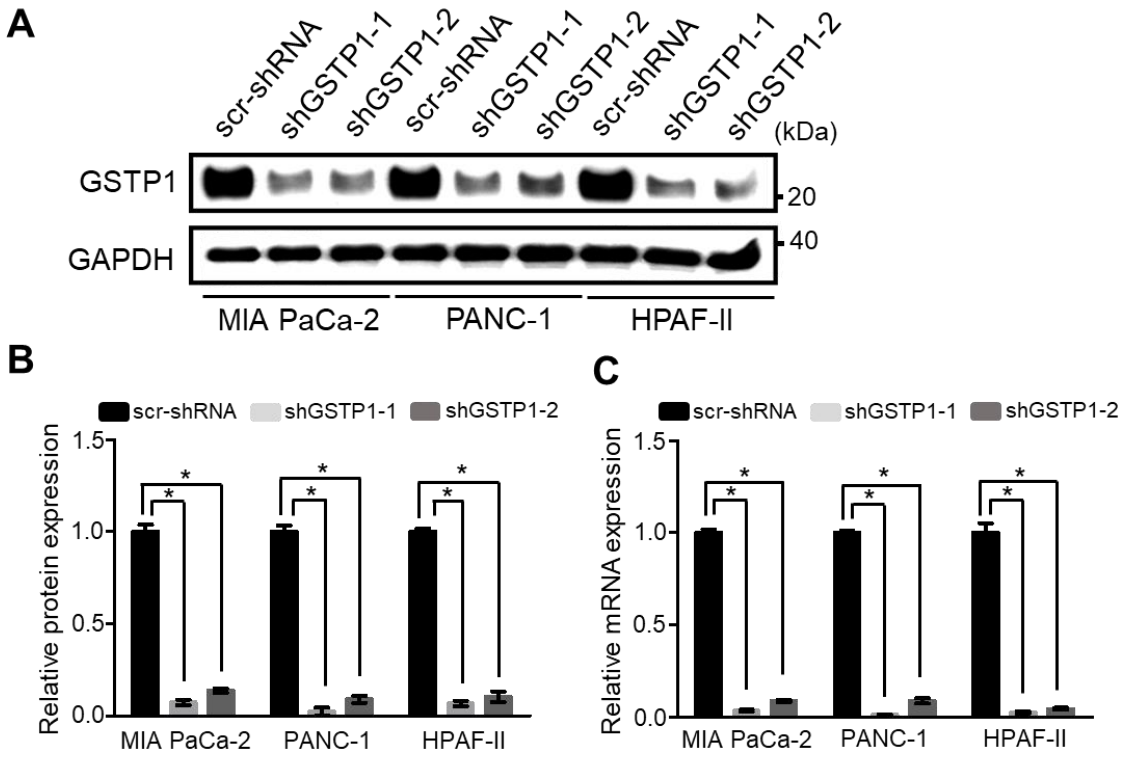

Figure 3.2. GSTP1 knockdown impairs PDAC cell viability. GSTP1 was knocked down in MIA PaCa-2, PANC-1, and HPAF-II PDAC cells using two independent shRNAs (shGSTP1-1 and shGSTP1-2) and expression was confirmed by (A, B) western blotting and (C) quantitative real-time (qRT)-PCR analysis. Western blot data were normalized to GAPDH for each cell line, and relative protein expression is shown for the scrambled control shRNA (scr-shRNA) compared to the GSTP1 shRNA sequences. Protein and mRNA levels of GSTP1 in scr-shRNA were compared to shGSTP1-1 and shGSTP1-2. The images are representative of three independent experiments. Student's t-test was used to evaluate the significance in the difference of GSTP1 expression among different groups. (D) CellTiter Glo® assays were used to detect the average cell viability of control and GSTP1 knockdown MIA PaCa-2, PANC-1, and HPAF-II cells for two independent experiments with eight technical replicates for each. The y-axis represents the luminescence recorded after 24, 48, 72, and 96 hours. The luminescence (cell viability) was compared between scr-shRNA and shGSTP1-1 and shGSTP1-2 independently. Student's t-test was used to analyze the significance between knockdown groups and the control. RLU: relative luminescence units (E) 50,000 cells for control and GSTP1 knockdown MIA PaCa-2, PANC-1, and HPAF-II were seeded and the number of viable cells was counted using a trypan blue dye exclusion test after 72 h. The live and the dead cell populations for shGSTP1-1 and shGSTP1-2 were compared to the scr-shRNA. Student's t-test was used to analyze for potentially significant differences. * denotes statistically significant differences between either GSTP1 knockdown and the control ($p < 0.05$). Unprocessed images for the western blotting results are shown in Figure S1.

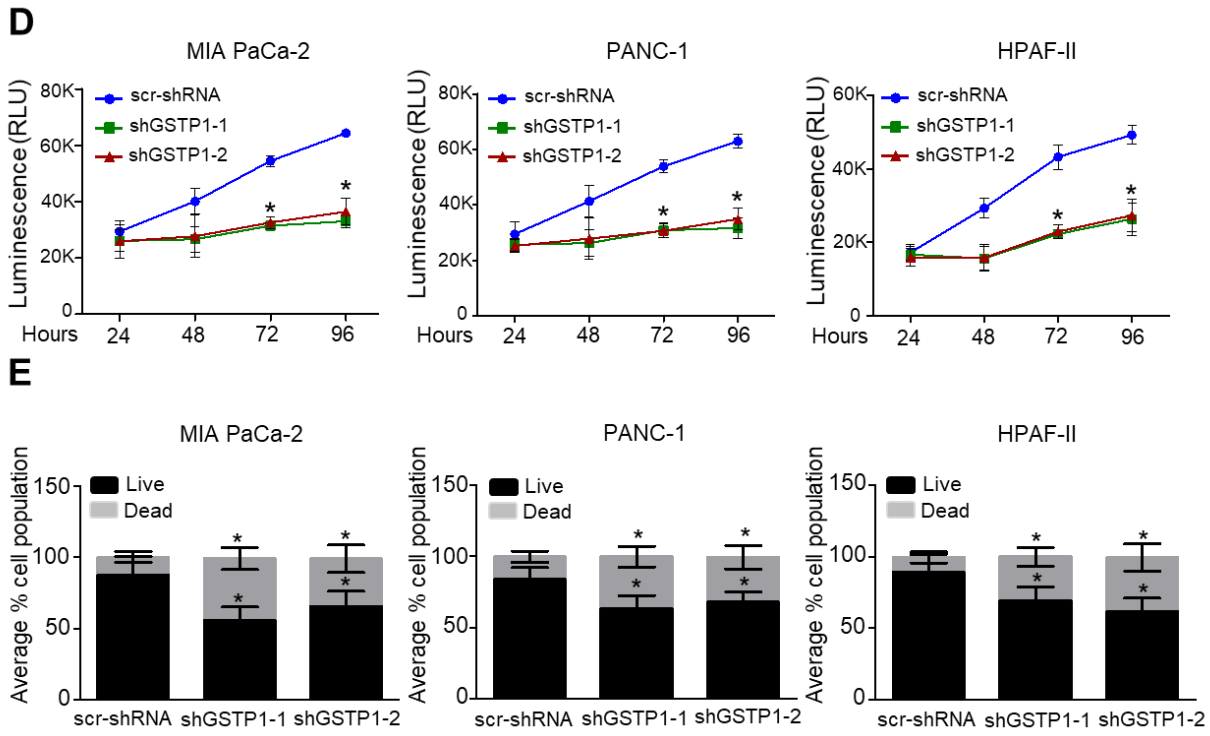

Figure 3.2. GSTP1 knockdown impairs PDAC cell viability (continued). GSTP1 was knocked down in MIA PaCa-2, PANC-1, and HPAF-II PDAC cells using two independent shRNAs (shGSTP1-1 and shGSTP1-2) and expression was confirmed by (A, B) western blotting and (C) quantitative real-time (qRT)-PCR analysis. Western blot data were normalized to GAPDH for each cell line, and relative protein expression is shown for the scrambled control shRNA (scr-shRNA) compared to the GSTP1 shRNA sequences. Protein and mRNA levels of GSTP1 in scr-shRNA were compared to shGSTP1-1 and shGSTP1-2. The images are representative of three independent experiments. Student's t-test was used to evaluate the significance in the difference of GSTP1 expression among different groups. (D) CellTiter Glo® assays were used to detect the average cell viability of control and GSTP1 knockdown MIA PaCa-2, PANC-1, and HPAF-II cells for two independent experiments with eight technical replicates for each. The y-axis represents the luminescence recorded after 24, 48, 72, and 96 hours. The luminescence (cell viability) was compared between scr-shRNA and shGSTP1-1 and shGSTP1-2 independently. Student's t-test was used to analyze the significance between knockdown groups and the control. RLU: relative luminescence units (E) 50,000 cells for control and GSTP1 knockdown MIA PaCa-2, PANC-1, and HPAF-II were seeded and the number of viable cells was counted using a trypan blue dye exclusion test after 72 h. The live and the dead cell populations for shGSTP1-1 and shGSTP1-2 were compared to the scr-shRNA. Student's t-test was used to analyze for potentially significant differences. * denotes statistically significant differences between either GSTP1 knockdown and the control ($p < 0.05$). Unprocessed images for the western blotting results are shown in Figure S1.

GSTP1 knockdown elevates ROS levels in PDAC cells

GSTP1, being a detoxification enzyme, has a key role in maintaining cellular homeostasis by scavenging reactive oxygen species (ROS) and protecting cells from oxidative damage [29]. We hypothesized that the growth inhibitory effects of knocking down GSTP1 result from the accumulation of ROS in PDAC cells. Control and GSTP1 knockdown (shGSTP1-1) MIA PaCa-2 and HPAF-II cells were stained with the fluorescent dye CM-H_2DCFDA to detect ROS, and fluorescence was determined using flow cytometry. We show GSTP1 knockdown elevates ROS levels by at least three-fold in PDAC cells (Figures 3.3A and B).

GSTP1 knockdown prolongs the G_0/G_1 phase of the cell cycle

Heightened ROS levels can activate transcription factors and several cell cycle regulatory proteins that inhibit the progression of cells through the cell cycle [21]. To elucidate the effects of GSTP1 knockdown on the cell cycle profile of PDAC cells, we identified the percentage of cells in each phase of the cell cycle via PI staining and flow cytometry. A larger percentage of GSTP1 knockdown PDAC cells were arrested in the G_0/G_1 phase compared to the control cells (Figure 3.3C). We found 57% of GSTP1 knockdown MIA PaCa-2 cells in G_0/G_1 phase compared to 47% of the control cells. Similarly, 38% GSTP1 knockdown HPAF-II cells were found in the G_0/G_1 phase compared to 31% of control cells. A complementary decrease in the G_2/M population was observed in the GSTP1 knockdown PDAC cells. These results suggest that GSTP1 knockdown prevents PDAC cell proliferation by prolonging the G_0/G_1 phase.

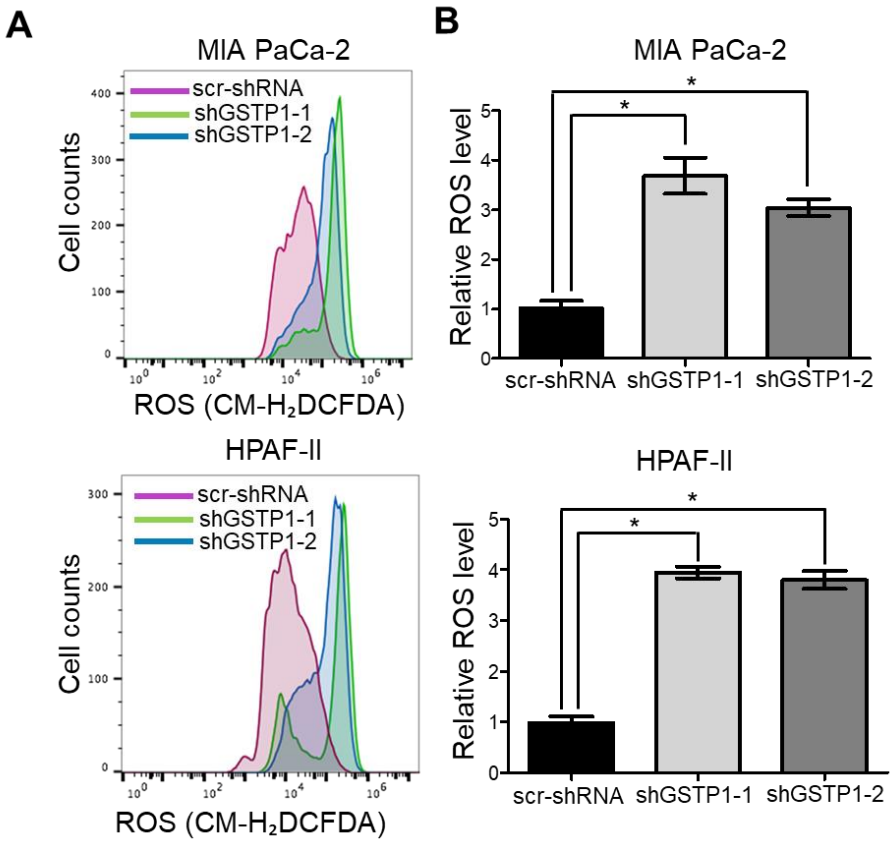

Figure 3.3. Effect of GSTP1 knockdown on the cell cycle profile and reactive oxygen species levels (ROS) levels in PDAC cells. (A) Histograms showing ROS levels determined using CM-H_2DCFDA and flow cytometry for control and GSTP1 knockdown MIA PaCa-2 and HPAF-II cells. The figure shows a representative image of three independent experiments. (B) Quantification of ROS levels in control and GSTP1 knockdown MIA PaCa-2 and HPAF-II cells. ROS levels in scr-shRNA were compared to that in shGSTP1-1 and shGSTP1-2 independently. Student's t-test was used to identify potential significant differences. (C) Control and GSTP1 knockdown MIA PaCa-2 and HPAF-II cells were analyzed for the percent cell population in different stages (G_0/G_1, S, and G_2/M) of the cell cycle. The data shown represent the average percent cell population in the given phases of the cell cycle. The experiment was conducted three times for each cell line. The percentage cell populations in G_0/G_1, S, and G_2/M phase of cell cycle were compared between scr-shRNA and shGSTP1-2. Student's t-test was used to identify significant differences. * denotes statistically significant differences between GSTP1 knockdown groups and control ($p < 0.05$).

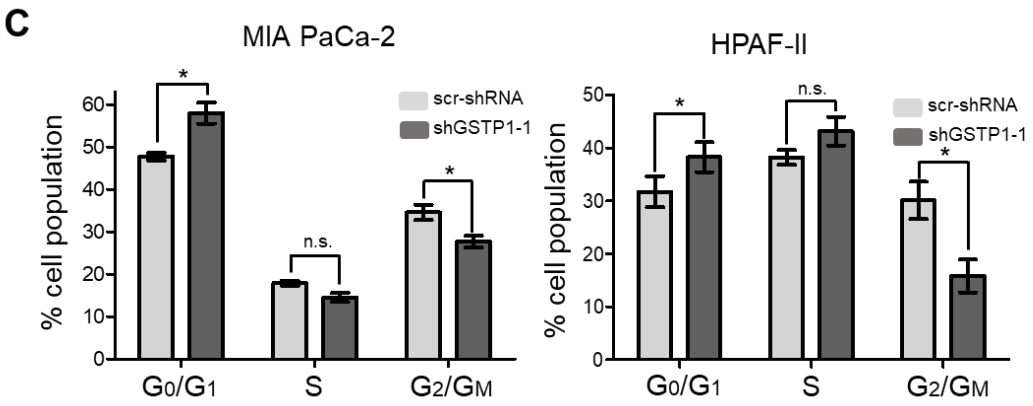

Figure 3.3. Effect of GSTP1 knockdown on the cell cycle profile and reactive oxygen species levels (ROS) levels in PDAC cells (continued). (A) Histograms showing ROS levels determined using CM-H_2DCFDA and flow cytometry for control and GSTP1 knockdown MIA PaCa-2 and HPAF-II cells. The figure shows a representative image of three independent experiments. (B) Quantification of ROS levels in control and GSTP1 knockdown MIA PaCa-2 and HPAF-II cells. ROS levels in scr-shRNA were compared to that in shGSTP1-1 and shGSTP1-2 independently. Student's t-test was used to identify potential significant differences. (C) Control and GSTP1 knockdown MIA PaCa-2 and HPAF-II cells were analyzed for the percent cell population in different stages (G_0/G_1, S, and G_2/M) of the cell cycle. The data shown represent the average percent cell population in the given phases of the cell cycle. The experiment was conducted three times for each cell line. The percentage cell populations in G_0/G_1, S, and G_2/M phase of cell cycle were compared between scr-shRNA and shGSTP1-2. Student's t-test was used to identify significant differences. * denotes statistically significant differences between GSTP1 knockdown groups and control ($p < 0.05$).

GSTP1 knockdown activates oxidative stress-mediated apoptotic signaling in PDAC cells

GSTP1 has previously been reported to regulate the phosphorylation and activation of mitogen-activated protein (MAP) kinases [30]. GSTP1 inhibits the JNK signaling pathway by binding to JNK and preventing its phosphorylation. In response to oxidative stress, the JNK-GSTP1 complex dissociates [31], JNK is activated, and the downstream signal transduction leads to apoptosis [19, 32]. Hence, we examined the effects of GSTP1 knockdown on the activation and phosphorylation of JNK1/2. We analyzed phosphorylated JNK1/2 protein expression through western blotting. GSTP1 knockdown cells showed elevated phosphorylated JNK1/2 and its target protein, c-Jun, compared to the scrambled controls in the PDAC cells (Figures 3.4A–C).

To elucidate the role of GSTP1 in cell proliferation and cell survival, we also analyzed the expression of extracellular signal-regulated kinase (ERK1/2), the p65 subunit of NF-κB, and specificity protein 1 (Sp1) transcription factor in GSTP1 knockdown cells. GSTP1 knockdown cells had low levels of phosphorylated ERK1/2 and p65, and reduced Sp1 compared to the scrambled control MIA PaCa-2 and HPAF-II cells (Figures 3.4A–C). To explain the cell-cycle arrest phenotype of GSTP1 knockdown PDAC cells, we also investigated the expression of important cell cycle regulators. Interestingly, we found a large reduction in cyclin D1 protein expression and a moderate decrease in CDK4 protein expression (Figures 3.4D and E). We also found elevated mRNA expression of the cyclin and CDK complex inhibitor, *CDKN1A* (p21) (Figures 3.4F and G). Further, pro-apoptotic protein, cleaved caspase-3 (Figures 3.4D and E), and genes, *Bax* and *Bak* (Figures 3.4F and G), were up-regulated, while the anti-apoptotic gene *Bcl2* was downregulation in GSTP1 knockdown PDAC cells. *HMOX1*, an oxidative stress-associated gene, was also upregulated in GSTP1 knockdown PDAC cells (Figures 3.4F and G).

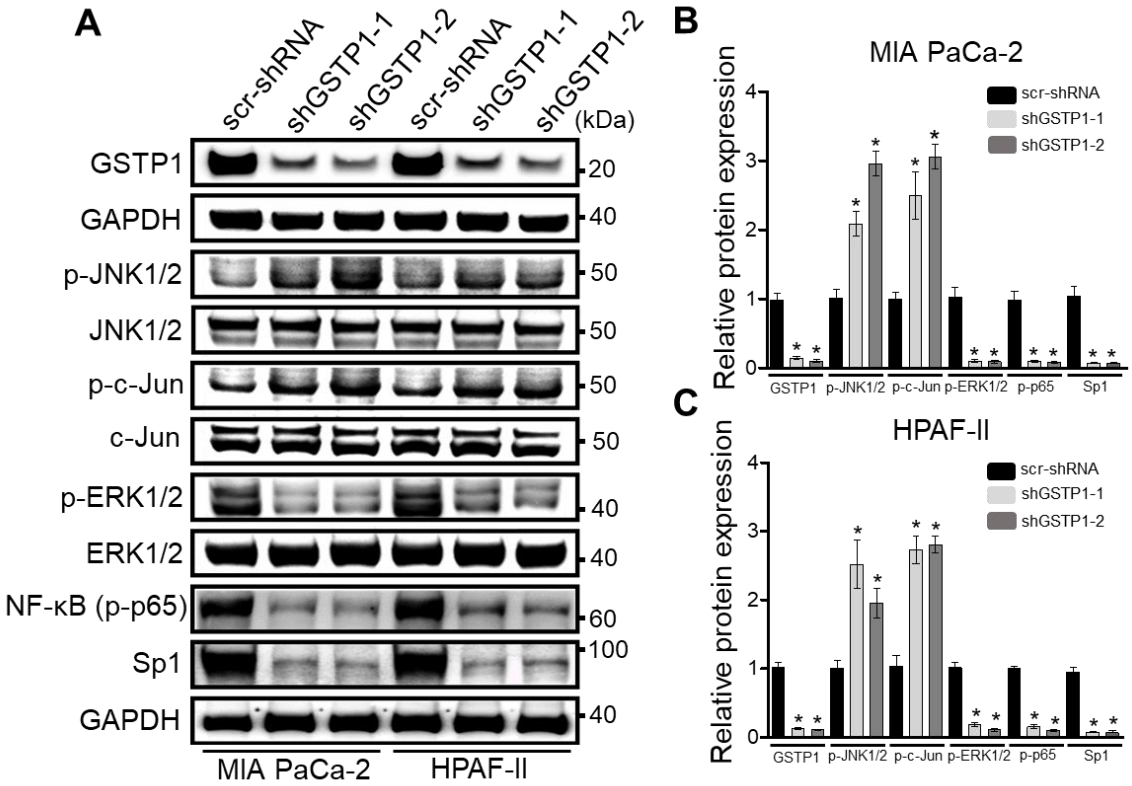

Figure 3.4. GSTP1 knockdown activates oxidative stress-mediated apoptotic and survival pathways in PDAC cells. (A) Phosphorylated (p-) levels of JNK1/2, c-Jun, extracellular signal-regulated kinase (ERK), and p65 and total specificity protein 1 (Sp1) protein expression were measured in GSTP1 knockdown PDAC cells via western blotting. Levels of total JNK/2, c-Jun, and ERK1/2 were determined to confirm that changes in phosphorylated proteins were not due to changes in total protein level and to normalize the phosphorylated protein levels. GAPDH was used as a loading control. Changes in protein expression were quantified using densitometry for control and GSTP1 knockdown (B) MIA PaCa-2 and (C) HPAF-II cells. The protein levels were compared between shGSTP1-1 or shGSTP1-2 and scr-shRNA groups. The graphs show the ratio of phosphorylated proteins to total proteins in the knockdown groups relative to the scr-shRNA control. The figures show representative images for three independent experiments. (D) Protein levels of cyclin D1, CDK4 and activation (cleavage) of caspase-3 was analyzed in GSTP1 knockdown PDAC cells using immunoblotting. GAPDH and total caspase-3 were used as loading controls. (E) Cyclin D1, CDK4, and cleaved caspase-3 protein expression was quantified using densitometry. The figures show representative images for three independent experiments. The protein levels were compared between shGSTP1-1 or shGSTP1-2 and scr-shRNA groups. (F, G) Relative mRNA levels of *CDKN1A*, *HMOX-1*, *Bax*, *Bad*, and *Bcl2* were quantified using qRT-PCR in control (scr-shRNA) and GSTP1 knockdown (shGSTP1-1 and shGSTP1-2) for MIA PaCa-2 and HPAF-II cells. Student's t-test was used to identify significant differences for the above experiments. Statistically significant changes in expression levels in GSTP1 knockdown groups compared to the control are shown with * ($p < 0.05$). Unprocessed images for the western blotting results are shown in Figure S1.

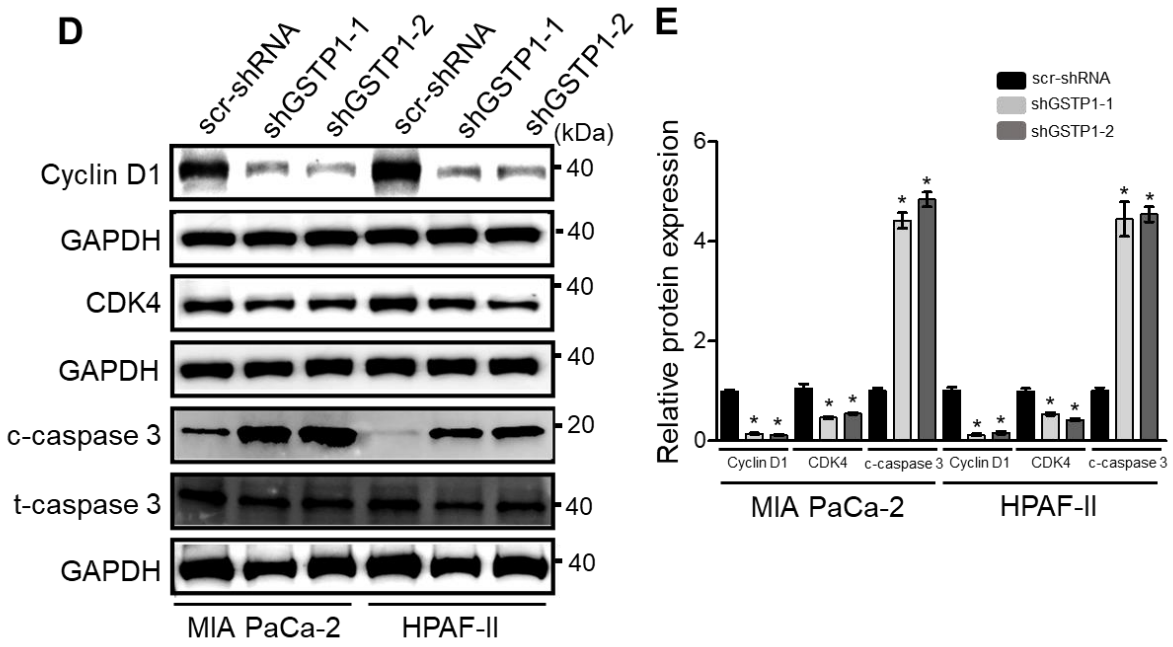

Figure 3.4. GSTP1 knockdown activates oxidative stress-mediated apoptotic and survival pathways in PDAC cells (continued). (A) Phosphorylated (p-) levels of JNK1/2, c-Jun, extracellular signal-regulated kinase (ERK), and p65 and total specificity protein 1 (Sp1) protein expression were measured in GSTP1 knockdown PDAC cells via western blotting. Levels of total JNK/2, c-Jun, and ERK1/2 were determined to confirm that changes in phosphorylated proteins were not due to changes in total protein level and to normalize the phosphorylated protein levels. GAPDH was used as a loading control. Changes in protein expression were quantified using densitometry for control and GSTP1 knockdown (B) MIA PaCa-2 and (C) HPAF-II cells. The protein levels were compared between shGSTP1-1 or shGSTP1-2 and scr-shRNA groups. The graphs show the ratio of phosphorylated proteins to total proteins in the knockdown groups relative to the scr-shRNA control. The figures show representative images for three independent experiments. (D) Protein levels of cyclin D1, CDK4 and activation (cleavage) of caspase-3 was analyzed in GSTP1 knockdown PDAC cells using immunoblotting. GAPDH and total caspase-3 were used as loading controls. (E) Cyclin D1, CDK4, and cleaved caspase-3 protein expression was quantified using densitometry. The figures show representative images for three independent experiments. The protein levels were compared between shGSTP1-1 or shGSTP1-2 and scr-shRNA groups. (F, G) Relative mRNA levels of *CDKN1A*, *HMOX-1*, *Bax*, *Bad*, and *Bcl2* were quantified using qRT-PCR in control (scr-shRNA) and GSTP1 knockdown (shGSTP1-1 and shGSTP1-2) for MIA PaCa-2 and HPAF-II cells. Student's t-test was used to identify significant differences for the above experiments. Statistically significant changes in expression levels in GSTP1 knockdown groups compared to the control are shown with * ($p < 0.05$). Unprocessed images for the western blotting results are shown in Figure S1.

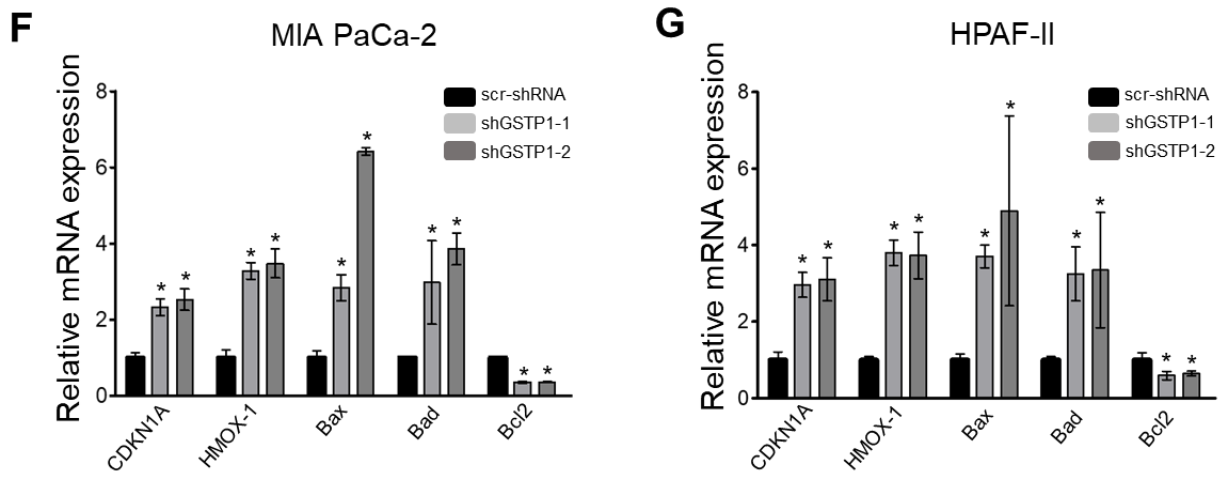

Figure 3.4. GSTP1 knockdown activates oxidative stress-mediated apoptotic and survival pathways in PDAC cells (continued). (A) Phosphorylated (p-) levels of JNK1/2, c-Jun, extracellular signal-regulated kinase (ERK), and p65 and total specificity protein 1 (Sp1) protein expression were measured in GSTP1 knockdown PDAC cells via western blotting. Levels of total JNK/2, c-Jun, and ERK1/2 were determined to confirm that changes in phosphorylated proteins were not due to changes in total protein level and to normalize the phosphorylated protein levels. GAPDH was used as a loading control. Changes in protein expression were quantified using densitometry for control and GSTP1 knockdown (B) MIA PaCa-2 and (C) HPAF-II cells. The protein levels were compared between shGSTP1-1 or shGSTP1-2 and scr-shRNA groups. The graphs show the ratio of phosphorylated proteins to total proteins in the knockdown groups relative to the scr-shRNA control. The figures show representative images for three independent experiments. (D) Protein levels of cyclin D1, CDK4 and activation (cleavage) of caspase-3 was analyzed in GSTP1 knockdown PDAC cells using immunoblotting. GAPDH and total caspase-3 were used as loading controls. (E) Cyclin D1, CDK4, and cleaved caspase-3 protein expression was quantified using densitometry. The figures show representative images for three independent experiments. The protein levels were compared between shGSTP1-1 or shGSTP1-2 and scr-shRNA groups. (F, G) Relative mRNA levels of *CDKN1A*, *HMOX-1*, *Bax*, *Bad*, and *Bcl2* were quantified using qRT-PCR in control (scr-shRNA) and GSTP1 knockdown (shGSTP1-1 and shGSTP1-2) for MIA PaCa-2 and HPAF-II cells. Student's t-test was used to identify significant differences for the above experiments. Statistically significant changes in expression levels in GSTP1 knockdown groups compared to the control are shown with * ($p < 0.05$). Unprocessed images for the western blotting results are shown in Figure S1.

Addition of glutathione reverses the effects of GSTP1 knockdown on cell viability and oxidative stress-response signaling

We next evaluated the ability of an exogenous antioxidant, glutathione (GSH), to reverse the cytotoxic effects of GSTP1 knockdown in PDAC cells. Control and GSTP1 knockdown MIA PaCa-2 and HPAF-II cells were treated with 5 mM GSH for 72 h. Our results show that GSH

treatment attenuated the effects of GSTP1 knockdown in PDAC cells. The growth inhibitory effects of GSTP1 knockdown were significantly diminished upon GSH treatment (Figure 3.5A), suggesting that the accumulation of endogenous ROS is a leading cause of reduced cell survival in GSTP1 knockdown cells. We not only see the reduced expression of p-JNK in GSH-supplemented GSTP1 knockdown cells, but also the protein expression of Sp1 was found to be restored (Figures 3.5B and C). Overall, these results indicate that the loss of GSTP1 function surges ROS levels, activates JNK, and suppresses Sp1, which leads to changes in gene expression associated with oxidative stress, cell proliferation, survival, and cell death (Figure 3.5D).

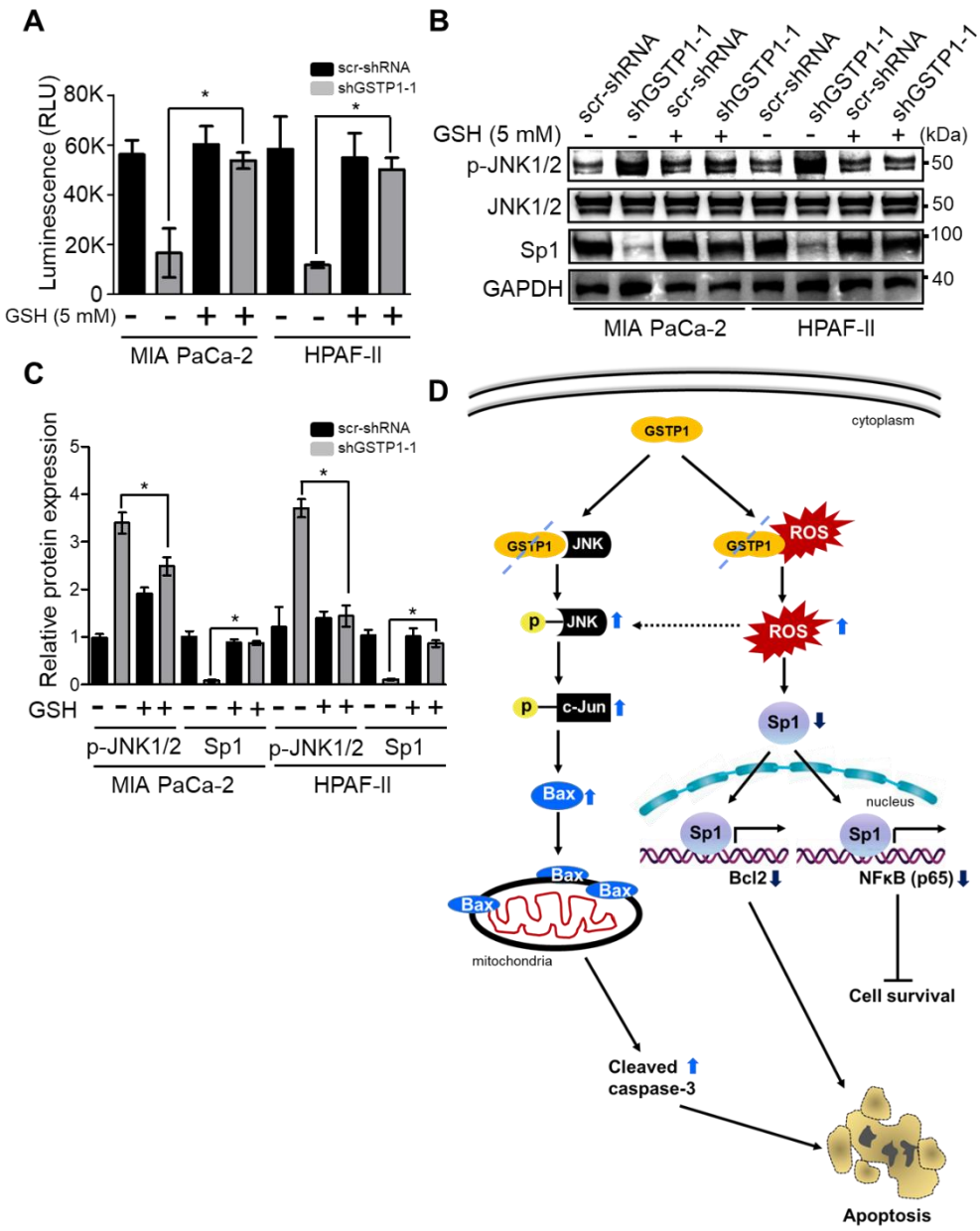

Figure 3.5. Exogenous antioxidant rescues the cytotoxic effects of GSTP1 knockdown in PDAC cells. Control and GSTP1 knockdown MIA PaCa-2 and HPAF-II cells were treated with 5 mM GSH for 72 hours. (A) CellTiter-Glo® assays were used to evaluate the average cell viability for three independent experiments with eight technical replicates for each. The luminescence (cell viability) was compared between shGSTP1-1 with and without GSH treatment. Student's t-test was used to identify significant differences in growth in GSTP1 knockdown cells treated with or without GSH. RLU: relative luminescence units (B) Effects of GSH treatment on the phosphorylation of JNK1/2 and expression of Sp1 were determined using western blotting. Total JNK and GAPDH were used as loading controls for the experiment. The figure shows one representative image of three independent experiments. Similar results were obtained in duplicate experiments. (C) Protein expression in two independent experiments was quantified using densitometry. p-JNK1/2 and Sp1 protein expression levels were compared between shGSTP1-1 with and without GSH treatment. Student's t-test was used to identify the significant differences in protein expression in the GSTP1 knockdown cells treated with or without GSH. (D) Proposed mechanisms underlying the role of GSTP1 in pancreatic cancer cell proliferation, survival, and apoptosis based on western blotting and qRT-PCR data. For all figures, * denotes statistically significant differences ($p < 0.05$). Unprocessed images for the western blotting results are shown in Figure S1.

GSTP1 knockdown impairs the growth of orthotopic PDAC tumors *in vivo*

Intrigued by the *in vitro* growth inhibitory effects of GSTP1 knockdown, we next explored these effects in an orthotopic animal model of PDAC. Control and GSTP1 knockdown MIA PaCa-2, PANC-1, and HPAF-II cells were orthotopically transplanted into the pancreata of nude mice (Figure 3.6A). The tumor volume was monitored every ten days using FUJIFILM Vevo3100 ultrasound imaging system and was compared among the control and the GSTP1 knockdown groups. At the conclusion of the experiment, we observed decreased tumor growth via abdominal ultrasounds in GSTP1 knockdown groups compared to the controls (Figures 3.6B and C). Furthermore, our results show that GSTP1 knockdown PDAC cells generated significantly smaller tumors ($p < 0.05$) with a 50–80% reduction in tumor weight compared to the control (Figures 3.6D and E).

Tumor cell proliferation is reduced and apoptosis is increased by GSTP1 knockdown in pancreatic tumors

To explain the dramatic reduction in tumor size in GSTP1 knockdown cells, we evaluated the expression of the nuclear proliferation marker Ki-67 and the apoptotic marker cleaved caspase-3 by immunohistochemistry in mouse tumor tissues. The scrambled controls from the two PDAC cell lines showed 64% and 67% Ki-67-positive cells (Figure 3.6F). In comparison, tumors obtained from GSTP1 knockdown cells showed a notable reduction in Ki-67 expression for MIA PaCa-2 (37% and 35% for shGSTP1-1 and shGSTP1-2, respectively) and HPAF-II (38% and 29% for shGSTP1-1 and shGSTP1-2, respectively) (Figure 3.6G). Additionally, tumors obtained from GSTP1 knockdown cells showed an impressive increase in the expression of cleaved caspase-3 compared to the scrambled controls (Figures 3.6H and I). These data provide additional affirmation

that GSTP1 knockdown impedes proliferation and promotes cell death via apoptosis in PDAC cells *in vivo*.

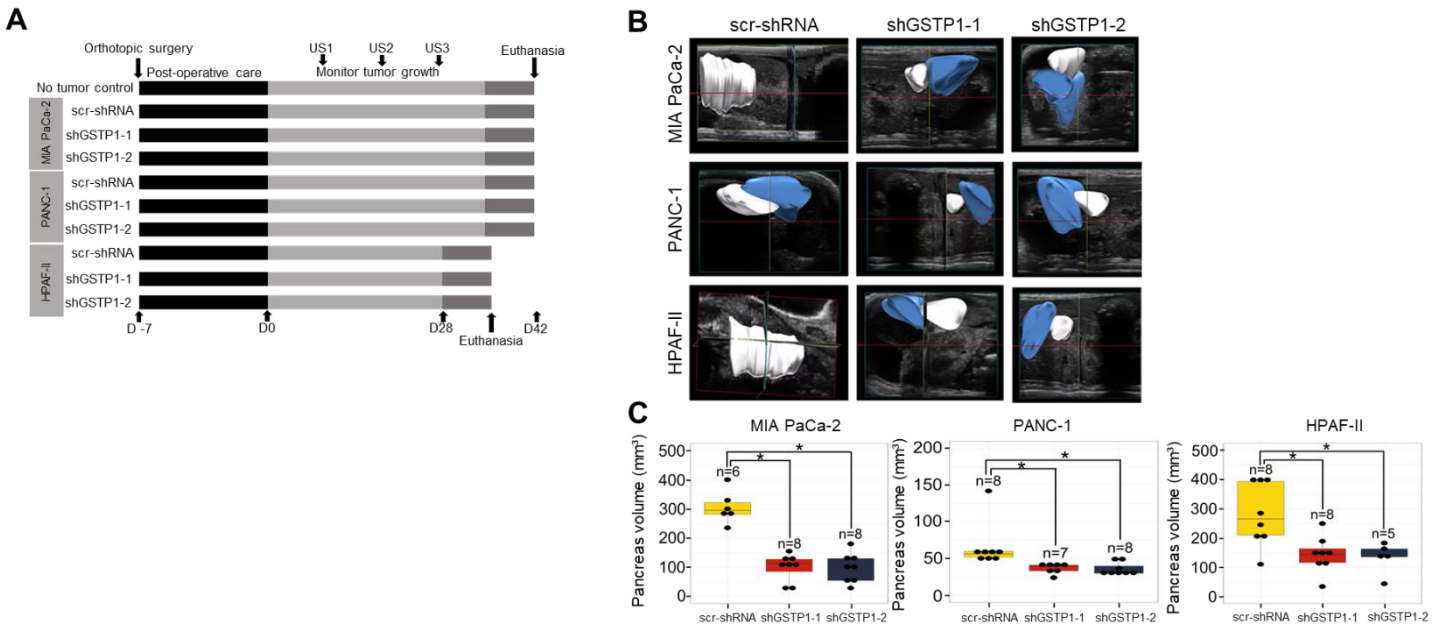

Figure 3.6. GSTP1 knockdown impedes the growth and proliferation of PDAC cells *in vivo*. (A) Schematic representation of animal experiments to assess the effects of GSTP1 knockdown on PDAC (MIA PaCa-2, PANC-1, or HPAF-II) tumor growth in nude mice for up to 42 days (D42). US1-3: ultrasound imaging was performed every 10 days to monitor tumor growth. For the HPAF-II group, the last ultrasound was done on D27 rather than D30. (B) Pancreatic tumor development was monitored and imaged using the FUJIFILM Vevo3100 ultrasound imaging system. The data show the tumor volume for one representative mouse for each group measured at US3 soon before euthanasia. Blue: healthy pancreatic tissue, white: pancreatic tumor tissue. (C) Total pancreata volumes were calculated using 3-dimensional ultrasound images for each cell line using the data collected at US3. (D) Size and (E) weight of the pancreata are shown for control and GSTP1 knockdown tumors. The figures show representative images of the tumor volumes (ultrasound) and tumor sizes of various treatment groups. The tumor volume and weight were compared between scr-shRNA and shGSTP1-1 and shGSTP1-2 independently. Welch's one-way analysis of variants was performed to analyze the significant differences in tumor volume and weight between knockdown groups and the control. Tumor tissue sections from GSTP1 knockdown and scrambled controls for MIA PaCa-2 and HPAF-II were subjected to immunohistochemistry. (F) Ki-67 staining for control and GSTP1 knockdown MIA PaCa-2 and HPAF-II tumors. Scale bar: 200 μm (G) The quantification of the Ki-67-positive cell population. (H) Cleaved caspase-3 staining for control and GSTP1 knockdown MIA PaCa-2 and HPAF-II tumors. Scale bar: 200 μm (I) The quantification of cleaved caspase-3-positive cells. One representative image for each treatment group is shown. The percentage of Ki-67- and cleaved caspase-3-positive cells was determined by normalizing the number of Ki-67- and cleaved caspase-3-positive cells to that of 4′,6-diamidino-2-phenylindole (DAPI)-stained cells. Each value in the graph is the mean ± SD from 5-6 mice from each treatment group. * denotes statistically significant differences for all graphs ($p < 0.05$).

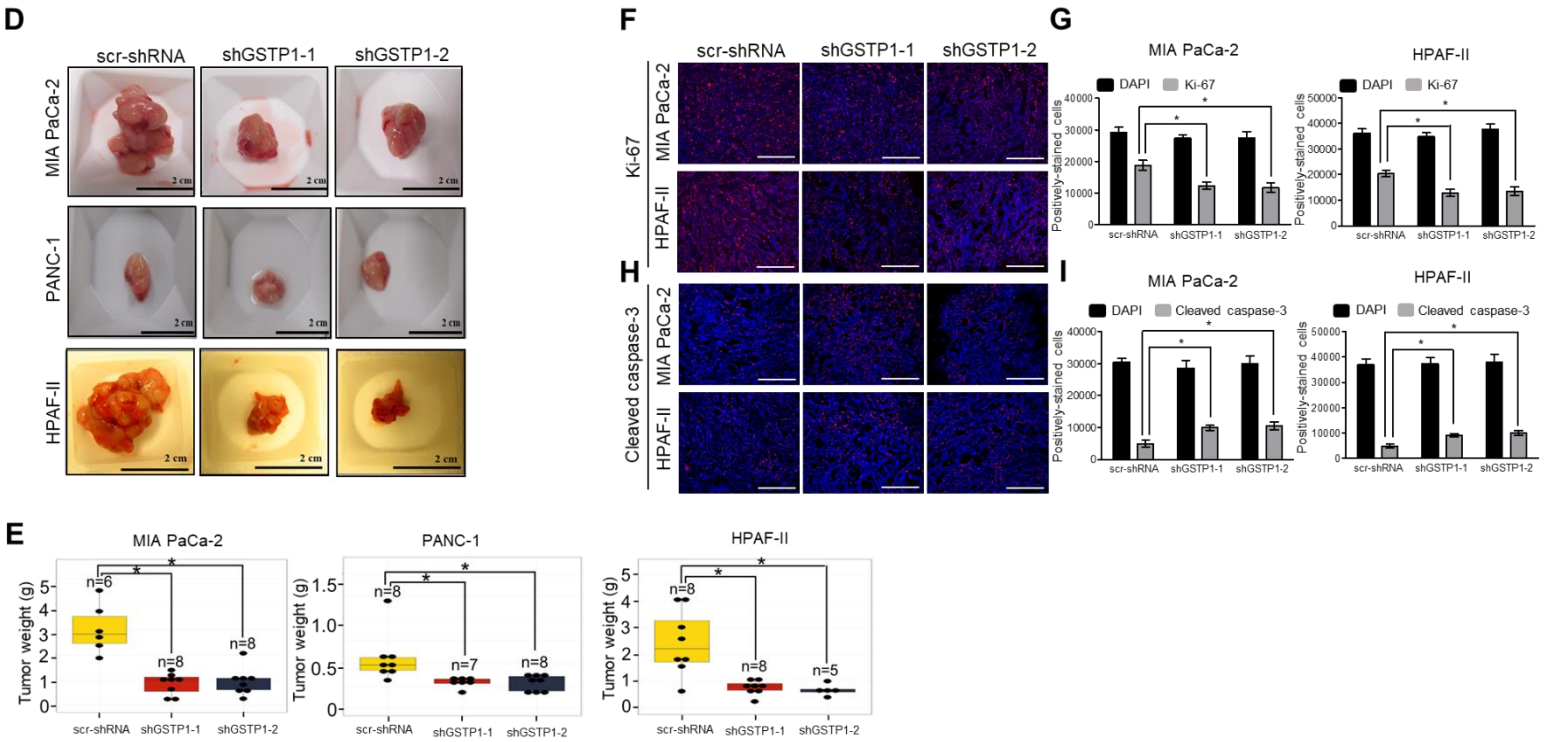

Figure 3.6. GSTP1 knockdown impedes the growth and proliferation of PDAC cells *in vivo* (continued). (A) Schematic representation of animal experiments to assess the effects of GSTP1 knockdown on PDAC (MIA PaCa-2, PANC-1, or HPAF-II) tumor growth in nude mice for up to 42 days (D42). US1-3: ultrasound imaging was performed every 10 days to monitor tumor growth. For the HPAF-II group, the last ultrasound was done on D27 rather than D30. (B) Pancreatic tumor development was monitored and imaged using the FUJIFILM Vevo3100 ultrasound imaging system. The data show the tumor volume for one representative mouse for each group measured at US3 soon before euthanasia. Blue: healthy pancreatic tissue, white: pancreatic tumor tissue. (C) Total pancreata volumes were calculated using 3-dimensional ultrasound images for each cell line using the data collected at US3. (D) Size and (E) weight of the pancreata are shown for control and GSTP1 knockdown tumors. The figures show representative images of the tumor volumes (ultrasound) and tumor sizes of various treatment groups. The tumor volume and weight were compared between scr-shRNA and shGSTP1-1 and shGSTP1-2 independently. Welch's one-way analysis of variants was performed to analyze the significant differences in tumor volume and weight between knockdown groups and the control. Tumor tissue sections from GSTP1 knockdown and scrambled controls for MIA PaCa-2 and HPAF-II were subjected to immunohistochemistry. (F) Ki-67 staining for control and GSTP1 knockdown MIA PaCa-2 and HPAF-II tumors. Scale bar: 200 μm (G) The quantification of the Ki-67-positive cell population. (H) Cleaved caspase-3 staining for control and GSTP1 knockdown MIA PaCa-2 and HPAF-II tumors. Scale bar: 200 μm (I) The quantification of cleaved caspase-3-positive cells. One representative image for each treatment group is shown. The percentage of Ki-67- and cleaved caspase-3-positive cells was determined by normalizing the number of Ki-67- and cleaved caspase-3-positive cells to that of 4′,6-diamidino-2-phenylindole (DAPI)-stained cells. Each value in the graph is the mean ± SD from 5-6 mice from each treatment group. * denotes statistically significant differences for all graphs ($p < 0.05$).

Discussion

Our data provide convincing evidence that GSTP1 plays a critical role in regulating PDAC cell growth, which was previously unknown. In this study, we show that the GSTP1 knockdown impairs the growth and proliferation of PDAC cells *in vitro*. We show, for the first time, that GSTP1 inhibition is associated with enhanced JNK activity and suppressed ERK, NF-κB, and Sp1 activity in PDAC cells. Furthermore, in an orthotopic pancreatic cancer mouse model, GSTP1 knockdown tumors showed an impressive reduction in growth compared to control tumors. Together, our results indicate that GSTP1 inhibition impairs PDAC cell growth, suggesting that GSTP1 is a viable target for PDAC therapy.

The ubiquitous expression of GSTP1 in a wide array of tissues and organisms provides evidence that GSTP1 has important cellular roles. We found GSTP1 protein expression was at least two times higher in five PDAC cell lines compared to normal pancreatic epithelial cells. Similarly, GSTP1 mRNA was reported in high levels in human PDAC tissue compared to the healthy pancreas tissue. Our analysis of The Human Protein Atlas [26] data revealed that elevated GSTP1 expression is associated with poor survival of PDAC patients, post-diagnosis of the disease. Previous research has shown that GSTP1 is expressed at high levels in a variety of human cancers, including colon, lung, breast, and ovarian cancers [25]. GSTP1 overexpression is associated with resistance to chemotherapeutic drugs like cisplatin, carboplatin, adriamycin, and bleomycin in ovarian and cervical cancer [33].

GSTP1 is associated with a variety of cellular processes, including detoxification [15], glutathionylation [21], actin polymerization [22], nitric oxide signaling [23], kinase signaling [31], and cellular metabolism [20]. To investigate the role of GSTP1 in PDAC cells, we generated two GSTP1 knockdown lines for each of the three metabolically diverse PDAC cell lines (MIA PaCa-

2, PANC-1, and HPAF-II). MIA PaCa-2 and PANC-1 cells are poorly differentiated mesenchymal-type PDAC cell lines compared to HPAF-II cells that belong to an epithelial subtype [27]. GSTP1 knockdown significantly impaired the *in vitro* viability of all three PDAC cell lines, suggesting that this protein is vital to PDAC growth regardless of metabolic subtype. Our cell viability data are in concordance with previous reports where Louie *et al*. [20] described that GSTP1 knockdown impairs the growth of triple-negative breast cancer cells. They concluded by demonstrating that GSTP1 inhibition disrupts glycolytic metabolism, resulting in reduced levels of lipids, nucleotides, and ATP. Furthermore, recently, Fujitani *et al*. [34] showed that knocking down GSTP1 in cancer cells of various anatomic origins gives rise to mitochondrial stress and severely impairs cell proliferation. Interestingly, they found that pancreatic cancer cell growth was particularly sensitive to GSTP1 knockdown.

Attempts have been made to disrupt the cellular redox balance through pharmacological regulation in favor of increasing intracellular ROS and inducing apoptosis for the treatment of cancer. Arrick *et al*. [35, 36] showed that specifically inhibiting the synthesis of GSH contributed to the destruction of neoplastic cells *in vitro*. Inhibiting GSTP1, an integral component of the cellular antioxidant system, is one avenue to disrupt redox balance. GSTP1 protects cells from electrophiles that cause oxidative damage to DNA, proteins, and lipids by conjugating electrophiles to GSH [18]. Here, we observed that the knockdown of GSTP1 in PDAC cells resulted in elevated ROS levels. Furthermore, the addition of GSH to GSTP1 knockdown cells enhanced cell viability and reduced the expression of stress and apoptosis-associated proteins. A previous study showed that an antioxidant (N-acetylcysteine) could reduce ROS levels in GSTP1 knockdown PDAC cells [34]. We speculate that GSTP1 knockdown impairs the ROS scavenging function that leads to ROS accumulation in PDAC cells. Our observations complement a previous

report that showed GSTP1 inhibition using siRNAs and a pharmacological inhibitor elevated ROS levels and caused DNA damage in prostate cancer cells [29]. Moreover, GSH also restored cell viability, reduced ROS, and decreased apoptosis-associated protein expression in PDAC cells treated with a GSTP1 inhibitor [37].

Elevated oxidative stress activates the JNK signaling pathway and triggers apoptosis [31]. In a non-stressed environment, GSTP1 binds and inhibits the phosphorylation of JNK preventing the transcriptional activation of downstream cell stress pathways. However, under oxidative stress conditions, GSTP1 dimerizes into aggregates and its binding to JNK is deterred, enabling JNK activation [38]. Previously, we showed that the interaction between JNK and GSTP1 is interrupted in PDAC cells treated with a GSTP1 inhibitor [39]. Additionally, complementing our current results, it was shown that a JNK inhibitor could restore viability of PDAC cells treated with a GSTP1 inhibitor [39]. As expected, GSTP1 knockdown increased the expression of phosphorylated JNK and its downstream target, c-Jun, in PDAC cells. This increase could be due to elevated levels of ROS that could activate JNK signaling and/or reduced levels of GSTP1 that would also result in enhanced JNK signaling. Our data are supported by a previous report that suggested GSTP1 knockdown elevated phosphorylated JNK expression in cervical cancer cells [24]. The extent and duration of JNK activation can lead to ER stress, mitotic arrest, and eventually apoptosis in cancer cells [31].

To elucidate additional mechanisms through which GSTP1 knockdown impedes growth and the proliferation of PDAC cells, we investigated the activation status of ERK, NF-κB, and Sp1 pathways. GSTP1 knockdown cells displayed reduced phospho-ERK and NF-κB, and reduced Sp1 protein expression. In support of this, ERK and NF-κB protein expression were reduced in cervical cancer cells upon GSTP1 inhibition [24]. Sp transcription factors are upregulated in various cancer

cells [40] and act as negative-prognostic markers for patient survival [41]. Our data are supported by previous reports that suggest ROS induction by chemotherapy and other anti-cancer agents lead to the downregulation of Sp proteins [42–45] and the reduced phosphorylation of ERK1/2 [46]. Similar to the previous studies [40, 47], we show that the restoration of Sp1 expression can be achieved by supplementing the cells with an exogenous antioxidant such as glutathione. Additionally, Sp (1, 3, or 4) knockdown induced similar cellular responses, such as enhanced cell death, and gene expression changes (increased apoptosis promoters and decreased apoptosis inhibitors) as we observed in GSTP1 knockdown PDAC cells [48]. Furthermore, we show the reduced expression of principal cell-cycle regulators, cyclin D1 [49] and CDK4 [50, 51]. Based on these results, we propose a mechanism through which GSTP1 alters MAP kinases and NF-κB signaling, averts apoptosis, and promotes cell survival and proliferation (Figure 3.5D). We speculate that in the absence of GSTP1, JNK is freely phosphorylated as a result of activating the downstream cell death pathways. Moreover, elevated ROS levels reduce the expression of Sp1 that transcribes Bcl2 [52, 53] and the p65 subunit of NF-κB [52, 54]. Reduced levels of Bcl2 and p65 in GSTP1 knockdown PDAC cells contribute to the apoptotic phenotype and decreased cell survival, respectively.

Intriguingly, we found that the orthotopic implantation of GSTP1 knockdown cells in the pancreata of athymic nude mice resulted in drastically smaller tumors compared to scrambled controls in terms of both tumor weight and volume. We also observed a lower percentage of proliferating cells and a larger population of apoptotic cells in tumors generated from GSTP1 knockdown PDAC cells. These results support our *in vitro* data as well as previously published literature. shRNAs targeting GSTP1 were shown to reduce breast cancer xenograft implants by

more than three-fold [20]. Similar results were observed when GSTP1 was inhibited using specific morpholinos in cervical cancer [24].

Given GSTP1's cytoprotective roles in xenobiotic detoxification, chemotherapeutics, and modulating oxidative stress, GSTP1 inhibitors emerged as promising anti-cancer compounds [55, 56] and have been used alone or in combination with chemotherapeutic drugs [57]. The selective targeting of GSTP1 using 6-(7-nitro-2,1,3-benzoxadiazol-4-ylthio)hexanol (NBDHEX) has shown increased efficiency of chemotherapeutic drugs in melanoma [56]. A potent GSTP1 inhibitor, TLK199 (Telik Inc.), has been shown to modulate cell proliferation in human myeloid leukemic cells [58] and is under clinical trial for myelodysplastic syndrome [59]. LAS17 was recently developed as a highly potent and selective GSTP1 inhibitor that impairs breast cancer pathogenicity [20]. The aforementioned GSTP1 inhibitors have shown effective impairment in GSTP1 activity; however, their toxicity in normal cells is not well characterized.

Collectively, our findings illustrate the crucial role of GSTP1 in the growth of PDAC cells. The loss of GSTP1 function leads to the activation of oxidative-stress response pathways that trigger a cell death mechanism. Taken together, our data suggest that GSTP1 is a potential and promising novel therapeutic target to treat pancreatic cancer patients.

Conclusions

Currently, pancreatic cancer is the third-leading cause of cancer-related deaths in the US and eighth in the world. PDAC continues to be a major unresolvable health issue at the start of the 21st century. Resistance of PDAC to the conventional treatment approaches has led to an increased interest in identifying promising therapeutic targets. GSTP1 has been associated with tumor promotion and drug resistance in breast, colon, and cervical cancers. Here, we report that GSTP1, a crucial cytoprotective antioxidant protein, plays a critical role in the growth and progression of

PDAC cells and tissues. We show that the knockdown of GSTP1 enhances JNK-mediated apoptosis and inhibits NF-κB and ERK-mediated cell survival and proliferation. Our findings are an important first step towards the validation of GSTP1 as a novel therapeutic target to treat pancreatic cancer patients.

Author contributions

R.R.S. and K.M.R. conceived and designed the study. All *in vitro* experiments were performed by R.R.S. *In vivo* experiments were performed by R.R.S. and J.M. M.O. performed the statistical analysis of the data. K.M.R. was responsible for the supervision and coordination of the project. All authors read and approve the final manuscript before submission.

Funding

NIH Grant number 1P20GM109024 (to KMR) and NSF Grant number DMR-1625704 made funding for this project possible. Its contents are solely the responsibility of the authors and do not necessarily represent the official views of the NIH or NSF.

Acknowledgments

We thank Jodie Haring, Jagadish Loganathan, Jeffrey Kittilson, John Wilkinson, Channing Der, Jiha Kim, and James Grunkemeyer for their technical support and assistance. We would like to acknowledge use of the Small Animal Core Facility for work described in this manuscript. This Core Facility is part of The Center for Diagnostic and Therapeutic Strategies in Pancreatic Cancer at North Dakota State University and is funded by National Institute of General Medical Sciences of the National Institutes of Health, Award Number 1P20GM109024. We thank Adrienne Cox for her excellent editorial comments and suggestions.

Conflict of interest

The authors declare no conflicts of interest.

Availability of data and materials

All data generated or analyzed during this study are presented in this article. The datasets used and/or analyzed during the current study are available from the corresponding author on reasonable request.

References

1. Siegel, R.L.; Miller, K.D.; Jemal, A. *Cancer statistics, 2020*. CA Cancer J. Clin. 2020, **70**, p. 7–30.

2. Drouillard, A.; Manfredi, S.; Lepage, C.; Bouvier, A.M. *Epidemiology of pancreatic cancer.* Bull. Cancer 2018, **105**, p. 63–69.

3. Rueff, J.; Rodrigues, A.S. *Cancer Drug Resistance: A Brief Overview from a Genetic Viewpoint.* Methods Mol. Biol. 2016, **1395**, p. 1–18.

4. Oettle, H.; Post, S.; Neuhaus, P.; Gellert, K.; Langrehr, J.; Ridwelski, K.; Schramm, H.; Fahlke, J.; Zuelke, C.; Burkart, C.; et al. *Adjuvant chemotherapy with gemcitabine vs observation in patients undergoing curative-intent resection of pancreatic cancer: A randomized controlled trial.* JAMA 2007, **297**, p. 267–277.

5. Oettle, H.; Neuhaus, P. *Adjuvant therapy in pancreatic cancer: A critical appraisal*. Drugs 2007, **67**, p. 2293–2310.

6. Ghaneh, P.; Costello, E.; Neoptolemos, J.P. Biology and management of pancreatic cancer. *Gut* **2007**, *56*, p. 1134–1152.

7. Chan, A.; Diamandis, E.P.; Blasutig, I.M. *Strategies for discovering novel pancreatic cancer biomarkers.* J. Proteom. 2013, **81**, p. 126–34.

8. Ma, W.W.; Xie, H.; Fetterly, G.; Pitzonka, L.; Whitworth, A.; LeVea, C.; Wilton, J.; Mantione, K.; Schihl, S.; Dy, G.K.; et al. *A Phase Ib Study of the FGFR/VEGFR Inhibitor Dovitinib With Gemcitabine and Capecitabine in Advanced Solid Tumor and Pancreatic Cancer Patients*. Am. J. Clin. Oncol. 2018, **42**, p. 184–189.

9. Zhen, D.B.; Coveler, A.; Zanon, S.; Reni, M.; Chiorean, E.G. *Biomarker-driven and molecularly targeted therapies for pancreatic adenocarcinoma.* Semin. Oncol. 2018, **45**, 3.

10. Deberardinis, R.J.; Sayed, N.; Ditsworth, D.; Thompson, C.B. *Brick by brick: Metabolism and tumor cell growth.* Curr. Opin. Genet. Dev. 2008, **18**, p. 54–61.

11. Ramsey, M.R.; Sharpless, N.E. *ROS as a tumour suppressor?* Nat. Cell Biol. 2006, **8**, p. 1213–1215.

12. Takahashi, A.; Ohtani, N.; Yamakoshi, K.; Iida, S.I.; Tahara, H.; Nakayama, K.; Nakayama, K.I.; Ide, T.; Saya, H.; Hara, E. *Mitogenic signalling and the p16INK4a-Rb pathway cooperate to enforce irreversible cellular senescence.* Nat. Cell Biol. 2006, **8**, p. 1291–1297.

13. Williamson, J.M.; Boettcher, B.; Meister, A. *Intracellular cysteine delivery system that protects against toxicity by promoting glutathione synthesis.* Proc. Natl. Acad Sci. USA 1982, **79**, p. 6246–6249.

14. Zhang, J.; Ye, Z.W.; Gao, P.; Reyes, L.; Jones, E.E.; Branham-O'Connor, M.; Blumer, J.B.; Drake, R.R.; Manevich, Y.; Townsend, D.M.; et al. *Glutathione S-transferase P influences redox and migration pathways in bone marrow*. PLoS ONE 2014, **9**, p. e107478.

15. Keen, J.H.; Jakoby, W.B. *Glutathione transferases. Catalysis of nucleophilic reactions of glutathione.* J. Biol. Chem. 1978, **253**, p. 5654–5657.

16. Medeiros, R.; et al. *Metabolic susceptibility genes and prostate cancer risk in a southern European population: The role of glutathione S-transferases GSTM1, GSTM3, and GSTT1 genetic polymorphisms.* Prostate 2004, **58**, p. 414–420.

17. Ye, Z.; et al. *Five glutathione s-transferase gene variants in 23,452 cases of lung cancer and 30,397 controls: Meta-analysis of 130 studies.* PLoS Med. 2006, **3**, p. e91.

18. Tew, K.D.; Townsend, D.M. *Glutathione-s-transferases as determinants of cell survival and death.* Antioxid. Redox Signal. 2012, **17**, p. 1728–1737.

19. Adler, V.; et al. *Regulation of JNK signaling by GSTp.* EMBO J. 1999, **18**, p. 1321–1334.

20. Louie, S.M.; et al. *GSTP1 Is a Driver of Triple-Negative Breast Cancer Cell Metabolism and Pathogenicity*. Cell Chem. Biol. 2016, **23**, p. 567–578.

21. Ye, Z.W.; et al. *Glutathione S-Transferase P-Mediated Protein S-Glutathionylation of Resident Endoplasmic Reticulum Proteins Influences Sensitivity to Drug-Induced Unfolded Protein Response.* Antioxid. Redox Signal. 2017, **26**, p. 247–261.

22. Yang, Y.; et al. *Regulation of Endothelial Permeability by Glutathione S-Transferase Pi Against Actin Polymerization.* Cell. Physiol. Biochem. 2018, **45**, p. 406–418.

23. Findlay, V.J.; et al. *Tumor cell responses to a novel glutathione S-transferase-activated nitric oxide-releasing prodrug.* Mol. Pharmacol. 2004, **65**, p. 1070–1079.

24. Checa-Rojas, A.; et al. *GSTM3 and GSTP1: Novel players driving tumor progression in cervical cancer*. Oncotarget 2018, **9**, p. 21696–21714.

25. Tew, K.D.; et al. *The role of glutathione S-transferase P in signaling pathways and S-glutathionylation in cancer*. Free Radic. Biol. Med. 2011, **51**, p. 299–313.

26. Uhlen, M.; et al. *Proteomics. Tissue-based map of the human proteome.* Science 2015, **347**, p. 1260419.

27. Daemen, A.; et al. *Metabolite profiling stratifies pancreatic ductal adenocarcinomas into subtypes with distinct sensitivities to metabolic inhibitors.* Proc. Natl. Acad Sci. USA 2015, **112**, p. E4410–E4417.

28. Deer, E.L.; et al. *Phenotype and genotype of pancreatic cancer cell lines.* Pancreas 2010, **39**, p. 425–435.

29. Kanwal, R.; et al. *Protection against oxidative DNA damage and stress in human prostate by glutathione S-transferase P1*. Mol. Carcinog. 2014, **53**, p. 8–18.

30. Wu, Y.; et al. *Human glutathione S-transferase P1-1 interacts with TRAF2 and regulates TRAF2-ASK1 signals.* Oncogene 2006, **25**, p. 5787–5800.

31. Wang, T.; et al. Glutathione S-transferase P1-1 (GSTP1-1) inhibits c-Jun N-terminal kinase (JNK1) signaling through interaction with the C terminus. J. Biol. Chem. 2001, **276**, p. 20999–21003.

32. Tew, K.D.; Townsend, D.M. *Regulatory functions of glutathione S-transferase P1-1 unrelated to detoxification*. Drug Metab. Rev. 2011, **43**, p. 179–193.

33. Tew, K.D. *Glutathione-associated enzymes in anticancer drug resistance.* Cancer Res. 1994, **54**, p. 4313–4320.

34. Fujitani, N.; et al. *Silencing of Glutathione S-Transferase Pi Inhibits Cancer Cell Growth via Oxidative Stress Induced by Mitochondria Dysfunction.* Sci. Rep. 2019, **9**, p. 14764.

35. Arrick, B.A.; et al. *Glutathione depletion sensitizes tumor cells to oxidative cytolysis.* J. Biol. Chem. 1982, **257**, p. 1231–1237.

36. Arrick, B.A.; Nathan, C.F. *Glutathione metabolism as a determinant of therapeutic efficacy: A review.* Cancer Res. 1984, **44**, p. 4224–4232.

37. Karki, K.; et al. *Piperlongumine Induces Reactive Oxygen Species (ROS)-Dependent Downregulation of Specificity Protein Transcription Factors.* Cancer Prev. Res. 2017, **10**, p. 467–477.

38. Elsby, R.; et al. *Increased constitutive c-Jun N-terminal kinase signaling in mice lacking glutathione S-transferase Pi.* J. Biol. Chem. 2003, **278**, p. 22243–22249.

39. Mohammad, J.; et al. *JNK inhibition blocks piperlongumine-induced cell death and transcriptional activation of heme oxygenase-1 in pancreatic cancer cells.* Apoptosis 2019, **24**, p. 730-744.

40. Pathi, S.S.; et al. *Pharmacologic doses of ascorbic acid repress specificity protein (Sp) transcription factors and Sp-regulated genes in colon cancer cells.* Nutr. Cancer 2011, **63**, p. 1133–1142.

41. Wang, L.; et al. *Transcription factor Sp1 expression is a significant predictor of survival in human gastric cancer.* Clin. Cancer Res. 2003, **9**, p. 6371–6380.

42. Jutooru, I.; et al. *Mechanism of action of phenethylisothiocyanate and other reactive oxygen species-inducing anticancer agents.* Mol. Cell. Biol. 2014, **34**, p. 2382–2395.

43. Safe, S.; et al. *Specificity Protein Transcription Factors and Cancer: Opportunities for Drug Development.* Cancer Prev. Res. 2018, **11,** p. 371–382.

44. O'Hagan, H.M.; et al. *Oxidative damage targets complexes containing DNA methyltransferases, SIRT1, and polycomb members to promoter CpG Islands.* Cancer Cell 2011, **20**, p. 606–619.

45. Pathi, S.S.; et al. *GT-094, a NO-NSAID, inhibits colon cancer cell growth by activation of a reactive oxygen species-microRNA-27a: ZBTB10-specificity protein pathway.* Mol. Cancer Res. 2011, **9**, p. 195–202.

46. Li, G.Z.; Tao, H.L.; Zhou, C.; Wang, D.D.; Peng, C.B. *Midazolam prevents motor neuronal death from oxidative stress attack mediated by JNK-ERK pathway.* Hum. Cell 2018, **31**, p. 64–71.

47. Chintharlapalli, S.; et al. *Betulinic acid inhibits colon cancer cell and tumor growth and induces proteasome-dependent and -independent downregulation of specificity proteins (Sp) transcription factors.* BMC Cancer 2011, **11**: 371.

48. Hedrick, E.; et al. *Specificity protein (Sp) transcription factors Sp1, Sp3 and Sp4 are non-oncogene addiction genes in cancer cells.* Oncotarget 2016, **7**, p. 22245–22256.

49. Qie, S.; Diehl, J.A. *Cyclin D1, cancer progression, and opportunities in cancer treatment.* J. Mol. Med. 2016, **94**, p. 1313–1326.

50. Laphanuwat, P.; et al. *Cyclin D1 depletion interferes with oxidative balance and promotes cancer cell senescence.* J. Cell Sci. 2018, **131**, doi: 10.1242/jcs.214726.

51. Dong, Y.; et al. *Cyclin D1-CDK4 complex, a possible critical factor for cell proliferation and prognosis in laryngeal squamous cell carcinomas.* Int. J. Cancer 2001, **95**, p. 209–215.

52. Jutooru, I.; et al. *Inhibition of NFkappaB and pancreatic cancer cell and tumor growth by curcumin is dependent on specificity protein down-regulation.* J. Biol. Chem. 2010, **285**, p. 25332–25344.

53. Sheng, L.; et al. *SP1-induced upregulation of lncRNA PANDAR predicts adverse phenotypes in retinoblastoma and regulates cell growth and apoptosis in vitro and in vivo.* Gene 2018, **668**, p. 140-145.

54. Hedrick, E.; et al. *Histone Deacetylase Inhibitors Inhibit Rhabdomyosarcoma by Reactive Oxygen Species-Dependent Targeting of Specificity Protein Transcription Factors.* Mol. Cancer Ther. 2015, **14**, p. 2143–2153.

55. Ascione, A.; et al. *The glutathione S-transferase inhibitor 6-(7-nitro-2,1,3-benzoxadiazol-4-ylthio)hexanol overcomes the MDR1-P-glycoprotein and MRP1-mediated multidrug resistance in acute myeloid leukemia cells.* Cancer Chemother. Pharmacol. 2009, **64**, p. 419–424.

56. Tregno, F.P.; Sau, A.; Pezzola, S.; Geroni, C.; Lapenta, C.; Spada, M.; Filomeni, G.; Bonanno, E.; Federici, G.; Caccuri, A.M. *In vitro and in vivo efficacy of 6-(7-nitro-2,1,3-benzoxadiazol-4-ylthio)hexanol (NBDHEX) on human melanoma.* Eur. J. Cancer 2009, **45**, p. 2606–2617.

57. Zhuo, R.; et al. *Targeting Glutathione S-transferase M4 in Ewing sarcoma.* Front. Pediatr. 2014, **2**, p. 83.

58. Ruscoe, J.E.; et al. *Pharmacologic or genetic manipulation of glutathione S-transferase P1-1 (GSTpi) influences cell proliferation pathways.* J. Pharmacol. Exp. Ther. 2001, **298**, 339–345.

59. Mahadevan, D.; Sutton, G.R. *Ezatiostat hydrochloride for the treatment of myelodysplastic syndromes.* Expert Opin. Investig. Drugs 2015, **24**, p. 725–733.

60. Dhillon, H.; et al. *Transcriptome Analysis of Piperlongumine-Treated Human Pancreatic Cancer Cells Reveals Involvement of Oxidative Stress and Endoplasmic Reticulum Stress Pathways.* J. Med. Food 2016, **19**, p. 578–585.

61. Livak, K.J.; Schmittgen, T.D. Schmittgen, *Analysis of relative gene expression data using real-time quantitative PCR and the 2(-Delta Delta C(T)) Method.* Methods 2001, **25**, p. 402–408.

62. Garber, J.C. *On the care and use of US lab animals.* Nature 2011, **476**, p. 152.

IV. GLUTATHIONE S-TRANSFERASE PI-1 KNOCKDOWN REDUCES mRNA OF GENES ASSOCIATED WITH TRANSLATION AND CAUSES SENESCENCE IN HUMAN PANCREATIC CANCER CELLS

Abstract

Glutathione S-transferase Pi-1 (GSTP1) is an important phase-II antioxidant enzyme that conjugates reduced glutathione with electrophilic compounds. It is well established that GSTP1 contributes to the process of tumorigenesis by detoxifying xenobiotic compounds such as chemotherapeutics. GSTP1 is overexpressed in numerous cancers where its high expression is associated with reduced survival. Conversely, a reduction in GSTP1 expression results in reduced cancer cell growth and survival. Recently, it was proposed that GSTP1 acts as a metabolic driver of triple negative breast cancer by triggering oxidative stress-mediated signaling and impairing glycolytic and lipid metabolism. However, the anticancer mechanisms underlying GSTP1 inhibition have not been comprehensively elucidated. In this study, we report changes in the transcriptome of MIA PaCa-2 human pancreatic cancer cells upon GSTP1 inhibition, using RNA-Sequencing technology. We found 847 genes to be differentially expressed in GSTP1-knockdown MIA PaCa-2 cells. The genes related to mRNA translation, ribosome machinery, and cell cycle were significantly downregulated, while the ones promoting apoptosis and senescence were upregulated. This study suggests that loss of GSTP1 results in significant transcriptomic changes in PDAC cells and underlines various potential mechanisms by which GSTP1 inhibition impairs cancer cell growth and survival.

Introduction

Pancreatic ductal adenocarcinoma (PDAC) is the most common type of pancreatic cancer and accounts for more than 45,000 deaths annually in the US alone [1]. Due to the lack of specific

symptoms at early stages, PDACs are often diagnosed at late, metastatic stages [2, 3]. PDACs are preceded by the occurrence of precancerous, hyperplastic lesions known as pancreatic intraepithelial neoplasias (PanINs) and intraductal papillary mucinous neoplasms (IPMNs) [4]. This course of evolution from precancerous lesions to the malignant disease is orchestrated by well-characterized genetic alterations: oncogenic KRAS mutation and inactivation of the tumor suppressors CDKN2A, TP53, and SMAD4 [5]. In addition, a multitude of other genes and metabolic changes contribute to the process of PDAC tumorigenesis [6]. Interpreting how various signaling pathways interact in different stages of PDAC progression is crucial for the development of selective and competent therapies to treat the disease.

Similar to other cancer cells, PDAC cells encounter higher oxidative stress due to accelerated metabolism [7]. It was previously shown that antioxidant enzymes, such as glutathione S-transferase Pi-1 (GSTP1), are overexpressed in PDAC cells and tissues to maintain the optimal redox balance [8]. GSTP1 is a primary phase-II detoxification enzyme and is indispensable in maintaining redox homeostasis [9]. GSTP1 protects cells from oxidative stress and subsequent macromolecular damage by conjugating reactive electrophiles to glutathione (GSH) [10]. Other than its cytoprotective functions, growing evidence suggests that GSTP1 plays an important role in cell signaling and metabolism [11, 12]. In particular, GSTP1 regulates stress-mediated signaling by inhibiting the phosphorylation of JNK [13]. Recent studies show that GSTP1 mediates S-glutathionylation of diverse proteins [14] and can detoxify antineoplastic drugs [15]. Interestingly, evidence suggests that the CRAF/ERK signaling cascade, critical for growth in mutant KRAS-driven cancers, is controlled by interactions of CRAF with GSTP1 [16]. Because of its emerging multifaceted role in cell survival [8, 12, 17], protein maturation [14], and drug resistance [18, 19],

it is important to understand the contributions of GSTP1 in tumor progression and cancer pathogenicity.

Genetic knockdown or pharmacological inhibition of GSTP1 resulted in a differential metabolic response in triple-negative breast cancer (TNBC) cells compared to the control [12]. It was concluded that GSTP1 inactivation leads to impaired glycolytic metabolism, reduced ATP production, and decreased macromolecules such as phospholipids and nucleotides. Additionally, doxycycline-inducible knockdown of GSTP1 showed significant reduction in xenograft models of breast, lung, and pancreatic cancer. It was reported that GSTP1 promotes dimerization and activation of CRAF protein and contributes to growth and survival of mutant KRAS cancer cells [16]. With its established role in cancer cell signaling and post-translational modification, we hypothesized that GSTP1 inhibition would alter the transcriptome of PDAC cells. This present study provides evidence that loss of GSTP1 expression for prolonged time causes dramatic effect on the transcriptome of PDAC cells. We find new evidence that GSTP1 maintains cellular homeostasis by contributing to mRNA translation and maturation, cell cycle, and inhibiting apoptosis. Furthermore, we report that GSTP1 knockdown causes senescence in PDAC cells.

Materials and methods

Chemicals

Puromycin was purchased from Sigma-Aldrich, St. Louis, MO, USA. Senescence β-galactosidase staining kit was purchased from Cell Signaling Technologies, Danvers, MA, USA.

Cell culture

MIA PaCa-2 (human PDAC cell line) was obtained from American Type Culture Collection (ATCC), Manassas, VA. MIA PaCa-2 cells were cultured in DMEM high-glucose media (GE Healthcare Life Sciences, Chicago, IL) containing 10% (v/v) fetal bovine serum

(Atlanta Biologicals, Flowery Branch, GA) and 2.5% (v/v) horse serum (Corning, Corning, NY). Cells were maintained at 37°C with 5% carbon dioxide. The cells were subcultured by enzymatic digestion with 0.25% trypsin/1 mM EDTA solution (GE Healthcare Life Sciences, Chicago, IL) when they were ~75% confluent. All cell lines tested negative for Mycoplasma contamination.

Constructing GSTP1 knockdown cell lines

Two independent short-hairpin oligonucleotides were used to knock down the expression of GSTP1. Lentiviral particles containing the shRNA (Sigma, St. Louis, MO) were used to infect the MIA PaCa-2 cells with polybrene (Sigma-Aldrich, St. Louis, MO). Transfected cells were selected over with 5 µg/ml puromycin (Sigma-Aldrich, St. Louis, MO). The short-hairpin sequences used to achieve the knockdown of GSTP1 expression were: shGSTP1-1, CCGGCCTCACCCTGTACCAGTCCAACTCGAGTTGGACTGGTACAGGGTGAGGTTTTG; and shGSTP1-2, CCGGCGCTGACTACAACCTGCTGGACTCGAGTCCAGCAGGTTGTAGT CAGCGTTTTTG. Scrambled GSTP1 shRNA, empty vector (pLKO.1), and shRNA targeting GFP were used as controls. GSTP1 knockdown was previously confirmed by qPCR and western blotting techniques.

RNA sequencing

Following GSTP1 knockdown, total RNA was extracted using Fisher SurePrep RNA isolation kit (Thermo Fisher Scientific, Waltham, MA) abiding by the manufacturer's instructions. RNA was quantified using a NanoDrop (Thermo Fisher Scientific, Waltham, MA). Three micrograms of total RNA per sample was sent to University of Minnesota Genomics Center, St. Paul, MN. All the samples passed quality control with an RNA integrity number (RIN) of ≥ 9.5. Illumina TruSeq library kit was used to generate six dual-indexed stranded libraries. Mean quality

scores of all libraries was > Q30. The libraries were pooled and sequences in two lanes of the flow cell on an Illumina HiSeq 2500. 50 nt single-end reads were generated using v4 chemistry.

Transcriptome analysis

The raw fastq files were trimmed using Trim Galore (Babraham Bioinformatics) to remove the adaptor sequences. Post-trimming, high-quality reads for each sample were aligned using HISAT2 to the most updated reference human genome (GRCh38) provided by the Genome Research Consortium. SAMtools and BAMtools were used to convert and sort the BAM files. Gene expression was calculated as the total number of reads for each sample that uniquely aligned to the reference genome, binned by gene coordinate annotations. Differential expression analysis between control and GSTP1knockodwn PDAC cells was performed using the Bioconductor package, DESeq2. To account for differences in sequencing depth across samples, raw read counts were normalized using methodologies implemented in DESeq2. Differential expression of the normalized read counts was performed using the negative binomial test with the Benjamini-Hochberg false discovery rate (FDR) adjustment method as applied by DESeq2. For our analysis, an FDR of 0.05 was applied, and any genes with a p-adjusted value of less than or equal to 0.05 and a log2fold change of less than -1 or greater than +1 were defined as significantly down- or upregulated.

RNA extraction and gene expression by qRT-PCR

Total RNA was extracted using QIAGEN RNeasy Mini Kit (Germantown, MD, USA) following the manufacturer's instructions. cDNA was synthesized using 500 ng of total RNA and the qScript cDNA synthesis kit (Quanta Biosciences, Beverly, MA, USA). The relative change in gene expression was calculated using the $2^{-\Delta\Delta Ct}$ method [20]. β-actin, β-tubulin, and HPRT were used as internal controls. The data represent the average ± standard deviation for three independent

experiments with two technical replicates each. The primer sequences of the genes analyzed are listed in Table 4.1.

Table 4.1. Primer sequences used for measuring mRNA expression via quantitative polymerase chain reaction.

Gene	Forward Sequence	Reverse Sequence
HPRT	5'-GAA CGT CTT GCT CGA GAT GTG-3′	5'TCC AGC AGG TCA GCA AAG AAT-3'
β-Actin	5'-TTG CCG ACA GGA TGC AGA-3′	5'-GCC GAT CCA CAC GGA GTA CTT-3'
β-Tubulin	5'-GTT CGC TCA GGT CCT TTT GG-3′	5'-CCC TCT GTG TAG TGG CCT TTG-3'
CSF2	5'- GTG GCC TGC AGC ATC TC -3′	5'- AGT GTC TCT ACT CAG GTT CAG G -3'
CDKN1A	5'-GGA CAG CAG AGG AAG ACC ATG T-3′	5'-GCC GTT TTC GAC CCT GAG A-3'
CTGF	5'- GGC GAG GTC ATG AAG AAG AA -3′	5'- TCT CCG TAC ATC TTC CTG TAG TA -3'
CYR61	5′- CTG ACC AGG ACT GTG AAG ATG -3′	5′- ATG CGG GCA GTT GTA GTT -3′
SERPINE1	5′- CTG GTG AAT GCC CTC TAC TTC -3′	5′- TGC TGC CGT CTG ATT TGT -3′

Analysis of cellular senescence

Senescence-associated β-galactosidase staining was performed according to the manufacturer's protocol. After removing the growth media from the control and GSTP1 knockdown MIA PaCa-2 cells, cells were washed with PBS before fixing. After 15 minutes of fixing, cells were washed twice with PBS and then stained with β-galactosidase staining solution (pH: 6.0). Cells were incubated overnight at 37 ºC without CO_2 before imaging using a microscope.

Results

GSTP1 knockdown induces a differential transcriptome in PDAC cells

We have previously shown that GSTP1 knockdown impairs the growth and survival in poorly differentiated mesenchymal (MIA PaCa-2) and epithelial (HPAF-II) PDAC cells. To determine the effects of GSTP1 knockdown on the transcriptome, RNA-Seq was performed for GSTP1 knockdown and scrambled-control PDAC cells. A total of 304,202,323 reads of single-

end, fifty base pair reads were obtained from six samples (three biological replicates of control and GSTP1 knockdown MIA PaCa-2 cells). We obtained an average of 50,683,526 high-quality reads for each sample. Approximately 97% of the reads were mapped to the human genome, and 61% aligned exclusively to the unique regions. The characteristics of the output reads are summarized in Table 4.2.

Table 4.2. Scrambled control (scr-shRNA) and GSTP1 knockdown (shGSTP1-1) PDAC cells were sequenced using Illumina HiSeq2500 with three replicates each.

Sample	QC Passed reads	Mapped reads	% mapped reads	Unique alignments	% unique alignments
MIA PaCa-2 scr-shRNA (Rep 1)	52,031,458	50,949,148	97.92	29,866,353	58.61
MIA PaCa-2 scr-shRNA (Rep 2)	52,488,084	51,123,371	97.40	28,841,113	56.41
MIA PaCa-2 scr-shRNA (Rep 3)	54,094,932	52,749,516	97.51	29,644,299	57.25
MIA PaCa-2 shGSTP1-1 (Rep 1)	50,292,802	48,904,134	97.24	29,826,699	60.99
MIA PaCa-2 shGSTP1-1 (Rep 2)	49,768,028	48,395,874	97.24	29,494,772	60.94
MIA PaCa-2 shGSTP1-1 (Rep 3)	52,156,706	50,668,940	97.15	30,949,765	61.08

A high correlation was observed between all three biological replicates of each sample, which is represented in the principal component analysis (PCA) plot (Figure 4.1A). A total of 2499 genes had significant changes in expression between control (scr-shRNA) and GSTP1 knockdown (shGSTP1-1) cells (Figure 4.1B). Of them, we classified 847 genes as differentially expressed. Differentially expressed genes were defined as genes with a log2fold change of less than -1 or greater than +1 and the p-adjusted value of less than 0.05. In GSTP1 knockdown MIA PaCa-2 cells, 460 genes were upregulated, and 387 were downregulated (Figure 4.1C).

The most significantly downregulated (Figure 4.1D) and upregulated (Figure 4.1E) were selected using DESeq2 with an increased cut-off defined as a p-adjusted value of less than or equal

to 0.01 and a fold-change of 2 or higher. The top differentially-expressed genes were visualized using the heatmap tool in the ggplot2 library.

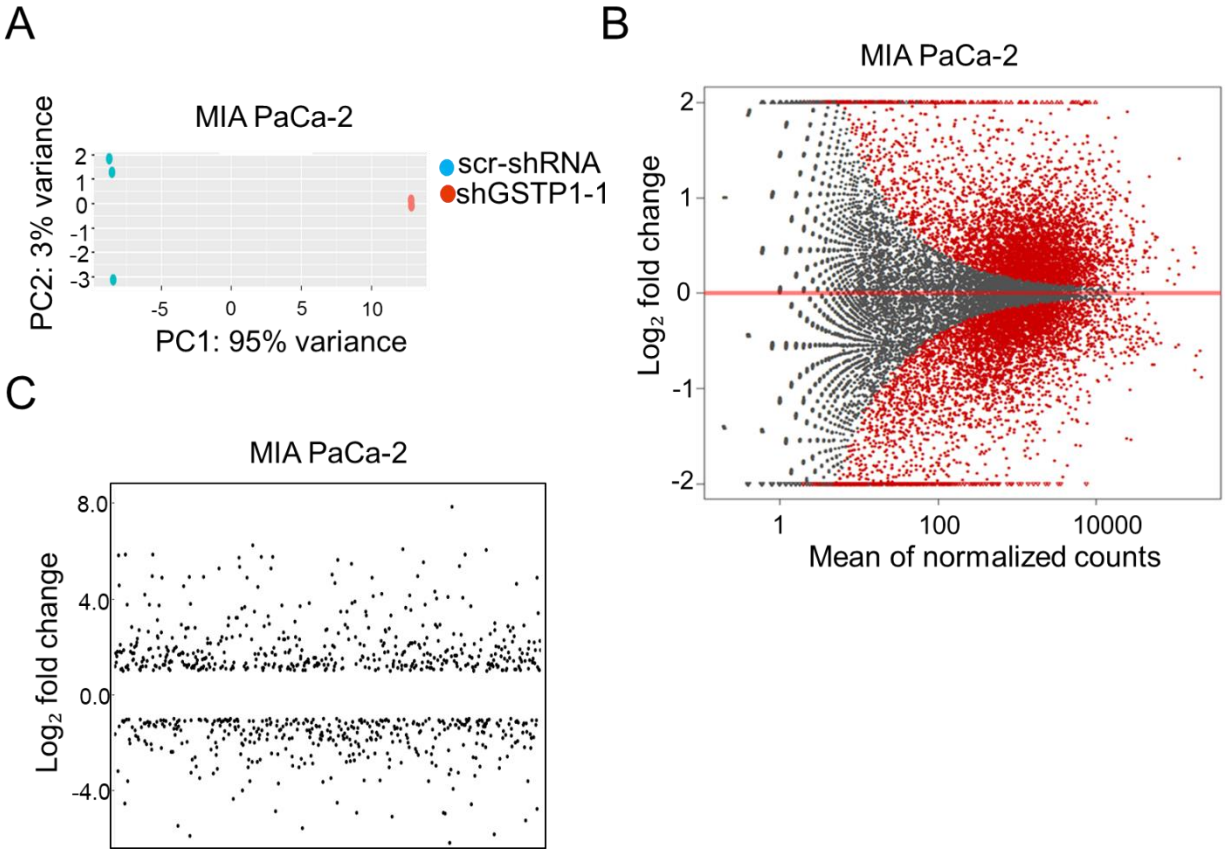

Figure 4.1. GSTP1 knockdown induces a differential transcriptome in PDAC cells. (A) Principal component analysis (PCA) plot showing the divergent transcriptome of GSTP1 knockdown MIA PaCa-2 cells compared to the control cells. (B) MA-plot showing differentially expressed genes (red) between GSTP1 knockdown and control cells. (C) Scatter plot showing the number of differentially expressed genes (p_{adj} <0.01 and log_2-fold <-1 or >1) in GSTP1 knockdown cells compared to the control. (D) Heatmap showing the most significant downregulated and (E) upregulated genes in GSTP1 knockdown MIA PaCa-2 cells compared to the control. Turquoise coloring indicates downregulation of genes in GSTP1 knockdown MIA PaCa-2 cells compared to the control and red indicates upregulation of genes.

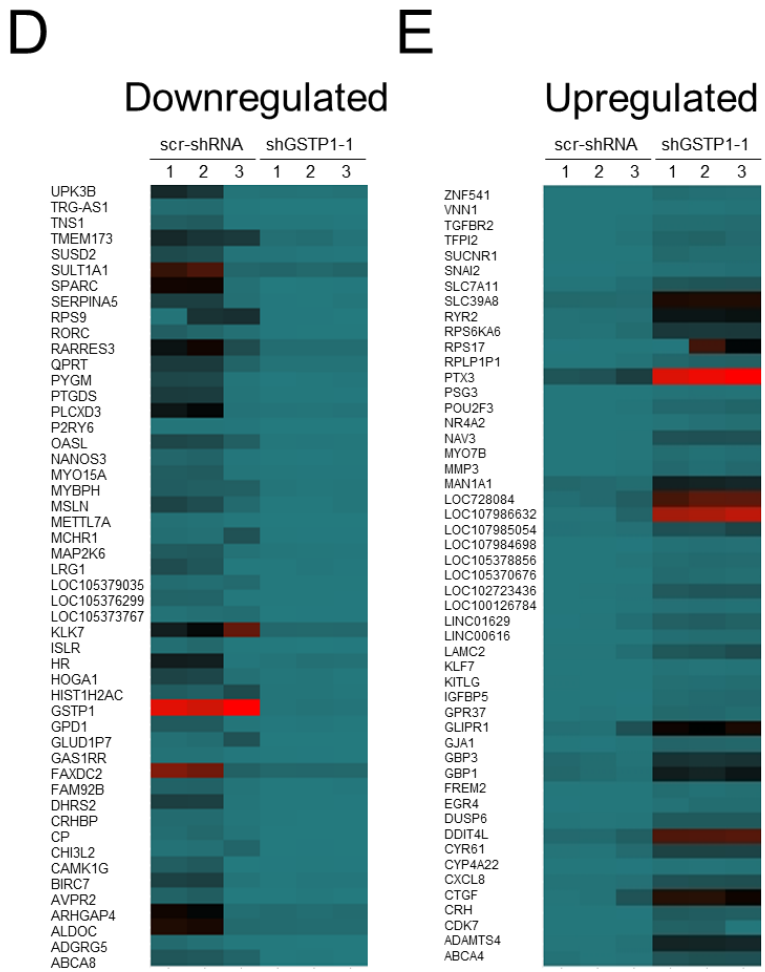

Figure 4.1. GSTP1 knockdown induces a differential transcriptome in PDAC cells (continued). (A) Principal component analysis (PCA) plot showing the divergent transcriptome of GSTP1 knockdown MIA PaCa-2 cells compared to the control cells. (B) MA-plot showing differentially expressed genes (red) between GSTP1 knockdown and control cells. (C) Scatter plot showing the number of differentially expressed genes (p_{adj} <0.01 and log_2-fold <-1 or >1) in GSTP1 knockdown cells compared to the control. (D) Heatmap showing the most significant downregulated and (E) upregulated genes in GSTP1 knockdown MIA PaCa-2 cells compared to the control. Turquoise coloring indicates downregulation of genes in GSTP1 knockdown MIA PaCa-2 cells compared to the control and red indicates upregulation of genes.

GSTP1 knockdown impairs the mRNA translation machinery

To determine the cellular and molecular changes associated with GSTP1 knockdown in PDAC cells, we used Ingenuity Pathway Analysis (IPA) software for functional pathway analysis. Gene-set enrichment analysis, using Enrichr, revealed that genes involved in mRNA translation

and modification were significantly downregulated in GSTP1 knockdown PDAC cells compared to the control (Table 4.3). In particular, cytoplasmic ribosomal proteins (p-value: 9.92E-28), cap-dependent translation initiation (p-value: 5.12E-18), protein metabolism (p-value: 1.24E-14), and activation of mRNA for translation (p-value: 1.12E-07) were among the top ten differentially regulated pathways (Figures 4.2A and B).

We report significant downregulation of ribosomal proteins of the small (RPSs) and the large (RPLs) subunits and the eukaryotic initiation factors (eIFs). To be specific, we report downregulation of 20 RPS and 41 RPL proteins. Because ribosomal proteins and initiation factors are indispensable in mRNA translation, we observe pathways such as translation initiation (Figure 4.2C), assembly of initiation complex (Figure 4.2D), and translation elongation (Figure 4.2E) to be negatively affected upon GSTP1 knockdown. To validate these results, enrichment analyses were performed using Reactome [21]. In addition to the above reported differentially regulated pathways, Reactome identified post-translation modification (Figure 4.2F), unfolded protein response (Figure 4.2G), and protein localization (Figure 4.2H) to be affected by GSTP1 knockdown in PDAC cells. Further, Gene Set Enrichment Analysis (GSEA 4.0.3) revealed a negative association of ribosome biogenesis (Figure 4.2I) and translation initiation factor (Figure 4.2J) with GSTP1 knockdown in PDAC cells.

Table 4.3. Significantly enriched pathways in GSTP1 knockdown PDAC cells. The q-value is an adjusted p-value calculated using the Benjamini-Hochberg method for correction for multiple hypotheses testing.

term	p-value	q-value
Cytoplasmic ribosomal proteins	9.92E-28	1.32E-24
Influenza infection	2.70E-24	1.79E-21
Influenza viral RNA transcription and replication	3.25E-23	1.44E-20
Translation	6.40E-21	2.13E-18
Cap-dependent translation initiation	5.12E-18	1.36E-15
Protein metabolism	1.24E-14	2.76E-12
Disease	1.40E-10	2.66E-08
Activation of mRNA upon binding of the cap-binding complex and eIFs, and subsequent binding to 43S	1.12E-07	1.86E-05
MAPK signaling pathway	3.78E-07	5.58E-05
FSH regulation of apoptosis	4.50E-07	5.98E-05
Interleukin-5 regulation of apoptosis	6.30E-07	7.61E-05
BDNF signaling pathway	1.66E-06	0.000184
MAP kinase signaling pathway	1.06E-05	0.00108
TGF-beta regulation of extracellular matrix	1.65E-05	0.001569
Interleukin-1 regulation of extracellular matrix	2.00E-05	0.001774
Prolactin regulation of apoptosis	3.67E-05	0.003052
Interleukin-2 signaling pathway	3.99E-05	0.00312
Gastrin pathway	4.42E-05	0.003261
Prolactin activation of MAPK signaling	8.29E-05	0.005799
Toll receptor cascades	0.000255	0.016949
Keratinocyte differentiation	0.000416	0.026324
Signal transduction through IL-1R	0.000454	0.026357
Integrin-mediated cell adhesion	0.000456	0.026357
TNF-alpha signaling pathway	0.000535	0.029647
Toll-like receptor signaling pathway regulation	0.000595	0.031626
RANKL signaling pathway	0.00066	0.03373
Fas signaling pathway	0.000796	0.038015
TNFR2 signaling pathway	0.000801	0.038015
NF-kappaB activation by non-typeable Hemophilus influenzae	0.000871	0.039899
Focal adhesion	0.001035	0.045836
TNF-alpha effects on cytokine activity, cell motility, and apoptosis	0.001101	0.047213
T cell receptor regulation of apoptosis	0.001198	0.049735
Oncostatin M	0.00182	0.073315
Selenium metabolism and selenoproteins	0.001922	0.075133
Post-translational protein modification	0.002059	0.078191
RIG-I-like receptor signaling pathway	0.002298	0.084818
MAP kinase pathway regulation through dual specificity phosphatases	0.002466	0.085785
ERBB1 downstream pathway	0.002539	0.085785
Tumor necrosis factor (TNF) pathway	0.002544	0.085785
Oxidative stress-induced gene expression via Nrf2	0.002638	0.085785
RhoA signaling pathway	0.002647	0.085785
Alternative NF-kappaB pathway	0.002954	0.093457
Glycosaminoglycan biosynthesis: heparan sulfate	0.003098	0.095738
CD40/CD40L signaling	0.003341	0.10092
Netrin-mediated signaling events	0.004324	0.120962
FRA pathway	0.004329	0.120962
Arrhythmogenic right ventricular cardiomyopathy (ARVC)	0.004347	0.120962
TGF-beta signaling pathway	0.004369	0.120962
JNK/MAPK pathway	0.004555	0.123553
Gene expression	0.00481	0.125206

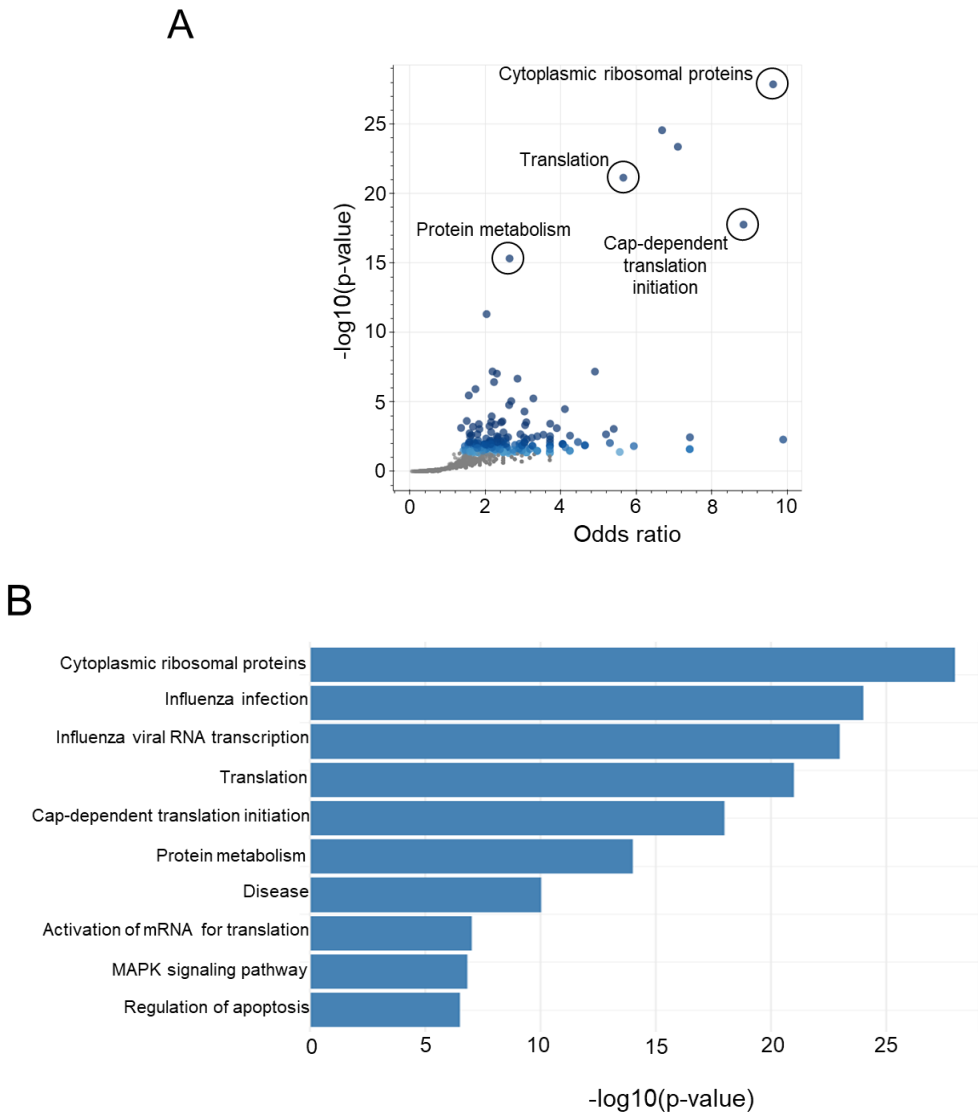

Figure 4.2. GSTP1 knockdown impairs the mRNA translation machinery. (A) The volcano plot shows the significance of each gene set versus its odds ratio analyzed using Enrichr. Each point represents a single gene set; the x-axis measures the odds ratio calculated for the gene set, while the y-axis gives the –log p-value of the gene set. (B) The bar chart shows the top 10 enriched terms. The y-axis shows the corresponding p-values. (C) Heatmap showing differential expression of genes associated with cap-dependent translation initiation, (D) translation initiation complex, (E) eukaryotic translation initiation, (F) post-translational modifications, (G) unfolded protein response, and (H) protein localization. Turquoise coloring indicates downregulation of genes in GSTP1 knockdown MIA PaCa-2 cells compared to the control, and red indicates upregulation of genes. (I) Gene Set Enrichment Analysis (GSEA) showing enrichment plot for ribosome biosynthesis and (J) mRNA translation initiation genes signatures.

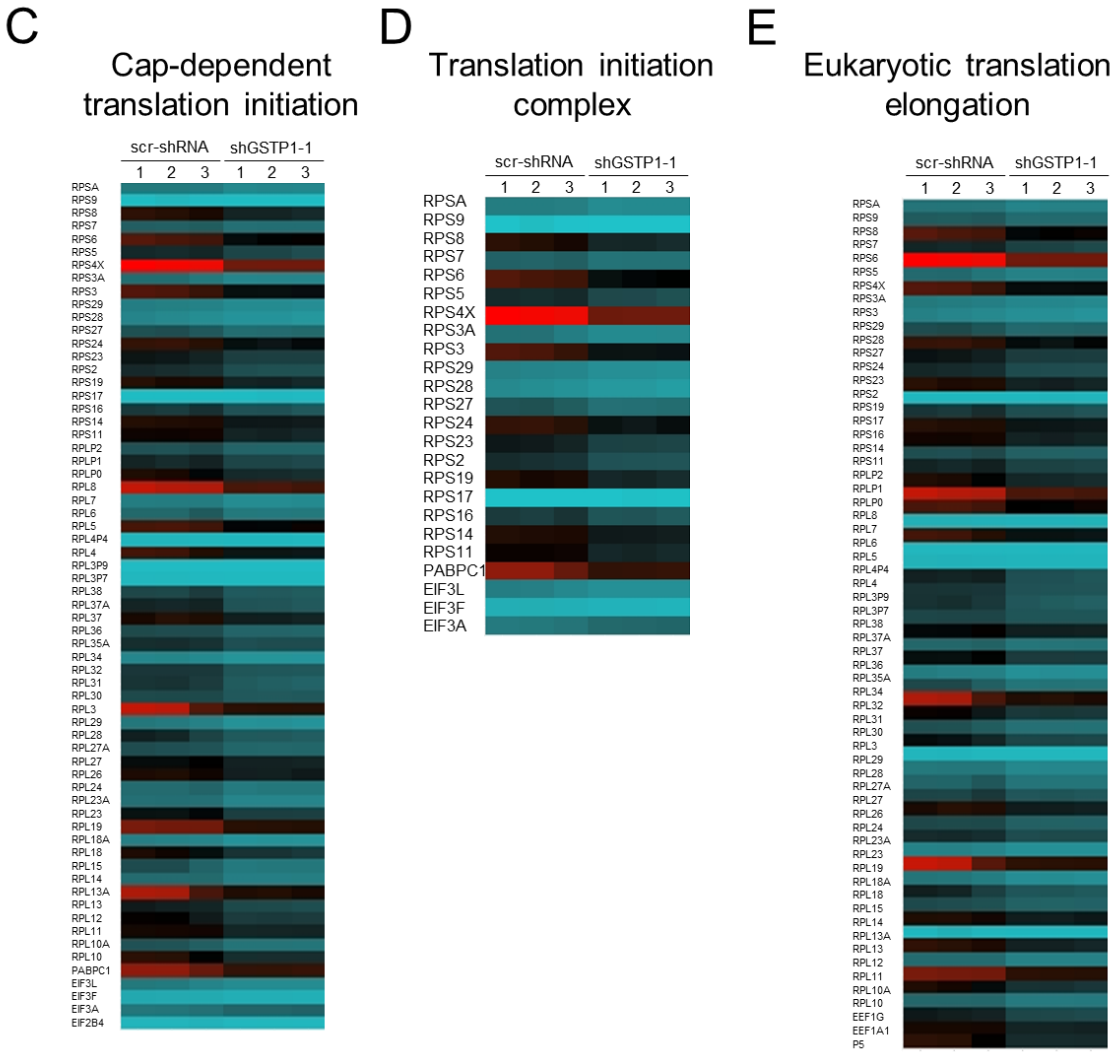

Figure 4.2. GSTP1 knockdown impairs the mRNA translation machinery (continued). (A) The volcano plot shows the significance of each gene set versus its odds ratio analyzed using Enrichr. Each point represents a single gene set; the x-axis measures the odds ratio calculated for the gene set, while the y-axis gives the –log p-value of the gene set. (B) The bar chart shows the top 10 enriched terms. The y-axis shows the corresponding p-values. (C) Heatmap showing differential expression of genes associated with cap-dependent translation initiation, (D) translation initiation complex, (E) eukaryotic translation initiation, (F) post-translational modifications, (G) unfolded protein response, and (H) protein localization. Turquoise coloring indicates downregulation of genes in GSTP1 knockdown MIA PaCa-2 cells compared to the control, and red indicates upregulation of genes. (I) Gene Set Enrichment Analysis (GSEA) showing enrichment plot for ribosome biosynthesis and (J) mRNA translation initiation genes signatures.

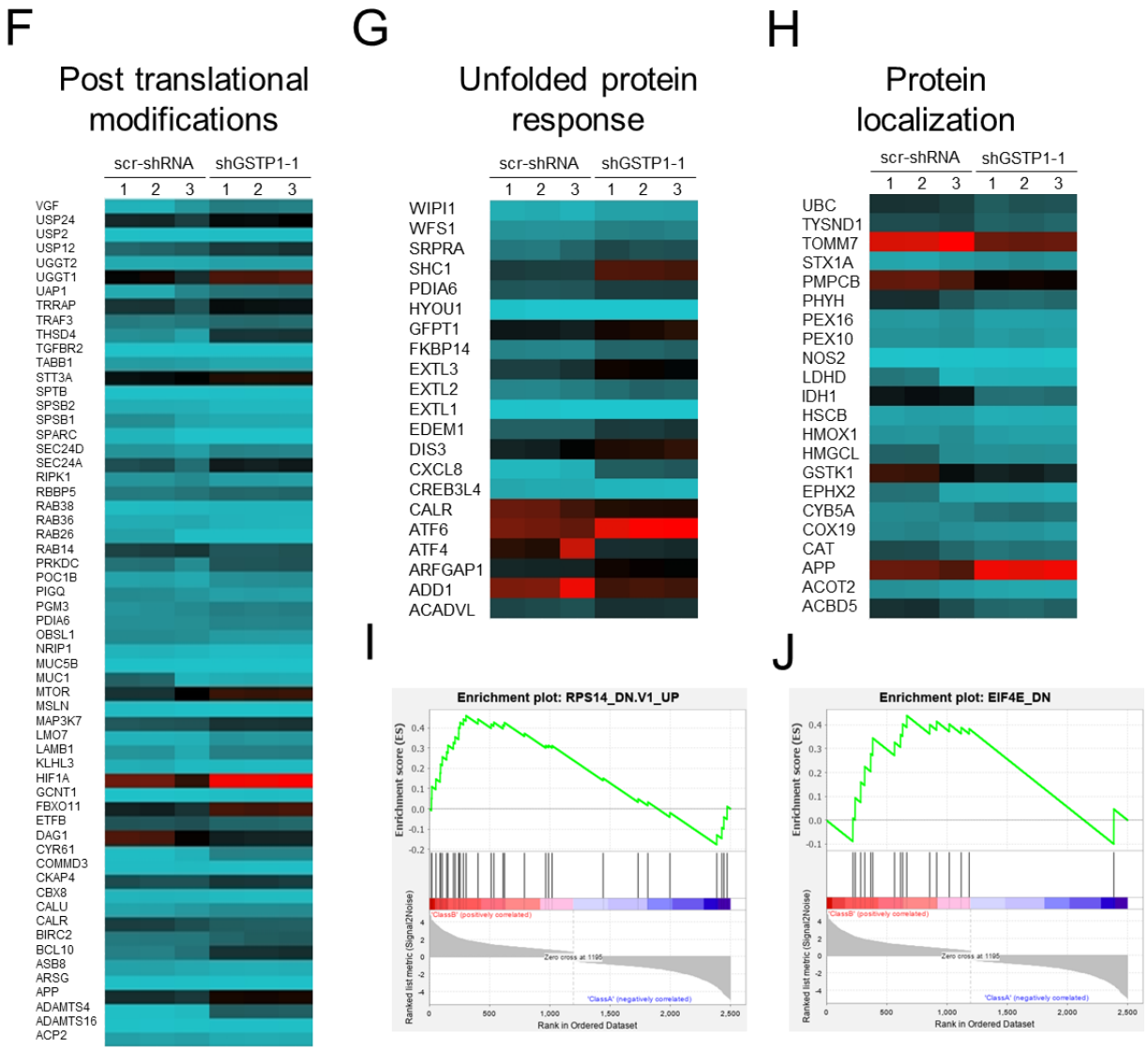

Figure 4.2. GSTP1 knockdown impairs the mRNA translation machinery (continued). (A) The volcano plot shows the significance of each gene set versus its odds ratio analyzed using Enrichr. Each point represents a single gene set; the x-axis measures the odds ratio calculated for the gene set, while the y-axis gives the –log p-value of the gene set. (B) The bar chart shows the top 10 enriched terms. The y-axis shows the corresponding p-values. (C) Heatmap showing differential expression of genes associated with cap-dependent translation initiation, (D) translation initiation complex, (E) eukaryotic translation initiation, (F) post-translational modifications, (G) unfolded protein response, and (H) protein localization. Turquoise coloring indicates downregulation of genes in GSTP1 knockdown MIA PaCa-2 cells compared to the control, and red indicates upregulation of genes. (I) Gene Set Enrichment Analysis (GSEA) showing enrichment plot for ribosome biosynthesis and (J) mRNA translation initiation genes signatures.

GSTP1 knockdown affects various cell survival pathways

In addition to mRNA translation, genes related to the cell cycle and programmed cell death were significantly enriched in the GSTP1 knockdown group. These included upregulation of cell-cycle inhibitory genes such as *CDKN1A* (p21), *ATR*, and *BRCA2* and downregulation of genes that promote mitotic entry, such as NEK7 (Figure 4.3A). Additionally, GSEA analysis shows enrichment of mitotic cell cycle (Figure 4.3B) and G_2/M checkpoint (Figure 4.3C) associated gene signatures. Further, we report that programmed cell death-promoting genes (*STAT3* and *CAD*) were upregulated in GSTP1 knockdown PDAC cells. However, the apoptosis-inhibiting genes, such as *PTK2* and *ADD1*, were found to be downregulated in GSTP1 knockdown cells (Figure 4.3D). Moreover, we report differential expression of genes associated with the JNK signaling pathway (Figure 4.3E). In addition, we found downregulation nuclear factor erythroid-derived 2-like 2, Nfe2l2/NRF2 (Figure 4.3F) that is an important regulator of redox control.

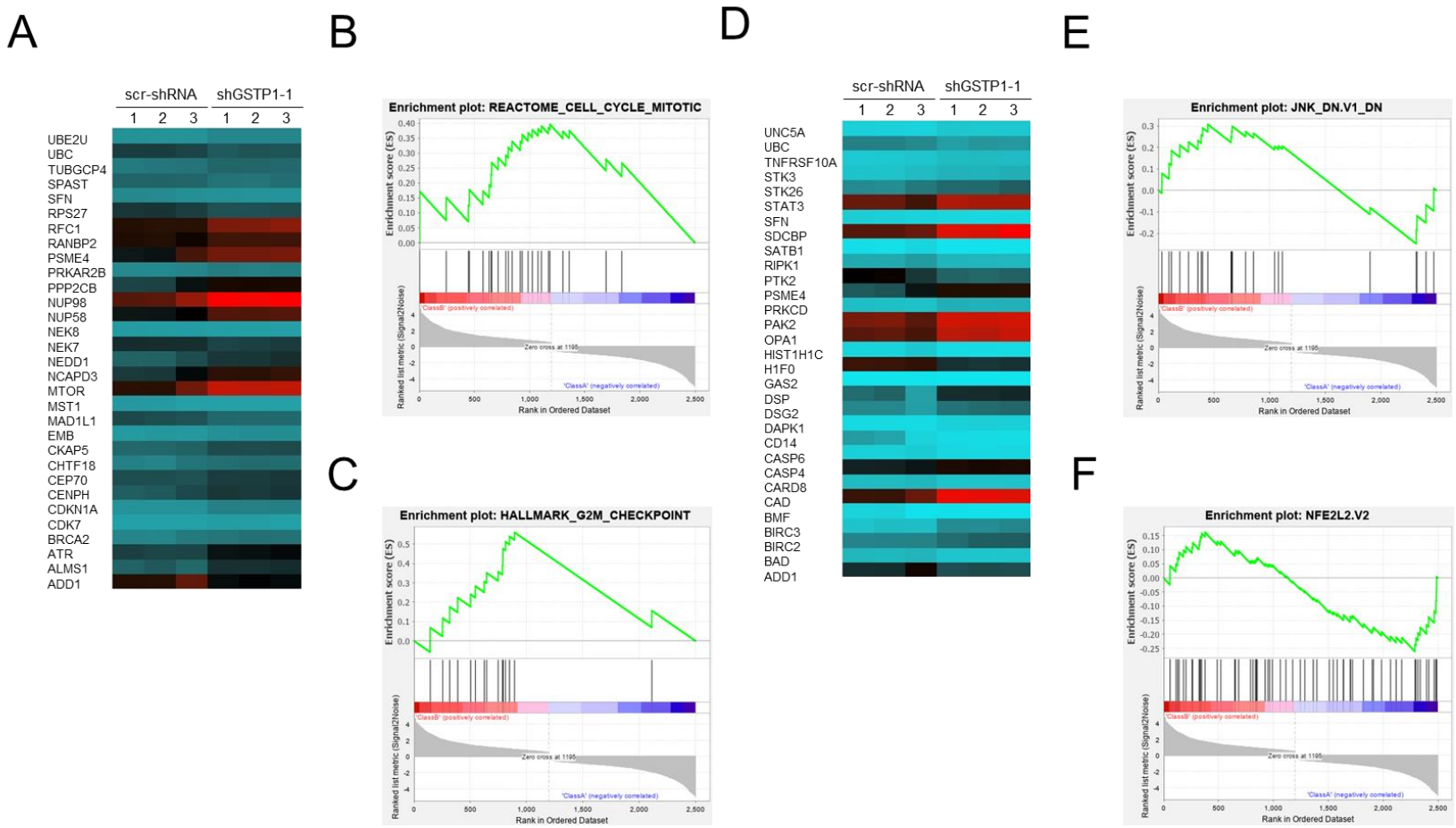

Figure 4.3. GSTP1 knockdown affects various cell survival pathways. (A) Heatmap showing differential expression of genes associated with cell cycle and (B) Gene Set Enrichment Analysis (GSEA) showing enrichment plot for mitotic cell cycle and (C) G_2/M checkpoint. (D) Heatmap showing the overexpression of programmed cell death-promoting genes in GSTP1 knockdown MIA PaCa-2 cells compared to the control. Turquoise coloring indicates downregulation of genes in GSTP1 knockdown MIA PaCa-2 cells compared to the control, and red indicates upregulation of genes. (E) Gene Set Enrichment Analysis (GSEA) showing enrichment plot for c-Jun N-terminal kinase (JNK) pathway, and (F) redox responsive transcription factor, nuclear factor erythroid-derived 2-like 2, Nfe2l2/NRF2.

GSTP1 knockdown causes senescence in PDAC cells

Among the differentially expressed genes, the ones that showed the most substantial change were found to be associated with cellular senescence. These included upregulation of several senescence-promoting genes, such as *CYR61*, *CTGF*, *CDKN1A* (p21), *SERPINE1*, *MAPK9*, *MAP2K3*, and *MSN*. Further, functional pathway analysis using Reactome revealed oxidative stress-induced senescence as one of the significantly regulated pathways (Figure 4.4A). To validate the RNA-Seq data, we analyzed the mRNA levels of senescence-associated genes. We report upre*gulation of senescence-promoting genes, such as CDKN1A, CTGF, CSF2, CYR61, and* SERPINE1, in GSTP1 knockdown PDAC cells compared to the control (Figure 4.4B). Additionally, we found increased expression of senescence-associated β-galactosidase, a characteristic hallmark of senescent cells, in GSTP1 knockdown PDAC cells (Figure 4.4C).

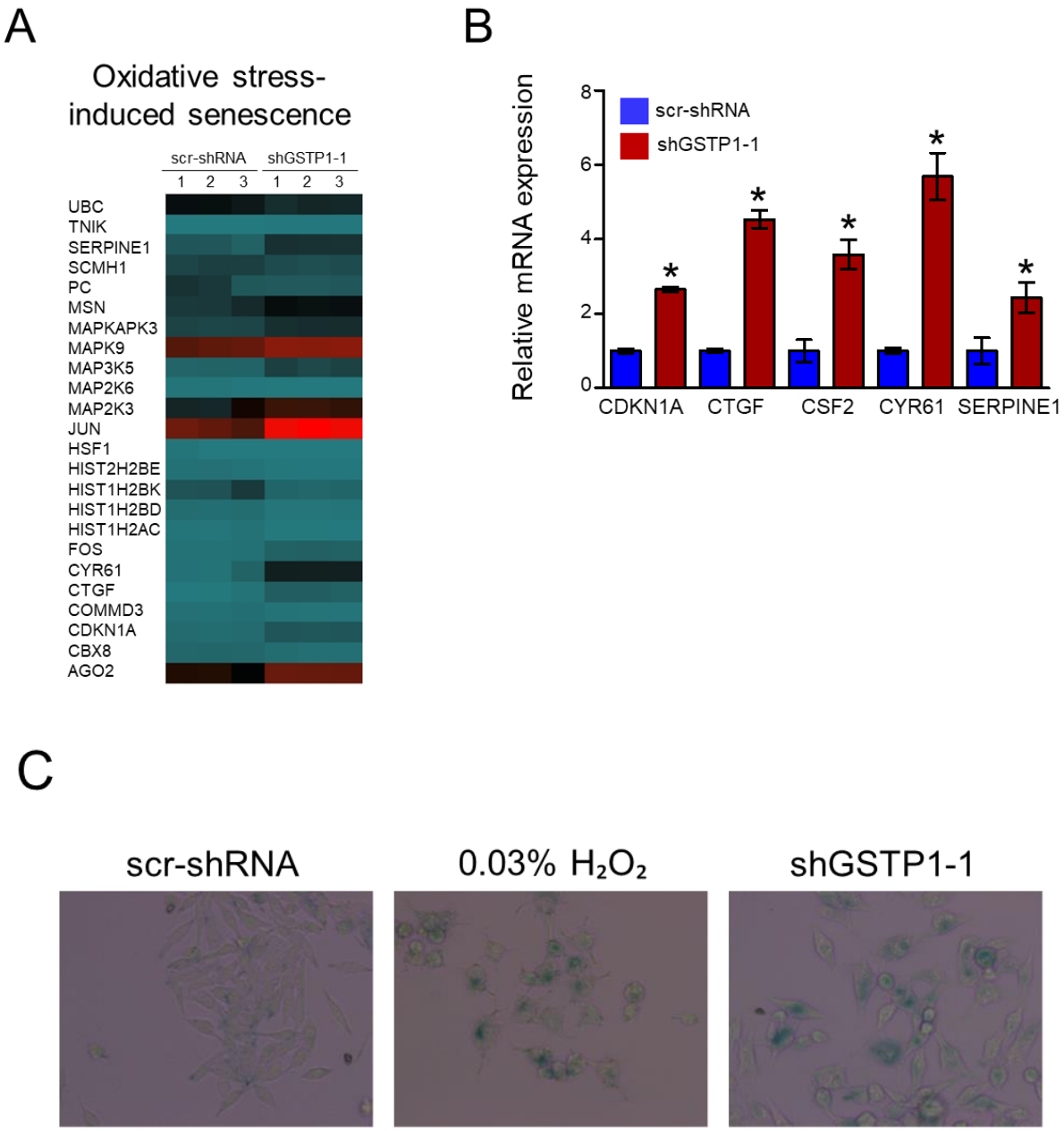

Figure 4.4. GSTP1 knockdown causes senescence in PDAC cells. (A) Heat map showing the genes associated with cellular senescence that are differentially expressed in GSTP1 knockdown cells (shGSTP1-1) compared to the scrambled controls (scr-shRNA) as predicted by RNA-Sequencing. (B) qPCR validation of selected genes associated with senescence. Significant changes in mRNA expression levels are denoted with * ($p < 0.05$) (C) Scrambled control and GSTP1 knockdown MIA PaCa-2 cells were stained for senescence-associated β-galactosidase. 0.03% H_2O_2 was used as a positive control.

Discussion

Using *in vitro* and pancreatic cancer mouse models, we have previously shown that GSTP1 contributes to PDAC pathogenicity [8]. Genetic knockdown of GSTP1 resulted in impaired cell survival and activation of oxidative stress-mediated apoptotic signaling. In this study, our goal was to comprehensively understand the underlying mechanisms of reduced cell growth upon GSTP1 inhibition. We used an RNA-Seq approach to investigate the global transcriptomic changes in GSTP1 knockdown PDAC cells and then validated the results of a subset of genes using RT-qPCR. Our data provide evidence that GSTP1 knockdown reduces cell growth and survival by weakening the mRNA translation machinery in PDAC cells.

Ubiquitous expression of GSTP1 in all mammalian tissues suggests that GSTP1 has important cellular roles [9]. Previously, it has been shown that GSTP1 contributes to the process of tumorigenesis in the breast [12], cervical [17], and pancreatic cancer [8]. GSTP1 overexpression in neoplastic tissue is often associated with resistance to chemotherapy and poor patient survival [22-24]. Evidence suggests that GSTP1 promotes the cell cycle [17] and inhibits oxidative-stress mediated apoptosis in cancer cells [8]. More recently, studies have shown that the cancer cell growth in mutant KRAS-driven neoplasms, such as PDAC [25], non-small cell lung [26], and colorectal cancers [27], is determined by the interactions between CRAF and GSTP1 [16]. These data have provided compelling evidence that GSTP1 is not only crucial in minimizing oxidative stress but plays an important role in cancer cell signaling and drug resistance. In the present study, for the first time, we report that GSTP1 knockdown impairs mRNA translation and causes senescence in PDAC cells.

Aberrant signal transduction pathways are important hallmarks of cancer [28]. It is known that abnormal activation of these signaling molecules drives tumorigenesis by modifying the

activity of translation factors [29]. For example, MYC, a key regulator of protein synthesis, is activated in many cancers [30] and transcribes the elements of the translation machinery [31]. In particular, MYC drives the transcription of most ribosomal proteins and translation initiation factors [32].

Individual ribosomal proteins have been found to be upregulated in hepatocellular carcinoma [33], non-small cell lung cancer [34], and some gynecologic tumors [35]. Interestingly, we observe reduced gene expression of various ribosomal proteins upon GSTP1 inhibition in PDAC cells. These include *RPLP1*, *RPL3*, *RPL8*, *RPL10*, *RPL11*, *RPL13A*, *RPL19*, *RPL23A*, *RPS3*, *RPS4X*, *RPS6*, *RPS8*, *RPS11*, *RPS14*, and *RPS19*. In addition, another transcription factor, Sp1, transcribes ribosomal proteins such as *RPS24* and *RPS27*. We have previously shown that GSTP1 knockdown activates oxidative stress-mediated signaling and reduces the protein expression of Sp1 [8]. Here, in our RNA-Seq experiment, we see downregulation of *RPS24* and *RPS27* that are the targets of Sp1.

In addition to their crucial role in ribosomal biogenesis and mRNA translation, ribosomal proteins have physiological roles independent of the translation machinery. Evidence shows that the ribosomal proteins of the large and the small subunit contribute to tumorigenesis by activating NF-kB [36, 37], cyclin D1 [38], and ITGB4 [39] and inhibiting the activity of p27 [40] and DNA damage-induced p53 [41]. Further, studies have shown that some ribosomal proteins are overexpressed in multidrug-resistant gastric cancer cells [42] and inhibit chemotherapy-induced cell death [40]. Based on these data, we hypothesize that ribosomal insufficiency and subsequent impairment in translation and cell signaling are the underlying causes of reduced growth in GSTP1-knockdown PDAC cells.

Because mRNA translation is an energy-intensive process [43], exposure to stress results in attenuation of global protein synthesis [44]. We have previously reported that GSTP1 knockdown in PDAC cells causes oxidative stress due to the accumulation of reactive oxygen species. Based on the RNA-Seq data, we believe that the GSTP1-knockdown mediated oxidative stress results in the reduction of ribosomal proteins and protein synthesis. Since translation is finely tuned with cell proliferation and survival [45], decreased protein synthesis is often associated with impaired cell cycle and increased apoptosis [46]. In GSTP1-knockdown PDAC cells, we observed upregulation of the cell-cycle inhibitory genes, such as *CDKN1A* (p21), *ATR*, and *BRCA2*. In normal cells, p21 exerts its antiproliferative effects by inhibiting the cyclin kinases essential for cell cycle progression [47]. Studies show that p21 is an effective, universal CDK inhibitor [48]. It binds to and inhibits the activity of CDK1, CDK2, and CDK4/6 complexes, therefore functioning as a checkpoint regulator during the G_1/S phase [49]. Similarly, upregulation of *ATR* and *BRCA2* in GSTP1-knockdown cells suggests GSTP1 plays an important role in cell cycle regulation [50, 51].

We have previously shown that GSTP1 protects the PDAC cells from oxidative-stress mediated apoptosis [8]. Complementing the previous findings, our RNA-Seq experiment shows an upregulation of the pro-apoptotic gene, *STAT3*, in GSTP1-knockdown PDAC cells. STAT3 is a DNA-binding transcription factor that is activated by the transmembrane receptor tyrosine kinase, EGFR [52]. Studies have shown that in EGFR-mediated apoptosis, STAT3 is a key regulator of programmed cell death in myeloid leukemia and prostate cancer [53]. Further, we found upregulation of caspase-activated DNase (CAD) in GSTP1-knockdown PDAC cells. Apoptotic signaling triggers the nucleolytic activity that results in genomic DNA fragmentation [54]. Liu *et al*. [55] and Halenbeck *et al*. [56] have previously shown that CAD is the primary

nuclease that is activated in pre-apoptotic cells. These results suggest that GSTP1 knockdown causes apoptosis in PDAC cells.

Interestingly, GSEA analysis of our RNA-Seq data shows activation of NRF2 signaling pathway in GSTP1 knockdown PDAC cells. NRF2 is the principal regulator of cellular antioxidant response that has numerous functions in cell growth and survival [57]. It is well known that mutant KRAS (G12D) and Myc increase the transcription of NRF2 to activate the antioxidant system in cancer cells and promote tumorigenesis [58]. Therefore, dysregulated NRF2 signaling in GSTP1 knockdown cells suggests that targeting GSTP1 holds the potential to develop standalone or combination therapies to effectively treat KRAS-driven cancers.

In addition to impaired mRNA translation, aberrant cell cycle, and increased apoptosis, GSTP1-knockdown PDAC cells also showed increased senescence. Cellular senescence is defined as stress-induced, stable cell-cycle arrest [59]. Interestingly, in our RNA-Seq experiment, we see an upregulation of the CCN family of proteins (*CYR61*/*CCN1* and *CTGF*/*CCN2*). Previously it was shown that overexpression of CCN proteins results in premature senescence in fibroblasts; however, Ccn dm/dm mice exhibited reduced senescence during maturation [60]. Further, we report upregulation of *SERPINE1*, also known as plasminogen activator inhibitor-1. Studies show that SERPINE1 is secreted from senescent cells to trigger cell-cycle arrest and senescence in other cells of the microenvironment [61]. Based on our data, we conclude that GSTP1 knockdown induces senescence in PDAC cells.

The dismal response of targeted therapies in the clinic is often attributed to the intra-tumor heterogeneity [62]. This is because most drugs are designed to eliminate the cells bearing a specific genetic lesion, while the ones that are powered by other mutations survive the treatment and cause tumor relapse [63, 64]. Because the mRNA translation machinery is hyperactive in many tumors

[29] and integrates almost all oncogenic signals [65], developing therapeutic modalities that target the protein synthesis holds promise for disease-free survival in cancer patients. In this study, we show that GSTP1 contributes to tumorigenesis by increasing the transcription of the ribosomal proteins. Further, loss of GSTP1 induces the oxidative-stress response pathway resulting in a stable cell-cycle arrest and activation of the apoptotic signaling pathway. Taken together, our data suggest that targeting GSTP1 in combination with conventional antineoplastic drugs is a potential therapy to treat pancreatic cancer patients.

References

1. Siegel, R.L., K.D. Miller, and A. Jemal, *Cancer statistics, 2020.* CA Cancer J Clin, 2020. **70**(1): p. 7-30.

2. Lowenfels, A.B. and P. Maisonneuve, *Epidemiology and risk factors for pancreatic cancer*. Best Pract Res Clin Gastroenterol, 2006. **20**(2): p. 197-209.

3. Ghaneh, P., E. Costello, and J.P. Neoptolemos, *Biology and management of pancreatic cancer*. Gut, 2007. **56**(8): p. 1134-52.

4. Hruban, R.H., et al., *Pancreatic intraepithelial neoplasia: a new nomenclature and classification system for pancreatic duct lesions.* Am J Surg Pathol, 2001. **25**(5): p. 579-86.

5. Hezel, A.F., et al., *Genetics and biology of pancreatic ductal adenocarcinoma.* Genes Dev, 2006. **20**(10): p. 1218-49.

6. Jones, S., et al., *Core signaling pathways in human pancreatic cancers revealed by global genomic analyses.* Science, 2008. **321**(5897): p. 1801-6.

7. Raffenne, J., et al., *Pancreatic Ductal Adenocarcinoma Arising in Young and Old Patients Displays Similar Molecular Features.* Cancers (Basel), 2021. **13**(6).

8. Singh, R.R., et al., *Glutathione S-Transferase pi-1 Knockdown Reduces Pancreatic Ductal Adenocarcinoma Growth by Activating Oxidative Stress Response Pathways.* Cancers (Basel), 2020. **12**(6).

9. Zhang, J., et al., *Pleiotropic functions of glutathione S-transferase P*. Adv Cancer Res, 2014. **122**: p. 143-75.

10. Kural, C., et al., *Glutathione S-Transferases and Cytochrome P450 Enzyme Expression in Patients with Intracranial Tumors: Preliminary Report of 55 Patients.* Med Princ Pract, 2019. **28**(1): p. 56-62.

11. Tew, K.D. and D.M. Townsend, *Regulatory functions of glutathione S-transferase P1-1 unrelated to detoxification.* Drug Metab Rev, 2011. **43**(2): p. 179-93.

12. Louie, S.M., et al., *GSTP1 Is a Driver of Triple-Negative Breast Cancer Cell Metabolism and Pathogenicity.* Cell Chem Biol, 2016. **23**(5): p. 567-578.

13. Adler, V., et al., *Regulation of JNK signaling by GSTp.* EMBO J, 1999. **18**(5): p. 1321-34.

14. Townsend, D.M., et al., *Novel role for glutathione S-transferase pi. Regulator of protein S-Glutathionylation following oxidative and nitrosative stress.* J Biol Chem, 2009. **284**(1): p. 436-45.

15. Singh, R.R. and K.M. Reindl, *Glutathione S-Transferases in Cancer.* Antioxidants (Basel), 2021. **10**(5).

16. Niitsu, Y., et al., *A CRAF/glutathione-S-transferase P1 complex sustains autocrine growth of cancers with KRAS and BRAF mutations.* Proc Natl Acad Sci U S A, 2020. **117**(32): p. 19435-19445.

17. Checa-Rojas, A., et al., *GSTM3 and GSTP1: novel players driving tumor progression in cervical cancer.* Oncotarget, 2018. **9**(31): p. 21696-21714.

18. Ogino, S., et al., *Glutathione S-transferase Pi 1 is a valuable predictor for cancer drug resistance in esophageal squamous cell carcinoma.* Cancer Sci, 2019. **110**(2): p. 795-804.

19. Satoh, T., et al., *[An immunohistological study on expression of glutathione S-transferase pi (form) in human ovarian carcinoma].* Nihon Sanka Fujinka Gakkai Zasshi, 1995. **47**(9): p. 931-8.

20. Livak, K.J. and T.D. Schmittgen, *Analysis of relative gene expression data using real-time quantitative PCR and the 2(-Delta Delta C(T)) Method.* Methods, 2001. **25**(4): p. 402-8.

21. Jassal, B., et al., *The reactome pathway knowledgebase.* Nucleic Acids Res, 2020. **48**(D1): p. D498-D503.

22. Mousseau, M., et al., *A study of the expression of four chemoresistance-related genes in human primary and metastatic brain tumours.* Eur J Cancer, 1993. **29A**(5): p. 753-9.

23. Geng, M., et al., *The association between chemosensitivity and Pgp, GST-pi and Topo II expression in gastric cancer.* Diagn Pathol, 2013. **8**: p. 198.

24. Yu, D.S., D.S. Hsieh, and S.Y. Chang, *Increasing expression of GST-pi MIF, and ID1 genes in chemoresistant prostate cancer cells.* Arch Androl, 2006. **52**(4): p. 275-81.

25. Waters, A.M. and C.J. Der, *KRAS: The Critical Driver and Therapeutic Target for Pancreatic Cancer.* Cold Spring Harb Perspect Med, 2018. **8**(9).

26. Ferrer, I., et al., *KRAS-Mutant non-small cell lung cancer: From biology to therapy.* Lung Cancer, 2018. **124**: p. 53-64.

27. Hayama, T., et al., *G12V and G12C mutations in the gene KRAS are associated with a poorer prognosis in primary colorectal cancer.* Int J Colorectal Dis, 2019. **34**(8): p. 1491-1496.

28. Hanahan, D. and R.A. Weinberg, *Hallmarks of cancer: the next generation.* Cell, 2011. **144**(5): p. 646-74.

29. Robichaud, N., et al., *Translational Control in Cancer.* Cold Spring Harb Perspect Biol, 2019. **11**(7).

30. Wang, T., et al., *c-Myc Overexpression Promotes Oral Cancer Cell Proliferation and Migration by Enhancing Glutaminase and Glutamine Synthetase Activity.* Am J Med Sci, 2019. **358**(3): p. 235-242.

31. Cargnello, M. and I. Topisirovic, *c-Myc steers translation in lymphoma.* J Exp Med, 2019. **216**(7): p. 1471-1473.

32. Destefanis, F., V. Manara, and P. Bellosta, *Myc as a Regulator of Ribosome Biogenesis and Cell Competition: A Link to Cancer.* Int J Mol Sci, 2020. **21**(11).

33. Kondoh, N., et al., *Enhanced expression of S8, L12, L23a, L27 and L30 ribosomal protein mRNAs in human hepatocellular carcinoma.* Anticancer Res, 2001. **21**(4A): p. 2429-33.

34. Liu, F., et al., *Cloning of novel tumor metastasis-related genes from the highly metastatic human lung adenocarcinoma cell line Anip973.* J Genet Genomics, 2007. **34**(3): p. 189-95.

35. Artero-Castro, A., et al., *Expression of the ribosomal proteins Rplp0, Rplp1, and Rplp2 in gynecologic tumors.* Hum Pathol, 2011. **42**(2): p. 194-203.

36. Wan, F., et al., *Ribosomal protein S3: a KH domain subunit in NF-kappaB complexes that mediates selective gene regulation.* Cell, 2007. **131**(5): p. 927-39.

37. Yang, Z.Y., et al., *Knockdown of metallopanstimulin-1 inhibits NF-kappaB signaling at different levels: the role of apoptosis induction of gastric cancer cells.* Int J Cancer, 2012. **130**(12): p. 2761-70.

38. Kuroda, K., et al., *Identification of ribosomal protein L19 as a novel tumor antigen recognized by autologous cytotoxic T lymphocytes in lung adenocarcinoma.* Cancer Sci, 2010. **101**(1): p. 46-53.

39. Yang, Z.Y., et al., *Metallopanstimulin-1 regulates invasion and migration of gastric cancer cells partially through integrin beta4.* Carcinogenesis, 2013. **34**(12): p. 2851-60.

40. Guo, X., et al., *Human ribosomal protein S13 promotes gastric cancer growth through down-regulating p27(Kip1).* J Cell Mol Med, 2011. **15**(2): p. 296-306.

41. Khalaileh, A., et al., *Phosphorylation of ribosomal protein S6 attenuates DNA damage and tumor suppression during development of pancreatic cancer.* Cancer Res, 2013. **73**(6): p. 1811-20.

42. Shi, Y., et al., *Ribosomal proteins S13 and L23 promote multidrug resistance in gastric cancer cells by suppressing drug-induced apoptosis.* Exp Cell Res, 2004. **296**(2): p. 337-46.

43. Sonenberg, N. and A.G. Hinnebusch, *Regulation of translation initiation in eukaryotes: mechanisms and biological targets.* Cell, 2009. **136**(4): p. 731-45.

44. Holcik, M. and N. Sonenberg, *Translational control in stress and apoptosis.* Nat Rev Mol Cell Biol, 2005. **6**(4): p. 318-27.

45. Stumpf, C.R., et al., *The translational landscape of the mammalian cell cycle.* Mol Cell, 2013. **52**(4): p. 574-82.

46. Barna, M., et al., *Suppression of Myc oncogenic activity by ribosomal protein haploinsufficiency.* Nature, 2008. **456**(7224): p. 971-5.

47. Fischer, M., et al., *The p53-p21-DREAM-CDE/CHR pathway regulates G2/M cell cycle genes.* Nucleic Acids Res, 2016. **44**(1): p. 164-74.

48. Xiong, Y., et al., *p21 is a universal inhibitor of cyclin kinases.* Nature, 1993. **366**(6456): p. 701-4.

49. Gartel, A.L. and S.K. Radhakrishnan, *Lost in transcription: p21 repression, mechanisms, and consequences.* Cancer Res, 2005. **65**(10): p. 3980-5.

50. Lecona, E. and O. Fernandez-Capetillo, *Targeting ATR in cancer.* Nat Rev Cancer, 2018. **18**(9): p. 586-595.

51. Lee, H., *Cycling with BRCA2 from DNA repair to mitosis.* Exp Cell Res, 2014. **329**(1): p. 78-84.

52. Fathi, N.N., et al., *Translocation-generated ITK-FER and ITK-SYK fusions induce STAT3 phosphorylation and CD69 expression.* Biochem Biophys Res Commun, 2018. **504**(4): p. 749-752.

53. Jackson, N.M. and B.P. Ceresa, *EGFR-mediated apoptosis via STAT3.* Exp Cell Res, 2017. **356**(1): p. 93-103.

54. Larsen, B.D. and C.S. Sorensen, *The caspase-activated DNase: apoptosis and beyond.* FEBS J, 2017. **284**(8): p. 1160-1170.

55. Liu, X., et al., *DFF, a heterodimeric protein that functions downstream of caspase-3 to trigger DNA fragmentation during apoptosis.* Cell, 1997. **89**(2): p. 175-84.

56. Halenbeck, R., et al., *CPAN, a human nuclease regulated by the caspase-sensitive inhibitor DFF45.* Curr Biol, 1998. **8**(9): p. 537-40.

57. Rojo de la Vega, M., E. Chapman, and D.D. Zhang, *NRF2 and the Hallmarks of Cancer.* Cancer Cell, 2018. **34**(1): p. 21-43.

58. DeNicola, G.M., et al., *Oncogene-induced Nrf2 transcription promotes ROS detoxification and tumorigenesis.* Nature, 2011. **475**(7354): p. 106-9.

59. Herranz, N. and J. Gil, *Mechanisms and functions of cellular senescence.* J Clin Invest, 2018. **128**(4): p. 1238-1246.

60. Jun, J.I. and L.F. Lau, *CCN2 induces cellular senescence in fibroblasts.* J Cell Commun Signal, 2017. **11**(1): p. 15-23.

61. Hansel, C., V. Jendrossek, and D. Klein, *Cellular Senescence in the Lung: The Central Role of Senescent Epithelial Cells.* Int J Mol Sci, 2020. **21**(9).

62. Dagogo-Jack, I. and A.T. Shaw, *Tumour heterogeneity and resistance to cancer therapies.* Nat Rev Clin Oncol, 2018. **15**(2): p. 81-94.

63. Zhao, D., et al., *Molecularly targeted therapies for p53-mutant cancers.* Cell Mol Life Sci, 2017. **74**(22): p. 4171-4187.

64. Griguolo, G., et al., *Olaparib for the treatment of breast cancer.* Expert Rev Anticancer Ther, 2018. **18**(6): p. 519-530.

65. Bhat, M., et al., *Targeting the translation machinery in cancer.* Nat Rev Drug Discov, 2015. **14**(4): p. 261-78.

V. MULTI-OMIC CHARACTERIZATION OF GLUTATHIONE S-TRANSFERASE PI-1 (GSTP1) KNOCKDOWN PDAC CELLS REVEALS DOWNREGULATION OF METABOLIC GENES, ALDH7A1 AND GLUT3[4]

Abstract

Glutathione S transferase pi-1 (GSTP1) maintains cellular homeostasis by conjugating the reactive electrophiles and by-products of aerobic respiration to glutathione. In addition to maintaining redox balance, convincing evidence suggests that GSTP1 promotes tumorigenesis by inhibiting the cell death signaling pathways. Although the loss of GSTP1 activity or expression reduces cancer cell survival in breast, pancreatic, and cervical cancer models, the anticancer mechanisms underlying GSTP1 inhibition remain poorly understood. Here, we show that loss of GSTP1 has direct implications on the redox homeostasis of PDAC cells. Further, we performed a detailed, multi-omic characterization of GSTP1 knockdown MIA PaCa-2 cells. Our results reveal unique changes in the global transcriptomic and proteomic signatures associated with GSTP1 knockdown. Precisely, we found 550 genes and 69 proteins to be differentially expressed in GSTP1 knockdown MIA PaCa-2 cells compared to the control. Among them, 41 were similarly upregulated or downregulated at the mRNA and the protein level. Pathway analyses using these differentially expressed genes revealed that cellular metabolism and energy production are the most affected physiological mechanisms in GSTP1 knockdown PDAC cells. Our data suggest that impaired energy production in GSTP1 knockdown cells is primarily due to the reduced expression of the metabolic genes- ALDH7A1 and GLUT3, which are crucial for fatty acid oxidation and glucose uptake, respectively. Thus, this study suggests that GSTP1 knockdown significantly

[4] The material in this chapter was co-authored by Rahul Raj Singh, Jenna Duttenheffner, and Katie M. Reindl. R.R.S. performed all experiments, collected and analyzed the data. Also, wrote the manuscript. Except; J.D. performed qPCR experiments. K.M.R. was responsible for the supervision and coordination of the project. All authors read and approve the final version of this chapter before submission.

changes the transcriptome and the proteome of PDAC cells and underlines impaired cellular metabolism by which GSTP1 inhibition reduces cancer-cell growth and survival. Collectively, our data show convincing evidence that GSTP1 is crucial in maintaining optimal redox and metabolic homeostasis in PDAC cells and targeting GSTP1 is a potential therapy for PDAC patients.

Introduction

Pancreatic ductal adenocarcinoma (PDAC), the most common type of pancreatic cancer, is a lethal malignancy [1]. Lack of early detection strategies, rapid metastasis, and resistance to conventional chemotherapy compound the ineffectiveness of treating the disease [2]. As a result, only 10% of the patients survive for more than five years after diagnosis [3]. Although surgical resection followed by radiation therapy is most effective, less than 20% of the patients are eligible for surgery due to the progressive nature of the disease at the time of diagnosis [4]. Current therapeutic recommendations for locally advanced or metastatic PDAC patients include either FOLFIRINOX (leucovorin, 5-fluorouracil, irinotecan, and oxaliplatin) or gemcitabine co-administered with nanoparticle albumin-bound (NAB) –paclitaxel, which has marginal effects on the overall clinical outcomes [5]. Therefore, to improve the efficacy of currently used therapy, identification of the novel targets unique to pancreatic cancer physiology is needed.

Among other avenues of discovering effective therapies, targeting cancer cell metabolism has shown remarkable promise [6, 7]. Cancer cells survive and proliferate in an alien environment, which is mediated by extensive metabolic rewiring [8]. Similar to oncogene addiction, where cancer cells become dependent on the activity of an oncogene for survival and proliferation [9], specific cancer cells become addicted to metabolic pathways for energy production and macromolecular biosynthesis [10]. Such dependencies can present vulnerabilities specific to

cancer cells, and recent studies in the field of pancreatic cancer metabolism have established the therapeutic advantage of these addictions [11].

PDAC is a solid tumor that survives and proliferates in a hypoxic, nutrient-poor environment [12, 13]. The hostile tumor microenvironment drives the molecular and physiological adaptations in cancer cells to maintain redox and metabolic homeostasis [14-16]. One such adaptation is a hyperactive antioxidant system in cancer cells [17]. Glutathione S-transferase Pi-1 (GSTP1), a primary detoxification enzyme, is overexpressed in various human cancers [18], including PDAC [19]. A higher expression of GSTP1 is often associated with tumor progression and, therefore, poor clinical outcomes for PDAC patients [19]. The canonical function of GSTP1 is to conjugate reduced glutathione (GSH) to the reactive electrophiles and xenobiotic compounds [20]. However, growing evidence suggests that GSTP1 plays a critical role in cancer cell metabolism, signaling, and drug resistance [21, 22].

Our previous work demonstrated that disrupting the antioxidant system via targeting GSTP1 activates apoptotic signaling in PDAC cells. We found that GSTP1 knockdown causes cell death primarily by increasing the reactive oxygen species (ROS) in PDAC cells [19]. However, little is known about the precise mechanism through which GSTP1 promotes pancreatic cancer cell growth and proliferation. Thus, in an effort to target the redox homeostasis and to further understand the biological role of GSTP1, we developed the doxycycline-inducible GSTP1-knockdown PDAC cells. We used multi-omics techniques to determine the global impacts of GSTP1 knockdown on the transcriptome and the proteome of the PDAC cells. We show that GSTP1 knockdown alters the transcriptomic and proteomic signature of the PDAC cells. Further, we report that GSTP1 knockdown impairs the metabolic efficacy of PDAC cells. Because GSTP1

is crucial in maintaining redox homeostasis and driving cancer cell metabolism, targeting GSTP1 and its adjoining metabolic pathways represent therapeutic opportunities for PDAC.

Materials and methods

Chemicals

Puromycin was purchased from Sigma-Aldrich, St. Louis, MO, USA. Doxycycline was purchased from MP Biomedicals, Albany, NY, USA. N-acetyl cysteine (NAC) was purchased from Amresco Biochemicals (ELITech group), Logan, UT, USA. GSTP1 and ALDH7A1 (Antiquitin) antibodies were obtained from Santa Cruz Biotechnology, Dallas, TX, USA. Antibodies to SLC2A3 (GLUT3) and 4-hydroxy nonenal (4-HNE) were purchased from Abcam, Waltham, MA, USA. GAPDH antibody was obtained from Cell Signaling Technology, Danvers, MA, USA. Horseradish peroxidase (HRP)-linked anti-mouse and anti-rabbit IgG secondary antibodies were obtained from Cell Signaling Technology. CellROX™ Deep Red Reagent was purchased from Invitrogen (by ThermoFisher Scientific), Eugene, OR, USA.

Cell culture

Human PDAC cell lines (MIA PaCa-2, PANC-1, HPAF-II, AsPC-1, and BxPC-3) were obtained from American Type Culture Collection, Manassas, VA, USA. hTERT-HPNE cells were obtained from Dr. Channing Der's laboratory at UNC, Chapel Hill, NC, USA. MIA PaCa-2 cells were cultured in Dulbecco's Modified Eagle Medium (DMEM) high-glucose media (GE Healthcare Life Sciences, Chicago, IL, USA) containing 10% (v/v) fetal bovine serum (Atlanta Biologicals, Flowery Branch, GA, USA) and 2.5% (v/v) horse serum (Corning, Corning, NY, USA). PANC-1 cells were cultured in DMEM high-glucose media containing 10% (v/v) FBS. HPAF-II cells were cultured in Eagle's Minimum Essential Medium (EMEM) (Corning, Corning, NY, USA) containing 10% v/v Fetal Bovine Serum (FBS). AsPC-1 were cultured in RPMI-1640

(GE Healthcare Life Sciences) containing 10% FBS (v/v). Cells were maintained at 37 °C with 5% CO_2. All cell-culture growth media were supplemented with 1% HyClone Antibiotic Antimycotic (Pen/Strep/Fungizone) Solution (Thomas Scientific, Swedesboro, NJ, USA. The cell lines were subcultured by enzymatic digestion with 0.25% trypsin/1 mM EDTA solution (GE Healthcare Life Sciences, Chicago, IL, USA) when they were 80% confluent. Lentiviral transfected (NS control and GSTP1 knockdown) cells were cultured with 5 µg/mL puromycin in growth media to maintain the selection. All cell lines tested negative for Mycoplasma contamination.

Western blotting

Cells were washed in cold PBS, trypsinized, and centrifuged for 4 minutes at 7,000 rpm. Cell pellets were resuspended in cell culture lysis buffer (Promega) containing protease/phosphatase inhibitor cocktail (Cell Signaling Technology) and incubated on ice for 30 minutes. The cell lysate was centrifuged at 13,000 rpm for 10 minutes at 4°C to collect the protein supernatant. The total protein concentration was measured using the PierceTM BCA Protein Assay Kit (ThermoFisher Scientific). The protein samples (10-80 µg) were prepared in loading buffer (Alfa Aesar) with 3-5% BME and subjected to thermal denaturation at 100°C. Samples were loaded in 7-10% SDS-polyacrylamide gels and separated at 100 V for 3-3.5 hours at 4°C. Proteins were transferred to nitrocellulose membrane (GE Healthcare) at 100 V for 70 minutes 4°C. Blots were blocked using 5% BSA for 3 hours and incubated overnight at 4°C in primary antibody (1:1000). The blots were washed in 1X TBS-T and probed for 1 hour at room temperature with a corresponding secondary antibody (1:2000) containing anti-biotin (1:5000). The blots were visualized using SuperSignal West Femto Maximum Sensitivity Substrate (ThermoFisher

Scientific), and chemiluminescence was detected with the FluorChem® FC2 Imaging System (Alpha Innotech).

Quantitative real-time PCR

RNA was isolated from cells using the Phenol-Free Total RNA Purification Kit (VWR Life Science) according to the manufacturer's protocol. RNA was eluted using 50 µL of nuclease-free water. The RNA concentration was measured using the NanoDrop 1000 Spectrophotometer (ThermoFisher Scientific), and 2 µg of RNA was used to generate cDNA using the qScript cDNA synthesis kit (Quanta Biosciences). Real-time qPCR was performed in triplicate using 10 µL PerfeCTa® SYBR® Green Supermix (Quanta Biosciences, 95056), 4 µL nuclease-free water, 4 µL 1:10 dilution of cDNA, and 1µL 3mM forward and reverse primers (Table 5.1). The 96-well PCR microplate (Sigma Aldrich) was run using the Stratagene Mx3000P® Multiplex Quantitative PCR System (Agilent Technologies) with the following conditions: 95°C for 2 minutes, then 45 cycles of 95°C for 15 seconds, 55°C for 30 seconds, and 72°C for 30 seconds. The results were normalized using β-actin and β-tubulin as housekeeping reference genes, and data were analyzed using the 2-ΔΔCt method [27].

Table 5.1. Primer sequences used for measuring mRNA expression via quantitative polymerase chain reaction.

Gene	Forward primer	Reverse primer
GSTP1	5′-CAG GAG GGC TCA CTC AAA GC-3′	5′-AGG TGA CGC AGG ATG GTA TTG-3′
ALDH7A1	5′-TTT CCC TGT GGC AGT GTA TG-3′	5′-CCT CCA GAA CCT TGG CTA TTA TC-3′
GLUT3	5′-TAC CAT CCT TCC TGC TAT CCT-3′	5′-GAC ATC CTT GCA CTC TCA TCT T-3′
β-Actin	5′-TTG CCG ACA GGA TGC AGA A-3′	5′-GCC GAT CCA CAC GGA GTA CTT-3′
β-Tubulin	5′-GTT CGC TCA GGT CCT TTT GG-3′	5′-CCC TCT GTG TAG TGG CCT TTG-3′

Cell viability assay

MIA PaCa-2 (125/well), PANC-1 (200/well), and HPAF-II (400/well) cells were seeded in 96-well plates. The viability of control (NS) and GSTP1 knockdown cells (shGSTP1-1 and

shGSTP1-2) was measured every 24 hours for ten days by adding 10 µl of 10 mg/mL 3-(4,5-dimethylthiazol-2-yl)-2,5-diphenyltetrazolium bromide (MTT) reagent to each well and incubating the plates for 3 hours at 37°C. The MTT reagent was removed, DMSO (100 µL/well) was added to solubilize the crystals, and absorbance was measured at 570 nm using a Bio-Rad xMark Microplate Absorbance Spectrophotometer. The data represent the average ± standard deviation for three independent experiments with twenty-four technical replicates for each treatment.

Detection of ROS

Following doxycycline treatment for 96 hours, NS control and GSTP1 knockdown PDAC cells were harvested and resuspended in complete culture media. CellRox™ Deep Red Reagent (Invitrogen) was added to a final concentration of 1000 nM to the samples. The samples were incubated for 60 minutes in an incubator at 37 ºC. After staining, cells were washed once with phosphate-buffered saline (PBS). The samples were immediately analyzed by flow cytometry using BD Accuri C6 system, using 635 nm excitation. Three technical replicates were included for each experiment, and the experiments were performed three times for each cell line. The data represent the average ± standard deviation of fluorescence values from three independent experiments with three technical replicates for each treatment. FLOWJO software was used to create histograms.

RNA-Seq analysis

RNA extraction and sequencing: Following doxycycline treatment for 96 hours, total RNA was extracted from four replicates of NS control and shGSTP1-1 MIA PaCa-2 cells, using RNeasy RNA isolation kit (Qiagen, Ann Arbor, MI) following the manufacturer's instructions. RNA was quantified using a NanoDrop (Thermo Fisher Scientific, Waltham, MA). Four micrograms of total

RNA per sample was sent to University of Minnesota Genomics Center, St. Paul, MN. All the samples passed quality control with an RNA integrity number (RIN) of ≥ 9.4. Unique, dual-indexed, TruSeq stranded mRNA libraries were created. Mean quality score for all libraries was greater than Q30. The libraries were pooled and sequences in two lanes of the flow cell on an Illumina NovaSeq 6000. The library pool was gel size-selected to have average inserts of ≈ 200bp.

Differential gene expression analysis: Reads from each sample were aligned to the most updated reference human genome (GRCh38) available on Ensembl. SAMtools [28] was used to generate, sort, and index BAM (binary alignment/map) files. Gene expression was calculated as the total number of reads for each sample that uniquely aligned to the reference genome, binned by gene coordinate annotations. The generated reads were assigned the genomic features using the featureCounts function. Differential gene expression analysis between the NS control and shGSTP1-1 (GSTP1 knockdown) MIA PaCa-2 cells was performed using the Bioconductor package, DESeq2 [29]. To account for differences in sequencing depth across samples, raw read counts were normalized using methodologies implemented in DESeq2. Differential expression of the normalized read counts was performed using the negative binomial test with the Benjamini-Hochberg false discovery rate (FDR) adjustment method as applied by DESeq2. For our analysis, an FDR of 0.01 was applied, and genes with a p-adjusted value of less than or equal to 0.01 and a $\log_2$-fold change of less than -1 or greater than +1 were defined as significantly down- or upregulated. The pathway analyses were performed using Ingenuity Pathway Analysis (IPA), Enrichr [30], and Reactome [31] tools.

Proteomics

Sample preparation: NS control and shGSTP1-1 MIA PaCa-2 cells were treated with doxycycline for 96 hours. Five million cells from NS control and shGSTP1-1 MIA PaCa-2 cells

were collected for mass spectrometry (MS)-based proteomics experiment. The samples were stored in -80 ºC until the proteomics experiment. Five biological replicates from each group were sent to the Proteomics Core Facility, University of Arkansas for Medical Sciences, Little Rock, AR.

Tandem mass tag (TMT) labeling and HPLC analysis: At the facility, the total protein was extracted. Proteins were reduced, alkylated, and purified by chloroform/methanol extraction prior to digestion with sequencing grade modified porcine trypsin (Promega, Madison, WI). Tryptic peptides were labeled using tandem mass tag isobaric labeling reagents (ThermoFisher, Waltham, MA) following the manufacturer's instructions and combined into one 10-plex sample group. The labeled peptide multiplex was separated into 46 fractions on a 100 x 1.0 mm Acquity BEH C18 column (Waters, Milford, MA) using an UltiMate 3000 UHPLC system (ThermoFisher, Waltham, MA) with a 50 min gradient from 99:1 to 60:40 buffer A:B ratio under basic pH conditions, and then consolidated into 18 super-fractions. Each super-fraction was then further separated by reverse phase XSelect CSH C18 2.5 um resin (Waters, Milford, MA) on an in-line 150 x 0.075 mm column using an UltiMate 3000 RSLCnano system (ThermoFisher, Waltham, MA). Peptides were eluted using a 60 min gradient from 98:2 to 60:40 buffer A: B ratio. Eluted peptides were ionized by electrospray (2.2 kV) followed by mass spectrometric analysis on an Orbitrap Eclipse Tribrid mass spectrometer (ThermoFisher, Waltham, MA) using multi-notch MS3 parameters. MS data were acquired using the FTMS analyzer in top-speed profile mode at a resolution of 120,000 over a range of 375 to 1500 m/z. Following CID activation with normalized collision energy of 35.0, MS/MS data were acquired using the ion trap analyzer in centroid mode and normal mass range. Using synchronous precursor selection, up to 10 MS/MS precursors were selected for HCD activation with normalized collision energy of 65.0, followed by acquisition of MS3 reporter ion

data using the FTMS analyzer in profile mode at a resolution of 50,000 over a range of 100-500 m/z. Buffer A = 0.1% formic acid and 0.5% acetonitrile. Buffer B = 0.1% formic acid and 99.9% acetonitrile. Both buffers were adjusted to pH 10 with ammonium hydroxide for offline separation.

Differential protein expression analysis: Protein TMT MS3 reporter-ion intensity values were assessed for quality using the in-house ProteiNorm app (University of Arkansas for Medical Sciences, Little Rock, AR) a user-friendly tool for a systematic evaluation of normalization methods, imputation of missing values and comparisons of different differential abundance methods. Popular normalization methods were evaluated including $\log_2$ normalization, median normalization, mean normalization, variance-stabilizing normalization [32], quantile normalization [33], cyclic loess normalization [34], global robust linear regression normalization (RLR) [35], and global intensity normalization [35]. The individual performance of each method were evaluated by comparing of the following matrices: total intensity, Pooled intragroup Coefficient of Variation (PCV), Pooled intragroup Median Absolute Deviation (PMAD), Pooled intragroup estimate of variance (PEV), intragroup correlation, sample correlation heatmap (Pearson), and $\log_2$-ratio distributions. The normalized data was used to perform statistical analysis using Linear Models for Microarray Data (limma) with empirical Bayes (eBayes) smoothing to the standard errors [34]. Proteins with an FDR adjusted p-value < 0.01 and a fold change > 2 were considered to be significant. The pathway analyses were performed using Ingenuity Pathway Analysis (IPA), Reactome [31], and Enrichr [30] tools.

Statistical analyses

For relative GSTP1 expression in different human PDAC cell lines, different cell lines and experimental replicate were the factors. Cell viability was analyzed separately for each PDAC cell line with knockdown line, time, and experimental replicate as the factors. Relative protein

expression of GSTP1, ALDH7A1, and SLC2A3 were analyzed with protein, knockdown line, and experimental replicate as the factors. All analyses were performed using the MIXED procedure in SAS software version 9.4 (SAS Institute, Cary NC).

Results

Establishment of doxycycline-inducible GSTP1-knockdown PDAC cells

Three PDAC cell lines (MIA PaCa-2, PANC-1, and HPAF-II) were seeded in 6 cm dishes. When the cells reached 50% confluence, they were treated with polybrene and lentiviral particles containing non-specific control (NS) and human GSTP1-specific shRNA (shGSTP1-1, shGSTP1-2, and shGSTP1-3) cloned in SMARTvector™ (Figure 5.1A). After 24 hours, the viral particles were removed, and the cells were provided with fresh culture media. The transfected cells were selected over five days with 5 µg/mL puromycin. Following puromycin selection, GSTP1 knockdown was induced by the treatment of 500 ng/mL doxycycline to the growth media. GSTP1 protein expression was evaluated every 24 hours via western blotting. We report more than 90% reduction in GSTP1 protein expression and mRNA expression after 96 hours of doxycycline treatment (Figures 5.1B-D). Two sequences with the most potent suppression (shGSTP1-1 and shGSTP1-2) were selected for all *in vitro* studies. Additionally, we show that GSTP1 protein expression can be restored to near untreated levels after 120 hours of doxycycline removal (Figures 5.1E-J).

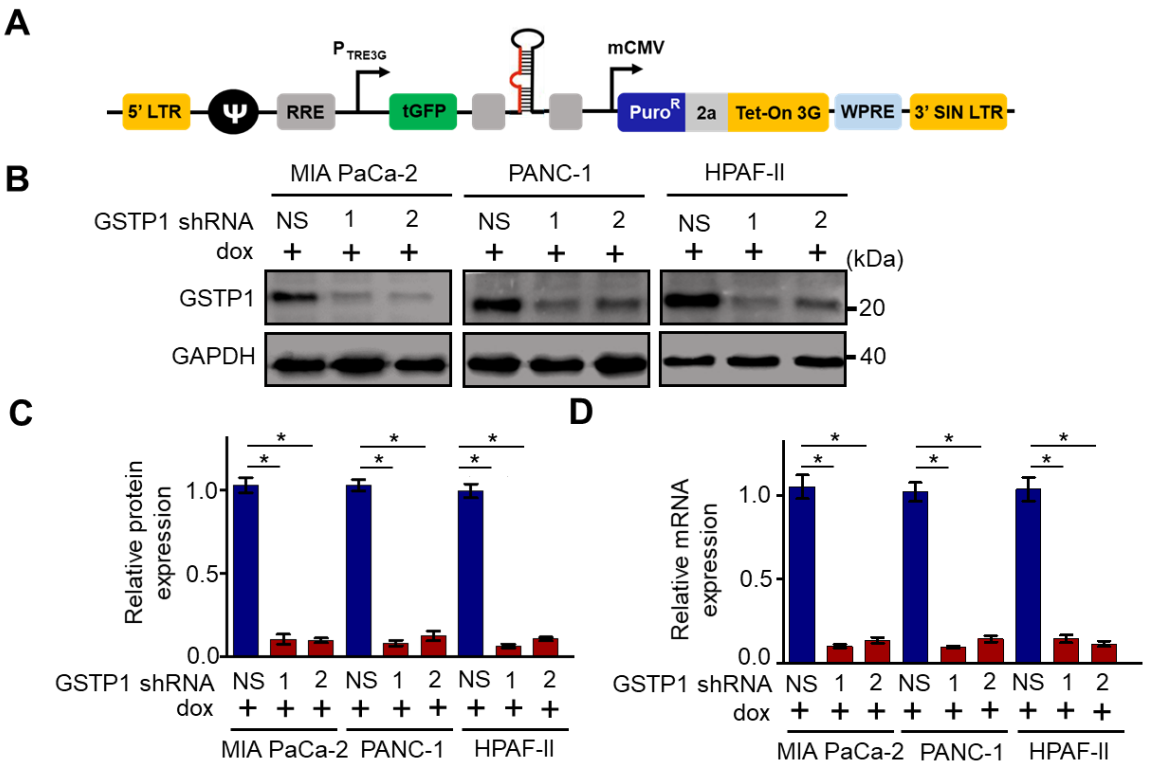

Figure 5.1. Establishment of the doxycycline (dox) inducible glutathione S–transferase pi-1 (GSTP1) knockdown pancreatic ductal adenocarcinoma (PDAC) cells. (A) Tet (doxycycline)-driven SMART™ vector for inducible expression of GSTP1 shRNA. GSTP1 was knocked down in MIA PaCa-2, PANC-1, and HPAF-II PDAC cells using two independent shRNAs (shGSTP1-1 and shGSTP1-2) and expression was confirmed by (B, C) western blotting and (D) quantitative real-time (qRT)-PCR analysis after 96 hours of dox treatment. To restore the expression of GSTP1, doxycycline was removed for 120 hours (dox +-) and the total protein was collected. Western blotting was used to confirm the levels of GSTP1 after doxycycline removal in MIA PaCa-2 (E, F), PANC-1 (G, H), and HPAF-II (I, J) cells. Western blot data were normalized to GAPDH for each cell line, and relative protein expression is shown for the non-specific control shRNA (NS control) compared to the GSTP1 shRNA sequences. Protein and mRNA levels of GSTP1 in NS control were compared to shGSTP1-1 and shGSTP1-2. The images are representative of three independent experiments. The Student's t-test was used to evaluate the significance in the difference of GSTP1 expression among different groups. Statistically significant changes in expression levels in GSTP1 knockdown groups compared to the NS control are shown with * ($p < 0.05$).

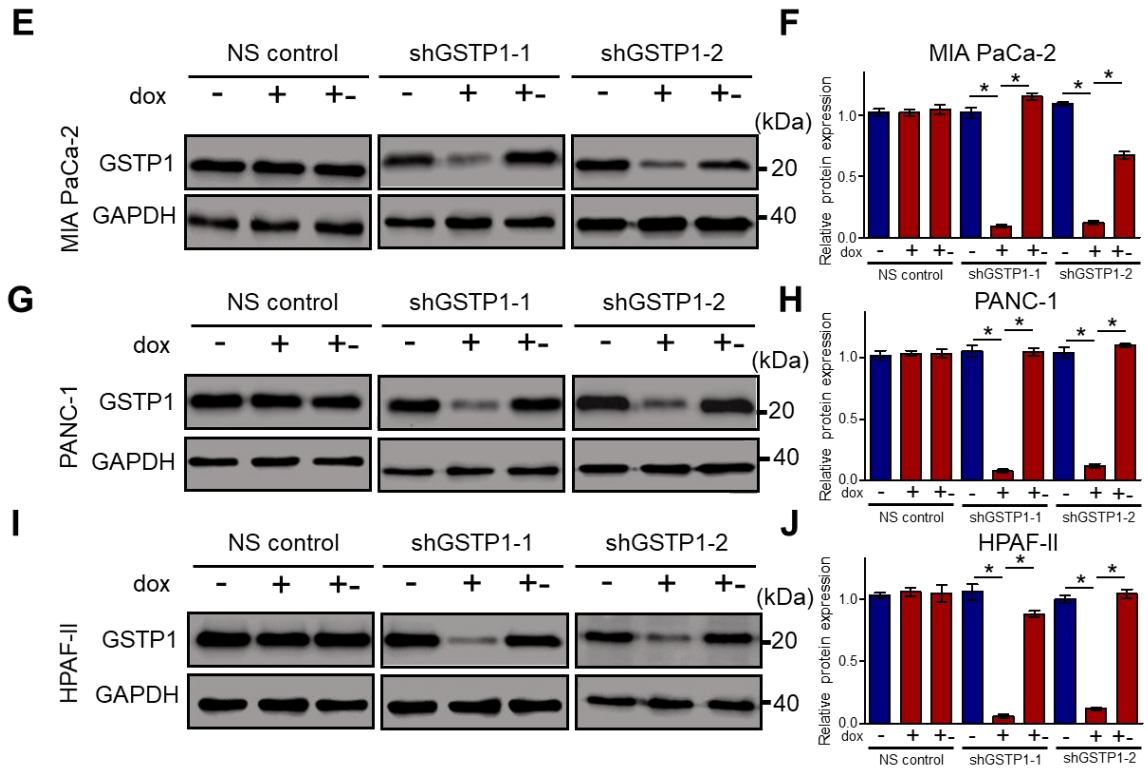

Figure 5.1. Establishment of the doxycycline (dox) inducible glutathione S–transferase pi-1 (GSTP1) knockdown pancreatic ductal adenocarcinoma (PDAC) cells (continued). (A) Tet (doxycycline)-driven SMART™ vector for inducible expression of GSTP1 shRNA. GSTP1 was knocked down in MIA PaCa-2, PANC-1, and HPAF-II PDAC cells using two independent shRNAs (shGSTP1-1 and shGSTP1-2) and expression was confirmed by (B, C) western blotting and (D) quantitative real-time (qRT)-PCR analysis after 96 hours of dox treatment. To restore the expression of GSTP1, doxycycline was removed for 120 hours (dox +-) and the total protein was collected. Western blotting was used to confirm the levels of GSTP1 after doxycycline removal in MIA PaCa-2 (E, F), PANC-1 (G, H), and HPAF-II (I, J) cells. Western blot data were normalized to GAPDH for each cell line, and relative protein expression is shown for the non-specific control shRNA (NS control) compared to the GSTP1 shRNA sequences. Protein and mRNA levels of GSTP1 in NS control were compared to shGSTP1-1 and shGSTP1-2. The images are representative of three independent experiments. The Student's t-test was used to evaluate the significance in the difference of GSTP1 expression among different groups. Statistically significant changes in expression levels in GSTP1 knockdown groups compared to the NS control are shown with * ($p < 0.05$).

GSTP1 knockdown reduces PDAC cell growth

To determine if GSTP1 knockdown impairs cell viability of PDAC cells, we performed MTT assays. We show that GSTP1 knockdown impairs cell viability of MIA PaCa-2 and PANC-1 cells by more than 20% and by 15% for HPAF-II cells (Figure 5.2A).

GSTP1 knockdown increases ROS levels in PDAC cells

GSTP1 is a key antioxidant enzyme that maintains optimal redox environment in the cells. We speculated that the loss of GSTP1 could result in an increased accumulation of ROS leading to oxidative stress. Non-specific control (NS) and GSTP1 knockdown (shGSTP1-1 and shGSTP1-2) MIA PaCa-2, PANC-1, and HPAF-II cells were stained with the fluorescent dye CellROX™ Deep Red Reagent to detect ROS, and fluorescence was determined using flow cytometry. We show GSTP1 knockdown elevates ROS levels by 2.1, 1.5, and 1.7 fold in MIA PaCa-2, PANC-1, and HPAF-II cells, respectively. Further, we show that ROS levels can be restored to near control levels by removing doxycycline for 48 hours from the growth media (Figures 5.2B and C).

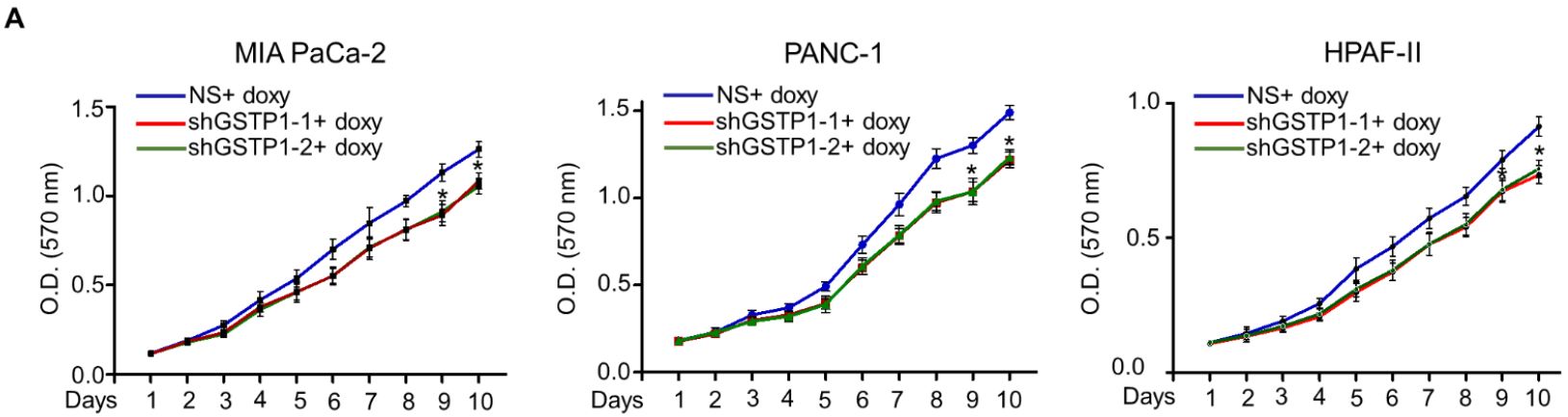

Figure 5.2. GSTP1 knockdown reduces PDAC cell growth and increases ROS levels. (A) MTT assays were used to detect the average cell viability of NS control and GSTP1 knockdown MIA PaCa-2, PANC-1, and HPAF-II cells for three independent experiments with twenty-four technical replicates for each. The y-axis represents the absorbance (570 nm) recorded every 24 hours for ten days. The absorbance (cell viability) was compared between NS control and shGSTP1-1 and shGSTP1-2 independently. The Student's t-test was used to analyze the significance between knockdown groups and the control. (B) Histograms showing ROS levels determined using CellROX™ Deep Red reagent and flow cytometry for NS control and GSTP1 knockdown MIA PaCa-2, PANC-1, and HPAF-II cells after 96 hours of dox treatment. GSTP1 was restored by withdrawing dox for 120 hours (dox +-) before analyzing the ROS levels. The figure shows a representative image of three independent experiments. (C) Quantification of ROS levels in NS control and GSTP1 knockdown PDAC cells. ROS levels in NS control were compared to that in shGSTP1-1 and shGSTP1-2 independently. The Student's t-test was used to identify potential significant differences. Statistically significant results in GSTP1 knockdown groups compared to the NS control are shown with * ($p < 0.05$).

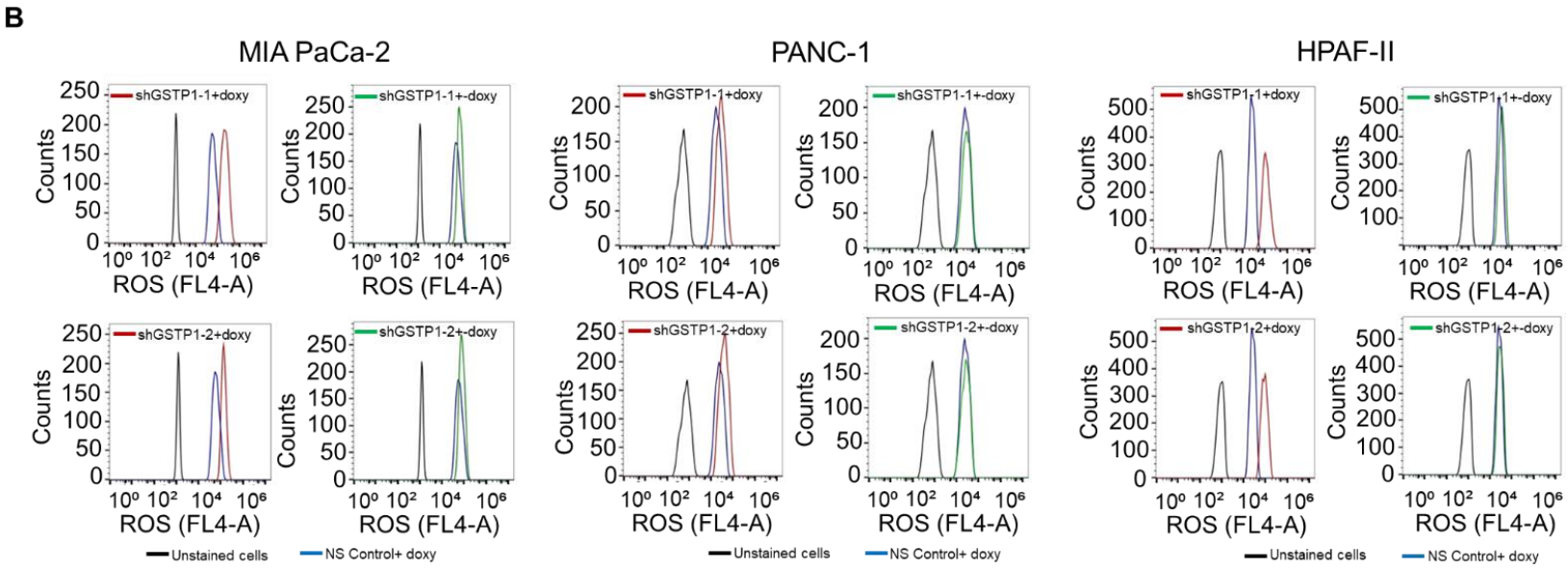

Figure 5.2. GSTP1 knockdown reduces PDAC cell growth and increases ROS levels (continued). (A) MTT assays were used to detect the average cell viability of NS control and GSTP1 knockdown MIA PaCa-2, PANC-1, and HPAF-II cells for three independent experiments with twenty-four technical replicates for each. The y-axis represents the absorbance (570 nm) recorded every 24 hours for ten days. The absorbance (cell viability) was compared between NS control and shGSTP1-1 and shGSTP1-2 independently. The Student's t-test was used to analyze the significance between knockdown groups and the control. (B) Histograms showing ROS levels determined using CellROX™ Deep Red reagent and flow cytometry for NS control and GSTP1 knockdown MIA PaCa-2, PANC-1, and HPAF-II cells after 96 hours of dox treatment. GSTP1 was restored by withdrawing dox for 120 hours (dox +-) before analyzing the ROS levels. The figure shows a representative image of three independent experiments. (C) Quantification of ROS levels in NS control and GSTP1 knockdown PDAC cells. ROS levels in NS control were compared to that in shGSTP1-1 and shGSTP1-2 independently. The Student's t-test was used to identify potential significant differences. Statistically significant results in GSTP1 knockdown groups compared to the NS control are shown with * ($p < 0.05$).

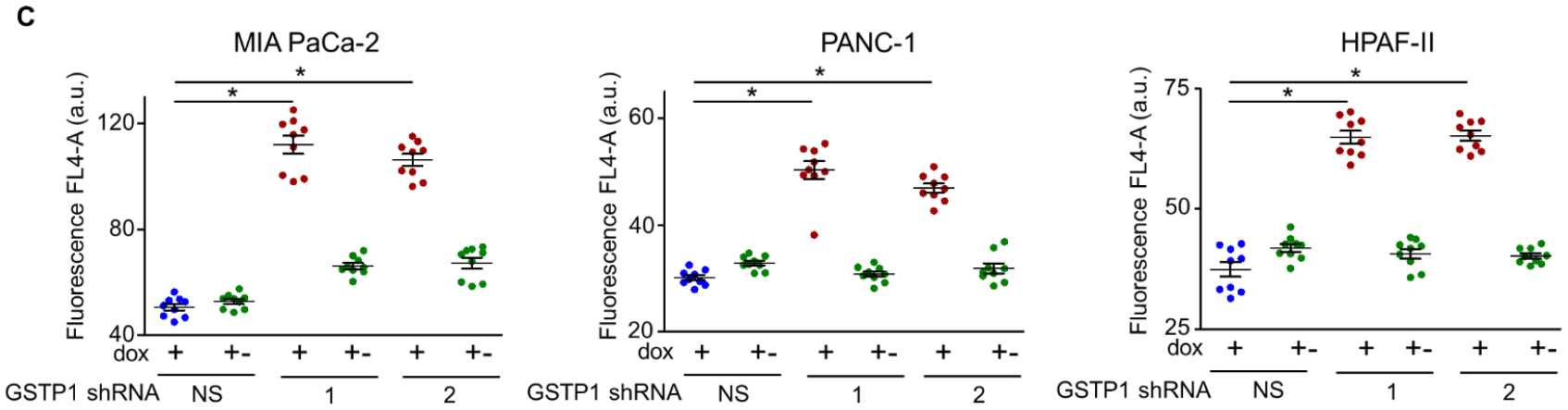

Figure 5.2. GSTP1 knockdown reduces PDAC cell growth and increases ROS levels (continued). (A) MTT assays were used to detect the average cell viability of NS control and GSTP1 knockdown MIA PaCa-2, PANC-1, and HPAF-II cells for three independent experiments with twenty-four technical replicates for each. The y-axis represents the absorbance (570 nm) recorded every 24 hours for ten days. The absorbance (cell viability) was compared between NS control and shGSTP1-1 and shGSTP1-2 independently. The Student's t-test was used to analyze the significance between knockdown groups and the control. (B) Histograms showing ROS levels determined using CellROX™ Deep Red reagent and flow cytometry for NS control and GSTP1 knockdown MIA PaCa-2, PANC-1, and HPAF-II cells after 96 hours of dox treatment. GSTP1 was restored by withdrawing dox for 120 hours (dox +-) before analyzing the ROS levels. The figure shows a representative image of three independent experiments. (C) Quantification of ROS levels in NS control and GSTP1 knockdown PDAC cells. ROS levels in NS control were compared to that in shGSTP1-1 and shGSTP1-2 independently. The Student's t-test was used to identify potential significant differences. Statistically significant results in GSTP1 knockdown groups compared to the NS control are shown with * ($p < 0.05$).

GSTP1 knockdown induces a differential transcriptomic response in PDAC cells

To identify the potential mechanisms underlying the impaired growth in GSTP1-knockdown cells and the effects of increased oxidative stress on the transcriptome of the PDAC cells, we performed an RNA-Seq experiment. A total of 211,535,272 single-end, one-hundred and fifty base pair reads were obtained from eight samples (four biological replicates each of NS control and GSTP1 knockdown MIA PaCa-2 cells). We obtained an average of 26,441,909 high-quality reads for each sample. More than 96% of the reads mapped successfully to the human genome, and approximately 90% aligned exclusively to the unique regions. The characteristics of the output reads are summarized in the Table 5.2.

Table 5.2. Non-specific control (NS) and GSTP1 knockdown (shGSTP1-1) MIA PaCa-2 cells were sequenced using Illumina NovaSeq6000 with four replicates each. The characteristics of the raw, output reads are summarized. QC: quality control.

Sample	QC Passed reads	% overall alignment	% unique alignments	% successfully assigned alignments
MIA PaCa-2 NS (Rep 1)	25,776,715	97.07	89.65	71.8
MIA PaCa-2 NS (Rep 2)	32,194,825	97.05	89.81	73.1
MIA PaCa-2 NS (Rep 3)	25,783,621	97.02	89.69	72.7
MIA PaCa-2 NS (Rep 4)	27,552,146	96.84	89.33	72.6
MIA PaCa-2 shGSTP1-1 (Rep 1)	32,942,440	96.68	89.93	74.3
MIA PaCa-2 shGSTP1-1 (Rep 2)	21,998,409	96.96	89.96	74.0
MIA PaCa-2 shGSTP1-1 (Rep 3)	21,904,880	96.81	90.02	74.5
MIA PaCa-2 shGSTP1-1 (Rep 4)	21,162,205	96.73	89.81	74.6

A high correlation was observed between all four biological replicates of each sample, which is represented in the principal component analysis (PCA) (Figure 5.3A). We found 1600 genes that had significant changes in gene expression between the NS control and the GSTP1 knockdown MIA PaCa-2 cells. Of them, we categorized 550 as differentially expressed between the two groups. Differentially expressed genes were defined as genes with a $\log_2$-fold change of less than -1 or greater than +1 and the p-adjusted value of less than 0.01. We found that GSTP1

knockdown upregulates the expression of 237 genes and downregulates the expression of 313 genes (Figure 5.3B). All differentially expressed genes are listed in Appendix A. The top differentially expressed genes were visualized using the heatmap tool in the ggplot2 [23] library (Figures 5.3C-E).

GSTP1 knockdown induces a differential proteomic response in PDAC cells

Encouraged by the transcriptomics results of GSTP1-knockdown PDAC cells, we next investigated the effects of GSTP1 knockdown on the global proteomic signature of the PDAC cells. We performed the comparative proteomics analysis with the quadrupole and the linear ion-trap technologies using the Orbitrap Tribrid LC-MS/MS for MIA PaCa-2 cells. In total, 5,965 proteins could be identified in each group. To identify the differentially expressed proteins, we compared the $\log_2$ cyclic Loess normalized exclusive tandem mass tag (TMT) intensities for the control and GSTP1 knockdown cells. A high correlation was observed between all five biological replicates of each sample, which is represented in the principal component analysis (PCA) (Figure 5.4A). We classified 69 proteins as differentially expressed in GSTP1 knockdown cells compared to the control. The proteins with a $\log_2$-fold change of less than -1 or greater than +1 and the adjusted p-value of less than 0.01 were categorized as differentially expressed. Out of the 69 differentially expressed proteins, 17 were upregulated, and 52 were downregulated in GSTP1 knockdown cells compared to the control (Figure 5.4B). All differentially expressed proteins are listed in Appendix B. These differentially expressed proteins were visualized using the heatmap tool in the ggplot2 [23] library (Figures 5.4C-E).

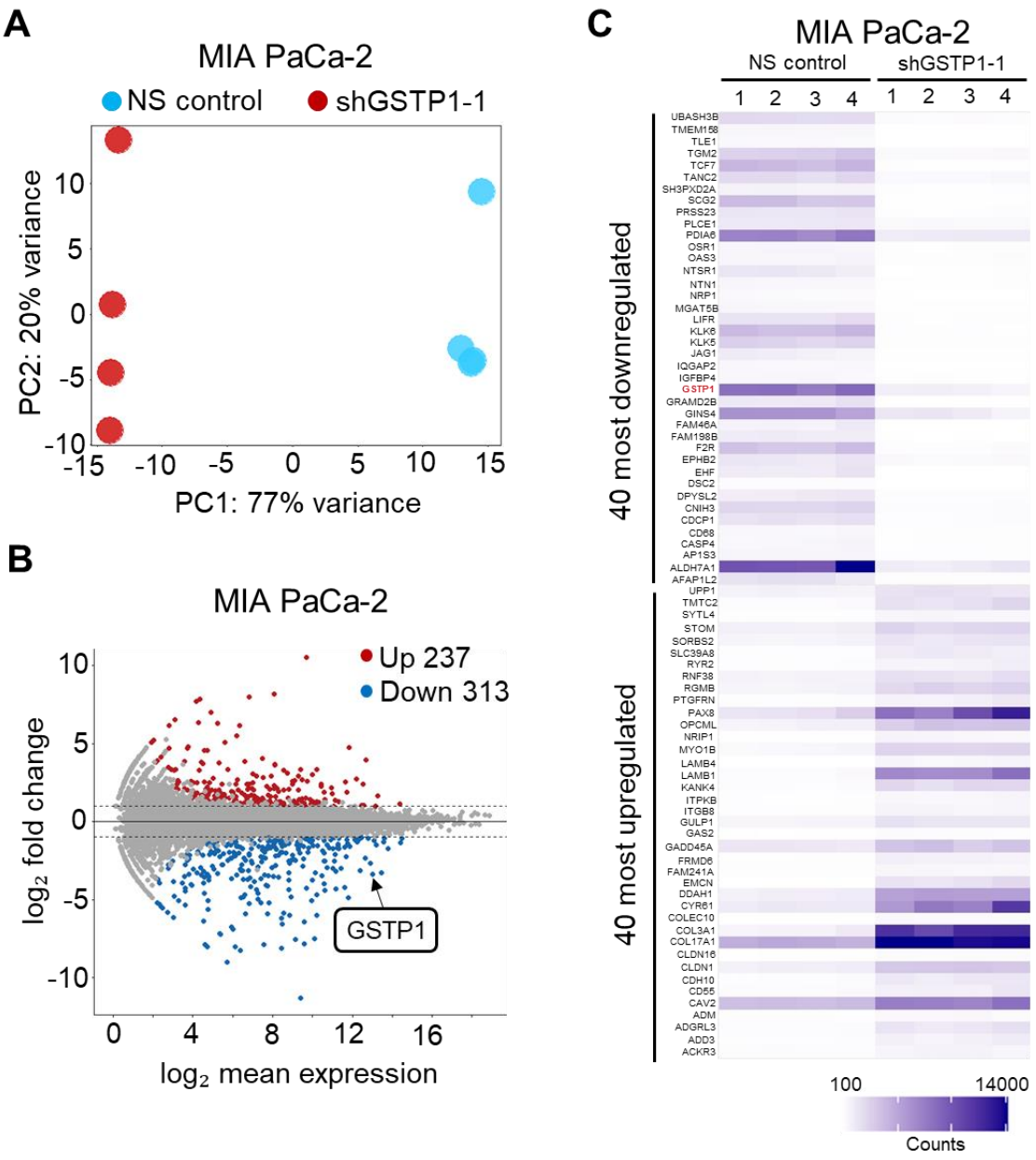

Figure 5.3. GSTP1 knockdown induces a differential transcriptome in PDAC cells. (A) Principal component analysis (PCA) plot showing the divergent transcriptome of GSTP1 knockdown MIA PaCa-2 cells compared to the NS control cells. (B) MA-plot showing upregulated (red) and downregulated (blue) genes in GSTP1 knockdown (shGSTP1-1) cells compared to the NS control (p_{adj} <0.01 and log_2-fold <-1 or >1). (C) Heatmap showing the forty most significant downregulated and upregulated genes in GSTP1 knockdown MIA PaCa-2 cells compared to the control. White color indicates downregulation of genes in GSTP1 knockdown MIA PaCa-2 cells compared to the control and dark blue indicates upregulation of genes. The thirty most significant (D) downregulated and (E) upregulated genes are represented in the bar graphs.

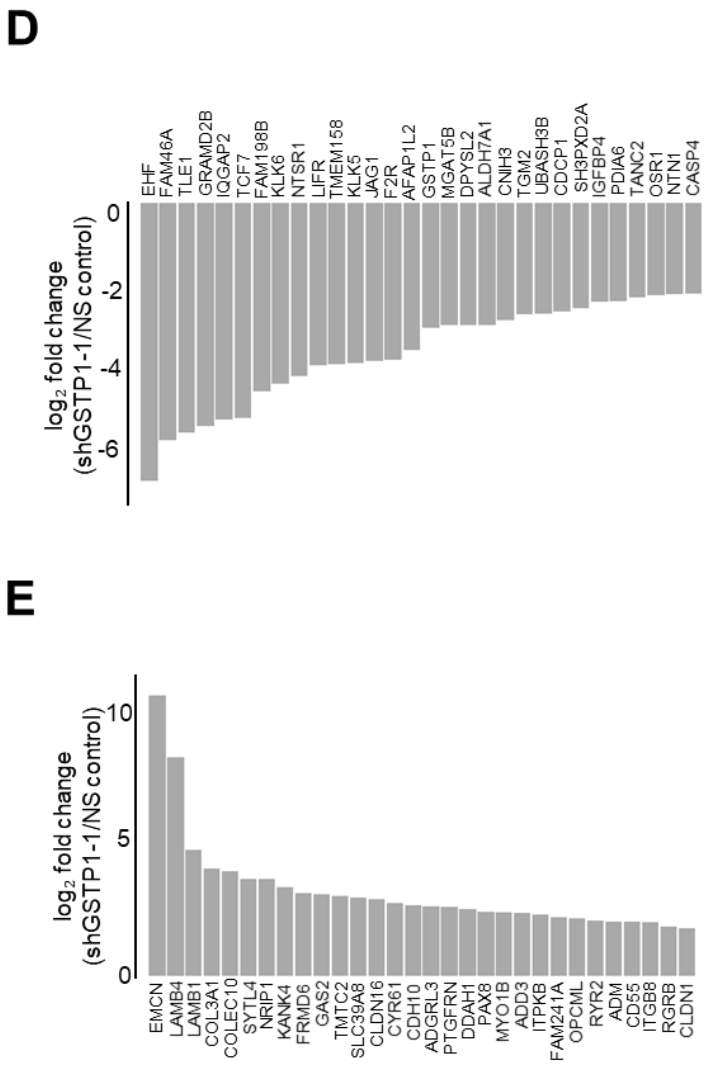

Figure 5.3. GSTP1 knockdown induces a differential transcriptome in PDAC cells (continued). (A) Principal component analysis (PCA) plot showing the divergent transcriptome of GSTP1 knockdown MIA PaCa-2 cells compared to the NS control cells. (B) MA-plot showing upregulated (red) and downregulated (blue) genes in GSTP1 knockdown (shGSTP1-1) cells compared to the NS control (p_{adj} <0.01 and log_2-fold <-1 or >1). (C) Heatmap showing the forty most significant downregulated and upregulated genes in GSTP1 knockdown MIA PaCa-2 cells compared to the control. White color indicates downregulation of genes in GSTP1 knockdown MIA PaCa-2 cells compared to the control and dark blue indicates upregulation of genes. The thirty most significant (D) downregulated and (E) upregulated genes are represented in the bar graphs.

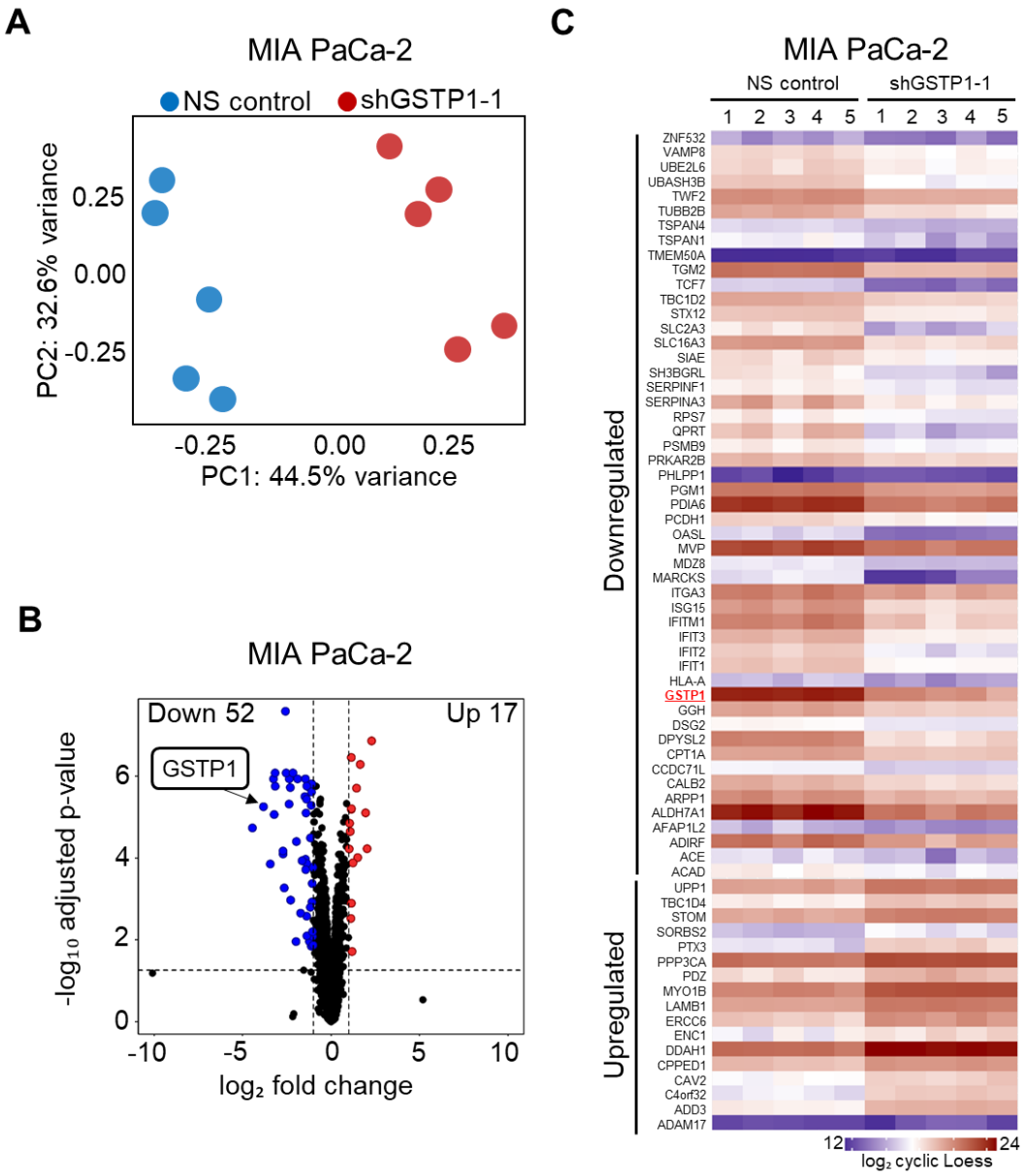

Figure 5.4. GSTP1 knockdown alters the global proteomic signature in PDAC cells. (A) Principal component analysis (PCA) plot showing the divergent proteome of GSTP1 knockdown MIA PaCa-2 cells compared to the NS control cells. (B) Volcano plot showing upregulated (red) and downregulated (blue) proteins in GSTP1 knockdown (shGSTP1-1) cells compared to the NS control (p_{adj} <0.01 and log_2-fold <-1 or >1). (C) Heatmap showing the fifty-two most significant downregulated and seventeen upregulated genes in GSTP1 knockdown MIA PaCa-2 cells compared to the control. Dark blue color indicates downregulated proteins in GSTP1 knockdown MIA PaCa-2 cells compared to the control and red indicates upregulated proteins. The fifteen most significant (D) downregulated and (E) upregulated proteins in GSTP1 knockdown cells are represented in the bar graphs.

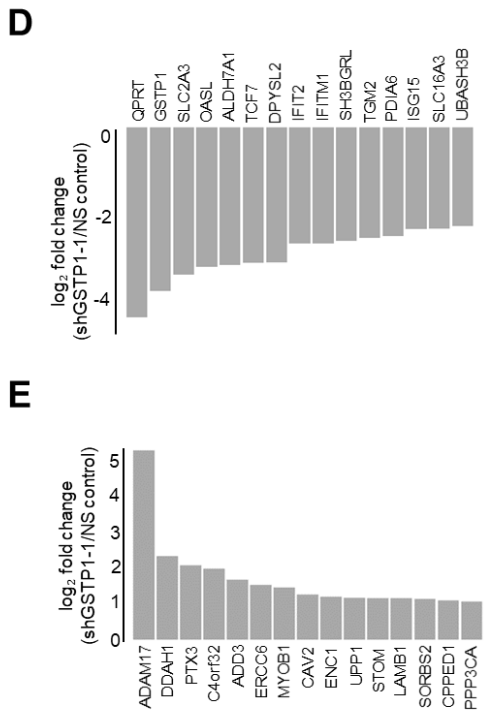

Figure 5.4. GSTP1 knockdown alters the global proteomic signature in PDAC cells (continued). (A) Principal component analysis (PCA) plot showing the divergent proteome of GSTP1 knockdown MIA PaCa-2 cells compared to the NS control cells. (B) Volcano plot showing upregulated (red) and downregulated (blue) proteins in GSTP1 knockdown (shGSTP1-1) cells compared to the NS control (p_{adj} <0.01 and log_2-fold <-1 or >1). (C) Heatmap showing the fifty-two most significant downregulated and seventeen upregulated genes in GSTP1 knockdown MIA PaCa-2 cells compared to the control. Dark blue color indicates downregulated proteins in GSTP1 knockdown MIA PaCa-2 cells compared to the control and red indicates upregulated proteins. The fifteen most significant (D) downregulated and (E) upregulated proteins in GSTP1 knockdown cells are represented in the bar graphs.

GSTP1 knockdown impairs the metabolic efficacy of PDAC cells

Interestingly, our bulk RNA sequencing and LC-MS/MS-based proteomics experiments revealed strong overlap in the genes that are differentially expressed at the mRNA and the protein levels respectively in GSTP1 knockdown cells compared to the control. To determine the changes in the cellular and molecular pathways associated with GSTP1 knockdown in PDAC cells, we performed functional pathway analysis using Ingenuity Pathway Analysis (Qiagen) software. We found cell function, maintenance, and signaling to be the most affected molecular pathways in

GSTP1 knockdown cells. Similarly, gene set enrichment analysis, using Enrichr, revealed that genes involved in metabolism, oxidative phosphorylation, and cellular signaling were differentially expressed in GSTP1 knockdown cells compared to the control. To be specific, cellular metabolism, pentose phosphate pathway, tricarboxylic-acid cycle, ATP synthesis, TGFβ signaling, and Wnt signaling pathways were among the top differentially regulated pathways in GSTP1 knockdown cells (Figures 5.5A and B). The significantly enriched pathways identified in our comparative transcriptomics and proteomics experiments are summarized in Tables 5.3 and 5.4, respectively.

Table 5.3. Significantly enriched pathways in doxycycline-inducible GSTP1 knockdown MIA PaCa-2 cells predicted by the comparative RNA-Seq analysis. The q-value is an adjusted p-value calculated using the Benjamini-Hochberg method for correction for multiple hypotheses testing.

Enriched pathway	p-value	q-value
Metabolism (*Homo sapiens*)	8.422E-07	2.671E-04
Insulin signaling pathway	3.702E-06	1.794E-04
Extracellular matrix organization	1.204E-06	3.063E-04
Downregulation of TGFβ signaling	1.646E-05	0.002
Downstream signal transduction	2.054E-05	0.002
Signaling by Wnt	4.922E-05	0.003
Prolonged ERK activation/signaling to ERKs	9.784E-05	0.004
Cellular senescence	1.042E-04	0.006
MAPK family cascade signaling	1.557E-04	0.006
Signaling by interleukins	1.942E-04	0.006
Post-translational protein modifications	2.113E-04	0.006
Signaling by NOTCH	2.414E-04	0.006
Interferon alpha/beta signaling	2.462E-04	0.006
Ca^{2+} signaling (*Homo sapiens*)	2.537E-04	0.006
Glucose metabolism	4.371E-04	0.008
Metabolism of carbohydrates	5.316E-04	0.011
Metabolism of lipids and lipoproteins	7.241E-04	0.013
Purine metabolism	1.072E-03	0.017
Metabolism of nucleotides	1.308E-03	0.019
Metabolism of proteins	1.384E-03	0.021
Insulin receptor signaling cascade	1.413E-03	0.021
Lipid digestion, mobilization, and transport	3.731E-03	0.045
Regulation of insulin secretion	4.099E-03	0.048
Fatty acid, triglycerides, and ketone body metabolism	4.262E-03	0.049
Pyruvate metabolism	4.352E-03	0.049

Table 5.4. Significantly enriched pathways in doxycycline-inducible GSTP1 knockdown MIA PaCa-2 cells predicted by the comparative proteomics experiment. The q-value is an adjusted p-value calculated using the Benjamini-Hochberg method for correction for multiple hypotheses testing.

Enriched pathway	p-value	q-value
Metabolism	1.322E-11	1.515E-08
Pentose phosphate pathway	2.561E-08	1.464E-05
Tricarboxylic acid (TCA) cycle and respiratory electron transport	2.603E-07	9.891E-05
L1CAM interactions	6.852E-07	1.953E-04
Respiratory electron transport/ATP biosynthesis	1.838E-06	4.191E-04
Immune system	4.072E-06	5.808E-04
Huntington's disease	4.427E-06	5.808E-04
Signaling by NGF	4.816E-06	5.808E-04
Recycling of adhesion molecule L1	5.022E-06	5.808E-04
Axon guidance	5.451E-06	5.808E-04
Immune system signaling by interferons, interleukins, and growth factors	9.419E-06	6.375E-04
Glucose metabolism	3.692E-05	1.619E-03
Electron transport chain	5.635E-05	2.294E-03
PDGFB signaling	6.567E-05	2.504E-03
Lipid and lipoprotein metabolism	9.797E-05	3.191E-03
Actin cytoskeleton regulation	1.456E-04	4.245E-03
Protein metabolism	1.773E-04	4.594E-03
Mitochondrial pathway of apoptosis	3.767E-04	8.102E-03
Purine metabolism	4.933E-04	9.696E-03
Fas signaling pathway	5.437E-04	0.011
Focal adhesion	5.632E-04	0.011
Activated NOTCH signaling in nucleus	6.551E-04	0.011
Glutathione metabolism	7.955E-04	0.013
MAPK signaling pathway	9.552E-04	0.014
Phospholipid metabolism	6.461E-03	0.048

We report significant downregulation of various solute carrier proteins (including SLC2A3, SLC6A12, SLC44A1, SLC2A3, SLC27A2, SLC16A3, and SLC25A16) and cytochrome proteins, such as CYP4A22 and CYP26B1 that primarily contribute for reduced metabolic efficacy in GSTP1 knockdown cells. Further, we found increased expression of ITGB8 and CYR61 that positively promote cellular senescence. In addition, we report decreased expression of PDIA6 and UBASH3B, suggesting impaired post-translational modifications and protein metabolism.

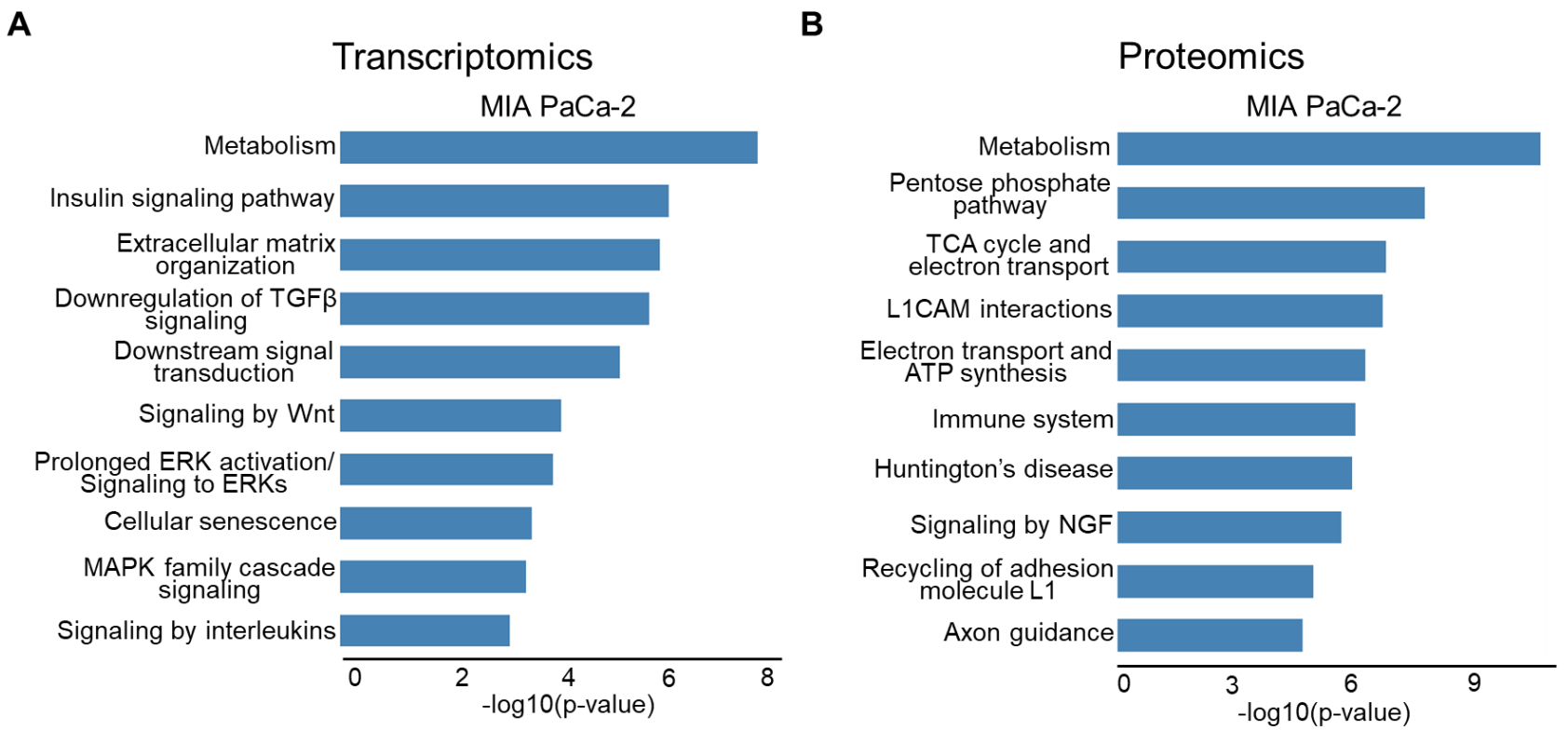

Figure 5.5. GSTP1 knockdown affects the metabolic efficacy of PDAC cells. (A, B) The bar charts show the top 10 enriched terms identified in our comparative transcriptomics and proteomics datasets using Enrichr. The x-axis shows the corresponding p-values. (C) Heatmaps showing differential expression of genes associated with cellular metabolism, (D-G) and pathways linked to lipid transport and metabolism in our RNA-Seq experiment. (H) Gene Set Enrichment Analysis (GSEA) of the transcriptomics data showing enrichment plot for decreased fatty acid metabolism in GSTP1 knockdown cells. White color indicates downregulation of genes in GSTP1 knockdown MIA PaCa-2 cells compared to the control and dark blue indicates upregulation of genes. (I) Heatmaps showing differential expression of proteins associated with cellular metabolism (J-L) and pathways linked to lipid and lipoprotein metabolism in our LC-MS/MS based proteomics experiment. (M) GSEA of the proteomics data showing enrichment plot for decreased fatty proteins genes in GSTP1 knockdown MIA PaCa-2 cells compared to the control.

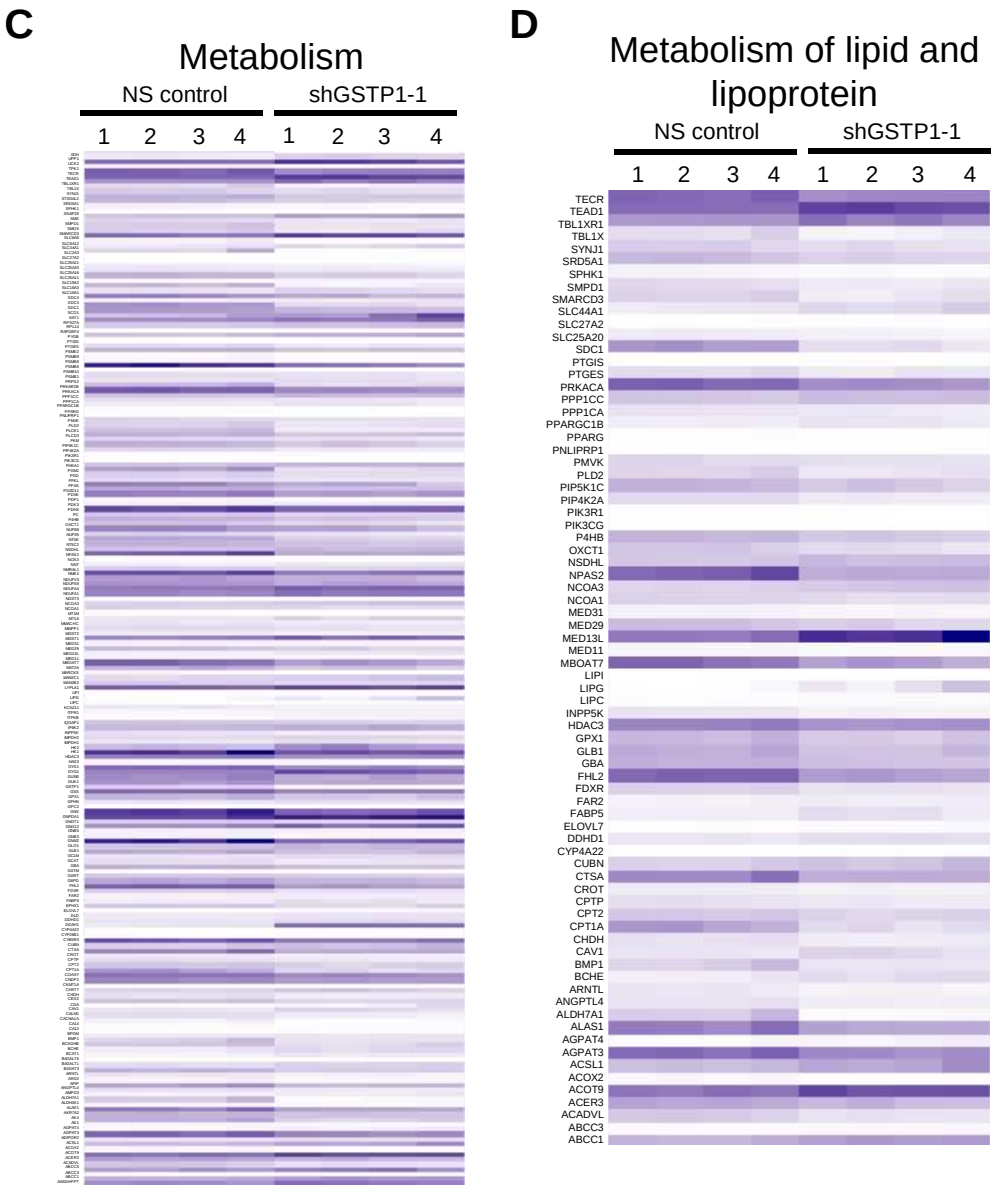

Figure 5.5. GSTP1 knockdown affects the metabolic efficacy of PDAC cells (continued). (A, B) The bar charts show the top 10 enriched terms identified in our comparative transcriptomics and proteomics datasets using Enrichr. The x-axis shows the corresponding p-values. (C) Heatmaps showing differential expression of genes associated with cellular metabolism, (D-G) and pathways linked to lipid transport and metabolism in our RNA-Seq experiment. (H) Gene Set Enrichment Analysis (GSEA) of the transcriptomics data showing enrichment plot for decreased fatty acid metabolism in GSTP1 knockdown cells. White color indicates downregulation of genes in GSTP1 knockdown MIA PaCa-2 cells compared to the control and dark blue indicates upregulation of genes. (I) Heatmaps showing differential expression of proteins associated with cellular metabolism (J-L) and pathways linked to lipid and lipoprotein metabolism in our LC-MS/MS based proteomics experiment. (M) GSEA of the proteomics data showing enrichment plot for decreased fatty proteins genes in GSTP1 knockdown MIA PaCa-2 cells compared to the control.

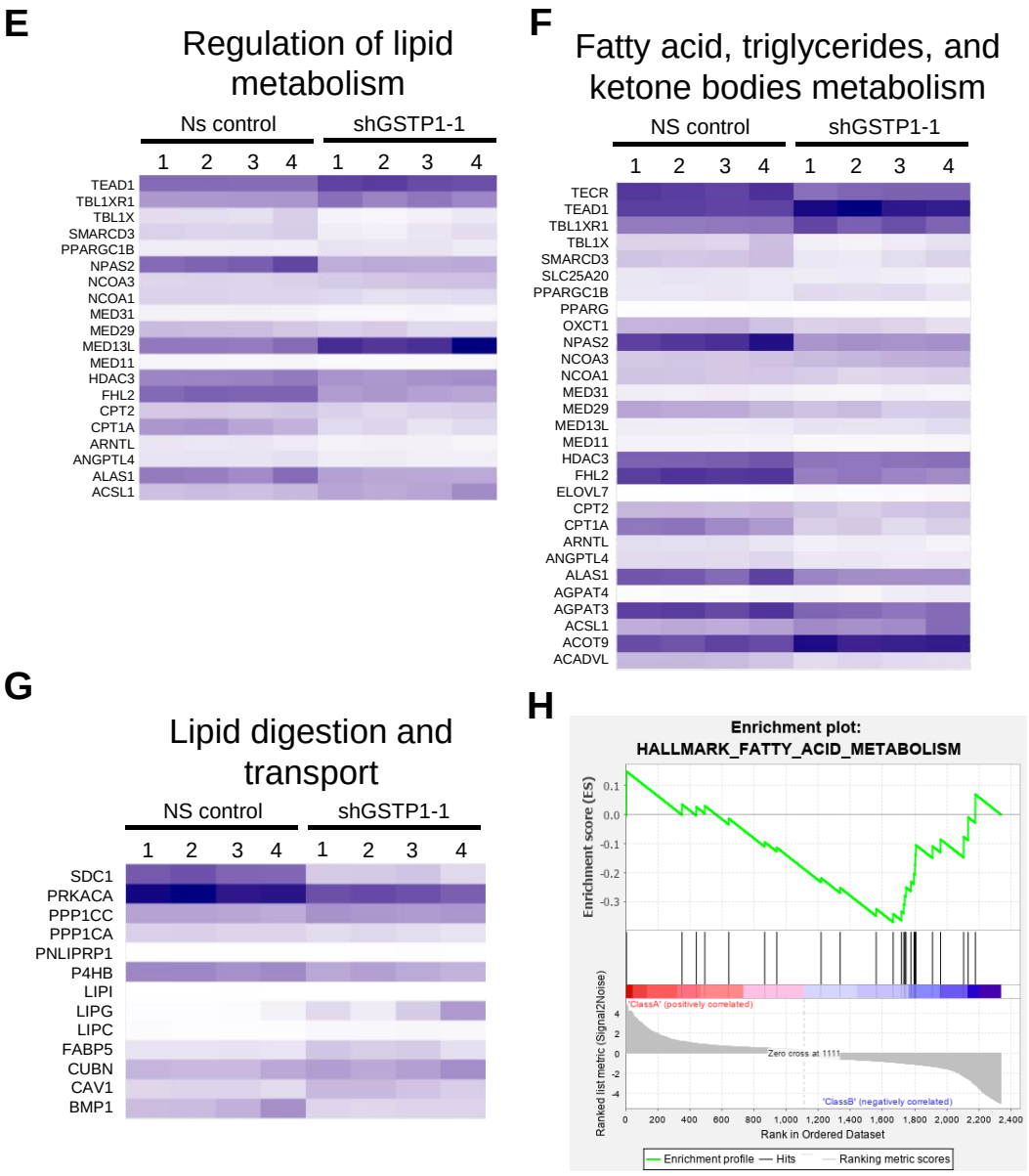

Figure 5.5. GSTP1 knockdown affects the metabolic efficacy of PDAC cells (continued). (A, B) The bar charts show the top 10 enriched terms identified in our comparative transcriptomics and proteomics datasets using Enrichr. The x-axis shows the corresponding p-values. (C) Heatmaps showing differential expression of genes associated with cellular metabolism, (D-G) and pathways linked to lipid transport and metabolism in our RNA-Seq experiment. (H) Gene Set Enrichment Analysis (GSEA) of the transcriptomics data showing enrichment plot for decreased fatty acid metabolism in GSTP1 knockdown cells. White color indicates downregulation of genes in GSTP1 knockdown MIA PaCa-2 cells compared to the control and dark blue indicates upregulation of genes. (I) Heatmaps showing differential expression of proteins associated with cellular metabolism (J-L) and pathways linked to lipid and lipoprotein metabolism in our LC-MS/MS based proteomics experiment. (M) GSEA of the proteomics data showing enrichment plot for decreased fatty proteins genes in GSTP1 knockdown MIA PaCa-2 cells compared to the control.

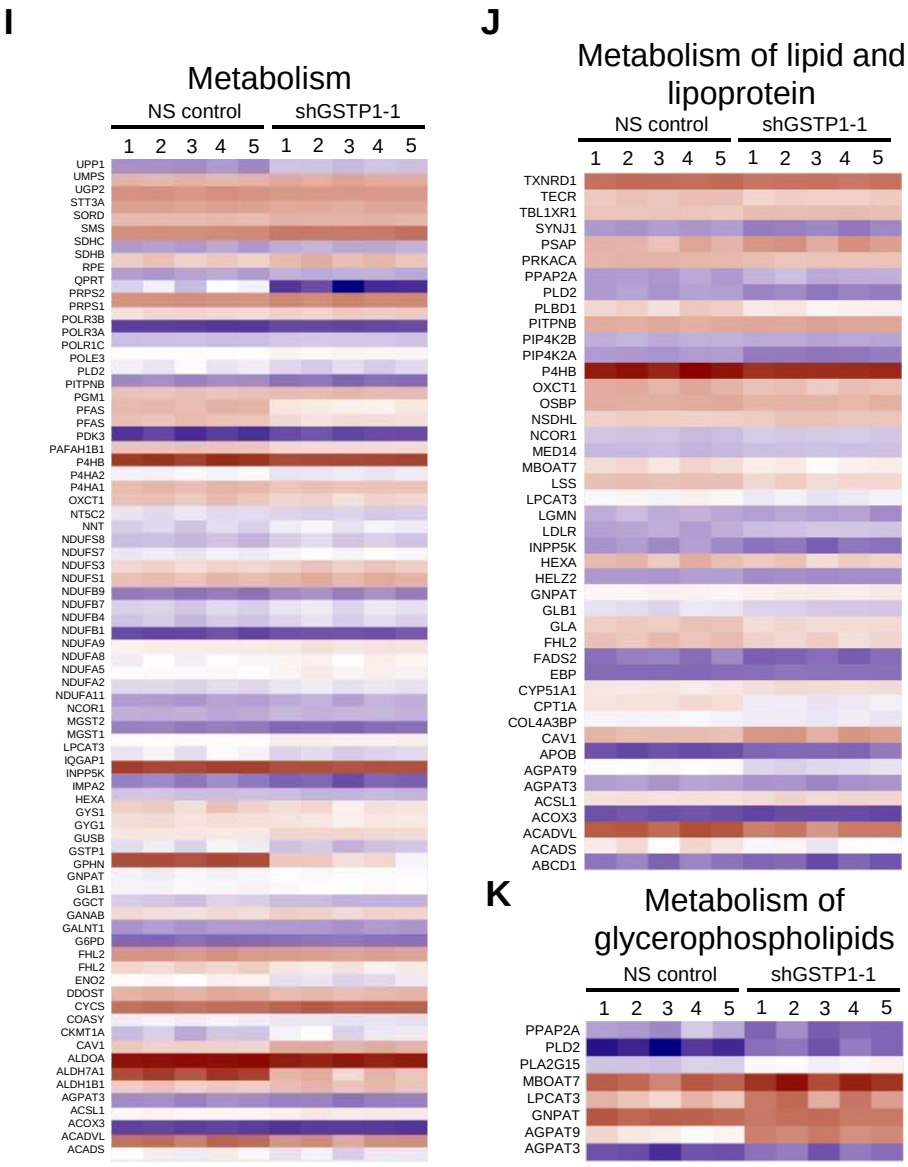

Figure 5.5. GSTP1 knockdown affects the metabolic efficacy of PDAC cells (continued). (A, B) The bar charts show the top 10 enriched terms identified in our comparative transcriptomics and proteomics datasets using Enrichr. The x-axis shows the corresponding p-values. (C) Heatmaps showing differential expression of genes associated with cellular metabolism, (D-G) and pathways linked to lipid transport and metabolism in our RNA-Seq experiment. (H) Gene Set Enrichment Analysis (GSEA) of the transcriptomics data showing enrichment plot for decreased fatty acid metabolism in GSTP1 knockdown cells. White color indicates downregulation of genes in GSTP1 knockdown MIA PaCa-2 cells compared to the control and dark blue indicates upregulation of genes. (I) Heatmaps showing differential expression of proteins associated with cellular metabolism (J-L) and pathways linked to lipid and lipoprotein metabolism in our LC-MS/MS based proteomics experiment. (M) GSEA of the proteomics data showing enrichment plot for decreased fatty proteins genes in GSTP1 knockdown MIA PaCa-2 cells compared to the control.

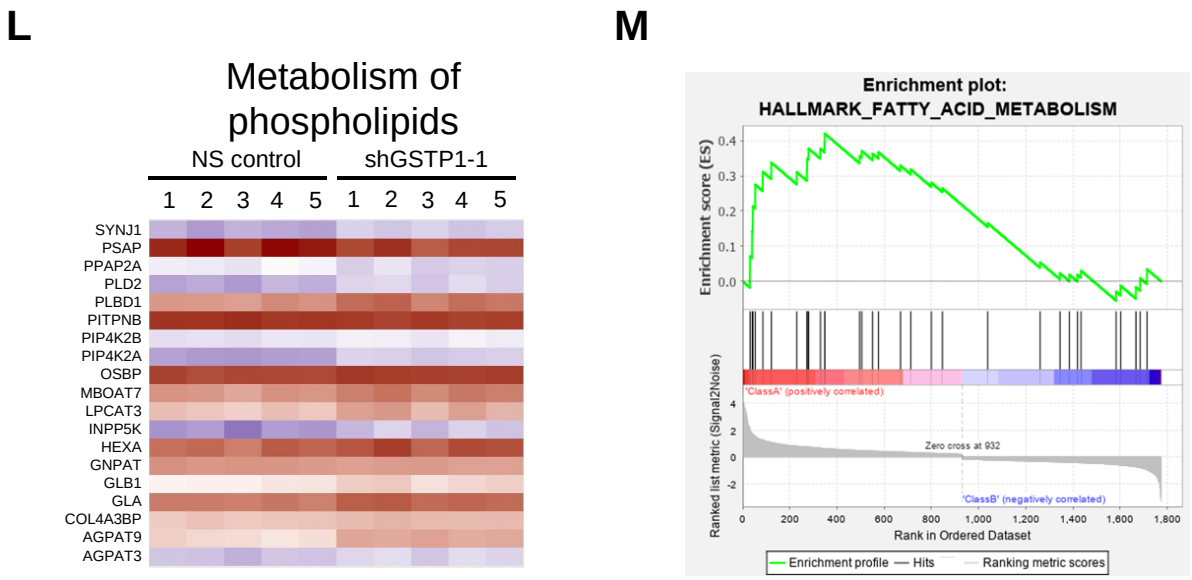

Figure 5.5. GSTP1 knockdown affects the metabolic efficacy of PDAC cells (continued). (A, B) The bar charts show the top 10 enriched terms identified in our comparative transcriptomics and proteomics datasets using Enrichr. The x-axis shows the corresponding p-values. (C) Heatmaps showing differential expression of genes associated with cellular metabolism, (D-G) and pathways linked to lipid transport and metabolism in our RNA-Seq experiment. (H) Gene Set Enrichment Analysis (GSEA) of the transcriptomics data showing enrichment plot for decreased fatty acid metabolism in GSTP1 knockdown cells. White color indicates downregulation of genes in GSTP1 knockdown MIA PaCa-2 cells compared to the control and dark blue indicates upregulation of genes. (I) Heatmaps showing differential expression of proteins associated with cellular metabolism (J-L) and pathways linked to lipid and lipoprotein metabolism in our LC-MS/MS based proteomics experiment. (M) GSEA of the proteomics data showing enrichment plot for decreased fatty proteins genes in GSTP1 knockdown MIA PaCa-2 cells compared to the control.

GSTP1 knockdown suppresses the lipid metabolic pathways in PDAC cells and inhibits the expression of ALDH7A1 and GLUT3

Comprehensive analysis of our comparative transcriptomics and proteomics datasets suggests that the dysregulated energy metabolism (Figures 5.5C and I) in GSTP1 knockdown cells is significantly contributed by impaired lipid metabolism. In addition to altered cellular homeostasis and signaling pathways described above, we found genes associated with lipid transport and breakdown to be differentially expressed at mRNA (Figures 5.5D-G) and protein levels (Figures 5.5J-L) in GSTP1 knockdown cells. In particular, pathways such as metabolism of

lipid macromolecules (including lipoproteins, glycerophospholipids, phospholipids, fatty acids, and ketone bodies), lipid digestion, and lipid transport were most significantly affected in GSTP1 knockdown cells.

Among the 550 genes and 69 proteins that were significant and differentially expressed in GSTP1 knockdown MIA PaCa-2 cells compared to the control, we found 41 genes that were similarly upregulated or downregulated at the mRNA and the protein level (Figure 5.6A and B). We then focused on the genes that play critical roles in lipid metabolic pathways and energy metabolism. Using qPCR and western blotting techniques, we validated the mRNA and protein expression, respectively, of aldehyde dehydrogenase 7A1 (ALDH7A1) and solute carrier 2A3 (also known as glucose transporter 3 or GLUT3). Apart from maintaining cellular homeostasis by detoxification of aldehydes, ALDH7A1 facilitates ATP production via fatty acid oxidation [24]. Likewise, GLUT3, responsible for cellular glucose uptake, controls the overall glycolytic process [25]. We report a more than 90% reduction in the mRNA and protein levels of (ALDH7A1). Similarly, the mRNA and the protein levels of GLUT3 were reduced by 70% in GSTP1 knockdown MIA PaCa-2 cells (Figures 5.6C-E).

A

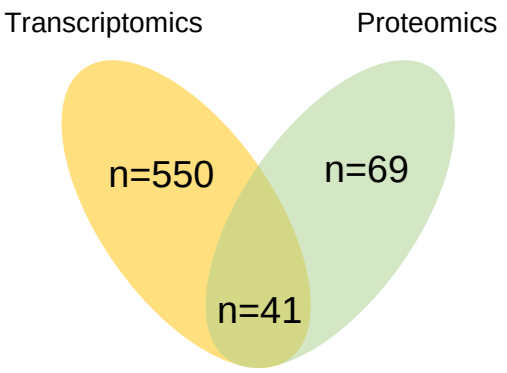

B

Protein/Gene	*KEGG class*
GSTP1	GSH metabolism/drug metabolism
GGH	
UPP1	
ALDH7A1	Lipid metabolism
SLC2A3	Carbohydrate metabolism
SLC16A3	
PGM1	
PDIA6	Protein metabolism
UBASH3B	
TCF7	Signal transduction
MVP	
SERPINF1	
TSPAN4	
ADD3	
PCDH1	TGFβ regulation of extracellular matrix
STOM	
LAMB1	Focal adhesion
CAV2	

Figure 5.6. GSTP1 knockdown reduces the expression of ALDH7A1 and GLUT3. (A) Venn diagram showing the number of genes that are differentially expressed at the mRNA and the protein level identified by the RNA-Seq and proteomics experiment, respectively. (B) Table of 18 differentially expressed genes and corresponding KEGG (Kyoto Encyclopedia of Genes and Genomes) class. Note-ALDH7A1 and SLC2A3 (GLUT3) are identified as differentially expressed by comparative transcriptomics and proteomics experiments. (C) qRT-PCR was used to validate the mRNA expression of ALDH7A1 and SLC2A3 in GSTP1 knockdown cells. (D, E) The protein levels of ALDH7A1 and SLC2A3 were quantified by western blotting. Protein and mRNA levels of ALDH7A1 and SLC2A3 in NS control MIA PaCa-2 cells were compared to shGSTP1-1 and shGSTP1-2. The images are representative of three independent experiments. The Student's t-test was used to evaluate the significance in the difference of GSTP1 expression among different groups. * denotes statistically significant differences between either GSTP1 knockdown and the control ($p < 0.05$).

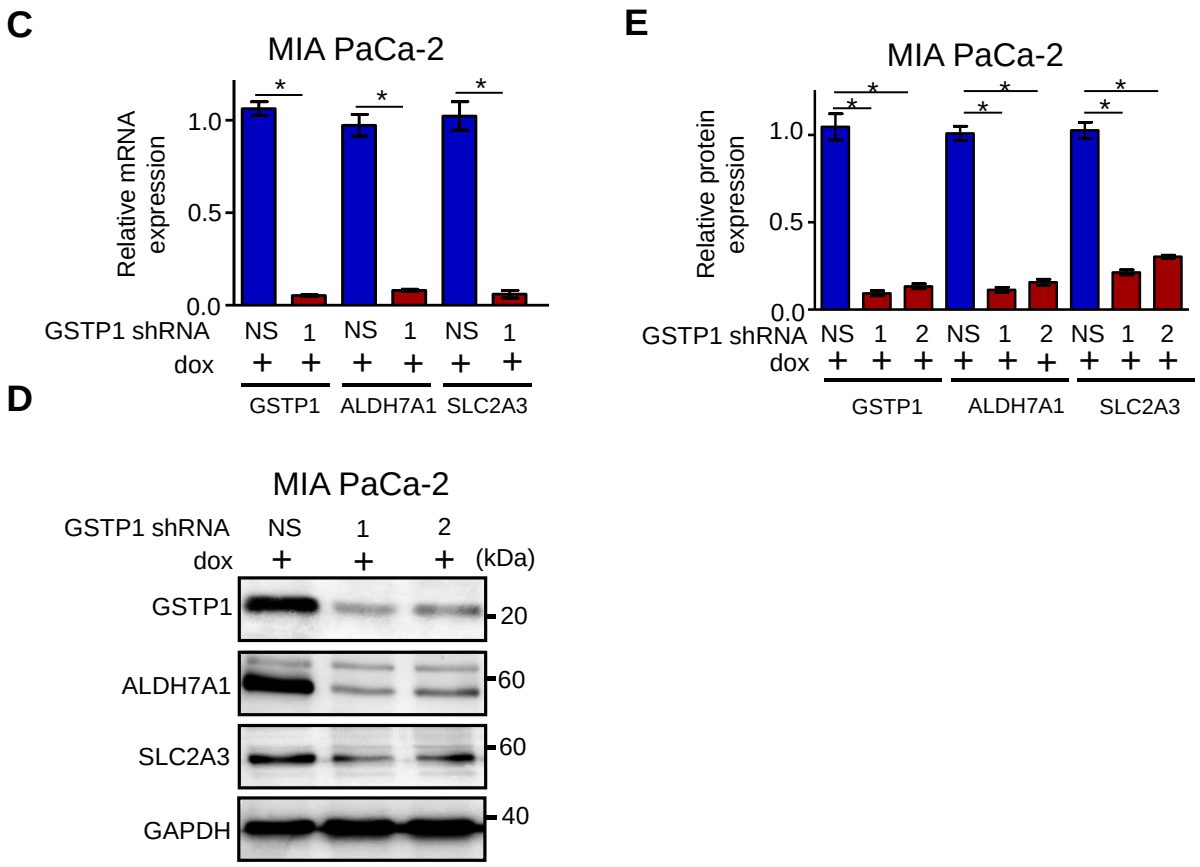

Figure 5.6. GSTP1 knockdown reduces the expression of ALDH7A1 and GLUT3 (continued). (A) Venn diagram showing the number of genes that are differentially expressed at the mRNA and the protein level identified by the RNA-Seq and proteomics experiment, respectively. (B) Table of 18 differentially expressed genes and corresponding KEGG (Kyoto Encyclopedia of Genes and Genomes) class. Note-ALDH7A1 and SLC2A3 (GLUT3) are identified as differentially expressed by comparative transcriptomics and proteomics experiments. (C) qRT-PCR was used to validate the mRNA expression of ALDH7A1 and SLC2A3 in GSTP1 knockdown cells. (D, E) The protein levels of ALDH7A1 and SLC2A3 were quantified by western blotting. Protein and mRNA levels of ALDH7A1 and SLC2A3 in NS control MIA PaCa-2 cells were compared to shGSTP1-1 and shGSTP1-2. The images are representative of three independent experiments. The Student's t-test was used to evaluate the significance in the difference of GSTP1 expression among different groups. * denotes statistically significant differences between either GSTP1 knockdown and the control ($p < 0.05$).

ALDH7A1 is overexpressed in PDAC cells and tissues

ALDH7A1 is overexpressed in various human cancers, such as breast cancer, colon adenocarcinoma, glioblastoma, and endometrial cancers [26]. A higher expression of ALDH7A1 is often associated with poor clinical outcomes [24]. To investigate if ALDH7A1 is overexpressed

in PDAC cell lines, we evaluated the protein expression of ALDH7A1 in various pancreatic cell lines. Interestingly, we found higher expression of ALDH7A1 in human pancreatic carcinoma cell lines (MIA PaCa-2, PANC-1, HPAF-II, and AsPC-1) compared to the normal Human Pancreatic Nestin-Expressing ductal cells (hTERT-HPNE) (Figures 5.7A and B). Additionally, to compare the *ALDH7A1* mRNA levels in healthy pancreas and PDAC tissues, we retrieved publicly available expression data from The Cancer Genome Atlas (TCGA) and Genotype-Tissue Expression (GTEx) projects. Similarly, we found significantly higher levels of *ALDH7A1* mRNA in basal and classical PDAC subtypes compared to the healthy pancreas (Figure 5.7C). Furthermore, using the mRNA gene expression and survival data from The Human Protein Atlas, we determined that the higher expression of *ALDH7A1* is negatively correlated with PDAC patient survival post-diagnosis (Figure 5.7D).

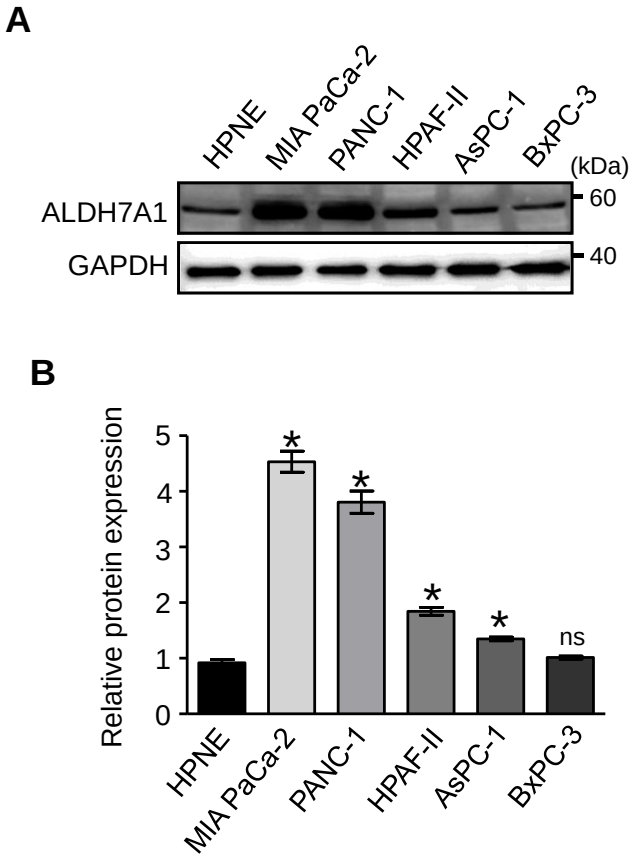

Figure 5.7. ALDH7A1 is overexpressed in human PDAC cells and tissues, and its expression is negatively correlated with patient survival. (A) Western blotting was used to determine the ALDH7A1 protein expression in a normal pancreatic cell line (Human Pancreatic Nestin-Expressing ductal cells (hTERT-HPNE)) and a panel of human PDAC cell lines (MIA PaCa-2, PANC-1, HPAF-II, AsPC-1, and BxPC-3). GAPDH protein levels were used as loading control. The images are representative of three independent experiments. (B) ALDH7A1 expression levels in MIA PaCa-2, PANC-1, HPAF-II, AsPC-1, and BxPC-3 cells were compared to ALDH7A1 expression in hTERT-HPNE cells. Densitometry values were determined using ImageJ software and normalized to GAPDH values. Student's t-test was used to identify potential significant differences in expression in the tumor cell lines compared to hTERT-HPNE cells. Significant changes in GSTP1 protein expression are denoted with * ($p < 0.05$). ns: non-significant. (C) *ALDH7A1* mRNA expression of healthy pancreatic tissue was compared with that of the basal and classical subtypes of PDAC tissue using the publicly available datasets in The Cancer Genome Atlas (TCGA) and Genotype-Tissue Expression (GTEx) projects. Student's t-test was used to analyze potential differences in *ALDH7A1* mRNA expression for PDAC tissue compared to normal pancreas tissue. Significant changes in *ALDH7A1* mRNA expression levels are denoted with * ($p < 0.05$). (D) The Human Protein Atlas was mined for *ALDH7A1* mRNA expression in PDAC patients ($n = 176$) relative to their corresponding years of survival post-diagnosis. The cut-off value of 5.6 FPKM was used to categorize patients in high- (red) and low- (blue) *ALDH7A1*-expressing groups. The Kaplan–Meier survival plot was constructed in RStudio using the survminer package.

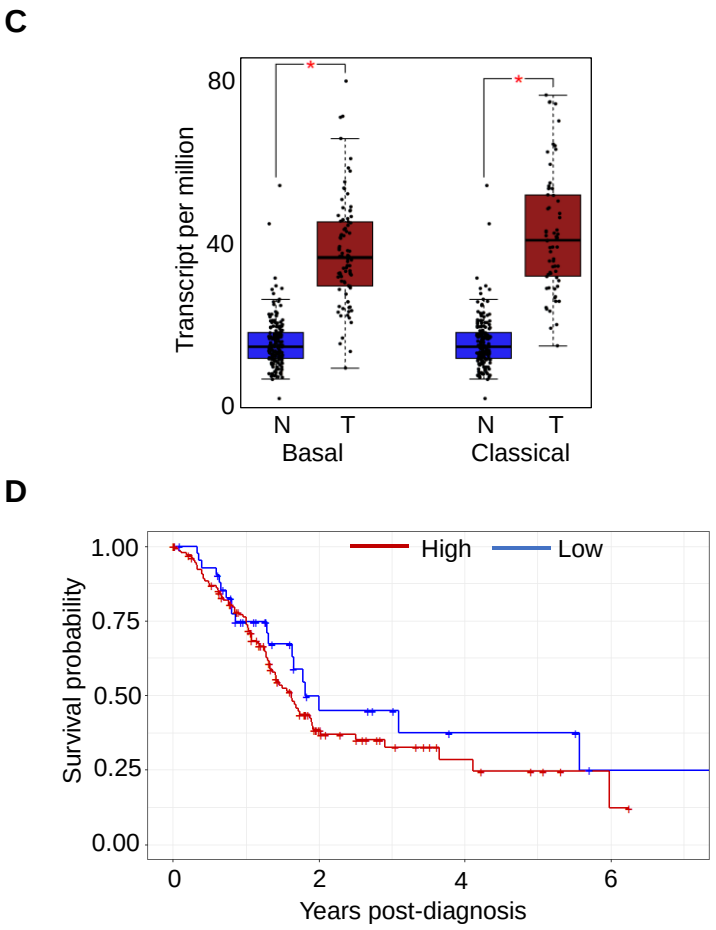

Figure 5.7. ALDH7A1 is overexpressed in human PDAC cells and tissues, and its expression is negatively correlated with patient survival (continued). (A) Western blotting was used to determine the ALDH7A1 protein expression in a normal pancreatic cell line (Human Pancreatic Nestin-Expressing ductal cells (hTERT-HPNE)) and a panel of human PDAC cell lines (MIA PaCa-2, PANC-1, HPAF-II, AsPC-1, and BxPC-3). GAPDH protein levels were used as loading control. The images are representative of three independent experiments. (B) ALDH7A1 expression levels in MIA PaCa-2, PANC-1, HPAF-II, AsPC-1, and BxPC-3 cells were compared to ALDH7A1 expression in hTERT-HPNE cells. Densitometry values were determined using ImageJ software and normalized to GAPDH values. Student's t-test was used to identify potential significant differences in expression in the tumor cell lines compared to hTERT-HPNE cells. Significant changes in GSTP1 protein expression are denoted with * ($p < 0.05$). ns: non-significant. (C) *ALDH7A1* mRNA expression of healthy pancreatic tissue was compared with that of the basal and classical subtypes of PDAC tissue using the publicly available datasets in The Cancer Genome Atlas (TCGA) and Genotype-Tissue Expression (GTEx) projects. Student's t-test was used to analyze potential differences in *ALDH7A1* mRNA expression for PDAC tissue compared to normal pancreas tissue. Significant changes in *ALDH7A1* mRNA expression levels are denoted with * ($p < 0.05$). (D) The Human Protein Atlas was mined for *ALDH7A1* mRNA expression in PDAC patients ($n = 176$) relative to their corresponding years of survival post-diagnosis. The cut-off value of 5.6 FPKM was used to categorize patients in high- (red) and low- (blue) *ALDH7A1*-expressing groups. The Kaplan–Meier survival plot was constructed in RStudio using the survminer package.

ALDH7A1 responds to the overall redox state of the cell

To interpret the mechanism through which GSTP1 knockdown reduces the expression of ALDH7A1, first, we restored GSTP1 expression by removing doxycycline from the culture media and evaluated the protein expression of ALDH7A1. We show that returning GSTP1 protein level to an unrepressed state restores the expression of ALDH7A1 (Figures 5.8A and B). Next, we treated MIA PaCa-2 cells with ezatiostat and piperlongumine (PL), which are known inhibitors of the catalytic activity of GSTP1. Our western blotting data show that 20 μM ezatiostat (for 48 and 72 hours) or 5 μM PL (for 24 and 48 hours) independently reduce the protein expression of ALDH7A1 (Figures 5.8C and D). Because genetic and pharmacological inactivation of GSTP1 cause oxidative stress, we then investigated the effects of adding an antioxidant, N-acetyl cysteine (NAC), to the GSTP1 knockdown cells. Interestingly, we found that treating the GSTP1-knockdown MIA PaCa-2 cells with 5 mM NAC for 48 hours increases the protein expression of ALDH7A1 by at least three fold (Figures 5. 8E and F). Lastly, to elucidate the effects of GSTP1 knockdown on lipid metabolism and fatty-acid oxidation (FAO), we evaluated the levels of 4-hydroxy nonenal (4-HNE), which is a byproduct of lipid peroxidation and a substrate of ALDH enzyme family for FAO, in GSTP1 knockdown cells. We show that GSTP1 knockdown increases the expression of 4-HNE by approximately twofold (Figures 5.8G and H). Collectively, our data suggest that the redox imbalance caused by GSTP1 knockdown reduces the expression of ALDH7A1.

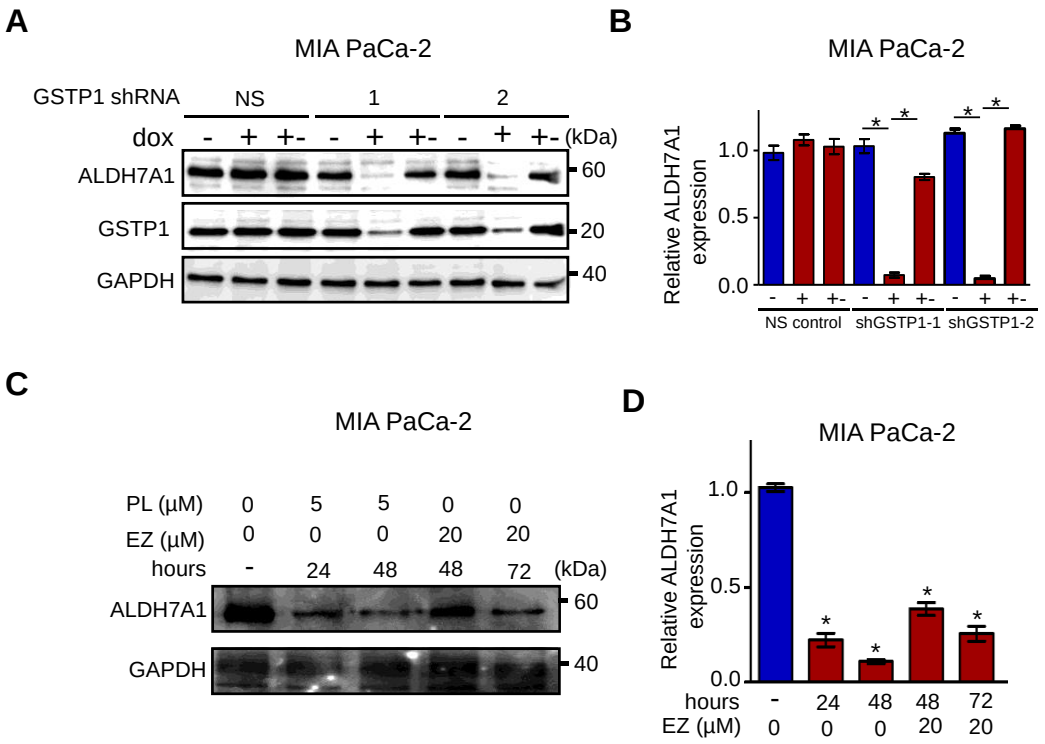

Figure 5.8. The redox state of the cell regulates the expression of ALDH7A1. (A) Western blotting showing expression of ALDH7A1 is restored upon removal of doxycycline for 120 hours (dox +-). (B) Protein expression in three independent experiments was quantified using densitometry. ALDH7A1 protein levels were compared between NS control and shGSTP1-1 and shGSTP1-2, independently. Relative levels of ALDH7A1 protein expression after 96 hours of dox treatment and after dox withdrawal for 120 hours are shown. (C) Effects of inhibiting enzymatic activity of GSTP1 on the protein expression of ALDH7A1 were determined using western blotting. GAPDH was used as loading control for the experiment. The figure shows one representative image of three independent experiments. Similar results were obtained in duplicate experiments. (D) Protein expression in three independent experiments was quantified using densitometry. ALDH7A1 protein levels were compared between NS control and shGSTP1-1 and shGSTP1-2, independently. Relative levels of ALDH7A1 protein expression after 48 and 72 hours of ezatiostat (20 μM) treatment and 24 and 48 hours of piperlongumine (PL) (5 μM) treatment. (E) Effects of N-acetyl cysteine (NAC) treatment on the protein expression of ALDH7A1 were determined using western blotting. GAPDH was used as loading control for the experiment. The figure shows one representative image of three independent experiments. Similar results were obtained in replicate experiments. (F) Protein expression in two independent experiments was quantified using densitometry. ALDH7A1 protein levels were compared between NS control and shGSTP1-1 and shGSTP1-2 independently with and without NAC treatment. (G) Western blotting showing the overexpression of 4-hydroxy nonenal (4-HNE) in GSTP1 knockdown cells. (H) Protein expression in two independent experiments was quantified using densitometry. 4-HNE protein levels were compared between NS control and shGSTP1-1 and shGSTP1-2 independently. Relative levels of 4-HNE protein expression after 96 hours of dox treatment. The Student's t-test was used to identify the significant differences in protein expression. * denotes statistically significant differences between either GSTP1 knockdown and the NS control ($p < 0.05$).

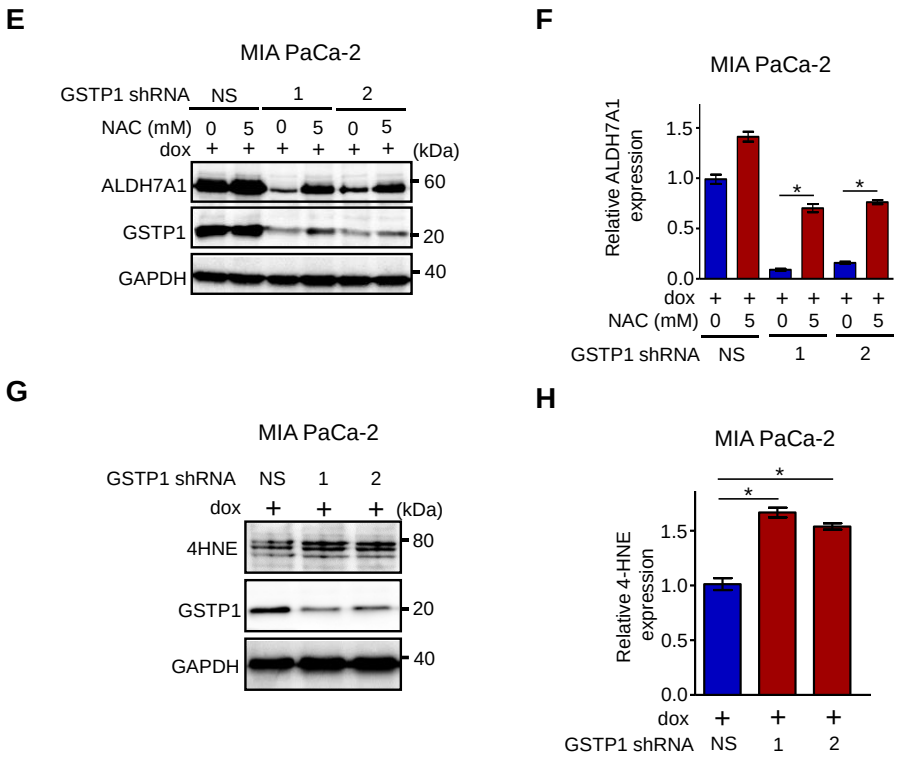

Figure 5.8. The redox state of the cell regulates the expression of ALDH7A1 (continued). (A) Western blotting showing expression of ALDH7A1 is restored upon removal of doxycycline for 120 hours (dox +-). (B) Protein expression in three independent experiments was quantified using densitometry. ALDH7A1 protein levels were compared between NS control and shGSTP1-1 and shGSTP1-2, independently. Relative levels of ALDH7A1 protein expression after 96 hours of dox treatment and after dox withdrawal for 120 hours are shown. (C) Effects of inhibiting enzymatic activity of GSTP1 on the protein expression of ALDH7A1 were determined using western blotting. GAPDH was used as loading control for the experiment. The figure shows one representative image of three independent experiments. Similar results were obtained in duplicate experiments. (D) Protein expression in three independent experiments was quantified using densitometry. ALDH7A1 protein levels were compared between NS control and shGSTP1-1 and shGSTP1-2, independently. Relative levels of ALDH7A1 protein expression after 48 and 72 hours of ezatiostat (20 µM) treatment and 24 and 48 hours of piperlongumine (PL) (5 µM) treatment. (E) Effects of N-acetyl cysteine (NAC) treatment on the protein expression of ALDH7A1 were determined using western blotting. GAPDH was used as loading control for the experiment. The figure shows one representative image of three independent experiments. Similar results were obtained in replicate experiments. (F) Protein expression in two independent experiments was quantified using densitometry. ALDH7A1 protein levels were compared between NS control and shGSTP1-1 and shGSTP1-2 independently with and without NAC treatment. (G) Western blotting showing the overexpression of 4-hydroxy nonenal (4-HNE) in GSTP1 knockdown cells. (H) Protein expression in two independent experiments was quantified using densitometry. 4-HNE protein levels were compared between NS control and shGSTP1-1 and shGSTP1-2 independently. Relative levels of 4-HNE protein expression after 96 hours of dox treatment. The Student's t-test was used to identify the significant differences in protein expression. * denotes statistically significant differences between either GSTP1 knockdown and the NS control ($p < 0.05$).

Discussion

GSTP1, a key antioxidant enzyme, maintains cellular homeostasis by conjugating GSH to the byproducts of aerobic respiration [36]. In addition, increasing evidence suggests that GSTP1 plays critical role in signaling [37], metabolism [21], and resistance to chemotherapy [38, 39] in cancer cells. We report that GSTP1 knockdown suppresses the growth of various PDAC cell lines and elevates the ROS levels. Additionally, our previous study demonstrated that GSTP1 knockdown causes PDAC cell death by activating the JNK signaling pathway [19]. The apoptotic phenotype upon GSTP1 knockdown was likely due to the disruption of redox homeostasis; however, the precise contributions of GSTP1 in promoting cancer cell growth are insufficiently characterized.

ROS are byproducts of aerobic respiration and cellular metabolism [40]. Higher accumulation of ROS causes macromolecular damage and promotes tumorigenesis [41]. The redox homeostasis in the cells is maintained by the meticulous activity of the antioxidant system [42]. Cancer cells, unlike their normal counterparts, are characterized by elevated levels of ROS [43], and, therefore, require a highly active antioxidant system [17]. The antioxidant system in cancer cells is rewired to scavenge excess ROS while maintaining pro-tumorigenic ROS levels allowing resistance to apoptosis and disease progression [44]. Therefore, therapies designed to cause redox imbalance by targeting the antioxidant system in cancer cells have shown potential in various tumor models [45, 46]. To demonstrate that GSTP1 is crucial in maintaining the redox balance in PDAC cells, we developed a doxycycline-inducible GSTP1 knockdown system. We show that knocking down GSTP1 expression for 96 hours can cause a significant elevation in the ROS levels. Interestingly, restoring GSTP1 protein levels returns the ROS levels to the inherent state. Thus,

our data provide convincing evidence that GSTP1 directly regulates the redox balance in PDAC cells and is a potential therapeutic target.

Intrigued by our previous observations, we next employed the multi-omics approaches to evaluate the comprehensive effects of GSTP1 knockdown in PDAC cells. Bulk RNA sequencing and mass spectrometry-based proteomics revealed significant changes in the global transcriptomic and proteomic signatures of the PDAC cells upon GSTP1 knockdown. Moreover, we found a strong overlap in differentially expressed genes identified by our transcriptomics and proteomics analyses. In particular, we found genes associated with cellular pathways such as energy metabolism, cellular signaling, and extracellular matrix organization to be substantially altered upon GSTP1 knockdown. Our data are supported by previous findings that suggest that GSTP1 binds to and increases the activity of glyceraldehyde-3-phosphate dehydrogenase (GAPDH), thus modulating glycolysis in triple-negative breast cancer (TNBC) cells [21]. These results provide strong evidence that GSTP1 resides at the intersection of redox homeostasis and cellular metabolism, two important and highly dysregulated elements in cancer cells.

Because cellular metabolism refers to broad physiological functions [47], we next wanted to identify the specific genes responsible for the altered metabolic state in GSTP1 knockdown PDAC cells. Consistent in our comparative transcriptomics and proteomics analyses, we found significant downregulation of ALDH7A1 in GSTP1 knockdown cells compared to the control. Like other aldehyde dehydrogenases, ALDH7A1 is an important detoxification enzyme [48]. To be specific, ALDH7A1 attenuates oxidative stress by metabolizing reactive aldehydes, including 4-HNE [49]. Further, ALDH7A1 contributes to energy metabolism by catabolizing 4-HNE to 4-hydroxy-2-nonenoic acid (4-HNA) and NADH, ultimately synthesizing acetyl Co-A for fatty acid oxidation [24]. Interestingly, recent evidence suggests that ALDH7A1 is associated with cancer

stem cell-like characteristics [50, 51] and provides resistance to chemotherapy and radiotherapy [52, 53]. Therefore, it is not surprising that a higher expression of ALDH7A1 is associated with poor patient survival. We speculate that downregulation of ALDH7A1 in GSTP1 knockdown cells contributes to oxidative stress, as seen by an increase in 4-HNE, and impairs the fatty acid oxidation mechanism. Further, our data suggest that the expression of ALDH7A1 is regulated by the general redox state of the cell. Our results show that increasing the oxidative stress in the PDAC cells reduces the expression of ALDH7A1, which can be restored by introducing an antioxidant in the growth media. In addition to impaired fatty acid oxidation, gene set enrichment analyses of our RNA-Seq and proteomics experiments reveal GSTP1 knockdown alters various lipid metabolism pathways, such as lipid transport, breakdown of triglycerides, ketone bodies, phospholipids, glycerophospholipids in PDAC cells. Although we show strong association of GSTP1 function with maintaining optimal lipid homeostasis in PDAC cells, to comprehensively understand this dependency, further validation of corresponding genes and pathways is critically needed.

Next, we directed our attention to GLUT3, which showed reduced mRNA and protein expression in GSTP1 knockdown cells. GLUT3 is a membrane protein that belongs to a family of solute carriers [54]. The primary function of GLUT3 is to enable the entry of glucose across the hydrophobic cell membrane [55]. Because most cancer cells depend extensively on glycolysis for ATP production [56], GLUT3 is often overexpressed in neoplastic tissue to accelerate metabolism [57]. In particular, comparative gene expression datasets show that GLUT3 is overexpressed in breast carcinoma, lung adenocarcinoma, ovarian carcinoma, colorectal carcinoma, and glioblastoma, where it contributes to tumorigenesis and results in poor patient outcomes [58, 59]. Although glucose intermediary breakdown has been a focus of recent investigations [60-63], the glucose uptake and the regulation of GLUT proteins remain poorly understood. Here, for the first

time, we show that mRNA and protein expression of GLUT3 are regulated by GSTP1. However, whether GLUT3 expression is affected by the overall redox state of the cell or through other functions of GSTP1 remains undetermined.

In addition to energy production, our comparative RNA-Seq and proteomics experiments reveal a set of genes associated with protein homeostasis are differentially expressed in GSTP1 knockdown PDAC cells. In particular, we report the downregulation of protein disulfide isomerase A6 (PDIA6) upon GSTP1 knockdown. Canonically, PDIA6 is crucial for protein folding and chaperone-mediated quality control of secretory and membrane proteins [64]. However, recent reports suggest that PDIA6 promotes tumorigenesis by modulating apoptosis in non-small cell lung cancer [65] and contributing to aerobic glycolysis in oral squamous cell carcinoma [66]. Further, mRNA expression data show higher levels of PDIA6 in the lung [65], bladder [67], and hepatocellular carcinoma [68], where it is believed to promote tumorigenesis. Similarly, our transcriptomics and proteomics datasets coincide in predicting a reduced expression of ubiquitin associated and SH3 domain containing B (UBASH3B). UBASH3B is a ubiquitin receptive, tyrosine phosphatase [69] that is aberrantly expressed in aggressive breast and prostate cancer cells and contributes to tumorigenesis and metastasis [70]. Therefore, it is possible that GSTP1 knockdown-mediated reduction in the expression of PDIA6 and UBASH3B is negatively associated with tumorigenesis and restores the near-normal phenotype in PDAC cells.

Collectively, our *in vitro* and multi-omic characterization of GSTP1 knockdown PDAC cells suggest a significant role of GSTP1 in the energy production processes of PDAC cells. For the first time, we show that GSTP1 knockdown not only causes oxidative stress but also affects lipid and carbohydrate metabolism by reducing the expression of ALDH7A1 and GLUT3, respectively. Because redox pathways and energy production mechanisms are significantly

rewired in cancer cells [71] and drive oncogenic phenotype [16], developing treatment modalities that target these vulnerabilities hold promise for disease-free survival in cancer patients. Our results identifying GSTP1 as an interjectory protein that regulates two important dimensions of cancer cell physiology are the first steps towards validation of GSTP1 as a novel therapeutic target to treat pancreatic cancer patients. Taken together, our observations suggest the efficacy of conventional antineoplastic drugs in pancreatic cancer patients can be improved by targeting GSTP1.

Author contributions

The material in this chapter was co-authored by Rahul Raj Singh, Jenna Duttenheffner, and Katie M. Reindl. R.R.S. performed all experiments, collected and analyzed the data. Also, wrote the manuscript. Except; J.D. performed qPCR experiments. K.M.R. was responsible for the supervision and coordination of the project. All authors read and approve the final version of this chapter before submission.

Acknowledgements

We thank Jeffrey Kittilson, Channing Der, Jiha Kim, Stephanie Byrum, and Philip Salu for their technical support and assistance. We acknowledge the use of the Proteomics Core Facility, a part of National Resource for Quantitative Proteomics, located at University of Arkansas for Medical Sciences, Little Rock, AR. Additionally; we acknowledge the use of IPA software provided by the Great Plains IDeA-Clinical & Translational Research collaborative project, funded at the University of Nebraska Medical Center, Omaha, NE.

Conflict of interest

The authors declare no conflict of interest.

Funding

This research is supported by NIH Research Enhancement Award 1R15CA249714-01 awarded to K.M.R. R.R.S. is partially supported by NIH COBRE Grant 1P20GM109024-04. The contents of this study are solely the responsibility of the authors and do not necessarily represent the official views of the NIH.

References

1. Hu, J.X., et al., *Pancreatic cancer: A review of epidemiology, trend, and risk factors.* World J Gastroenterol, 2021. **27**(27): p. 4298-4321.

2. Barcellini, A., et al., *Locally Advanced Pancreatic Ductal Adenocarcinoma: Challenges and Progress.* Onco Targets Ther, 2020. **13**: p. 12705-12720.

3. Siegel, R.L., K.D. Miller, and A. Jemal, *Cancer statistics, 2020.* CA Cancer J Clin, 2020. **70**(1): p. 7-30.

4. Hidalgo, M., et al., *Addressing the challenges of pancreatic cancer: future directions for improving outcomes.* Pancreatology, 2015. **15**(1): p. 8-18.

5. Sohal, D.P., et al., *Metastatic Pancreatic Cancer: American Society of Clinical Oncology Clinical Practice Guideline.* J Clin Oncol, 2016. **34**(23): p. 2784-96.

6. Kim, E.S., *Enasidenib: First Global Approval.* Drugs, 2017. **77**(15): p. 1705-1711.

7. Kremer, D.M., et al., *GOT1 inhibition promotes pancreatic cancer cell death by ferroptosis.* Nat Commun, 2021. **12**(1): p. 4860.

8. Hanahan, D. and R.A. Weinberg, *Hallmarks of cancer: the next generation.* Cell, 2011. **144**(5): p. 646-74.

9. Weinstein, I.B. and A. Joe, *Oncogene addiction.* Cancer Res, 2008. **68**(9): p. 3077-80; discussion 3080.

10. Mayers, J.R., et al., *Tissue of origin dictates branched-chain amino acid metabolism in mutant Kras-driven cancers.* Science, 2016. **353**(6304): p. 1161-5.

11. Vander Heide, M., *Targeting cancer metabolism: a therapeutic window opens.* Nature Reviews Drug Discovery, 2011. **10**: p. 671-684.

12. Kamphorst, J.J., et al., *Human pancreatic cancer tumors are nutrient poor and tumor cells actively scavenge extracellular protein.* Cancer Res, 2015. **75**(3): p. 544-53.

13. Koong, A.C., et al., *Pancreatic tumors show high levels of hypoxia.* Int J Radiat Oncol Biol Phys, 2000. **48**(4): p. 919-22.

14. Guillaumond, F., et al., *Strengthened glycolysis under hypoxia supports tumor symbiosis and hexosamine biosynthesis in pancreatic adenocarcinoma.* Proc Natl Acad Sci U S A, 2013. **110**(10): p. 3919-24.

15. Guillaumond, F., et al., *Cholesterol uptake disruption, in association with chemotherapy, is a promising combined metabolic therapy for pancreatic adenocarcinoma.* Proc Natl Acad Sci U S A, 2015. **112**(8): p. 2473-8.

16. Ying, H., et al., *Oncogenic Kras maintains pancreatic tumors through regulation of anabolic glucose metabolism.* Cell, 2012. **149**(3): p. 656-70.

17. Zhang, Y., et al., *Upregulation of Antioxidant Capacity and Nucleotide Precursor Availability Suffices for Oncogenic Transformation.* Cell Metab, 2021. **33**(1): p. 94-109 e8.

18. Ye, Z., et al., *Five glutathione s-transferase gene variants in 23,452 cases of lung cancer and 30,397 controls: meta-analysis of 130 studies.* PLoS Med, 2006. **3**(4): p. e91.

19. Singh, R.R., et al., *Glutathione S-Transferase pi-1 Knockdown Reduces Pancreatic Ductal Adenocarcinoma Growth by Activating Oxidative Stress Response Pathways.* Cancers (Basel), 2020. **12**(6).

20. Bakhiya, N., et al., *Directing role of organic anion transporters in the excretion of mercapturic acids of alkylated polycyclic aromatic hydrocarbons.* Drug Metab Dispos, 2007. **35**(10): p. 1824-31.

21. Louie, S.M., et al., *GSTP1 Is a Driver of Triple-Negative Breast Cancer Cell Metabolism and Pathogenicity.* Cell Chem Biol, 2016. **23**(5): p. 567-578.

22. Singh, R.R. and K.M. Reindl, *Glutathione S-Transferases in Cancer.* Antioxidants (Basel), 2021. **10**(5).

23. Wickham, H., *ggplot2: Elegant Graphics for Data Analysis*. 2016: Springer-Verlag New York.

24. Lee, J.S., et al., *Overall survival of pancreatic ductal adenocarcinoma is doubled by Aldh7a1 deletion in the KPC mouse.* Theranostics, 2021. **11**(7): p. 3472-3488.

25. Valentin Jacquier, D.G., Samuel Fritsch, Sandrine Bonnet, Balázs Győrffy, Stéphan Jalaguier, Laetitia K. Linares, Vincent Cavaillès, Catherine Teyssier, *RIP140 inhibits glycolysis-dependent proliferation of breast cancer cells by regulating GLUT3 expression through transcriptional crosstalk between hypoxia induced factor and p53.* bioRxiv, 2020.

26. Tang, Z., et al., *GEPIA: a web server for cancer and normal gene expression profiling and interactive analyses.* Nucleic Acids Res, 2017. **45**(W1): p. W98-W102.

27. Livak, K.J. and T.D. Schmittgen, *Analysis of relative gene expression data using real-time quantitative PCR and the 2(-Delta Delta C(T)) Method.* Methods, 2001. **25**(4): p. 402-8.

28. Li, H., et al., *The Sequence Alignment/Map format and SAMtools.* Bioinformatics, 2009. **25**(16): p. 2078-9.

29. Love, M.I., W. Huber, and S. Anders, *Moderated estimation of fold change and dispersion for RNA-seq data with DESeq2.* Genome Biol, 2014. **15**(12): p. 550.

30. Kuleshov, M.V., et al., *Enrichr: a comprehensive gene set enrichment analysis web server 2016 update.* Nucleic Acids Res, 2016. **44**(W1): p. W90-7.

31. Jassal, B., et al., *The reactome pathway knowledgebase.* Nucleic Acids Res, 2020. **48**(D1): p. D498-D503.

32. Huber, W., et al., *Variance stabilization applied to microarray data calibration and to the quantification of differential expression.* Bioinformatics, 2002. **18 Suppl 1**: p. S96-104.

33. B., B., *preprocessCore: A collection of pre-processing functions.* 2021. p. R package version 1.54.0.

34. Ritchie, M.E., et al., *limma powers differential expression analyses for RNA-sequencing and microarray studies.* Nucleic Acids Res, 2015. **43**(7): p. e47.

35. Chawade, A., E. Alexandersson, and F. Levander, *Normalyzer: a tool for rapid evaluation of normalization methods for omics data sets.* J Proteome Res, 2014. **13**(6): p. 3114-20.

36. Zhang, J., et al., *Pleiotropic functions of glutathione S-transferase P.* Adv Cancer Res, 2014. **122**: p. 143-75.

37. Dowling, R.J., et al., *Metformin inhibits mammalian target of rapamycin-dependent translation initiation in breast cancer cells.* Cancer Res, 2007. **67**(22): p. 10804-12.

38. Yu, D.S., D.S. Hsieh, and S.Y. Chang, *Increasing expression of GST-pi MIF, and ID1 genes in chemoresistant prostate cancer cells.* Arch Androl, 2006. **52**(4): p. 275-81.

39. Geng, M., et al., *The association between chemosensitivity and Pgp, GST-pi and Topo II expression in gastric cancer.* Diagn Pathol, 2013. **8**: p. 198.

40. Zorov, D.B., M. Juhaszova, and S.J. Sollott, *Mitochondrial reactive oxygen species (ROS) and ROS-induced ROS release.* Physiol Rev, 2014. **94**(3): p. 909-50.

41. Sabharwal, S.S. and P.T. Schumacker, *Mitochondrial ROS in cancer: initiators, amplifiers or an Achilles' heel?* Nat Rev Cancer, 2014. **14**(11): p. 709-21.

42. Williamson, J.M., B. Boettcher, and A. Meister, *Intracellular cysteine delivery system that protects against toxicity by promoting glutathione synthesis.* Proc Natl Acad Sci U S A, 1982. **79**(20): p. 6246-9.

43. Kang, S.W., S. Lee, and E.K. Lee, *ROS and energy metabolism in cancer cells: alliance for fast growth.* Arch Pharm Res, 2015. **38**(3): p. 338-45.

44. Gorrini, C., I.S. Harris, and T.W. Mak, *Modulation of oxidative stress as an anticancer strategy.* Nat Rev Drug Discov, 2013. **12**(12): p. 931-47.

45. Nogueira, V., et al., *Akt determines replicative senescence and oxidative or oncogenic premature senescence and sensitizes cells to oxidative apoptosis.* Cancer Cell, 2008. **14**(6): p. 458-70.

46. Trachootham, D., et al., *Selective killing of oncogenically transformed cells through a ROS-mediated mechanism by beta-phenylethyl isothiocyanate.* Cancer Cell, 2006. **10**(3): p. 241-52.

47. Judge, A. and M.S. Dodd, *Metabolism.* Essays Biochem, 2020. **64**(4): p. 607-647.

48. Marchitti, S.A., et al., *Non-P450 aldehyde oxidizing enzymes: the aldehyde dehydrogenase superfamily.* Expert Opin Drug Metab Toxicol, 2008. **4**(6): p. 697-720.

49. Singh, S., et al., *Aldehyde dehydrogenases in cellular responses to oxidative/electrophilic stress.* Free Radic Biol Med, 2013. **56**: p. 89-101.

50. Xu, X., et al., *Aldehyde dehydrogenases and cancer stem cells.* Cancer Lett, 2015. **369**(1): p. 50-7.

51. Alison, M.R., et al., *Finding cancer stem cells: are aldehyde dehydrogenases fit for purpose?* J Pathol, 2010. **222**(4): p. 335-44.

52. Prabhu, V.V., et al., *Cancer stem cell-related gene expression as a potential biomarker of response for first-in-class imipridone ONC201 in solid tumors.* PLoS One, 2017. **12**(8): p. e0180541.

53. Duru, N., et al., *HER2-associated radioresistance of breast cancer stem cells isolated from HER2-negative breast cancer cells.* Clin Cancer Res, 2012. **18**(24): p. 6634-47.

54. Ancey, P.B., C. Contat, and E. Meylan, *Glucose transporters in cancer - from tumor cells to the tumor microenvironment.* FEBS J, 2018. **285**(16): p. 2926-2943.

55. Hediger, M.A., et al., *The ABCs of membrane transporters in health and disease (SLC series): introduction.* Mol Aspects Med, 2013. **34**(2-3): p. 95-107.

56. Lunt, S.Y. and M.G. Vander Heiden, *Aerobic glycolysis: meeting the metabolic requirements of cell proliferation.* Annu Rev Cell Dev Biol, 2011. **27**: p. 441-64.

57. Barron, C.C., et al., *Facilitative glucose transporters: Implications for cancer detection, prognosis and treatment.* Metabolism, 2016. **65**(2): p. 124-39.

58. Flavahan, W.A., et al., *Brain tumor initiating cells adapt to restricted nutrition through preferential glucose uptake.* Nat Neurosci, 2013. **16**(10): p. 1373-82.

59. Chai, Y.J., et al., *Upregulation of SLC2 (GLUT) family genes is related to poor survival outcomes in papillary thyroid carcinoma: Analysis of data from The Cancer Genome Atlas.* Surgery, 2017. **161**(1): p. 188-194.

60. Poff, A., et al., *Targeting the Warburg effect for cancer treatment: Ketogenic diets for management of glioma.* Semin Cancer Biol, 2019. **56**: p. 135-148.

61. Ganapathy-Kanniappan, S. and J.F. Geschwind, *Tumor glycolysis as a target for cancer therapy: progress and prospects.* Mol Cancer, 2013. **12**: p. 152.

62. Abdel-Wahab, A.F., W. Mahmoud, and R.M. Al-Harizy, *Targeting glucose metabolism to suppress cancer progression: prospective of anti-glycolytic cancer therapy.* Pharmacol Res, 2019. **150**: p. 104511.

63. Chae, Y.C. and J.H. Kim, *Cancer stem cell metabolism: target for cancer therapy.* BMB Rep, 2018. **51**(7): p. 319-326.

64. Gorasia, D.G., et al., *A prominent role of PDIA6 in processing of misfolded proinsulin.* Biochim Biophys Acta, 2016. **1864**(6): p. 715-723.

65. Bai, Y., et al., *PDIA6 modulates apoptosis and autophagy of non-small cell lung cancer cells via the MAP4K1/JNK signaling pathway.* EBioMedicine, 2019. **42**: p. 311-325.

66. Mao, L., et al., *PDIA6 contributes to aerobic glycolysis and cancer progression in oral squamous cell carcinoma.* World J Surg Oncol, 2021. **19**(1): p. 88.

67. Cheng, H.P., et al., *The Inhibitory Effect of PDIA6 Downregulation on Bladder Cancer Cell Proliferation and Invasion.* Oncol Res, 2017. **25**(4): p. 587-593.

68. Negroni, L., et al., *Integrative quantitative proteomics unveils proteostasis imbalance in human hepatocellular carcinoma developed on nonfibrotic livers.* Mol Cell Proteomics, 2014. **13**(12): p. 3473-83.

69. Krupina, K., et al., *UBASH3B-mediated silencing of the mitotic checkpoint: Therapeutic perspectives in cancer.* Mol Cell Oncol, 2018. **5**(2): p. e1271494.

70. Lee, S.T., et al., *Protein tyrosine phosphatase UBASH3B is overexpressed in triple-negative breast cancer and promotes invasion and metastasis.* Proc Natl Acad Sci U S A, 2013. **110**(27): p. 11121-6.

71. Halbrook, C.J. and C.A. Lyssiotis, *Employing Metabolism to Improve the Diagnosis and Treatment of Pancreatic Cancer.* Cancer Cell, 2017. **31**(1): p. 5-19.

VI. CONCLUSIONS AND FUTURE DIRECTIONS

Pancreatic ductal adenocarcinoma (PDAC), the most common form of pancreatic cancer, is a lethal malignancy with a five-year survival rate of less than 10% [1]. The dismal clinical outcomes for PDAC patients are primarily due to the lack of early detection markers, rapid metastasis, and inadequate response to conventional antineoplastic drugs [2]. Because the majority of the PDAC patients develop resistance to chemotherapy, there is a pressing need to develop therapeutic modalities based on the characteristic physiology of pancreatic cancer. The present studies evaluated the antitumor activity and mechanisms of glutathione S-transferase pi-1 (GSTP1) knockdown in PDAC cells.

GSTs, a family of phase II detoxification enzymes, are essential constituents of the mammalian antioxidant system [3]. GSTs maintain cellular homeostasis by conjugating glutathione (GSH) to reactive electrophiles generated by cytochrome P450 metabolism [4]. Although most cell types express GST isoforms, different human organs are believed to present unique expression signatures. Using publicly available expression datasets, we found that GSTK1 and GSTM1 were abundantly expressed in hepatic tissues while GSTP1 was mostly found in extra-hepatic tissues. Further, we report that some GST isoforms such as GSTK1 and GSTP1 are overexpressed in neoplastic tissue and contribute to poor patient survival post-diagnosis. However, these observations are not uniformly consistent with all GST isoforms.

We then focused our attention on GSTP1, the most abundant isoform of the GST enzyme family, and found it is overexpressed in PDAC cells and tissue. To determine the role of GSTP1 in promoting PDAC cell growth and survival, we generated three knockdown PDAC cell lines (MIA PaCa-2, PANC-1, and HPAF-II). Using *in vitro* and *in vivo* PDAC models, we show that GSTP1 is crucial in maintaining cellular homeostasis and inhibits apoptotic signaling in PDAC

cells. In particular, we report that GSTP1 knockdown activates the JNK signaling pathway, reduces the phosphorylation of ERK, and decreases the expression of Sp1 [5]. Our observations provide convincing evidence that GSTP1 plays a crucial role in PDAC cell growth, which was previously unknown. To determine the molecular mechanisms underlying the growth-inhibitory effects of prolonged GSTP1 knockdown, we used bulk RNA sequencing. Our findings suggest that long-term knockdown of GSTP1 impairs the mRNA translation machinery. Further, we show that the redox imbalance due to GSTP1 knockdown creates a cascade of events, such as aberrant cell-cycle checkpoint regulation and senescence, which leads to the activation of cell death pathways.

Because GSTP1 is instrumental in maintaining redox homeostasis, we next wanted to evaluate the short-term effects of GSTP1 knockdown in PDAC cells. To address this, we generated doxycycline-inducible GSTP1 knockdown PDAC cells. Using this model, we show that, similar to long-term knockdown, short-term GSTP1 knockdown increases the reactive oxygen species (ROS) in the PDAC cells. Furthermore, restoring GSTP1 levels to an unrepressed state rescues the cells from oxidative stress, suggesting GSTP1 directly influences the redox homeostasis of PDAC cells. To comprehensively characterize GSTP1 knockdown PDAC cells, we next used a multi-omic approach. Our comparative bulk RNA sequencing and LC-MS/MS proteomics experiments revealed significant global transcriptomic and proteomic changes in PDAC cells upon GSTP1 knockdown. A thorough gene set enrichment and pathway analysis revealed genes associated with cellular metabolism and energy production to be most differentially expressed in GSTP1 knockdown PDAC cells compared to the control. Interestingly, our transcriptomics and proteomics dataset showed a significant reduction in critical metabolic genes, such as aldehyde dehydrogenase 7A1 (ALDH7A1) and solute carrier 2A3 (SLC2A3), also known as glucose transporter 3

(GLUT3). These results were validated using qPCR and western blotting techniques, and we indeed found a significant reduction in the expression of these genes. ALDH7A1, another antioxidant enzyme, is crucial for ATP production via fatty acid oxidation [6] and is directly regulated by the levels of GSTP1 in the cell. Because ALDH7A1 utilizes 4-hydroxy nonenal (4-HNE) for ATP production via fatty acid oxidation, we next investigated the levels of 4-HNE in GSTP1 knockdown cells. We report a significant increase in 4-HNE in GSTP1 knockdown cells, suggesting lipid peroxidation and impaired fatty oxidation pathways in GSTP1 knockdown cells. Our observations from these studies are intriguing because they provide preliminary evidence that GSTP1 resides at the junction of cellular redox and metabolic mechanisms.

The dire clinical outcomes for PDAC patients are primarily due to poor response and resistance to conventional chemotherapy [7]. The recent understanding of rewired cancer cell metabolism has shown that targeting metabolic vulnerabilities of cancer cells is a potential treatment strategy for PDAC patients [8, 9]. Taken together, our findings highlight the crucial role of GSTP1 in PDAC cell growth and metabolism. The loss of GSTP1 causes oxidative stress, affects the cell cycle pathways, and induces apoptotic-signaling mechanisms. Further, we report significant changes in the global transcriptomic and proteomic signature of PDAC cells upon GSTP1 knockdown. Our data suggest that GSTP1 is a potential and novel therapeutic target to treat pancreatic cancer patients. However, the precise mechanisms underlying the GSTP1 action in PDAC cells are still not fully understood. Therefore, to comprehensively characterize the diverse functions of GSTP1 in cancer cells, the following ***future directions*** are recommended.

1. Because we found genes associated with cellular metabolism and energy production pathways to be most differentially expressed in GSTP1 knockdown PDAC cells, we propose executing a real-time assay to measure and quantify the rate of ATP production

from glycolytic and mitochondrial systems using a Seahorse Bioanalyzer. We speculate a reduction in metabolic efficacy of GSTP1 knockdown PDAC cells. Specifically, we expect a reduction in ATP levels in GSTP1 knockdown cells due to the reduced levels of ALDH7A1. Moreover, because we observed a significant reduction of glucose transporter-protein, GLUT3, we predict impaired glycolysis in GSTP1 knockdown cells.

2. Our data provide convincing evidence that GSTP1 knockdown causes oxidative stress in PDAC cells. The free radicals produced by redox imbalance cause oxidative damage to cellular membranes, lipoproteins, and other molecules that contain lipids. To comprehensively evaluate the effects of GSTP1-knockdown mediated oxidative stress on lipid peroxidation, we will use a mass spectrometry-based approach to identify the phospholipid composition in control and GSTP1 knockdown PDAC cells.
3. We saw a significant increase in 4-HNE, which is a metabolic byproduct of lipid peroxidation, in GSTP1 knockdown cells. This observation suggests that GSTP1 knockdown induces a differential metabolic response in PDAC cells. Therefore, we propose to compare the bulk metabolome of GSTP1 knockdown cells to the control. For a comparative metabolomics experiment, the methanol extract of control and GSTP1 knockdown MIA PaCa-2 cells will be used to evaluate hydrophilic metabolites in the two groups
4. Significant evidence suggests that GSTP1 provides resistance to platinum-based chemotherapy in various neoplastic tissues. However, this function of GSTP1 remains undetermined in PDAC cells and tissues. We propose to evaluate the combined effects of GSTP1 knockdown and cisplatin or oxaliplatin treatment on PDAC cell death, redox

imbalance, and cell signaling using the *in vitro* cell culture and patient-derived xenograft (PDX) models.

5. Our bulk RNA sequencing and LC-MS/MS-based proteomics experiments revealed a significant reduction in ALDH7A1 and GLUT3 mRNA and protein levels. These results were validated using RT-qPCR and Western blotting. However, the precise mechanism through which GSTP1 regulates the expression of these metabolic genes is currently unknown. Therefore, we propose to restore ALDH7A1 and GLUT3 levels and investigate the effects on cell growth and oxidative stress in GSTP1 knockdown PDAC cells.
6. We [5, 10], and others, have previously shown that GSTP1 inhibits apoptotic signaling by binding to JNK [11]. Additionally, evidence suggest that GSTP1 plays crucial role in cell signaling by binding to tumor necrosis factor (TNF)-receptor-associated factor 2 (TRAF2) [12]. Further, GSTP1 post-translationally modify various proteins through glutathionylation [13]. However, the comprehensive interactome of GSTP1 remains poorly characterized. We suggest that identifying the interacting partners of GSTP1 and investigating the significance of these interactions will substantially expand the existing knowledge about GSTP1.

References

1. Siegel, R.L., K.D. Miller, and A. Jemal, *Cancer statistics, 2020.* CA Cancer J Clin, 2020. **70**(1): p. 7-30.
2. Hidalgo, M., et al., *Addressing the challenges of pancreatic cancer: future directions for improving outcomes.* Pancreatology, 2015. **15**(1): p. 8-18.
3. Zhang, J., et al., *Pleiotropic functions of glutathione S-transferase P.* Adv Cancer Res, 2014. **122**: p. 143-75.
4. Singh, R.R. and K.M. Reindl, *Glutathione S-Transferases in Cancer.* Antioxidants (Basel), 2021. **10**(5).

5. Singh, R.R., et al., *Glutathione S-Transferase pi-1 Knockdown Reduces Pancreatic Ductal Adenocarcinoma Growth by Activating Oxidative Stress Response Pathways.* Cancers (Basel), 2020. **12**(6).

6. Lee, J.S., et al., *Overall survival of pancreatic ductal adenocarcinoma is doubled by Aldh7a1 deletion in the KPC mouse.* Theranostics, 2021. **11**(7): p. 3472-3488.

7. Barcellini, A., et al., *Locally Advanced Pancreatic Ductal Adenocarcinoma: Challenges and Progress.* Onco Targets Ther, 2020. **13**: p. 12705-12720.

8. Halbrook, C.J. and C.A. Lyssiotis, *Employing Metabolism to Improve the Diagnosis and Treatment of Pancreatic Cancer.* Cancer Cell, 2017. **31**(1): p. 5-19.

9. Kremer, D.M., et al., *GOT1 inhibition promotes pancreatic cancer cell death by ferroptosis.* Nat Commun, 2021. **12**(1): p. 4860.

10. Mohammad, J., et al., *JNK inhibition blocks piperlongumine-induced cell death and transcriptional activation of heme oxygenase-1 in pancreatic cancer cells.* Apoptosis, 2019. **24**(9-10): p. 730-744.

11. Adler, V., et al., *Regulation of JNK signaling by GSTp.* EMBO J, 1999. **18**(5): p. 1321-34.

12. De Luca, A., et al., *The fine-tuning of TRAF2-GSTP1-1 interaction: effect of ligand binding and in situ detection of the complex.* Cell Death Dis, 2014. **5**: p. e1015.

13. Townsend, D.M., et al., *Novel role for glutathione S-transferase pi. Regulator of protein S-Glutathionylation following oxidative and nitrosative stress.* J Biol Chem, 2009. **284**(1): p. 436-445.

APPENDIX A: DIFFERENTIALLY EXPRESSED GENES IN GSTP1 KNOCKDOWN CELLS

The most significant, differentially expressed genes in GSTP1 knockdown MIA PaCa-2 cells compared to the control as reported by bulk RNA sequencing experiment. The log_2-fold change, p-adjusted, and the raw count values for four replicates of each group are shown here.

Gene	log2-fold change	Adjusted p-value	NS control Rep 1	NS control Rep 2	NS control Rep 3	NS control Rep 4	shGSTP1-1 Rep 1	shGSTP1-1 Rep 2	shGSTP1-1 Rep 3	shGSTP1-1 Rep 4
EHF	-7.51012	7.8E-152	2922.522	2010.653	1845.445	1991.265	11.78259	14.18768	7.256729	15.00266
FAM71D	-6.57144	8.85E-96	842.0491	664.2125	632.8963	713.2364	6.284046	9.458456	9.675639	5.000886
FAM46A	-6.40533	1.86E-92	2227.388	1240.699	1283.875	1263.974	23.56517	11.82307	24.1891	10.00177
TLE1	-6.20256	1.2E-106	626.1138	649.3304	717.2824	747.4928	11.78259	4.729228	7.256729	12.50222
GRAMD2B	-6.01841	5E-197	2991.542	2166.523	2085.544	2186.263	43.98832	34.2869	33.86474	31.25554
P2RY6	-6.00328	8.06E-11	1566.764	736.2733	592.7124	756.2765	34.56225	16.5523	2.41891	2.500443
SH3BGRL	-5.90161	8.44E-47	608.3657	405.7336	375.7194	303.0376	4.713035	4.729228	4.83782	15.00266
TCF7	-5.80483	8.2E-249	7688.875	6513.669	7052.273	7405.537	103.6868	101.6784	129.4117	181.2821
SCG2	-5.69391	0	5638.968	5530.666	6859.39	6797.705	139.82	107.5899	104.0131	125.0222
C15orf48	-5.19805	1.49E-67	289.8858	331.323	367.6826	343.4426	9.426069	7.093842	7.256729	12.50222
OAS2	-5.19481	1.78E-06	821.343	290.593	381.747	251.2138	29.84922	7.093842	0	10.00177
FAM198B	-5.07857	7E-212	1830.027	1839.9	2138.788	1950.86	45.55933	61.47997	48.3782	77.51374
MDFIC	-4.99098	3.5E-47	228.7534	293.7261	345.5815	312.6997	4.713035	7.093842	16.93237	10.00177
KLK6	-4.88173	3.4E-118	7615.91	6451.791	6334.99	7042.77	136.678	261.2899	232.2153	305.0541
CCL5	-4.82618	3.5E-12	379.6123	104.1748	140.6436	83.44514	1.571012	11.82307	9.675639	2.500443
KLK7	-4.81799	2.42E-10	1590.428	693.1935	674.0848	750.1279	70.69552	23.64614	4.83782	31.25554
NTSR1	-4.66628	4.18E-45	1664.378	2312.995	2678.256	2539.368	152.3881	61.47997	102.8037	42.50753
VWA5A	-4.59239	1.53E-16	564.9814	245.9466	180.8275	198.5116	12.56809	9.458456	2.41891	25.00443
ADAMTSL1	-4.58233	1.93E-10	40.42625	35.24713	42.19308	59.72916	2.356517	2.364614	2.41891	0
LIFR	-4.3862	4.41E-63	3489.475	2852.667	2855.065	2855.581	193.2344	165.523	65.31056	150.0266
MARCKS	-4.37975	1.96E-27	267.2076	196.6006	306.4022	327.632	10.99708	28.37537	7.256729	6.251108
TMEM158	-4.35287	9.7E-136	761.1966	802.8512	970.4409	930.1938	38.48978	46.10997	45.95929	40.00709
KLK5	-4.3243	1.3E-262	4426.181	3885.8	4438.311	4711.576	240.3648	232.9145	172.952	222.5394
JAG1	-4.26045	3E-103	1199.969	1376.988	1774.119	1937.684	93.47519	78.03226	70.14838	85.01507
F2R	-4.22631	3.9E-70	6783.721	5383.411	5474.05	6202.17	475.231	288.4829	187.4655	318.8065
TMEM173	-4.18319	2.47E-09	414.1225	195.0341	147.6758	137.0257	32.99124	7.093842	4.83782	2.500443
OXR1	-4.11064	2.96E-70	431.8706	400.2507	416.9079	358.3749	32.99124	22.46383	15.72291	18.75332
PMAIP1	-4.07979	3.02E-37	537.3733	382.2355	349.5998	261.7542	26.7072	16.5523	31.44583	15.00266
AFAP1L2	-3.96918	8.8E-115	2085.403	3239.603	3316.176	2895.107	201.0895	199.8099	174.1615	160.0284
GPR39	-3.95449	7.23E-08	19.72012	66.57791	46.21147	36.01317	1.571012	4.729228	2.41891	2.500443
RASAL2	-3.85756	1.73E-47	259.3196	245.9466	215.9884	274.9298	15.71012	14.18768	12.09455	27.50488
SLC2A3	-3.76502	1.41E-11	3158.177	1445.132	1503.882	1515.188	273.356	102.8607	64.10111	118.7711
APOL1	-3.72532	7.36E-10	388.4864	161.3535	129.593	111.553	23.56517	11.82307	2.41891	21.25377

Gene	log2-fold change	Adjusted p-value	NS control Rep 1	NS control Rep 2	NS control Rep 3	NS control Rep 4	shGSTP1-1 Rep 1	shGSTP1-1 Rep 2	shGSTP1-1 Rep 3	shGSTP1-1 Rep 4
SAMD9	-3.70641	3.45E-27	219.8793	133.1558	152.6988	173.0389	18.85214	11.82307	12.09455	7.50133
SYTL2	-3.64222	1.35E-66	339.1861	306.2584	296.3562	310.943	31.42023	22.46383	24.1891	20.00355
PDE1A	-3.62185	1.38E-40	216.9213	223.2318	183.8413	228.3762	23.56517	11.82307	12.09455	20.00355
PIK3CG	-3.55991	1.94E-09	43.38426	43.86309	37.1701	46.55361	6.284046	2.364614	0	5.000886
NRP1	-3.55615	3.5E-45	459.4788	536.5396	616.8227	689.5204	43.98832	30.73998	48.3782	73.76308
PRICKLE1	-3.55347	5.55E-10	35.49622	39.16347	66.30342	55.33731	6.284046	2.364614	2.41891	5.000886
CORO2B	-3.53564	4.61E-74	564.9814	439.4142	484.2159	458.5091	32.99124	49.6569	38.70256	48.75864
SERPINE2	-3.49927	1.79E-08	68.03441	64.2281	36.1655	28.10784	3.142023	2.364614	7.256729	5.000886
PNMA2	-3.47268	7.93E-13	731.6165	306.2584	278.2734	299.5242	69.91001	34.2869	21.77019	17.5031
PRSS23	-3.47148	4.72E-35	2863.361	2505.679	2508.479	2615.786	382.5413	256.5606	133.04	170.0301
DDX60	-3.41577	2.13E-11	631.0438	271.7945	269.2321	231.8897	65.19698	24.82845	12.09455	27.50488
GSTP1	-3.37029	8.8E-115	15834.27	13740.11	15369.33	15024.52	1058.862	1481.431	1704.122	1560.277
GBP3	-3.36994	2.78E-11	57.18835	43.86309	44.20228	42.16176	4.713035	5.911535	4.83782	2.500443
CPEB2	-3.32146	5.22E-08	85.78252	70.49425	65.29882	50.06709	15.71012	2.364614	4.83782	2.500443
MGAT5B	-3.3013	1.2E-105	757.2526	766.8208	839.8433	863.4377	95.8317	67.3915	70.14838	91.26618
DPYSL2	-3.29399	1.85E-82	2379.232	2183.755	1916.772	1775.186	253.7184	221.0914	152.3913	211.2875
ALDH7A1	-3.29361	3.57E-60	27199.96	17750.45	18078.73	18413.27	2750.056	2098.595	1631.555	1821.573
PTPRK	-3.2669	1.22E-05	31.55219	36.0304	39.17929	21.08088	1.571012	0	7.256729	5.000886
VWA2	-3.20639	2.42E-07	49.3003	42.29655	38.1747	29.86458	3.142023	7.093842	7.256729	0
CNIH3	-3.16917	7.9E-246	4496.187	3932.013	3961.127	4086.177	508.2222	430.3598	446.2889	441.3282
OAS1	-3.15872	9.95E-06	305.6619	97.12542	100.4597	108.0395	39.27529	16.5523	3.628365	7.50133
IFITM3	-3.1585	2.59E-10	15833.28	7620.429	7633.935	7611.076	1816.089	975.4033	605.9369	935.1658
GBP2	-3.13911	4.6E-13	251.4315	148.0379	124.5701	126.4853	32.99124	14.18768	12.09455	12.50222
F2RL1	-3.12118	4.74E-12	350.0321	131.5893	139.639	158.1066	21.99416	28.37537	29.02692	10.00177
ACOX2	-3.10743	5.45E-23	332.284	209.9162	313.4343	223.106	45.55933	35.46921	21.77019	20.00355
TENM3	-3.03742	4.82E-12	66.0624	60.31175	46.21147	58.85079	10.21158	7.093842	4.83782	5.000886
44265	-3.03631	1.62E-05	35.49622	27.41443	20.09195	25.47273	1.571012	2.364614	2.41891	7.50133
HKDC1	-3.03114	1.68E-16	211.9913	125.3231	113.5195	133.5122	14.1391	28.37537	16.93237	12.50222
TGM2	-3.00254	7E-142	5921.952	4848.438	4608.088	4468.268	672.3929	586.4243	603.518	611.3584
UBASH3B	-2.99152	1.1E-277	3638.362	3509.047	3770.253	3793.68	435.9557	457.5528	446.2889	513.8411
PALM2-AKAP2	-2.96257	1.67E-12	781.9028	341.5055	292.3378	361.8884	91.11867	62.66227	41.12147	31.25554
CDCP1	-2.93354	3.98E-74	3109.863	2811.154	3182.564	2841.527	502.7237	417.3544	321.715	316.3061
B4GALT6	-2.92972	4.02E-07	41.41225	43.86309	30.13792	28.10784	6.284046	7.093842	2.41891	2.500443
PARP10	-2.90057	4.2E-09	444.6887	223.2318	215.9884	209.9304	70.69552	36.65152	13.304	23.75421
EGLN3	-2.874	1.66E-05	87.75453	39.16347	33.15171	55.33731	11.78259	11.82307	2.41891	2.500443
SH3PXD2A	-2.83692	6.63E-29	1267.018	1138.091	1384.335	1343.028	285.9241	135.9653	122.1549	170.0301
SLC6A12	-2.80823	1.17E-12	710.9103	444.1138	415.9033	438.3066	100.5447	106.4076	50.79711	27.50488
NOS3	-2.77152	1.76E-13	69.02042	85.37637	82.37697	63.24264	14.92461	11.82307	6.047274	10.00177
JAM2	-2.7702	8.39E-08	97.61459	85.37637	83.38157	42.16176	19.63764	11.82307	7.256729	5.000886
MID1IP1	-2.74938	3.87E-10	233.6834	113.5741	140.6436	123.8502	30.63473	29.55768	7.256729	22.50399
PMP22	-2.68449	2.83E-39	214.9493	224.7983	220.0068	202.0251	31.42023	26.01075	37.4931	40.00709

Gene	log2-fold change	Adjusted p-value	NS control Rep 1	NS control Rep 2	NS control Rep 3	NS control Rep 4	shGSTP1-1 Rep 1	shGSTP1-1 Rep 2	shGSTP1-1 Rep 3	shGSTP1-1 Rep 4
IGFBP4	-2.65757	1.67E-52	714.8544	856.8968	779.5675	790.533	110.7563	120.5953	169.3237	98.76751
PDIA6	-2.65556	7.6E-159	14380.9	12059.22	13081.87	12884.81	2239.477	2168.351	2097.195	1807.82
ZMAT1	-2.58078	2.71E-09	391.4444	314.8743	278.2734	223.106	102.1158	37.83383	29.02692	30.00532
TANC2	-2.5463	5.67E-53	4136.295	3213.755	3711.987	3730.437	845.9897	550.9551	573.2816	556.3486
ISG15	-2.54065	4.56E-11	1278.85	578.8361	677.0985	510.3329	224.6547	99.31379	96.75639	100.0177
ZNF703	-2.53473	9.78E-21	158.747	202.8668	257.1769	220.4709	44.77383	23.64614	33.86474	41.25731
SEMA6B	-2.5128	0.001025	3526.943	2146.158	2281.44	2596.462	1024.3	388.979	104.0131	330.0585
SLC16A3	-2.5121	3.64E-16	2928.438	2320.044	2697.344	2690.447	809.8565	409.0782	250.3572	391.3194
FZD4	-2.50062	7.37E-16	83.81051	89.29272	94.43214	98.37743	18.06663	21.28153	9.675639	15.00266
OSR1	-2.48795	1.45E-46	904.1675	1002.585	1008.616	934.5856	170.4548	198.6276	114.8982	202.5359
CNTNAP2	-2.48679	2.88E-13	242.5575	149.6045	171.7861	111.553	27.4927	41.38075	21.77019	30.00532
NTN1	-2.45999	1.58E-45	830.2171	758.9881	750.4341	911.748	194.0199	127.6892	123.3644	141.275
CASP4	-2.44635	3.3E-34	1207.857	860.0299	821.7606	743.9793	201.0895	154.8822	170.5331	137.5244
C13orf46	-2.40704	0.005298	11.83207	11.74904	18.08275	44.79687	3.142023	3.546921	4.83782	5.000886
IFITM2	-2.39082	0.000163	2017.368	920.3416	1066.882	1047.017	498.7962	197.4453	104.0131	161.2786
GINS4	-2.35282	3.31E-22	9339.449	11073.08	11172.13	11330.97	1128.772	2072.584	2692.247	2511.695
AMOTL1	-2.34985	1.17E-09	112.4047	101.0418	121.5563	72.90471	10.99708	16.5523	31.44583	22.50399
MCHR1	-2.34888	1.27E-10	329.326	296.0759	374.7148	316.2132	91.11867	61.47997	21.77019	82.51463
ETS2	-2.32632	0.000172	72.96444	108.8745	120.5517	89.59373	4.713035	9.458456	27.81746	37.50665
LONRF3	-2.31713	7.87E-21	169.593	150.3877	146.6712	167.7687	42.41731	28.37537	31.44583	22.50399
PDP1	-2.29853	8.19E-14	315.5219	260.0455	319.4619	333.7806	100.5447	47.29228	36.28365	62.51108
SERPINF1	-2.26369	1.88E-05	8138.494	4380.826	4667.359	4639.55	2120.08	1068.806	547.8831	806.3929
SATB2	-2.25215	1.87E-06	281.9977	299.9922	302.3838	242.4301	124.8954	49.6569	25.39855	33.75598
CEBPD	-2.23357	0.000201	127.1948	40.73001	58.26664	33.37806	9.426069	11.82307	19.35128	15.00266
SH2D6	-2.21971	2.9E-07	141.9849	117.4904	76.34939	114.1881	32.99124	35.46921	16.93237	10.00177
C1S	-2.18901	7.15E-05	730.6304	386.9351	377.7286	378.5774	215.2286	96.94918	29.02692	67.51197
CD68	-2.17508	5.83E-32	974.1739	745.6725	803.6778	823.0326	239.5793	153.6999	194.7222	148.7764
MT1M	-2.16829	9.82E-06	58.17435	159.0037	64.29422	154.5931	16.49562	21.28153	30.23637	30.00532
PSMB9	-2.16442	0.000157	262.2776	148.0379	170.7815	156.3499	94.26069	28.37537	16.93237	22.50399
CACNA1A	-2.16098	1.77E-05	722.7424	426.8819	402.8435	476.9549	241.9358	98.13148	43.54038	67.51197
FAM155B	-2.14988	0.003812	24.65015	28.1977	22.10114	12.29718	3.142023	9.458456	2.41891	5.000886
GOLGA8Q	-2.12927	0.001868	39.44024	25.06462	59.27124	19.32414	6.284046	14.18768	3.628365	8.751551
TSPAN1	-2.10218	0.001967	6210.852	2819.77	2923.378	2761.595	1702.977	879.6364	390.6539	452.5802
WSCD1	-2.09453	5.73E-05	37.46823	42.29655	55.25285	45.67524	18.85214	9.458456	4.83782	7.50133
RTN1	-2.08897	0.008881	25.63616	10.96577	24.11033	15.81066	1.571012	4.729228	7.256729	5.000886
CA14	-2.07464	8.25E-09	244.5295	141.7718	156.7172	182.7009	54.1999	62.66227	29.02692	25.00443
MYBPH	-2.06937	0.000873	38.45423	48.56271	46.21147	80.81004	7.855058	4.729228	26.60801	12.50222
DOC2B	-2.0373	0.005576	119.3067	45.42963	42.19308	87.83699	29.84922	23.64614	2.41891	15.00266
EPHB2	-2.02801	3.47E-44	2697.712	2099.162	2527.567	2630.718	670.0364	647.9043	471.6874	648.865
RBM47	-2.02324	1.29E-10	902.1955	495.0263	610.7951	593.7781	243.5068	166.7053	94.33748	132.5235
AP1S3	-1.99777	2.47E-35	1007.698	1119.292	1087.979	1021.544	194.0199	263.6545	319.2961	288.8012

Gene	log2-fold change	Adjusted p-value	NS control Rep 1	NS control Rep 2	NS control Rep 3	NS control Rep 4	shGSTP1-1 Rep 1	shGSTP1-1 Rep 2	shGSTP1-1 Rep 3	shGSTP1-1 Rep 4
CACNG8	-1.99757	1.78E-08	160.719	132.3725	91.41835	113.3097	43.20282	26.01075	36.28365	17.5031
PPFIBP2	-1.96089	1.46E-24	1017.558	1378.554	1370.271	1751.47	284.3531	365.3329	396.7012	373.8163
MUC1	-1.95858	5.92E-06	477.2269	258.4789	238.0895	252.9705	136.678	56.75074	38.70256	81.2644
CALB2	-1.95168	7.06E-12	876.5593	487.1936	471.1561	448.847	145.3186	198.6276	116.1077	130.023
CXXC5	-1.9511	2.66E-22	529.4852	521.6575	495.2664	600.805	189.3069	126.5069	102.8037	132.5235
TBC1D9	-1.9038	0.005331	25.63616	50.12925	18.08275	19.32414	6.284046	4.729228	9.675639	10.00177
CSF3	-1.88264	0.000106	69.02042	62.66156	47.21607	39.52665	9.426069	26.01075	14.51346	10.00177
PLCE1	-1.8715	9.2E-137	2445.295	2324.744	2221.165	2235.452	622.1206	615.982	651.8962	632.6121
SIGLEC10	-1.87009	8.91E-07	55.21634	68.14444	52.23906	61.4859	12.56809	21.28153	21.77019	10.00177
PSMB8	-1.84517	4.73E-10	401.3044	246.7299	245.1217	232.768	96.61721	75.66765	48.3782	91.26618
P2RY2	-1.77748	2.01E-16	570.8975	404.1671	397.8205	423.3743	160.2432	144.2415	95.54694	121.2715
OAS3	-1.76949	9.36E-27	1176.305	861.5964	950.349	884.5185	340.9095	290.8475	261.2423	238.7923
STK39	-1.75219	2.46E-07	155.7889	153.5208	143.6574	97.49906	28.27821	30.73998	43.54038	62.51108
WT1	-1.74467	1.39E-17	213.9633	181.7185	169.7769	182.7009	63.62597	47.29228	48.3782	62.51108
RUNX1	-1.74411	2.29E-37	2802.229	3256.051	3236.812	3404.562	772.9377	885.548	1037.712	1100.195
44258	-1.74342	7.47E-10	266.2216	329.7565	329.5079	384.726	56.55642	126.5069	123.3644	87.51551
SDC1	-1.73781	4.09E-30	3695.55	3709.564	4242.414	4002.732	864.0563	1382.117	1238.482	1212.715
ITGA3	-1.72603	9.2E-48	26553.14	18944.16	20859.46	21434.86	7085.262	6636.289	6425.834	6387.382
DSG2	-1.70315	2.28E-36	2937.312	2587.922	2851.047	2815.176	1070.644	825.2503	726.8824	807.6432
SOCS3	-1.69546	1.55E-13	508.7791	323.4903	323.4803	292.4972	106.0433	100.4961	123.3644	117.5208
PALM3	-1.67934	0.001185	77.89447	37.59693	53.24365	47.43198	25.13618	21.28153	9.675639	10.00177
FBXO27	-1.67293	1.62E-11	1587.47	1221.9	1322.05	1397.487	634.6887	471.7405	314.4583	308.8047
PGM1	-1.67263	2.41E-28	4295.042	3305.397	3650.706	3453.751	1424.907	1149.202	956.6788	1076.441
NDRG1	-1.65962	8.13E-06	419.0526	278.8439	309.416	270.5379	179.8808	66.20919	72.56729	82.51463
LZTS1	-1.65545	6.12E-05	213.9633	92.4258	112.5149	77.29656	40.8463	44.92767	36.28365	35.00621
PCGF5	-1.65123	1.09E-13	452.5768	422.9655	410.8803	374.1856	186.9504	118.2307	96.75639	122.5217
ROBO4	-1.65087	2.75E-09	393.4164	215.3991	253.1585	222.2276	109.1853	85.12611	74.9862	73.76308
OPHN1	-1.64489	3.14E-18	996.8521	899.1934	852.9031	1047.017	402.9645	314.4937	250.3572	241.2928
MVP	-1.62642	2.11E-06	6485.947	3953.161	4283.603	4219.689	2683.288	1425.862	944.5843	1077.691
TUBB2B	-1.60234	2.69E-59	5696.157	4969.062	5634.786	5994.875	1632.281	1886.962	1970.202	1857.829
SHROOM3	-1.59437	5.39E-11	560.0514	416.6994	541.4779	618.3724	120.1824	185.6222	162.067	242.543
GGH	-1.59125	1.89E-16	977.1319	1232.866	1149.259	1101.476	254.5039	357.0567	419.6808	453.8304
C5AR1	-1.58404	0.000655	29.58018	72.06079	43.19768	53.58057	15.71012	20.09922	14.51346	16.25288
ITGA10	-1.57492	0.003603	408.2065	210.6995	154.708	157.2282	128.0374	94.58456	55.63493	32.50576
LMO4	-1.57151	7.92E-07	99.58661	133.1558	140.6436	87.83699	47.13035	26.01075	45.95929	35.00621
TRIB2	-1.57112	1.27E-24	4344.342	3476.15	3444.764	3532.804	1345.571	1431.774	951.841	1248.971
TBC1D2	-1.56476	6.1E-37	3624.558	3873.268	3710.982	3702.329	1128.772	1183.489	1565.035	1166.457
MAPK11	-1.55775	7.87E-19	432.8566	372.053	365.6734	375.064	159.4577	137.1476	124.5739	100.0177
CCDC71L	-1.54414	1.08E-17	1881.299	1408.319	1522.969	1333.366	657.4683	477.652	546.6736	421.3247
ENDOD1	-1.53716	9.16E-16	295.8018	379.8857	349.5998	267.9028	102.1158	99.31379	133.04	112.5199
ICOSLG	-1.53655	9.32E-05	50.28631	91.64253	91.41835	66.75612	17.28113	26.01075	26.60801	35.00621

Gene	log2-fold change	Adjusted p-value	NS control Rep 1	NS control Rep 2	NS control Rep 3	NS control Rep 4	shGSTP1-1 Rep 1	shGSTP1-1 Rep 2	shGSTP1-1 Rep 3	shGSTP1-1 Rep 4
ARNTL2	-1.5347	8.75E-65	1760.021	1803.086	1883.62	1807.685	555.3526	637.2635	676.0853	641.3637
C1QTNF6	-1.50127	1.14E-16	2873.221	2253.466	2394.96	2505.111	1178.259	887.9126	703.9027	766.3858
KCNAB3	-1.49805	0.002769	78.88048	90.07599	73.3356	50.06709	12.56809	36.65152	16.93237	38.75687
PPARG	-1.49504	6.93E-05	118.3207	79.89349	88.40456	60.60753	42.41731	22.46383	26.60801	30.00532
PRRG4	-1.48431	1.34E-43	12862.45	13766.74	14983.57	14255.07	4359.557	4672.477	5455.851	5485.972
SLFN5	-1.48269	5.24E-10	655.694	613.3	574.6296	514.7248	301.6342	212.8153	181.4182	143.7755
GALNT6	-1.47856	0.000677	930.7897	805.201	941.3076	872.2214	590.7003	340.5044	126.9928	212.5377
KIAA1549L	-1.47728	0.004645	47.32829	39.94674	40.18389	35.1348	25.13618	11.82307	12.09455	7.50133
TMEM154	-1.42943	0.000127	103.5306	64.2281	59.27124	86.08025	20.42315	30.73998	38.70256	27.50488
CPT1A	-1.42737	1.2E-17	2898.858	3387.64	4100.766	3977.259	1365.209	1046.342	1561.406	1367.742
ABLIM3	-1.40917	0.001671	98.6006	64.2281	56.25745	48.31035	36.13327	18.91691	26.60801	17.5031
FGFR1	-1.40889	3.47E-17	739.5045	990.8359	1006.606	1106.746	421.0311	319.2229	339.8568	365.0647
PDGFA	-1.40802	4.27E-06	825.287	586.6688	652.9882	548.9812	375.4718	264.8368	152.3913	188.7835
SLC46A3	-1.40517	3.13E-07	418.0665	416.6994	356.632	368.037	230.1532	119.413	105.2226	130.023
PARM1	-1.40391	0.003667	48.31429	54.04559	58.26664	43.9185	8.640563	30.73998	19.35128	20.00355
GRAMD1B	-1.38916	2.96E-64	4789.031	4899.351	5266.099	4983.871	1726.542	1969.724	2047.607	1874.082
SLC20A1	-1.34984	6.38E-20	31095.67	33007.76	30436.28	30013.9	9063.951	12720.44	14504.99	12583.48
SPON1	-1.3488	0.000605	150.8589	79.11022	84.38617	82.56677	29.84922	30.73998	41.12147	55.00975
PLPPR3	-1.32891	0.00756	717.8124	471.5282	515.3584	526.1436	463.4484	177.3461	141.5062	102.5182
TBL1X	-1.32595	9.34E-06	1810.307	1128.691	1277.848	1253.434	838.9202	552.1374	348.323	438.8278
BACE2	-1.32491	2.44E-19	1071.789	757.4216	880.0272	774.7223	350.3356	365.3329	333.8096	340.0603
BTC	-1.31326	1.47E-07	592.5896	655.5966	598.74	643.8452	358.1906	277.8422	191.0939	171.2804
PTPN3	-1.30993	4.38E-31	8220.332	6474.506	6380.197	6602.707	2691.143	3010.154	2614.841	2848.005
STX12	-1.26369	7.37E-16	1463.233	1190.57	1305.976	1261.339	648.0423	530.8559	573.2816	417.574
KIAA1755	-1.26011	0.002411	65.0764	48.56271	53.24365	40.40502	25.13618	26.01075	12.09455	22.50399
CTSC	-1.25272	1E-10	604.4217	585.1023	580.6572	723.7768	211.3011	211.633	321.715	305.0541
ZFP3	-1.22954	1.22E-14	298.7598	311.7413	394.8067	336.4157	150.0316	152.5176	130.6211	137.5244
GOLGA8H	-1.21994	5.6E-07	580.7575	476.2278	378.7332	383.8477	206.588	247.1022	136.6684	190.0337
IZUMO4	-1.21831	0.00289	112.4047	97.12542	66.30342	96.62069	64.41147	34.2869	29.02692	30.00532
SQOR	-1.20835	8.74E-07	479.1989	381.4522	421.9308	334.6589	241.1503	135.9653	137.8779	181.2821
CTNNBIP1	-1.20292	2.15E-12	2108.081	1960.524	2199.063	2224.033	1218.319	919.8349	801.8686	742.6316
RASL11A	-1.2016	4.99E-07	1239.41	1388.737	1487.809	1503.769	352.6921	704.655	667.6191	722.6281
PCDH1	-1.1958	6.33E-24	11818.27	10887.45	12339.47	12935.75	4287.291	5717.637	5500.601	5445.965
TPK1	-1.1903	2.6E-13	537.3733	462.129	424.9446	433.9148	229.3677	171.4345	183.8371	227.5403
SPNS2	-1.17425	0.002685	149.8729	244.3801	258.1815	269.6596	56.55642	80.39688	147.5535	126.2724
OSMR	-1.17087	2.15E-16	8798.132	6215.243	6234.531	6058.118	3057.188	2917.934	3085.319	3066.794
NUCB2	-1.16456	1.04E-14	7346.731	6776.848	7237.119	6773.989	4084.63	2778.422	2709.179	2971.777
POLE3	-1.16049	4.05E-06	4709.165	6454.141	6926.698	6901.353	1767.388	2521.861	3722.702	3171.812
PSMB10	-1.15887	0.00188	99.58661	114.3573	95.43674	69.39123	35.34776	43.74536	27.81746	63.7613
SORT1	-1.1564	6.94E-38	2664.188	2645.884	2699.353	2675.515	1304.725	1252.063	1048.597	1182.71
SPHK1	-1.15612	0.000512	275.0957	428.4484	487.2297	525.2652	137.4635	137.1476	267.2895	230.0408

Gene	log2-fold change	Adjusted p-value	NS control Rep 1	NS control Rep 2	NS control Rep 3	NS control Rep 4	shGSTP1-1 Rep 1	shGSTP1-1 Rep 2	shGSTP1-1 Rep 3	shGSTP1-1 Rep 4
FAM20C	-1.14535	5.31E-07	585.6876	568.6536	543.4871	644.7235	380.9703	243.5552	232.2153	197.535
ARMCX2	-1.14531	1.56E-17	4464.635	4521.031	4872.297	4917.993	2565.462	2084.407	1716.216	2116.625
ADORA1	-1.13992	0.006624	679.3581	1207.018	1295.93	1223.569	201.0895	489.4751	711.1595	600.1064
GPAT3	-1.12828	7.1E-30	6838.938	7144.201	7454.112	7235.133	2795.615	3271.444	3544.912	3511.873
DLK2	-1.12748	0.007954	215.9353	162.9201	121.5563	136.1473	109.1853	60.29766	36.28365	83.76485
TNS2	-1.12666	3.86E-05	1537.183	1020.6	1002.588	1102.354	690.4596	639.6281	335.019	467.5829
DHRS3	-1.11772	0.002266	479.1989	280.4105	328.5033	398.78	268.643	166.7053	95.54694	151.2768
NXN	-1.10469	1.61E-11	1414.919	1063.68	1084.965	1170.867	541.999	669.1858	453.5456	536.3451
ARTN	-1.10108	5.39E-06	178.4671	195.8174	148.6804	150.2013	100.5447	78.03226	70.14838	62.51108
RNF167	-1.09634	1.25E-26	2559.672	2536.227	2783.739	2764.23	1238.743	1223.688	1417.481	1097.695
PRKAR2B	-1.09121	1.83E-13	2968.864	2478.265	2437.153	2345.248	1433.548	1139.744	985.7057	1237.719
GLCCI1	-1.08817	0.001542	389.4724	287.4599	327.4987	308.3079	250.5763	150.153	96.75639	116.2706
HSPA13	-1.08536	7.64E-54	3602.866	3479.283	3584.403	3380.846	1743.037	1557.098	1701.703	1612.786
TUBB2A	-1.08004	0.000134	12815.12	16011.59	18428.33	19512.99	4303.001	7958.109	10086.85	9237.887
NT5E	-1.07335	1.2E-41	31154.83	30515.4	32132.04	31710.03	14450.95	13466.48	16096.64	15634.02
SERPINH1	-1.07197	2.52E-24	9418.329	9200.283	10216.75	9641.867	4716.962	3848.409	5072.454	4663.327
PIK3R1	-1.06859	0.002305	88.74054	99.47522	74.3402	84.32351	32.99124	49.6569	26.60801	57.51019
ECM1	-1.06132	0.000362	649.778	431.5815	428.963	432.158	351.1211	183.2576	181.4182	211.2875
RAC3	-1.04404	3.32E-05	674.4281	536.5396	474.1699	543.711	326.7704	341.6867	182.6277	227.5403
TMEM220	-1.04397	7.2E-13	497.933	669.6954	584.6756	536.684	295.3502	258.9252	296.3164	258.7959
TSPAN4	-1.04291	2.06E-12	3527.929	2759.458	2596.884	2810.784	1588.293	1525.176	1181.637	1377.744
ANKRD18A	-1.04115	0.000806	136.0688	168.4029	142.6528	105.4044	44.77383	70.93842	67.72947	87.51551
ZFYVE28	-1.04069	0.005097	401.3044	340.7222	348.5952	286.3486	252.9329	206.9037	100.3848	106.2688
BTG3	-1.02805	2.81E-29	1277.864	1340.174	1312.004	1281.542	622.9061	593.5181	622.8693	718.8774
TAPBP	-1.02552	8.3E-06	9520.874	6613.144	6842.312	6889.055	5015.454	3873.238	2922.043	2855.506
GATM	-1.02443	0.000362	171.565	101.825	138.6344	147.5662	87.97665	59.11535	60.47274	65.01152
FP565260.1	-1.02406	3.7E-10	661.61	581.9692	585.6802	665.8044	231.7242	334.5929	328.9717	336.3096
C21orf2	-1.02367	7.59E-06	1030.376	1817.185	1870.56	1987.751	732.0914	800.4219	934.9086	832.6476
FAM111A	-1.0133	5.06E-09	1545.071	2246.417	2012.208	1936.806	754.0855	1043.977	1094.557	946.4178
CTXN1	-1.01099	1.29E-13	539.3453	438.6309	569.6066	498.0358	245.8633	257.7429	272.1274	238.7923
NPAS2	-1.00837	7.67E-26	7258.976	6289.654	6039.639	5726.094	3199.365	3121.291	3211.103	3050.541
SH3D21	-1.00241	1.86E-05	1038.264	1133.391	837.8341	891.5455	673.1784	483.5636	440.2416	346.3114
TMEM179	-1.0024	0.006218	201.1452	311.7413	345.5815	339.9292	95.8317	222.2737	171.7426	110.0195
RILP	-1.00233	2.02E-07	279.0397	269.4447	295.3516	262.6326	170.4548	109.9546	118.5266	150.0266
SUSD4	1.000097	0.00141	116.3487	61.09502	90.41375	77.29656	213.6576	143.0592	194.7222	135.0239
POU5F1B	1.009263	2.51E-08	267.2076	210.6995	190.8735	167.7687	461.0919	396.0729	413.6336	410.0727
ARHGEF28	1.010915	1.24E-37	1347.87	1502.311	1508.905	1364.109	2999.847	2725.218	2905.111	2901.764
C12orf56	1.014363	3.98E-09	251.4315	173.1026	175.8045	180.9442	384.1123	390.1613	429.3565	372.566
LGALSL	1.014466	1.45E-05	658.652	460.5625	495.2664	406.6853	1340.858	1021.513	777.6795	937.6662
COL6A3	1.014596	7.63E-11	7877.202	5278.453	5275.14	5652.311	12627.01	11644.54	11453.54	12927.29
BMI1	1.016671	0.00019	145.9289	286.6766	275.2596	295.1323	395.8949	520.2151	543.0452	573.8517

Gene	log2-fold change	Adjusted p-value	NS control Rep 1	NS control Rep 2	NS control Rep 3	NS control Rep 4	shGSTP1-1 Rep 1	shGSTP1-1 Rep 2	shGSTP1-1 Rep 3	shGSTP1-1 Rep 4
TOX2	1.018327	0.004435	111.4187	107.3079	82.37697	110.6746	277.2835	236.4614	105.2226	213.7879
TRGV4	1.018705	0.003667	42.39826	40.73001	48.22067	29.86458	56.55642	101.6784	91.91857	77.51374
KLHL29	1.020088	1.23E-05	69.02042	56.3954	57.26204	47.43198	104.4723	131.2361	118.5266	112.5199
TRABD2A	1.03041	1.32E-05	1331.108	773.8702	796.6456	767.6953	2085.518	2044.209	1450.136	1911.589
IGSF3	1.032388	0.000159	305.6619	175.4524	241.1033	237.1599	652.7553	507.2097	341.0663	456.3309
CAV2	1.035612	2.17E-37	3857.255	3577.975	3720.024	3629.425	8393.129	7050.097	7359.533	7495.079
ABCA10	1.046497	3.93E-10	5041.449	4067.518	3328.231	3321.117	8595.79	8695.868	7001.534	8253.963
MAP1LC3B2	1.049058	0.001803	231.7114	169.1862	167.7677	139.6608	576.5612	313.3114	253.9855	317.5563
CA12	1.05154	8.41E-05	45.35628	42.29655	39.17929	40.40502	77.76507	83.9438	77.40511	108.7693
HOXA3	1.054838	0.000467	203.1172	155.0874	101.4643	106.2828	375.4718	273.1129	258.8233	266.2972
SAMD4A	1.055691	1.3E-08	271.1517	299.2089	369.6918	291.6188	560.8511	524.9443	765.5849	710.1259
FBXO25	1.058703	4.25E-06	182.4111	139.422	161.7402	115.9448	395.1094	309.7644	261.2423	277.5492
RIMS4	1.078205	5.5E-06	206.0753	143.3383	126.5793	149.3229	412.3905	339.3221	264.8706	300.0532
VASH2	1.095409	0.001178	58.17435	51.69579	52.23906	56.21568	160.2432	133.6007	73.77675	96.26706
REEP1	1.096908	0.001551	27.60817	36.0304	29.13332	27.22947	51.84338	81.57919	72.56729	52.50931
CNNM1	1.103062	0.000248	117.3347	68.14444	71.32641	57.09405	196.3764	178.5284	148.763	147.5262
DGKA	1.104862	0.006555	375.6683	219.3155	206.947	160.7417	764.2971	597.0651	309.6205	396.3203
KLF4	1.114154	1.54E-09	570.8975	597.6346	615.8181	649.1154	935.5374	1267.433	1619.46	1450.257
IL1RAP	1.135545	0.001062	37.46823	45.42963	66.30342	50.06709	78.55058	89.85533	131.8306	138.7746
UPP1	1.14061	2.21E-21	640.9039	738.6231	828.7927	729.9254	1466.539	1610.302	1823.858	1580.28
PHLDB2	1.147259	5.3E-13	11618.11	14088.67	14279.35	12878.66	22829.15	26831.28	35388.65	32048.18
PAQR5	1.155416	0.005916	124.2368	95.55888	84.38617	67.63449	357.4051	140.6945	171.7426	155.0275
CCDC3	1.179955	4.26E-10	199.1732	170.7527	209.9608	179.1875	556.1381	381.8852	372.5121	402.5714
CKMT1A	1.192615	0.000577	76.90847	53.26232	56.25745	40.40502	164.1707	156.0645	101.5942	93.76662
HEG1	1.194039	3.95E-24	325.382	336.8059	387.7745	370.6721	811.4275	815.7919	724.4635	897.6591
ADGRG1	1.199793	2.79E-09	351.0181	469.9617	545.4963	519.1166	970.0996	867.8134	1331.61	1163.956
APLF	1.203538	0.000193	57.18835	59.52848	50.22986	35.1348	152.3881	126.5069	89.49966	95.01684
SOX8	1.203676	6.86E-06	197.2012	126.1064	106.4873	156.3499	439.8832	310.9468	269.7084	326.3078
NFIA	1.205995	5.79E-27	338.2001	331.323	321.4711	268.7812	692.8161	738.9419	736.558	738.881
FAM107B	1.214168	1.48E-14	222.8374	179.3687	147.6758	187.9712	449.3093	444.5474	395.4918	421.3247
LARGE1	1.21687	0.003342	19.72012	36.0304	24.11033	24.59436	62.84046	62.66227	38.70256	80.01418
ADRB2	1.223588	0.003667	17.74811	23.49808	33.15171	28.98621	67.5535	52.02151	81.03348	40.00709
GULP1	1.223803	1.67E-35	689.2182	626.6156	622.8503	613.9806	1402.128	1441.232	1446.508	1674.047
ADGRE2	1.228739	3.57E-07	176.4951	111.2243	106.4873	108.0395	318.9153	289.6652	233.4248	332.5589
MGAT4A	1.232029	0.001898	57.18835	39.16347	26.11953	33.37806	126.4664	89.85533	65.31056	82.51463
LIPC	1.234094	3.69E-06	91.69856	72.06079	53.24365	108.9179	176.7388	221.0914	181.4182	188.7835
SPTBN2	1.237437	1.83E-09	1084.607	684.5775	657.0066	628.9129	2093.373	1775.825	1629.136	1700.301
PLCXD2	1.242475	2.05E-05	67.04841	57.17867	58.26664	52.7022	175.1678	145.4238	87.08075	146.2759
PTPRZ1	1.261294	4.86E-08	2128.787	1407.535	1233.645	1225.326	4368.983	3825.946	2739.415	3433.109
SORBS2	1.263972	1.93E-23	702.0363	581.9692	539.4687	606.0753	1578.081	1512.171	1252.995	1487.764
RNF38	1.266857	3.9E-30	704.0083	716.6916	648.9698	732.5605	1889.141	1468.425	1617.041	1766.563

Gene	log2-fold change	Adjusted p-value	NS control Rep 1	NS control Rep 2	NS control Rep 3	NS control Rep 4	shGSTP1-1 Rep 1	shGSTP1-1 Rep 2	shGSTP1-1 Rep 3	shGSTP1-1 Rep 4
FSTL1	1.270068	0.008843	279.0397	120.6235	130.5976	158.1066	730.5204	404.349	206.8168	315.0558
AGPAT4	1.270903	0.00063	314.5359	157.4372	162.7448	124.7285	605.625	522.5797	304.7826	396.3203
AL031777.3	1.289325	0.007319	24.65015	20.36501	18.08275	14.93229	74.62305	41.38075	37.4931	35.00621
NKX1-2	1.304036	2.56E-12	72.96444	93.99234	87.39996	89.59373	178.3098	223.456	237.0532	215.0381
PTPRU	1.307364	2.45E-06	168.607	98.69195	132.6068	129.9988	435.9557	358.239	229.7964	282.5501
TBC1D4	1.3075	1.62E-14	476.2409	393.2013	434.9906	309.1862	1071.43	1126.739	869.5981	921.4133
NKD1	1.319991	1.57E-06	130.1528	81.46003	127.5839	108.9179	384.1123	268.3837	203.1884	257.5457
SLC16A10	1.322389	2E-13	165.649	110.441	122.5609	130.8771	323.6284	378.3383	318.0866	301.3034
SOCS2	1.329167	2.1E-12	78.88048	79.89349	111.5103	84.32351	221.5126	206.9037	209.2357	251.2945
SOX4	1.336068	4.73E-06	49.3003	36.81367	46.21147	28.98621	118.6114	95.76687	81.03348	108.7693
JCAD	1.341101	1.27E-21	331.298	257.6957	299.37	318.8483	791.7898	637.2635	810.3348	815.1445
CARMIL1	1.346259	0.000203	21.69213	24.28135	25.11493	21.08088	69.12451	37.83383	66.52002	60.01064
GADD45A	1.347609	5.81E-29	1153.627	1278.296	1359.22	1335.122	3329.759	2713.395	3696.094	3306.836
PCDH9	1.362804	4.49E-08	71.97844	70.49425	114.5241	93.10721	172.0258	221.0914	256.4044	251.2945
GPC2	1.389913	0.003603	57.18835	28.98097	44.20228	25.47273	152.3881	114.6838	56.84438	81.2644
PPP3CA	1.39572	2.3E-12	679.3581	506.7754	550.5193	361.8884	1430.406	1429.409	1180.428	1477.762
CPPED1	1.397793	7.45E-09	126.2088	113.5741	72.331	81.68841	213.6576	251.8314	301.1543	273.7985
E2F5	1.412359	7.65E-07	87.75453	46.2129	83.38157	76.41819	246.6488	202.1745	172.952	155.0275
STOM	1.413087	4.53E-42	958.3978	800.5014	838.8387	813.3706	2336.88	2265.3	2024.627	2451.685
GLB1L2	1.420428	3.14E-16	436.8007	299.9922	351.609	307.4295	1122.488	926.9287	818.801	860.1525
SLC27A2	1.434947	0.001723	21.69213	17.23193	22.10114	14.05392	33.77675	73.30304	38.70256	57.51019
WNT11	1.442535	0.001736	15.7761	16.44866	9.041375	12.29718	32.99124	49.6569	31.44583	32.50576
DUSP8	1.446062	0.000106	89.72655	50.12925	52.23906	35.1348	211.3011	151.3353	134.2495	118.7711
IGKV1OR2-108	1.486729	0.006886	8.874054	6.266156	19.08735	17.5674	38.48978	33.1046	43.54038	28.7551
APLN	1.516322	3.86E-05	65.0764	73.62733	102.4689	67.63449	141.391	143.0592	299.9448	300.0532
ST6GAL1	1.517657	1.01E-09	602.4497	390.0682	360.6504	338.1724	1593.006	1237.875	913.1384	1093.944
COL27A1	1.534431	2.74E-08	122.2647	102.6083	71.32641	74.66145	338.553	305.0352	224.9586	203.7861
WDR63	1.534696	0.000148	23.66414	16.44866	20.09195	14.05392	66.76799	35.46921	50.79711	60.01064
ACKR3	1.535219	1.46E-18	242.5575	214.6158	251.1493	187.9712	548.283	743.6711	745.0242	560.0993
SLC47A2	1.545038	0.005541	35.49622	18.79847	16.07356	21.95925	102.9013	76.84996	27.81746	60.01064
CD302	1.56279	0.001736	46.34228	14.09885	20.09195	17.5674	94.26069	72.12073	58.05383	62.51108
SLITRK3	1.565272	0.001997	46.34228	20.36501	38.1747	36.89154	183.8084	80.39688	55.63493	96.26706
HRASLS	1.596626	9.02E-17	124.2368	165.2699	146.6712	124.7285	355.8341	483.5636	364.0459	497.5882
SLC19A2	1.613497	6.7E-27	129.1668	115.9239	107.4919	109.7962	311.8458	398.4375	356.7892	350.0621
IL12A	1.61353	3.27E-11	37.46823	39.94674	26.11953	36.89154	110.7563	98.13148	105.2226	117.5208
ABHD17C	1.619674	1.53E-09	50.28631	45.42963	52.23906	68.51286	150.8171	228.1853	142.7157	143.7755
EGR2	1.649485	8.38E-05	17.74811	12.53231	22.10114	12.29718	36.13327	49.6569	65.31056	51.25909
RGS2	1.653371	3.93E-10	57.18835	86.15964	70.32181	45.67524	224.6547	154.8822	228.587	208.787
TNFAIP3	1.658872	1.79E-05	19.72012	26.63116	16.07356	14.05392	51.84338	52.02151	82.24293	57.51019
COL17A1	1.659648	1.5E-154	4416.321	4797.526	4985.816	4632.523	14742.37	14517.55	15124.23	15116.43
ANKRD20A1	1.685762	0.004635	15.7761	6.266156	12.05517	15.81066	47.13035	61.47997	24.1891	26.25465

Gene	log2-fold change	Adjusted p-value	NS control Rep 1	NS control Rep 2	NS control Rep 3	NS control Rep 4	shGSTP1-1 Rep 1	shGSTP1-1 Rep 2	shGSTP1-1 Rep 3	shGSTP1-1 Rep 4
TMEM236	1.701519	1.16E-05	173.5371	82.2433	78.35859	80.81004	518.4338	315.676	215.283	296.3025
ARHGAP15	1.703866	1.38E-09	67.04841	36.0304	34.15631	42.16176	141.391	139.5122	130.6211	171.2804
ITGB6	1.721099	1.99E-12	50.28631	42.29655	78.35859	54.45894	177.5243	193.8984	159.648	208.787
FOXL1	1.723949	0.000413	13.80408	14.09885	10.04597	10.54044	48.70136	54.38612	24.1891	32.50576
FAM171B	1.726395	7.92E-07	21.69213	28.1977	23.10574	12.29718	60.48394	70.93842	82.24293	70.01241
SPAG6	1.742433	1.69E-05	15.7761	16.44866	16.07356	17.5674	73.83754	63.84458	36.28365	45.00798
BNC1	1.757852	1.17E-07	38.45423	31.33078	21.09654	24.59436	78.55058	112.3192	123.3644	77.51374
CLDN1	1.795403	4.24E-75	996.8521	901.5432	954.3674	780.8709	3045.406	3301.001	3186.914	3074.295
KLHL4	1.802973	8.1E-06	8.874054	23.49808	18.08275	22.83762	56.55642	66.20919	53.21602	82.51463
CYP26B1	1.834127	8.87E-06	18.73411	51.69579	32.14711	47.43198	79.33608	141.8768	171.7426	146.2759
RGMB	1.865573	4.45E-45	805.5669	657.9464	609.7905	577.0891	2578.815	2357.52	2566.463	2150.381
ERCC6	1.884714	7.1E-16	1923.698	1528.159	1257.756	1038.233	7137.891	5355.851	4314.126	4413.282
MPZL3	1.900921	1.35E-11	21.69213	28.1977	27.12413	28.98621	98.18822	105.2253	74.9862	118.7711
RGS16	1.916317	7.49E-10	29.58018	29.76424	24.11033	17.5674	78.55058	85.12611	96.75639	122.5217
SYDE2	1.927591	7.31E-25	160.719	123.7566	143.6574	96.62069	489.3701	449.2767	579.3289	473.834
DUSP6	1.992745	0.000151	15.7761	9.399234	20.09195	10.54044	65.98248	23.64614	67.72947	62.51108
ADRB1	1.995063	0.003151	6.902042	8.615964	6.027584	2.63511	30.63473	26.01075	12.09455	27.50488
PECAM1	2.007157	8.43E-06	25.63616	10.96577	10.04597	15.81066	67.5535	47.29228	84.66184	50.00886
EPHA8	2.012843	4.66E-09	49.3003	23.49808	26.11953	22.83762	135.107	137.1476	88.29021	127.5226
CYP4Z1	2.014015	8.5E-10	67.04841	72.06079	42.19308	28.98621	249.7908	245.9199	181.4182	172.5306
ITGB8	2.031947	2.11E-39	123.2508	135.5056	161.7402	174.7956	605.625	529.6736	656.734	642.6139
CD55	2.046647	9.3E-20	309.6059	234.1976	206.947	224.8627	1430.406	829.9795	904.6723	860.1525
GPM6A	2.051749	0.00882	25.63616	7.832695	6.027584	7.02696	87.19114	54.38612	24.1891	25.00443
ADM	2.05663	4.78E-21	70.00643	94.77561	99.45513	91.35047	265.501	445.7298	373.7216	398.8207
NDST3	2.063337	9.28E-05	7.888048	14.09885	8.036778	7.02696	34.56225	26.01075	36.28365	60.01064
WIPF3	2.088256	7.61E-05	72.96444	30.54751	27.12413	31.62132	331.4834	131.2361	112.4793	111.2697
RYR2	2.090593	1.22E-20	234.6694	169.1862	124.5701	161.6201	926.8968	718.8427	597.4707	692.6228
CCDC80	2.099994	3.83E-29	145.9289	87.72618	113.5195	107.1611	523.1468	465.829	416.0525	535.0949
LPAR3	2.107939	4.44E-09	150.8589	112.7908	100.4597	46.55361	629.1901	424.4482	353.1608	360.0638
TES	2.130752	5.94E-11	36.48222	63.44483	20.09195	43.9185	183.0228	164.3407	178.9993	197.535
CDHR1	2.1345	6.87E-05	13.80408	9.399234	6.027584	8.783699	65.98248	33.1046	38.70256	27.50488
PELI1	2.144213	6.1E-17	35.49622	57.17867	51.23446	42.16176	252.1474	156.0645	228.587	186.283
OPCML	2.170291	2.24E-48	814.441	806.7676	676.094	557.7649	3395.741	3260.803	3442.109	2751.738
FAM241A	2.21078	7.36E-59	112.4047	101.825	96.44134	93.98558	432.8137	448.0944	482.5725	511.3406
PKD1L1	2.240401	0.000209	817.399	467.6119	348.5952	298.6458	4209.525	2247.566	1130.84	1540.273
SLITRK6	2.26114	4.04E-33	68.03441	72.84406	69.31721	75.53982	363.6892	370.0621	256.4044	380.0674
ITPKB	2.305033	1.07E-19	132.1248	83.02656	60.27584	92.22884	560.0656	441.0005	366.4648	446.3291
ADD3	2.384347	1.84E-22	218.8933	151.171	157.7218	122.0934	1134.27	815.7919	599.8896	836.3983
MYO1B	2.39059	2.15E-57	577.7995	436.2811	401.8389	360.1317	2326.668	2290.129	2256.843	2434.181
KCND3	2.396347	0.000137	25.63616	7.832695	12.05517	9.662069	125.6809	66.20919	67.72947	27.50488
PAX8	2.411721	3.04E-21	2742.083	1713.01	1544.066	1443.162	13494.2	10502.43	7291.804	8306.472

Gene	log2-fold change	Adjusted p-value	NS control Rep 1	NS control Rep 2	NS control Rep 3	NS control Rep 4	shGSTP1-1 Rep 1	shGSTP1-1 Rep 2	shGSTP1-1 Rep 3	shGSTP1-1 Rep 4
MPP7	2.416426	1.01E-12	29.58018	17.23193	38.1747	45.67524	234.0807	154.8822	146.344	157.5279
ELOVL7	2.419619	2.66E-12	51.27231	21.14828	34.15631	35.1348	269.4285	157.2468	137.8779	187.5332
TNN	2.426581	1.48E-07	11.83207	24.28135	30.13792	22.83762	51.84338	120.5953	152.3913	156.2777
ZNF525	2.479804	5.79E-05	8.874054	7.832695	3.013792	1.75674	36.13327	28.37537	25.39855	30.00532
ELMOD1	2.49814	3.04E-27	33.5242	36.0304	40.18389	45.67524	171.2403	205.7214	252.7761	251.2945
RGCC	2.508063	0.006907	11.83207	3.133078	2.009195	1.75674	43.98832	24.82845	9.675639	26.25465
AL603750.1	2.520661	4.92E-05	3.944024	17.23193	2.009195	8.783699	51.84338	42.56305	47.16874	46.2582
DDAH1	2.529898	2.9E-132	1070.803	992.4024	930.2571	794.9248	5470.262	5450.435	5603.405	5350.949
PNLIPRP1	2.569645	0.001008	6.902042	2.349808	2.009195	5.27022	19.63764	43.74536	21.77019	12.50222
PTGFRN	2.590312	1.09E-18	214.9493	115.1406	148.6804	108.9179	1283.516	905.6472	626.4976	715.1268
ADGRL3	2.611603	1.27E-48	299.7458	204.4333	249.1401	209.052	1780.742	1380.935	1190.104	1517.769
KRT13	2.629728	6.14E-10	272.1377	130.806	100.4597	111.553	1247.383	1292.262	395.4918	867.6538
CDH10	2.669247	2.52E-40	261.2916	179.3687	191.8781	148.4445	1351.855	1384.482	950.6315	1272.726
RAPGEF4	2.697937	3.24E-05	41.41225	14.09885	2.009195	22.83762	179.8808	124.1422	113.6888	102.5182
CYR61	2.756298	3.46E-41	1233.494	1207.802	1333.101	1097.962	11885.49	7314.934	7861.457	5851.037
MEST	2.776626	5.96E-06	7.888048	7.832695	8.036778	8.783699	112.3273	47.29228	31.44583	30.00532
HMSD	2.809452	7.74E-11	59.16036	46.2129	31.14251	45.67524	531.0019	371.2444	126.9928	246.2937
CLDN16	2.899065	2.13E-30	47.32829	39.94674	28.12872	23.71599	303.2052	260.1075	212.8641	260.0461
TTC39C	2.903509	7.09E-42	78.88048	38.3802	59.27124	56.21568	453.2368	401.9844	396.7012	477.5847
SLC39A8	2.943905	3.05E-86	153.8169	153.5208	143.6574	122.0934	909.6157	1106.639	1274.765	1122.699
TMTC2	3.019386	2.66E-48	311.5779	189.5512	202.9286	196.7549	2350.233	1732.08	1513.028	1696.551
GAS2	3.07109	3.4E-27	31.55219	28.1977	19.08735	29.86458	157.8867	224.6383	237.0532	298.803
FRMD6	3.127972	2.84E-28	140.0129	97.12542	66.30342	50.06709	662.9669	770.8642	786.1457	868.904
MEFV	3.2833	2.07E-05	3.944024	4.699617	0	5.27022	23.56517	33.1046	61.6822	20.00355
CDA	3.285702	3.48E-11	117.3347	44.64636	52.23906	64.99938	1408.412	598.2474	290.2692	420.0745
LIPG	3.323385	0.000403	314.5359	75.19387	48.22067	50.06709	2389.509	1178.76	443.8699	870.1542
KANK4	3.342784	3.8E-91	279.0397	184.0683	184.8459	194.9981	2188.419	2275.941	1780.318	2295.407
WDR17	3.359075	1.95E-10	7.888048	14.09885	12.05517	3.51348	148.4606	47.29228	84.66184	105.0186
SYTL4	3.643375	4.9E-80	41.41225	33.68059	46.21147	41.28339	439.8832	470.5582	611.9842	501.3389
NRIP1	3.649707	2.32E-42	61.13237	32.89732	38.1747	32.49969	384.8978	443.3651	581.7478	648.865
ANKRD29	3.704025	5.52E-08	1.972012	6.266156	4.018389	0	43.98832	54.38612	31.44583	32.50576
CYP4X1	3.763468	1.41E-06	7.888048	3.133078	0	10.54044	138.249	73.30304	43.54038	37.50665
RPS6KA6	3.812709	2.59E-10	3.944024	3.133078	2.009195	1.75674	34.56225	30.73998	37.4931	50.00886
SRPX2	3.854557	0.000866	0	0	4.018389	1.75674	6.284046	26.01075	29.02692	20.00355
SLC9C1	3.867376	2.14E-09	23.66414	14.88212	6.027584	5.27022	391.9674	156.0645	82.24293	95.01684
COL3A1	3.949953	2.84E-87	1160.529	697.1098	710.2503	593.7781	12951.42	12915.52	10680.7	12293.43
COLEC10	4.037145	4.01E-75	21.69213	20.36501	17.07815	22.83762	297.7067	331.046	330.1812	392.5696
ADM2	4.543129	0.000648	6.902042	1.566539	0	0	136.678	30.73998	19.35128	7.50133
RBMS3	4.586941	1.09E-10	3.944024	1.566539	2.009195	0	60.48394	42.56305	33.86474	37.50665
TSPAN6	4.69977	6.1E-05	1.972012	0	0	1.75674	25.13618	18.91691	7.256729	43.75776
NEUROG2	4.702122	0.004749	0	1.566539	0	0	14.1391	2.364614	14.51346	15.00266

Gene	log2-fold change	Adjusted p-value	NS control Rep 1	NS control Rep 2	NS control Rep 3	NS control Rep 4	shGSTP1-1 Rep 1	shGSTP1-1 Rep 2	shGSTP1-1 Rep 3	shGSTP1-1 Rep 4
LAMB1	4.748397	1.5E-115	393.4164	245.1633	200.9195	216.9574	8404.912	6609.096	6516.543	6844.963
AFF3	4.814775	1E-05	0	2.349808	0	0.87837	36.13327	17.73461	12.09455	32.50576
NRCAM	5.073576	1.12E-16	5.916036	3.133078	2.009195	0	90.33316	80.39688	59.26329	137.5244
TRGV5	5.219152	0.008113	0	0	0	0	12.56809	7.093842	2.41891	2.500443
DDIT4L	5.488146	1.07E-22	7.888048	4.699617	0	0	168.0982	165.523	112.4793	120.0213
LHFPL6	6.158145	2.7E-29	0	6.266156	0	1.75674	172.0258	132.4184	164.4859	166.2795
MAL2	6.170303	1.56E-05	0	0	0	0	14.1391	11.82307	14.51346	7.50133
PLXNA2	6.309936	5.2E-14	3.944024	0	0	0	78.55058	62.66227	74.9862	72.51285
CD200	6.330353	9.76E-07	0	0	0	1.75674	55.77091	40.19844	14.51346	35.00621
ADGRF5	6.534704	3.01E-06	0	0	0	0	25.13618	14.18768	12.09455	10.00177
TMPRSS15	7.007854	1.21E-09	0	0	0	1.75674	51.05788	76.84996	48.3782	57.51019
PTGIS	7.700124	6.46E-09	0	0	0	0	67.5535	16.5523	31.44583	22.50399
CYP4A22	7.864922	2.04E-08	0	0	0	0	72.26653	53.20382	9.675639	20.00355
MACC1	7.973208	4.6E-24	0	3.133078	0	0	210.5155	266.0191	188.675	238.7923
LAMB4	8.201434	1.19E-48	3.944024	1.566539	2.009195	0	628.4046	524.9443	407.5863	571.3513
EMCN	10.518	5.06E-53	1.972012	0	1.004597	1.75674	2130.292	1619.761	1318.306	1569.028

APPENDIX B: DIFFERENTIALLY EXPRESSED PROTEINS IN GSTP1 KNOCKDOWN CELLS

The most significant, differentially expressed proteins in GSTP1 knockdown MIA PaCa-2 cells compared to the control as reported by LC-MS/MS based proteomics experiment. The log_2-fold change, p-adjusted, and the log_2 Cyclic Loess normalized intensities for TMT values for four replicates of each group are shown here.

Protein	log2-fold change	Adjusted p-value	NS Rep 1	NS Rep 2	NS Rep 3	NS Rep 4	NS Rep 5	shGSTP1-1 Rep 1	shGSTP1-1 Rep 2	shGSTP1-1 Rep 3	shGSTP1-1 Rep 4	shGSTP1-1 Rep 5
MARCKS	-10.08	0.0653474	17.74	17.99	18.61	18.29	18.26	0.00	12.49	13.01	14.97	0.00
QPRT	-4.441	1.835E-05	20.96	21.65	20.45	21.93	21.69	17.14	17.77	15.84	16.82	16.91
GSTP1	-3.820	5.555E-06	26.67	26.74	26.56	26.85	26.67	23.41	23.38	22.78	23.04	21.78
SLC2A3	-3.437	0.0001393	19.49	20.28	19.58	20.25	20.45	15.80	16.99	15.82	16.43	17.81
OASL	-3.255	1.155E-06	17.64	18.04	17.23	18.09	17.66	14.41	14.22	14.31	14.59	14.86
ALDH7A1	-3.217	8.601E-06	26.64	27.16	26.38	27.32	27.00	23.88	24.15	22.96	23.94	23.49
TCF7	-3.162	8.286E-07	17.50	17.61	17.50	17.51	17.14	14.26	14.24	13.91	14.87	14.17
DPYSL2	-3.156	1.758E-06	23.54	23.36	23.37	23.47	23.12	19.99	20.33	19.65	20.28	20.82
IFIT2	-2.716	6.721E-05	20.79	20.88	20.33	21.02	20.98	18.64	18.50	17.15	18.34	17.79
IFITM1	-2.714	7.925E-05	23.38	23.51	23.19	24.02	23.57	21.16	21.46	19.82	20.90	20.76
SH3BGRL	-2.651	0.0005376	20.26	20.12	19.66	19.93	19.21	17.55	17.62	17.71	17.24	15.80
TGM2	-2.578	2.567E-08	24.10	23.95	23.84	23.95	24.04	21.28	21.38	21.32	21.34	21.65
PDIA6	-2.538	8.286E-07	26.10	26.38	26.02	26.40	26.30	23.76	23.74	23.32	23.64	24.05
ISG15	-2.374	4.784E-06	22.47	22.89	22.16	22.99	22.87	20.31	20.40	19.94	20.42	20.43
SLC16A3	-2.365	1.155E-06	22.49	22.68	22.77	22.47	22.61	20.12	20.37	19.87	20.21	20.64
UBASH3B	-2.301	1.889E-06	20.96	21.13	21.02	21.16	20.98	19.00	19.00	18.20	18.81	18.73
SERPINA3	-2.284	0.0010628	21.92	22.77	20.95	22.67	21.48	19.62	20.15	19.29	19.90	19.42
IFIT3	-2.155	8.286E-07	21.68	21.79	21.34	21.92	21.92	19.68	19.60	19.39	19.66	19.54
TSPAN1	-1.982	0.0110034	18.76	18.43	18.30	19.47	18.59	17.25	17.96	15.53	17.09	15.80
TUBB2B	-1.960	3.936E-05	22.18	21.93	22.26	22.07	21.63	20.21	20.30	20.37	19.93	19.46
IFIT1	-1.893	1.155E-06	21.06	21.26	20.76	21.27	21.30	19.38	19.15	19.12	19.27	19.27
ADIRF	-1.722	0.0022265	24.00	24.25	23.29	24.49	24.09	22.64	22.66	21.32	22.59	22.30
MVP	-1.639	0.0001159	25.37	25.65	25.06	25.87	25.46	23.97	24.11	23.29	23.91	23.92
GGH	-1.479	3.147E-06	22.19	22.38	22.04	22.52	22.15	20.79	20.93	20.60	20.82	20.75
CALB2	-1.442	0.0001070	21.92	22.05	21.48	21.77	21.35	20.46	20.51	19.98	20.35	20.07
TBC1D2	-1.416	7.898E-06	22.15	22.11	22.10	21.86	21.71	20.80	20.59	20.46	20.63	20.37
STX12	-1.384	3.640E-06	20.97	21.03	21.13	21.17	21.21	19.72	19.66	19.61	19.56	20.04
ITGA3	-1.380	0.0026366	23.55	23.74	23.13	24.08	23.47	22.33	22.77	21.51	22.47	22.01
PGM1	-1.373	1.736E-06	23.79	23.86	23.71	23.99	23.95	22.62	22.51	22.36	22.31	22.61
SERPINF1	-1.369	0.0001358	19.44	19.82	19.31	19.79	19.48	18.55	18.10	18.47	17.90	17.97
AFAP1L2	-1.367	0.0079548	17.15	16.13	17.67	16.48	16.27	15.34	15.87	15.19	15.05	15.42
CPT1A	-1.260	1.840E-06	22.17	22.23	22.24	22.50	22.34	21.06	21.09	20.89	20.98	21.16

Protein	log2-fold change	Adjusted p-value	NS Rep 1	NS Rep 2	NS Rep 3	NS Rep 4	NS Rep 5	shGSTP1-1 Rep 1	shGSTP1-1 Rep 2	shGSTP1-1 Rep 3	shGSTP1-1 Rep 4	shGSTP1-1 Rep 5
HLA-A	-1.226	0.0109119	16.89	17.13	16.36	17.49	17.24	15.51	16.17	14.99	16.04	16.28
PCDH1	-1.173	0.0015951	20.72	20.58	20.46	20.63	20.15	19.55	19.80	19.22	19.40	18.71
TSPAN4	-1.163	3.200E-05	17.90	17.63	17.73	17.93	17.53	16.71	16.79	16.33	16.51	16.58
CCDC71L	-1.127	5.136E-06	18.70	18.66	18.54	18.54	18.54	17.22	17.54	17.52	17.42	17.64
ZNF532	-1.125	0.0620328	16.57	15.00	16.08	15.41	16.55	14.77	14.71	14.28	15.86	14.35
DSG2	-1.108	2.427E-06	19.28	19.44	19.35	19.18	19.12	18.21	18.27	18.17	18.07	18.10
TWF2	-1.095	1.527E-06	22.99	23.11	22.84	23.16	23.04	21.94	21.99	21.88	21.96	21.91
PSMB9	-1.081	0.0011825	19.51	19.91	19.20	20.01	19.90	18.63	18.89	18.32	18.53	18.75
VAMP8	-1.065	0.0004191	20.32	20.52	20.28	20.64	20.14	19.39	19.49	19.01	19.64	19.07
UBE2L6	-1.055	0.0063319	20.37	20.65	19.84	20.90	20.68	19.57	19.74	18.86	19.58	19.40
PRKAR2B	-1.027	0.0001681	21.48	21.79	21.22	21.68	21.42	20.43	20.66	20.22	20.63	20.51
SIAE	-1.015	0.0134196	20.29	20.43	19.64	20.91	20.49	19.52	19.65	18.69	19.40	19.43
TBC1D4	1.0202	5.980E-05	17.48	17.68	17.28	17.54	17.31	18.60	18.65	18.34	18.54	18.27
PPP3CA	1.0458	1.407E-05	20.94	20.70	20.61	20.61	20.45	21.81	21.73	21.65	21.72	21.62
CPPED1	1.0797	2.247E-05	18.90	18.89	18.61	18.65	18.46	19.87	19.73	19.72	19.91	19.68
SORBS2	1.1187	0.0029833	15.63	15.31	15.05	15.21	15.23	16.89	16.69	16.05	16.54	15.85
LAMB1	1.1392	3.462E-07	19.41	19.43	19.40	19.35	19.41	20.57	20.55	20.64	20.53	20.41
STOM	1.1413	6.460E-06	19.31	19.14	19.45	19.12	19.29	20.25	20.42	20.53	20.52	20.29
UPP1	1.1471	6.17E-06	19.47	19.42	19.34	19.68	19.26	20.63	20.65	20.42	20.66	20.54
ENC1	1.1814	0.0191522	16.77	15.99	17.41	16.26	17.44	17.82	17.51	18.32	17.82	18.32
CAV2	1.2355	0.0001310	16.90	16.65	17.28	17.02	17.06	18.23	18.14	17.94	18.18	18.59
MYO1B	1.4374	1.958E-06	20.18	20.16	20.39	20.34	19.92	21.49	21.64	21.65	21.72	21.68
ERCC6	1.5012	9.714E-05	18.65	18.53	18.22	18.36	17.93	20.06	19.91	19.57	20.12	19.56
ADD3	1.6465	5.144E-07	17.60	17.51	17.37	17.39	17.27	18.93	19.07	19.05	19.23	19.10
C4orf32	1.9506	7.851E-06	16.27	16.66	16.82	16.45	16.01	18.17	18.42	18.37	18.60	18.41
PTX3	2.0358	5.907E-05	16.41	16.29	16.46	16.31	15.48	18.26	18.40	18.19	18.51	17.78
DDAH1	2.2903	1.36E-07	20.98	20.91	20.87	20.94	20.52	23.21	23.20	23.05	23.16	23.05
ADAM17	5.1881	0.2911827	0.00	12.77	12.70	0.00	12.52	11.94	12.92	13.33	13.29	12.43